

UNIVERSITÀ DEGLI STUDI DI NAPOLI FEDERICO II



Scuola Politecnica e delle Scienze di Base

**Dipartimento di Ingegneria Chimica, dei Materiali e della
Produzione Industriale**

**XXVIII PHD PROGRAMME
IN
PRODUCTION TECHNOLOGIES AND SYSTEMS**

**Cognitive Sensor Monitoring of Machining Processes
for Zero Defect Manufacturing**

PHD PROJECT SUPERVISOR

Prof. Roberto Teti

PHD PROGRAM COORDINATOR

Prof. Luigi Carrino

PHD CANDIDATE

Ing. Piera Centobelli

Index

ACKNOWLEDGMENTS	i
LIST OF FIGURES	i
LIST OF TABLES.....	iii
1. Introduction.....	1
2. Sensor monitoring of manufacturing processes.....	3
2.1 Monitoring Scopes	3
<i>2.1.1 Tool condition</i>	<i>3</i>
<i>2.1.2 Chip form</i>	<i>4</i>
<i>2.1.3 Process conditions.....</i>	<i>4</i>
<i>2.1.4 Surface integrity.....</i>	<i>5</i>
<i>2.1.4 Machine tool state</i>	<i>6</i>
2.2 Sensors for machining process monitoring.....	6
<i>2.2.1 Motor Power and Current</i>	<i>7</i>
<i>2.2.2 Force and torque</i>	<i>7</i>
<i>2.2.3 Acoustic emission.....</i>	<i>8</i>
<i>2.2.4 Vibration</i>	<i>9</i>
<i>2.2.5 Other sensors.....</i>	<i>10</i>
2.3 Advanced sensor signal processing	10
<i>2.3.1 Signal pre-processing</i>	<i>11</i>
<i>2.3.2 Feature extraction.....</i>	<i>12</i>
<i>2.3.2.1 Time domain</i>	<i>12</i>
<i>2.3.2.2 Frequency domain</i>	<i>13</i>
<i>2.4.3 Signal feature selection</i>	<i>14</i>
2.4 Cognitive decision making systems	15
<i>2.4.1 Neural networks</i>	<i>16</i>
<i>2.4.2 Fuzzy logic.....</i>	<i>17</i>
<i>2.4.3 Genetic algorithms</i>	<i>18</i>
2.5 Sensor fusion concept and paradigm	19
3. Cognitive sensor monitoring of robot assisted polishing.....	21
3.1 Surface roughness.....	23
<i>3.1.1 2 Profile roughness parameters.....</i>	<i>23</i>
<i>3.1.2 3D Surface roughness parameters</i>	<i>25</i>
3.2 Polishing of AISI 52100 steel	25
<i>3.2.1 Experimental procedure and workpiece details.....</i>	<i>27</i>
<i>3.3.2 Identification of possible vital parameters and sensor monitoring system implemented.....</i>	<i>28</i>
<i>3.2.3 Sensor monitoring system.....</i>	<i>29</i>
3.4 Experimental Test 1.....	30
<i>3.4.1 Features Extraction and selection for experimental Test1</i>	<i>33</i>

3.4.2 <i>Neural Network Pattern Recognition for Surface Roughness Identification</i>	35
3.4.2.1 <i>Discussion of results for NN training set 1</i>	37
3.4.2.2 <i>Discussion of results for NN training set 2</i>	39
3.5 Experimental Test 2	42
3.5.1 <i>Features Extraction and selection for experimental Test2</i>	45
3.5.2 <i>Neural Network Pattern Recognition for Surface Roughness Identification</i>	47
3.5.2.1 <i>Discussion of results for NN training set 2</i>	49
3.5.2.2 <i>Discussion of results for NN training set 2</i>	53
4. Cognitive sensor monitoring of drilling of composite materials	58
4.1 Characteristics of composite materials	58
4.2 Classification of composite laminates	58
4.3 Drilling operations	60
4.4 Tool wear analysis	62
4.5 Hole quality evaluation for drilling of composite laminates	64
4.5.1 <i>Delamination</i>	65
4.5.2 <i>Spalling and fuzzing</i>	67
4.5.3 <i>Diameter error and circularity</i>	70
4.5.4 <i>Roughness</i>	71
4.6 Drilling of CFRP/CFRP stacks	71
4.6.1 <i>Workpiece details</i>	72
4.6.2 <i>Experimental procedure</i>	73
4.7 Multiple sensor monitoring system	75
4.8 Advanced signal processing	79
4.9 Features extraction	81
4.9.1 <i>Time domain features</i>	81
4.9.2 <i>Frequency domain features</i>	83
4.10 Tool wear	85
4.11 Hole quality assessment	87
4.12 Features selection	89
4.13 Neural network paradigm for decision making	90
4.14 Discussion of results	95
5. Conclusions and future developments	98
APPENDIX A	100
APPENDIX B	102
APPENDIX C	113
APPENDIX D	116
References	121

ACKNOWLEDGMENTS

The research activities described in the first part of this PhD thesis work have been developed within the EC FP7 Integrated Project (IP) on Intelligent Fault Correction and self Optimizing Manufacturing systems (IFaCOM) under grant agreement n. 285489. Jes Ramsing of Strecon, partner in the IFaCOM project, is thankfully accredited for supplying the sensorial data set of the polishing process and surface roughness measures.

The activities of the second part of this thesis have been developed in the context of the national MIUR PON Project on “Development of eco-compatible materials and technologies for robotised drilling and assembly processes – STEP FAR” (2014-2016). I would like to thank also Prof. Luigi Nele for his scientific support concerning drilling of carbon fibre reinforced plastic laminates.

The Fraunhofer Joint Laboratory of Excellence on Advanced Production Technology (Fh-J_LEAPT Naples) at the Department of Chemical, Materials and Industrial Production Engineering, University of Naples Federico II, is gratefully acknowledged for its support to this work.

This thesis would not have been possible without the support of my supervisor Prof. Roberto Teti. I would like to express to him my sincere gratitude for his significant suggestions, inspiring guidance and immense knowledge.

I would like to thank also my colleagues Dr. Dorian M. D’Addona, Dr. Tiziana Segreto, Dr. Sara Karam, Davide Matarazzo, Vittorio Balsamo, Alberto Bottillo, Francesco Napolitano, Roberta Angelone and, last but not least, Dr. Alessandra Caggiano for her time and valuable feedback on my research activities.

I would like to give my special thanks and gratitude to Roberto Cerchione for his infinite patience, unconditional support and lovely care.

I will be forever thankful to my family for their love, understanding and emotional support. Words cannot express how grateful I am to my mother and my father for all of the sacrifices they made for me. Thank you, I love you!

LIST OF FIGURES

Figure 1. Spindle motor with integrated sensor ring (Byrne & O'Donnell, 2007).....	8
Figure 2. Advanced signal processing procedure (Teti, Jemielniak, & O'Donnell, 2010)	11
Figure 3. Fuzzy inference system implementation steps (Teti, Jemielniak, & O'Donnell, 2010).....	18
Figure 4. General steps of the polishing process (IFaCOM deliverable 4.1)	22
Figure 5. Evolution of surface roughness in polishing operation (IFaCOM deliverable 4.1)	22
Figure 6. Roughness Average (Ra).....	24
Figure 7. Standard deviation of surface slopes (Whitehouse, 2012).....	25
Figure 8. (a) STRECON® RAP-225 MACHINE for polishing tools, machine components and other similar applications with 2D rotation-symmetric geometry as well as simplified 3D geometries; (b) close-up of the vibration polishing module (right) (Pilný & Bissacco, 2015).....	26
Figure 9. Initial test piece proposed by STRECON.....	27
Figure 10. Measuring principle of Non-Contact Surface Metrology by means of Light Scattering.....	28
Figure 11. Sensors mounted on the RAP machine (IFaCOM deliverable 4.1)	29
Figure 12. Aqm roughness values versus number of passes_Test1	31
Figure 13. Sa and Sz roughness values versus number of passes_Test1	33
Figure 14. Surface roughness average measurement values and surface roughness interpolation curves for polished workpieces WP1, WP2, WP3, WP5	36
Figure 15. NN training set 1: WP1, WP2, WP3, WP5 plots of the 7 average surface roughness values, the desired surface roughness interpolation values and the NN predicted surface roughness values obtained using the 12-12-1 and 12-24-1 NN configurations	39
Figure 16. NN training set 2: WP1, WP2, WP3, WP5 plots of the 7 average surface roughness values, the desired surface roughness interpolation values and the NN predicted surface roughness values obtained using the 13-13-1 and 13-26-1 NN configurations	41
Figure 17. Aqm roughness values versus number of passes_Test2	43
Figure 18. Sa and Sz roughness values versus number of passes_Test2	45
Figure 19. Surface roughness average measurement values and surface roughness interpolation curves for polished workpieces WP1, WP2, WP3, WP4, WP5	48
Figure 20. NN training set 1: WP1, WP2, WP3, WP4, WP5 plots of the desired surface roughness interpolation values and the NN predicted surface roughness values obtained.....	52
Figure 21. NN training set 2: WP1, WP2, WP3, WP4, WP5 plots of the desired surface roughness interpolation values and the NN predicted surface roughness values obtained.....	56
Figure 22. (a) Unidirectional fibres orientation; (b) Bidirectional fibre orientations; (c) Laying-up sequence of unidirectional-plies	58
Figure 23. Standard geometry of a twist drill (Groover, 2010)	60
Figure 24. Drilling basic motions	61
Figure 25. Schematic representation of twist drill (Stephenson & Agapiou, 2006)	63
Figure 26. Tool wear as a function of cutting time (Marinov, 2004).....	63
Figure 27. Effect of cutting speed on tool wear and tool life for three cutting speeds	64
Figure 28. Entry and exit delamination representation (Faraz, Biermann, & Weinert, 2009).....	66
Figure 29. Delamination factor.....	66
Figure 30. Representation of holes delamination factor and delaminated area (Voß, Henerichs, Rupp, Kuster, & Wegener, 2016)	67
Figure 31. Formation process of the spalling defect: (a) Thrust action of the chisel edge; (b) Thrust action of the cutting edges; (c) Twist action of the cutting edges.....	68
Figure 32. Spalling defect (Zhang L. , 2013)	68

Figure 33. Uncut fibres – fuzzing (Zhang, Chen, Chen, & Zhang, 2001).....	69
Figure 34. Covered relative circumference (Voß, Henerichs, Rupp, Kuster, & Wegener, 2016)	69
Figure 35. Covered relative bore area (Voß, Henerichs, Rupp, Kuster, & Wegener, 2016)	70
Figure 36. Hole defects observed in a unidirectional plate	71
Figure 37. (a) Vacuum bag moulding; (b) Autoclave	73
Figure 38. Laminates profiles and their surface textures	73
Figure 39. Drill bit geometry.....	74
Figure 40. Drilling centre used for the experimental campaign	74
Figure 41. (a) Kistler-9257A piezoelectric dynamometer; (b) Kistler-9277A25 piezoelectric dynamometer	75
Figure 42. Kistler 5007 amplifiers	76
Figure 43. (a) Vibration and high frequency Acoustic Emission sensor - Montronix BV100™; (b) Montronix TSVA4G amplifier	76
Figure 44. Acoustic Emission and Vibration Acceleration amplifier settings	77
Figure 45. Data acquisition device - NI USB-6361	78
Figure 46. NI SignalExpress software interface	79
Figure 47. Thrust force raw signal and its corresponding conditioned signal for hole n. 6 (6000 rpm, 0.20 mm/rev).....	80
Figure 48. (a) thrust force; (b) torque; (c) acoustic emission; (d) vibration acceleration - operating conditions 6000 rpm – 0.15 mm/rev	81
Figure 49. Thrust force statistical features plots for all operating conditions: (a) Arithmetic Mean; (b) Variance; (c) Kurtosis; (d) Skewness; (e) Power.....	83
Figure 50. Single-Sided Amplitude Spectrum of Force (6000 rpm – 0.15 mm/rev)	84
Figure 51. Evolution of peaks detected in frequency domain using discrete Fourier Transform	85
Figure 52. (a) drill secured in the vine; (b) optical measuring machine Tesa Visio V-200	85
Figure 53. Tool wears types for the determination of tool-life during drilling (Dolinšek, Šuštaršič, & Kopač, 2001)	86
Figure 54. Measured flank wear values: (a) VB and (b) VBmax	86
Figure 55. Measured flank wear values and interpolated tool wear curves.....	87
Figure 56. Entry delamination (6000 rpm - 0.20 mm/rev) for holes 1,30 and 60.....	87
Figure 57. Exit delamination (6000 rpm - 0.20 mm/rev) for holes 1,30 and 60.....	88
Figure 58. (a) Measured entry delamination; (b) Measured exit delamination	88
Figure 59. Delaminated area (6000 rpm - 0.20 mm/rev) for holes 1,30 and 60	88
Figure 60. Measured delaminated area	89
Figure 61. Results comparison	94
Figure 62. Exit diameter error, tool flank wear, exit delamination and delaminated area measures for all drilling conditions.....	97

LIST OF TABLES

Table 1. Sensors used in the monitoring of the process analysed.....	29
Table 2. Number of passes for each band	30
Table 3. Number of passes for each band and surface roughness values (Aqm and Aqs)_Test1	31
Table 4. Number of passes for each band and surface roughness values (Sa and Sz)_Test1	32
Table 5. Visual checking of significant signals features_Test 1.....	34
Table 6. NN training set 1: desired surface roughness interpolation values and NN predicted surface roughness values, obtained with the 12-12-1 and 12-24-1 NN configurations, for each WP and polishing pass	38
Table 7. NN training set 2: desired surface roughness interpolation values and NN predicted surface roughness values, obtained with the 13-13-1 and 13-26-1 NN configurations, for each WP and polishing pass	40
Table 8. NN results for training set 1 and training set 2 in terms of MAPE_Test1	42
Table 9. Number of passes for each band	42
Table 10. Number of passes for each band and surface roughness values (Aqm and Aqs)_Test2.....	43
Table 11. Number of passes for each band and surface roughness values (Sa and Sz)_Test2	44
Table 12. Visual checking of significant signals features_Test 2.....	46
Table 13. NN training set 1: desired surface roughness interpolation values and NN predicted surface roughness values, obtained.....	50
Table 14. NN training set 2: desired surface roughness interpolation values and NN predicted surface roughness values, obtained.....	54
Table 15. NN results for training set 1 and training set 2 in terms of MAPE_Test2	57
Table 16. Experimental testing conditions	74
Table 17. AE Amplifier Specifications	76
Table 18. Data acquisition device NI USB-6361	78
Table 19. NN performances in terms of RMSE and MAPE	92
Table 20. Overall results	96

1. Introduction

The research work developed in this thesis, focused on cognitive sensor monitoring of machining processes for zero defect manufacturing, has been addressed within the framework of the international research project EC FP7 CP-IP “IFaCOM – Intelligent Fault Correction and self Optimizing Manufacturing systems” (2011-2015; FoF NMP – 285489) and the national MIUR PON Project on “Development of eco-compatible materials and technologies for robotised drilling and assembly processes – STEP FAR” (2014-2016).

The vision of the IFaCOM project is to achieve near zero defect level of manufacturing with particular emphasis on the production of high value, large variety and high performance products.

This goal is achieved through the development of improved methodologies for monitoring and control of the performance of manufacturing processes with the aim to detect abnormal process conditions leading to defects on the produced parts.

The overall aim of the STEP FAR project is the study of issues related to drilling and cutting techniques of advanced lightweight components, such as composite material parts, and their relative assembly, using cooperating anthropomorphic robots. The use of innovative materials and processes developed in this research will lead to a reduction in weight and environmental impact in the construction and maintenance of primary aircraft structures. At least a 5% reduction in weight of the structures is foreseen without increase of costs (a possible rise in the cost of raw materials is compensated with the reduction of process costs).

In aeronautical industry, the reduction of aircraft weight is becoming an increasingly important aim both for environmental requirements (lower emissions) and contraction of the management costs (lower fuel consumption). Therefore, new structural architectures have been developed through the use of innovative materials and technologies.

One of the innovative processes analysed in this project is the drilling of carbon fibre reinforced plastic (CFRP) stacks.

With reference to the two different industrial manufacturing applications defined in the framework of these projects, the objective of this thesis work is focused on the development of cognitive condition monitoring procedures for zero defect machining processes.

Chapter 2 reviews the general concept of sensor monitoring of manufacturing processes and provides a comprehensive survey of sensor technologies, advanced signal processing techniques, sensor fusion approach, and cognitive decision making strategies for process monitoring.

In Chapter 3, the IFaCOM project industrial case focused on improving repeatability and predictability of the surface finish produced by a Robot Automated Polishing (RAP) process at STRECON A/S, Denmark, is discussed and analysed.

In order to establish a robust method for the detection of the polishing process end-point, i.e. the determination of the right moment for tool and abrasive paste change, STRECON sensor system selection focuses on monitoring the progress of the surface quality during the polishing process by means of variation in VQCs (Vital Quality Characteristics), i.e. roughness and gloss of the polished surface. The output data have been used to train a neural network. The employed NN learning procedure was the leave-k-out method where k cases from the training set are put aside in turn, while the other cases are used for NN training.

In Chapter 4, the Alenia Aermacchi industrial case, as coordinator and partner of the STEP FAR project, is discussed and analysed. The Alenia Aermacchi user case is focused on cognitive

sensor monitoring for drilling of stacks made of two overlaid carbon fibre reinforced plastic composite laminates. In this case, a neural network based cognitive paradigm based on a bootstrap procedure has been used for the identification of correlations between the sensor signal features and the tool wear development and product hole quality.

Finally, Chapter 5 reports the concluding remarks and future developments of this work.

2. Sensor monitoring of manufacturing processes

Many studies conducted in the last years showed that the success of modern flexible manufacturing systems is largely based on the availability of real-time data about the process operating conditions (material, tool, process). Reliable models of production systems performance prediction are, in many cases, very difficult to find. In order to avoid errors, defects and malfunctions are therefore needed, in addition to a careful modelling of production processes, methods of monitoring and control of production. The use of reliable and intelligent sensory devices helps the production system to achieve optimal performances: so that nowadays the use of monitoring systems is widespread. In order to increase the efficiency of these systems, it is necessary to develop improved sensors and more sophisticated techniques for processing the sensor data output.

The design of advanced sensor systems with innovative technologies for signal processing allows to obtain more comprehensive information about the process conditions, with the aim of increasing economic efficiency through the optimization and control of the process.

The research studies carried out in recent years by several authors have shown the effectiveness of sensor techniques based on the signals detection and analysis (Teti, Jemielniak, & O'Donnell, 2010). The purpose of sensor monitoring is to increase the information reliability in order to make correct decisions about the status of the process through the extraction of the appropriate features.

2.1 Monitoring Scopes

Advanced monitoring of machining operations may have several scopes such as tool condition monitoring (TCM), chip form classification, monitoring of the process conditions, surface integrity and monitoring of the machine tool state (Teti, Jemielniak, & O'Donnell, 2010).

2.1.1 Tool condition

The following list summarizes some of the most important and notable applications in tool condition monitoring:

- Analysis of acoustic emission (AE) using the wavelet packet decomposition method (WPD) for automatic classification of tool wear in milling (Wu, et al., 2014)
- Development of correlations in broaching between tool conditions and output signals of multiple sensors, i.e. AE, vibration, cutting force, hydraulic pressure and spindle power of the broaching machine, mounted on the machine tool (Axinte & Gindy, 2003). The spindle power signal was used for tool condition monitoring in milling, drilling and turning, it turned out to be successful in continuous turning and drilling but not efficient in discontinuous milling.
- Application to identify real-time tool breakage in milling operations based on the analysis of indirect measurements of cutting force through feed drive AC motor current (Lee, Choi, Kim, & Chu, 1995).

- Development of a laser displacement meter for online tool geometry measurement (Ryabov, Mori, & Kasashima, 1996).
- Development of an online tool condition monitoring system based on vibrations and cutting forces monitoring (Dimla & Lister, 2000).
- Online estimation of drill wear during drilling operations based on spindle motor power signal (Kim H. , Ahn, Kim, & Takata, 2002).
- Use of micro-scale thermal imaging to identify effects of steel machinability on cutting zone temperature and related tool wear mechanisms (Arrazola, Arriola, Davies, Cooke, & Dutterer, 2008).
- Analysis and comparison of cost effective methods for tool breakage detection by performing trials on ultra-precision micro-milling machine (Gandarias, et al., 2006).

2.1.2 Chip form

As regards the applications developed for chip conditions, the following papers illustrates effective applications:

- Govekar, Gradisek, & Grabec (2000) employed filtered AE spectrum components for chip form classification.
- Monitoring method based on neural network and spindle motor power to detect the state of chip disposal in drilling (Kim & Ahn, 2002).
- Chip form recognition based on wavelet packet transform (WPT) and spectral estimation of cutting force signals (Teti, et al., 2006).
- Chip form characterization (chip entanglements, chip size, and chip shape) under different dry cutting conditions using geometric transformations of the control variables (Venuvinod & Djordjevich, 1996).
- Development and testing of a system for the automatic chip breaking detection using frequency analysis of cutting forces (Andreasen & De Chiffre, 1998).

2.1.3 Process conditions

Another aspect of monitoring of machining processes is monitoring of process conditions. The following illustrates important applications and developments:

- Classification of drilling operations in *normal* and *abnormal*, e.g. tool breakage or missing tool, based on spindle power signals (Brophy, Kelly, & Byrne, 2002).
- Fault detection method in tapping under different fault conditions based on torque and radial force (Mezentsev, Zhu, DeVor, Kapoor, & Kline, 2002).
- Development of an online machining monitoring system for machining operations of aero engine materials experimentally validated on PXI and LabVIEW platforms (Shi, Axinte, & Gindy, 2007).
- Development of a process monitoring system in Al alloy milling based on sound energy sensors, frequency analysis and cognitive processing of audible sound signal features to identify variable process conditions (Rubio & Teti, 2009).

- Implementation of a generalised internet-based process monitoring facility for process optimisation and simulation forming a Remote Machine Monitoring System (RMMS) (Chen, Bender, Renton, & El-Wardany, 2002).
- Development of an online polishing expert system based on AE signals integrated with a multiple sensor systems which can detect in real time polishing status and subsequently adjust the polishing parameters initially set (Ahn, Shen, Kim, Jeong, & Cho, 2001).
- Assessment of cutting variables, such as shear angle, chip thickness, tool vibration amplitude, strain, strain rate, and chip type in orthogonal turning tests using high speed photography combined with laser printed square grid (Pujana, Arrazola, & Villar, 2008).
- Development of an innovative non-stationary process condition monitoring method based on time-frequency distribution analysis and a singular value decomposition approach (Gu, Ni, & Yuan, 2002).

2.1.4 Surface integrity

Concerning monitoring and control of surface integrity in manufacturing processes, a number of applications and studies have been developed. The most remarkable ones are illustrated below:

- Online estimation of surface roughness (Ra) and dimensional deviation (DD) in turning using neural network. Cutting feed, depth of cut and two components of the cutting force (the feed and radial force components) appears to be the most significant features to be monitored (Azouzi & Guillot, 1997).
- Correlation of surface and cutting force in end milling processes based on a statistical approach (Huang & Chen, 2003).
- Prediction of surface roughness in turning based on cutting vibration parameters and FFT analysis (Abouelatta & Mádl, 2001).
- Decomposition of the vibration signals for in-process prediction of surface roughness in turning based on singular spectrum analysis (Salgado D. , Alonso, Cambero, & Marcelo, 2009).
- Real-time surface roughness prediction and machining trouble during cutting operation through time series analysis of vibration acceleration signals measured (Song, et al., 2005).
- Assessment of machined surface quality after broaching, in terms of geometrical accuracy, burr formation, chatter marks and surface anomalies, based on the monitoring of multiple sensors signals, i.e. acoustic emission, vibration and cutting force. Cutting force in broaching proved to be efficient in detecting of small surface anomalies (Axinte D. , Gindy, Fox, & Unanue, 2004).
- Development of a real-time monitoring system in hard machining to correlate AE parameters and white layer, surface finish and tool wear. The results showed that AE_{RMS} , frequency and count rate seems to be correlated with white layer formation and therefore suitable to monitor surface integrity factors (Guo & Ammula, 2005).
- Recognition of grinding burns in cylindrical plunge grinding processes through AE signal analysis (Kwak & Song, 2001).
- Real-time surface roughness prediction method based on a simple linear regression model using the displacement signal of spindle motion (Chang, Kim, Kim, Jang, & Han, 2007).

- Process monitoring in abusive broaching and milling of difficult-to-machine aerospace materials for surface anomalies detection based on AE signals and cutting force data (Axinte, Boud, Penny, Gindy, & Williams, 2005; Marinescu & Axinte, 2009).
- Analysis of the dynamics of broaching of complex part features. Inclined chatter surface marks, because of cutting edges specific geometry were linked through force and acceleration signal analysis revealed (Axinte D. , 2007).
- Detection of workpiece surface discontinuities during multiple cutting edge machining through an array of three AE sensors (Axinte, Natarajan, & Gindy, 2005; Marinescu & Axinte, 2008).
- Determination of the cutting speed and feed rate effect on the quality of drilled holes in carbon fibre composites through cutting forces and temperature analysis (Rawat & Attia, 2009).

2.1.4 Machine tool state

Finally, as far as machine tool state monitoring, the main applications studied and developed are the followings:

- Detection and comparison between characteristic parameters of signals available in controlled drives (position, speed and motor current) and the current ones (Verl, Heisel, Walther, & Maier, 2009).
- Design and implementation of an integrated intelligent monitoring system, with modular and reconfigurable structure. This system monitors a total of 72 diagnostic features (power, vibration, temperature and pressure of the drives and spindles) (Zhou, Chen, Fuh, & Nee, 2000).
- Condition monitoring technique based on vibration, acoustic emission, Shock Pulse Method (SPM) and surface roughness for fault detection of critical subsystems identified by a failure frequency analysis (Saravanan, Yadava, & Rao, 2006).

2.2 Sensors for machining process monitoring

The purpose of the application of sensors in machining processes is to continuously monitor the machining process in order to optimise the machining process performance.

Monitoring of machining operations is typically done through diverse measuring techniques that can be classified into direct and indirect approaches.

Direct techniques are based on measuring the actual quantity of a given variable, e.g. tool wear. Some examples of direct measurement techniques applicable to monitoring of machining operations are the use of cameras for visual inspection, radioactive isotopes, laser beams, and electrical resistance.

Direct techniques may be limited only to laboratory environments due to the practical limitations caused by access problems during machining, illumination and the use of cutting fluid. In addition, direct measurement techniques are highly accurate and have been extensively used in research laboratories to closely monitor fundamental measurable variables in machining processes.

Instead, as regards indirect measurement techniques, an auxiliary quantity is correlated to the actual quantity of a measured variable through already existing correlations. However, indirect

measuring techniques are less accurate compared to direct ones but have the advantage of being less complex and more suitable for practical cases.

2.2.1 Motor Power and Current

For material removal from the workpiece, the mechanical force is provided by the electric drives and spindles. Process power and machine tool measures and conditions can be obtained through measurement of motor related parameters such as motor power or current. Most importantly, the embedded devices used to measure motor related parameters do not disturb the machining process. Moreover, it is possible to measure power through the drive control loop, particularly interesting in production environment (Byrne, et al., 1995).

A cheap and economical monitoring solution in machining operations is retrofit power measurements. However, the most recent control systems give a direct access to motor power and motor current signals using the numerical controller (Oliveira, Ferraz Jr., Coelho, & Silva, 2008). Furthermore, recently, in order to provide the user a Human Machine Interface (HMI), software have been integrated with the CNC control. This has become more common in the industrial sector. Extending the earlier approach the Adaptive Control Optimise (ACO) and Adaptive Control Constraint (ACC) algorithms have been developed and implemented based on internal control signals and additional sensors (Klocke, Wirtz, & Veselovac, 2009). This aspect leads to the direct monitoring in the drive control. Power measurement is already enabled in the drive controller and is adequate for use in the machining environments (Byrne, et al., 1995). A technique based on power measurement technology have been applied in order to demonstrate high quality signal information for process and drive condition monitoring (Pritschow & Kramer, 2005).

2.2.2 Force and torque

During machining operations a given force is required to separate and/or remove material. Therefore, in almost every machining operation the monitoring of cutting forces is essential for the verification of analytical models, cutting tool failure detection, workpiece quality, and so on (Byrne, Dornfeld, & Denkena, 2003). It has been noted that cutting force signals are highly sensitive to changes in the cutting states. Deformation could also be measure using torque sensors, however torque sensors measure torsional applied load corresponding to deformation. Even though the measurement technology is the same, the application and the method of signal transmission of torque and force sensors are quite different.

Force and torque sensors are generally used to measure the deformation of an elastic element and convert it into the applied force element or torsional load. There are several types of sensors and they can be divided into two basic groups: *piezoelectric* and *strain based sensors*.

For direct force measurement, *piezoelectric sensors* should be mounted in line with the force path. In laboratory experimental environments, where applications request for more flexibility, multi-component force transducers have been used. Another type are rotating cutting force dynamometers that are able to acquire and measure both torque and the three components of the force. These dynamometers have been used in monitoring of high speed milling in aerospace industry and operate at speeds of up to 20,000 rpm. During the last decade, integration of force and torque sensor into the machine tool structure have increased especially in drilling (Byrne & O'Donnell, 2007) and milling (Qiao & Zhu, 2012) machine tools. The following figure (Figure 1) shows an integrated force sensor ring in the motor spindle. The process of sensor integration

in machine tools is complex and requires strategy development in order to isolate the process phenomena from spindle and machine dynamics (Jun, et al., 2002; Korkut, 2003).

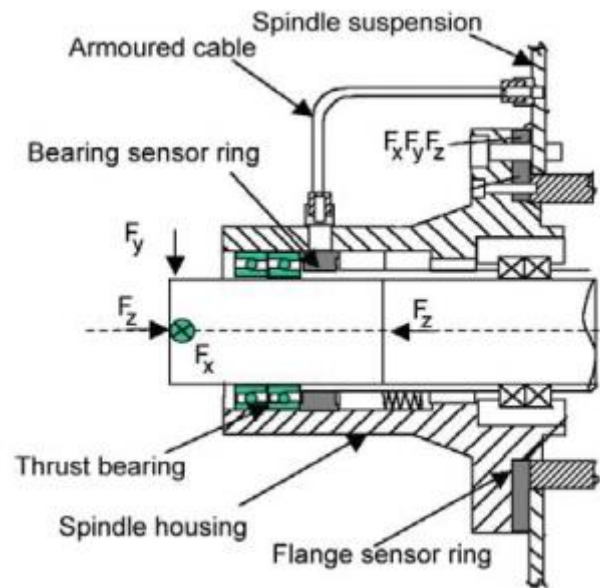


Figure 1. Spindle motor with integrated sensor ring (Byrne & O'Donnell, 2007)

Strain gauges are force sensors that deform under a force; they are considered stable and offer a reasonably high frequency response. One of the first application developed combined strain gauges and piezoelectric sensor into a single instrument in order to acquire the static force measurements from the strain gauges and the dynamic force measurements using a piezoelectric thin film accelerometer (Kim & Kim, 1997). The overall cutting force was determined by summing both static and dynamic force components. Another application was based on the development of a strain based force sensor to detect and measure the three cutting components of the force during milling (Korkut, 2003).

Moreover, another research group has developed a strain based sensor to be placed between the cutting tool and the tool holder. This strain based sensor would be used to monitor conventional milling. This sensor provided torque measurements for a 100 mm diameter face-milling cutter (Smith, Smith, & Tlustý, 1998).

2.2.3 Acoustic emission

In machining process monitoring, the piezoelectric sensor is one of the most adequate technology to measure acoustic emission (AE) (Rogers, 1979). Having a rather wide sensor bandwidth (100 to 900 kHz), AE is able to detect a big part of the phenomena in machining. Bandpass filters are of great help for AE detection and signal process once selected appropriate frequency ranges. The working principle of AE pre-processing is the following: the AE sensor signals are the input of a preamplifier with a high input impedance and low output impedance. In addition, a root mean square (RMS) converter, a gain selection unit, and filters are embedded in the preamplifier.

Several principles can be used to detect and monitor AE signals. An example is capacitance as it changes as the distance between two parallel plate changes. This is considered a highly accurate technique for AE detecting and it is highly adequate to be used for calibrating other AE sensors.

Yet, it should be taken into consideration that capacitance sensors for AE detection are highly sensitive and are highly affected by sensor position and mounting. This makes this type of sensors inadequate in monitoring machining processes where the operating environment is harsh (Hundt, Leuenberger, Rehsteiner, & Gygax, 1994).

Another type of method is based on a piezoelectric thin film sensor placed between the cutting insert and the tool holder. This type of sensor is noted to have several advantages with respect to other commercial AE sensors. It is more sensitive to changes due to the fact that is very closely located to the cutting process. It is also characterised by a very large frequency bandwidth. In addition, the acquired signal is usually characterized by good quality, especially in the high frequency range.

An alternative and innovative approach was developed based on the use of fibre optics (Carolan, et al., 1997; Carolan, et al., 1997). This method shows several strengths compared to the traditional AE technology. It operates over a broader bandwidth with respect to the other conventional methods, flat frequency response and absolute calibration. In addition, a significant advantage is the fact that is a no contact method which allows the signal transmission between the source and the sensor.

However the piezoelectric thin film sensor and fibre optics based AE sensor types have been extensively developed in laboratory environments but not yet in industrial contexts.

AE signals are characterized by a high frequency and low amplitude nature, allowing signal transmission through a coupling fluid. If the AE sensor was placed on the coolant supply nozzle, the coolant fluid represents the transmission mechanism (Inasaki, 1998). A widely used application implements a nonintrusive coupling fluid to link the AE sensor to the spindle drive shaft (Hutton & Hu, 1999; Li, Dong, & Yuan, 1999).

This method using a coupling fluid is advantageous in milling and drilling, i.e. for machining operations with rotating cutting tools. Several other techniques are available for signal transmission and coupling between the AE sensor and the AE signal processor. Some examples are slip rings, inductive coupling, and radio frequency transmission (Inasaki, 1998; Karpuschewski, Wehmeier, & Inasaki, 2000). AE signal processing in machining has been widely investigated by Jemielniak (2001). He proposed that the AE signals should be continuously reflected from the inner surfaces of the structure where the AE sensor is mounted, during the machining operation.

As mentioned earlier, in order to correctly mount an AE sensor, a couplant is required between the sensor and the work material surface which should be clean and free from any barrier that may influence the acoustic coupling. The distance between the sensor the AE source should not be big due to the fact that the further the sensor is placed from the source in order to obtain an adequate representation of AE signals. The possible change in distance between sensor and AE source should be taken into consideration due to the fact that affect the correct representation and acquisition of AE. Therefore, the best location of the AE is the workpiece or an a stationary part of the machine tool.

2.2.4 Vibration

There is a wide variety of ways to detect vibrations, nevertheless piezoelectric transduction is the most common one in machining operations.

Actually, vibrations occurring during metal cutting can be considered as dependant or independent of the cutting process. These two of vibrations are not independent. Forced vibration

created by other machines or machine components are considered vibrations independent from the machining process, e.g. vibration transmitted through foundations. As for vibrations derived from metal cutting, it is possible to identify a large number of characteristics related to the functioning of the machining process. An example would be interrupted cutting. Varying cutting forces can be caused by several reasons, e.g. non-homogeneity in the work material. In addition, the cutting tool conditions during machining has a significant impact on the vibration produced. Chatter, defined as self-excited vibration, is one of the common known types of vibration in machining. It is very destructive and negatively affect finish and tool life. The main reason behind chatter is the interaction between surface material and tool under some cutting conditions.

2.2.5 Other sensors

Several other sensor types have been studied and used in research for monitoring and control of machining processes. An example would be the integration of micro sensors for temperature measurements in the cutting tool insert (Biermann, Kirschner, Pantke, Tillmann, & Herper, 2013; Yang, Hou, Zhou, Zhu, & Duan, 2014). In literature, monitoring and measurement of temperature variations in machining operation has been exhaustively studied (Davies, Ueda, M'Saoubi, Mullany, & Cooke, 2007). The implementation of vision systems for tool condition monitoring based on temperature measurement has been of great interest (Kurada & Bradley, 1997). A great factor that may negatively affect machine vision is illumination. Another application implemented lasers for measuring cutting edge profile of cutting tool inserts in milling (Ryabov, Mori, & Kasashima, 1996). This technique allows to realise a 3D image of the cutting tool. Subsequently, the tool condition was assessed based on a histogram method of noisy input signals and a hybrid technique for detection and measurement of tool failures. Over the years, many researchers have tried to combine multiple sensors to monitor tool conditions.

Other techniques are based on strain and temperature sensors (Shinno & Hashizume, 1997) or sound and image analysis (Mannan, Kassim, & Jing, 2000).

Another field of interest is the examination of displacement in order to find the correlation between tool wear and the workpiece dimension and surface quality. Some of these applications include the ultrasound technique (Abu-Zahra & Yu, 2000), laser light with reflected light intensity measurement (Wong, Nee, Li, & Reisdorf, 1997) and bifurcated optic fibre with reflected light intensity measurement (Choudhury, Jain, & Rama Rao, 1999).

2.3 Advanced sensor signal processing

Reliable process condition monitoring should be based on the identification and extraction of a proper number of sensor signal features (SFs) that can be correlated to the monitoring output, e.g. tool wear and process condition (Dimla Snr., 2000; Li, 2002; Sick, 2002). This may be obtained through advanced signal processing methodologies according to the steps reported in Figure 2. The first stage involves signal pre-processing (filtering, amplification, A/D conversion, and segmentation) including, on occasion, signal transformation into frequency or time–frequency domain (Fourier Transform, wavelet transform, etc.). The next stage is the extraction of signal or signal transform features changing with tool or process conditions. There are many diverse descriptors from different sensor signals, but most cannot be easily related with the process being monitored. Thus, feature selection is of critical importance and the identified relevant features are finally integrated into the tool or process condition diagnosis system.

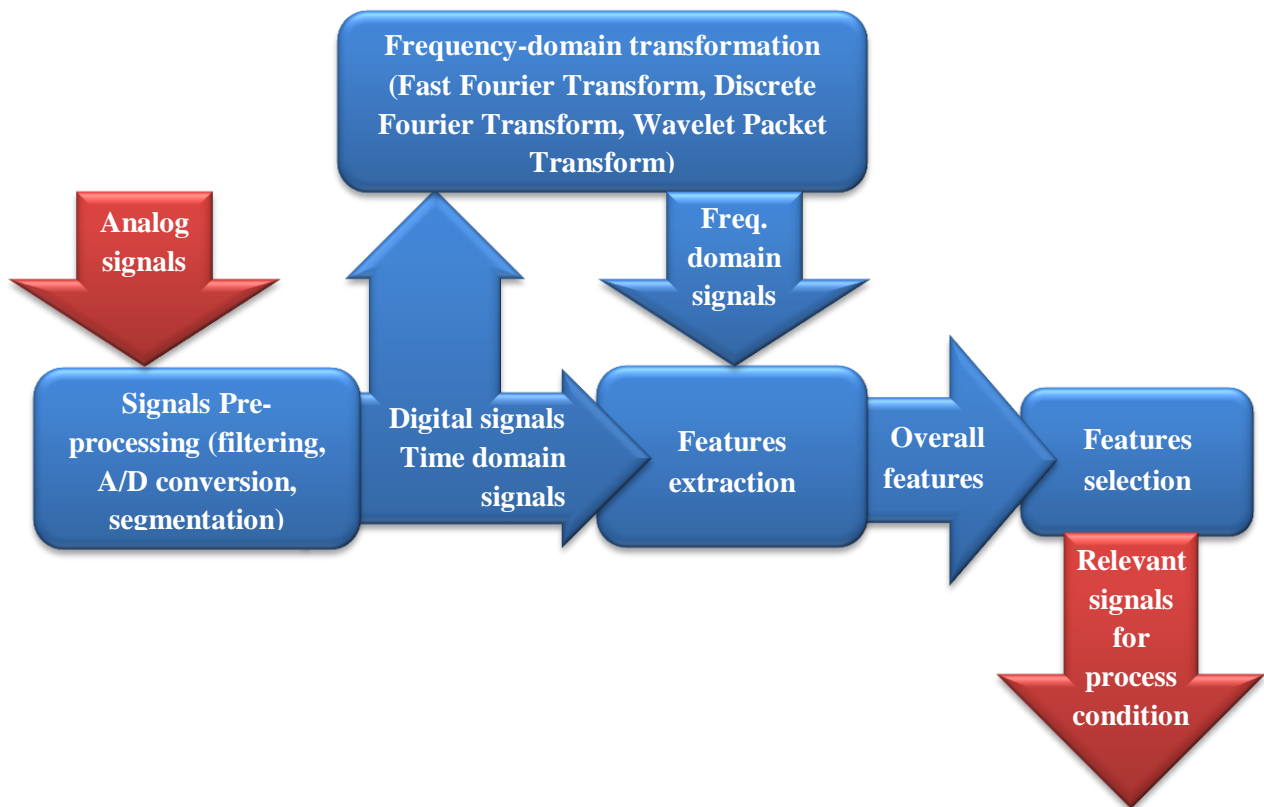


Figure 2. Advanced signal processing procedure (Teti, Jemielniak, & O'Donnell, 2010)

2.3.1 Signal pre-processing

Pre-processing is required for analogue signals in order to be converted into digital signals. Each sensor is characterized by a specific conditioner (e.g. charge amplifier, piezotron coupler, etc.). As described above, the piezoelectric AE sensor must be localized close to the cutting zone. Due to its high impedance, the sensor should be connected to an amplifier. The buffer amplifier transforms the raw signal derived from the sensor in a proportional voltage one. Also dynamometers and accelerometers have the same requirements. To respect the range of sensor frequency response and avoid high frequency noise, it is necessary to filter the analogue signal. Then the filtered signal may be furtherly processed.

As far as raw acoustic emission signals, the frequency range could reach 1 MHz (typically 80–700 kHz). Therefore, a high sampling frequency (>1 MS/s) is required. Therefore, in order to obtain a low frequency variable, the AE sensors acquire usually RMS (Root Mean Square) signals (AE_{RMS}), which require cheaper devices.

Several sensor signal features (e.g. burst rate, event counts, signal average) can be calculated.

During the cutting process, the acoustic emission energy can be considerable. Due to the pre-processing characteristics the acoustic emission energy may cause an excess of load of the buffer amplifier. High-pass filtering lead to misleading data evaluation temporary fading of the signal value due to the of saturated signals (Jemielniak K. , 2000). A solution method would be setting the gain of the buffer amplifier to the smallest possible value. Consequently, especially using AE_{RMS} instead of AE_{raw} , any additional required amplification should be carried out after signal filtering (Jemielniak K. , 2000).

The signal is amplified before A/D conversion in order to achieve the best possible accuracy. In addition, further pre-processing is usually required for digital signals. Digital filtering is

fundamental for reduction of frequency bands that are not related to the analysed process. It may also extract information required for pattern recognition.

Scheffer & Heyns (2004) investigate the signal features concerning the tool wear in interrupted turning. This was performed through the application of digital filters to divide cutting force signals into two frequency ranges. Another case investigates the detection of catastrophic tool failure in turning using a low-pass filter of cutting force signals (Jemielniak & Szafarczyk, 1992).

In several applications, a digital signal filtering was necessary to avoid signal oscillations and high frequency noise (Ghosh, et al., 2007; Li, Ouyang, & Liang, 2008).

Also segmentation is considered a sensor signal pre-processing method. The only interesting portion of the signal is the signal detected when the tool is removing metal. Signal information should be extracted only in that phase because this is the only portion which contains valuable information regarding the tool conditions or the process monitored (Bhattacharyya, Sengupta, & Mukhopadhyay, 2007; Marinescu & Axinte, 2008).

2.3.2 Feature extraction

2.3.2.1 Time domain

Several SFs can be extracted from sensor signals in the time domain. From the sensor signals, SFs to be extracted are selected to be extracted based on their ability to adequately describe the signal and maintain the related information concerning the process as well as tool conditions. Several SFs can be extracted from time domain signal. The most common signal features in the time domain are:

- arithmetic mean, average value, magnitude (Sick, 2002; Dong, Subrahmanyam, Wong, Hong, & Mohanty, 2006; Salgado & Alonso, 2006; Ghosh, et al., 2007);
- effective value (root mean square) (Sick, 2002; Ghosh, et al., 2007);
- conventional statistical features: variance (or standard deviation) (Scheffer & Heyns, 2001; Guo & Ammula, 2005; Dong, Subrahmanyam, Wong, Hong, & Mohanty, 2006; Ghosh, et al., 2007); skewness (Al-Habaibeh & Gindy, 2000; Dong, Subrahmanyam, Wong, Hong, & Mohanty, 2006; Salgado & Alonso, 2006; Zhu, Wong, & Hong, 2009); kurtosis (Al-Habaibeh & Gindy, 2000; Binsaeid, Asfour, Cho, & Onar, 2009; Zhu, Wong, & Hong, 2009); signal power (Al-Habaibeh & Gindy, 2000; Bhattacharyya, Sengupta, & Mukhopadhyay, 2007; Binsaeid, Asfour, Cho, & Onar, 2009);
- peak-to-peak range, or peak-to-valley amplitude (Sick, 2002; Scheffer & Heyns, 2004; Al-Habaibeh & Gindy, 2000; Ghosh, et al., 2007);
- crest factor (Scheffer & Heyns, 2001; Sick, 2002; Sun, Hong, Rahman, & Wong, 2004; Dong, Subrahmanyam, Wong, Hong, & Mohanty, 2006);
- ratios of the signals, signal increments (Sick, 2002; René de Jesús, Gilberto, Iván, & Carlos, 2004).

There are some signal features relevant only for vibration and acoustic emission signals, e.g.:

- ring down count or pulse rate, i.e. the number of times the AE_{raw} signal exceeds the threshold level (Jemielniak, 2000; Kwak & Song, 2001; Sick, 2002; Guo & Ammula, 2005);

- pulse width, i.e. the percentage of time during which AE_{raw} remains above the threshold level (Jemielniak, Kwiatkowski, & Wrzosek, 1998; Jemielniak K, 2000);
- burst rate, i.e. number of times AERMS signal exceeds preset thresholds per second (Jemielniak, 2000; Li, 2002; Binsaeid, Asfour, Cho, & Onar, 2009);
- burst width, i.e. percentage of time AERMS signal remains above each threshold (Jemielniak, Kwiatkowski, & Wrzosek, 1998; Jemielniak, 2000).

These features reveals to be particularly useful for the detection of the catastrophic tool failure (Jemielniak, 1998a; Jemielniak, 1998b) and for the monitoring of the cutting tool flank wear (Kannatey-Asibu Jr. & Dornfeld, 1982).

2.3.2.2 Frequency domain

Fast Fourier transform. Signal features extraction from sensor signals in the frequency domain is usually performed using the discrete Fast Fourier Transform method (FFT). In the Discrete Fourier Transform (DFT), data are converted from their original domain (typically time or samples) to the frequency domain. For this purpose, practically, a fast Fourier transform (FFT) algorithms is chosen to be used out of the several commonly known ones. The main aim behind FFT is to give an inside view of the process. An example would be its use for tool wear influences (Prakash, Kanthababu, & Rajurkar, 2015).

The signal features usually taken into consideration are:

- amplitude of dominant spectral peaks (Kwak & Song, 2001; Sick, 2002; Marinescu & Axinte, 2008; Binsaeid, Asfour, Cho, & Onar, 2009);
- signal power in particular frequency ranges (Jemielniak K. , 2000; Govekar, Gradisek, & Grabec, 2000; Sick, 2002; Sun, Hong, Rahman, & Wong, 2004; Binsaeid, Asfour, Cho, & Onar, 2009);
- energy in given frequency bands (Scheffer & Heyns, 2001; Altintas & Park, 2004; Marinescu & Axinte, 2008);
- statistical characteristics of band power spectrum: mean frequency, variance, skewness, kurtosis (Binsaeid, Asfour, Cho, & Onar, 2009);
- frequency of the spectrum highest peak (Abouelatta & Mádl, 2001; Sick, 2002; Guo & Ammala, 2005).

The sensor signals acquired during machining are dynamic rather than static. FFT provides the averages of the frequency composition with a fixed predetermined resolution along the entire frequency spectrum over the signal duration. Therefore, a time-frequency analysis, i.e. the Short Time Fourier Transform, can be adopted to overcome this problem. The Short Time Fourier Transform allows to analyse the frequency components in different time intervals using a sliding window. For this sample of data, spectral coefficients are calculated and the window is moved to a new position where the calculation procedure is repeated. The Short Time Fourier Transform gives information along different consecutive short time intervals and, consecutively, put them together. The Short Time Fourier Transform was applied in milling operations to acoustic emission signals to identify tool and workpiece failures (Marinescu & Axinte, 2008; Marinescu & Axinte, 2009).

Wavelet transform. The wavelet transform was firstly introduced by Mallat (1989) and Daubechies (1990) to overcome the problem of the window width of the Short-Time Fourier Transform, i.e. it is not possible obtain an high time and frequency resolution at the same time. Therefore, according to the frequency values to be investigated, they use different windows, wide windows are used for low frequencies analysis while narrow windows are used for high frequencies.

Wavelet transform has been widely used in literature also for the machine condition monitoring (Kunpeng, San, & Soon, 2012; Liu, Li, & Shen, 2014), flank wear estimation (Kamarthi & Pittner, 1997; Kamarthi, Kumara, & Cohen, 2000), tool failure and breakage (Hong, Rahman, & Zhou, 1996; Tarnng & Lee, 1999; Kwak, 2006) very often in combination with neural network (Tansel, Mekdeci, & Mclaughlin, 1995).

Through discrete wavelet transform (DWT), the original signal may decomposed into scaling coefficients and wavelet coefficients representing the signal convolution and its impulse response to the filters applied.

Wavelet transform coefficients are considered signals from which, in turn, it is possible to extract significant time domain features:

- average (Hong, Rahman, & Zhou, 1996; Wu & Du, 1996)
- crest factor (Wu & Du, 1996; Scheffer & Heyns, 2001)
- kurtosis (Wu & Du, 1996; Scheffer & Heyns, 2001; Teti, et al., 2006)
- peak-to-peak and peak-to-valley values (Wu & Du, 1996; Teti, et al., 2006)
- Root Mean Square (Teti, et al., 2006)
- standard deviation and variance (Wu & Du, 1996; Grzesik & Bernat, 1998; Teti, et al., 2006)

2.4.3 Signal feature selection

From a given number of sensor signals, a large number of signal features can be extracted and calculated. However, not all these features can give adequate information concerning the process conditions. Therefore, the extracted SFs should be selected on the basis of their relevancy and sensitivity to process conditions. However, any given well correlated and selected signal feature can be randomly become distorted. Therefore, an appropriate number of SFs should be chosen in such a way to avoid possible disturbances caused by any single SF. In some decision making systems, such as neural networks, a bigger number of training samples is required when faced with a bigger number of features (Hong, Rahman, & Zhou, 1996). In cases where the system should work after the first training session, a large number of SF inputs might not be adequate due to the fact that the amount of training samples is not big enough (Jemielniak, 2000). Therefore, signal processing may be able to maintain the relevant system information by eliminating repeated or irrelevant SFs. Applying these systems and concepts in industrial contexts, minimum operator intervention should be required, i.e. the selection of the relevant SFs should be automatic. An interesting classification of feature selection procedures for tool wear estimation in turning was proposed by (Sick, 2002). The study reveals that, of the 138 papers reviewed, the 38% selected SFs without any valid reason or just on the basis of the literature review, the 26% selected SFs on basis of the measured signals analysis, the other 21% doesn't selected the SFs considering the behaviour of the tool wear model and the only the remaining 15 % selected SFs after a careful analysis of the influence of different SFs on tool wear estimation.

As concern tool wear condition monitoring, the Pearson correlation coefficient r has been used to find the features that can best characterize it (Quan, Zhou, & Luo, 1998). The correlation coefficient (r) represents the correlation between a selected feature (x) and a tool wear value (y), where \bar{x} and \bar{y} represent the average values:

$$r^2 = \frac{(\sum_i (x_i - \bar{x})(y_i - \bar{y}))^2}{\sum_i (x_i - \bar{x})^2 \sum_i (y_i - \bar{y})^2}$$

The correlation coefficient represents the measure of the linear correlation between two variables and it ranges from -1 to +1. Usually, a lower value of r means that that SF is not correlated with the phenomenon, so the probability to select it is low (Scheffer & Heyns, 2001; Scheffer & Heyns, 2004). However, in some cases, SFs are not perfectly linearly correlated with tool wear and is <1 . This fact is usually ignored.

Another correlation index, the coefficient of determination, was used by (Jemielniak, Kwiatkowski, & Wrzosek, 1998) in order to investigate the correlation between signal features and tool wear:

$$R^2 = \frac{RSS}{TSS} = \frac{TSS - ESS}{TSS} = \frac{\sum_i (y_i - \bar{y}_i)^2 - \sum_i (y_i - \hat{y}_i)^2}{\sum_i (y_i - \bar{y}_i)^2}$$

where

y_i : is the signal feature value

\bar{y} : is the mean value

\hat{y}_i : is the signal feature predicted value based on tool wear function

However, automated feature selection methods have a major drawback. These methods select very similar SFs or ones that are dependent on each other. Therefore, sensor fusion through automated feature selection methods cannot be completed. In such cases, manual intervention of engineers and scientists would be required for feature selection instead of automated methods. However, such manual procedures are not encouraged in industrial contexts and are, therefore, considered only on the level of laboratory experimental conditions. Still, removing similar features became fundamental due to the fact that they do not contain any additional information. A method would be calculating the Root Mean Square Error (RMSE), set a threshold and then select the best SFs (Jemielniak & Bombiński, 2006; Jemielniak, Bombiński, & Aristimuno, 2008; Jemielniak & Arrazola, 2008). Any SFs having an RMSE higher than the set threshold was rejected. Following the most adequate signal features are selected and the ones correlated to them are rejected.

2.4 Cognitive decision making systems

Cognitive computing methods play a crucial and fundamental role in the realization of intelligent multiple sensor monitoring systems for modern manufacturing systems (Teti & Kumara, 1997). During the last years several paradigms, schemes, and techniques have been developed for the construction of decision making support systems based on sensor monitoring and signal features extraction and processing. These cognitive paradigms include, but are not limited to, fuzzy logic, genetic algorithms, neural networks, and hybrid systems that can combine different capabilities.

2.4.1 Neural networks

In machine learning, artificial neural networks (ANNs) are a family of models based on the functioning of the central nervous system of animals, in particular the brain. Computation is based on developing and adjusting connections between single elements called neurons or nodes, which operate in parallel. A NN can be given as a map through which input points are associated with their corresponding output points. This correlation between input and output nodes is based on given values, e.g. class membership. NNs have several positive aspects and they can be summarized in the following:

- the knowledge domain is based on known examples
- they are able to handle continuous and discrete data
- they have a good generalisation capability

NN builds its knowledge through training phase. A typical NN training method is the supervised training, which consist in providing both input and the corresponding output patterns. The error between the output values predicted and the expected ones is used to adjust the weights of the links between the neurons of the network. On another hand, unsupervised training is performed through feeding to the NN only input pattern vectors. The NN learns and divides these input pattern vectors in groups depending on similarities between them.

Supervised learning: There are several supervised learning paradigms. Backpropagation neural network (BPNN) is one of those training paradigms and it has been very popular for their performance. It is based on the calculation of a loss function according to the descent gradient so it requires a pattern of output values. The initial weight values highly influence the training results. In order to obtain satisfactory results, random distortions to the weight system may be introduced in order to lead the NN performance function in local minima. Another effective method is apply alternately positive and negative shifts to the NN weights. Other supervised NN paradigms are also considered, e.g. artificial cellular neural network (ACNN) (Daisuke & Tomoharu, 2001), fuzzy logic neural network (FLNN) or neuro-fuzzy inference systems (NFS) which combines the benefits of both paradigms (Halgamuge & Glesner, 1994), probabilistic neural network (PNN) (Specht, 1990), recurrent neural network (RNN) (Schmidhuber, Wierstra, Gagliolo, & Gomez, 2007).

Unsupervised learning: Contrary to supervised leaning, only input are fed to the NN in unsupervised learning. The NN tends to organise and sort the given data in such a way that the hidden processing nodes respond equally or similarly to closely related group of stimuli which represent distinct real concepts. The self-organising map (SOM) NN is known for its high performance among several other unsupervised learning paradigms (Kohonen, 1989). The SOM NN uses the input data to create a 2D feature map. The order of the data is kept. If two or more of these input vectors are similar, then these input vectors will be mapped to close processing elements in the 2D layer representing the features of the input data.

A probabilistic neural network has been used for the detection and classification of tool malfunctions in broaching monitoring the cutting force acquired data (Axinte, 2006). The simulation of the roughing industrial broaching stage was performed using short broaching tools. These trials were carried out to produce square profile slots while detecting cutting force signals.

The broaching tools were tested in different conditions in order to reproduce the real tool failures: with fresh and worn teeth, chipped teeth and broken ones.

Simple architecture NN was repeatedly used in turning operation for tool wear evaluation (Kamarthi, Kumara, & Cohen, 2000; Bukkapatnam, Kumara, & Lakhtakia, 2000; Bukkapatnam, Kumara, Lakhtakia, & Srinivasan, 2002).

Kuljanic, Totis, & Sortino (2009) used two accelerometers and a monoaxial force sensor to develop an intelligent multi-sensor detection system for milling. To test the applicability of the system in different application ranges, different milling machines, milling cutters, sensor systems and work materials were tested.

A combined approach was employed for decision making using artificial cellular neural network for acceleration signals (Daisuke & Tomoharu, 2001) and a fuzzy neural network for axial force signals [190]. The NN gave good results for each sensor signal monitoring. Later on, the NN outputs were combined in order to realise the concept of multi-sensor chatter detection. Several combinations have been used and tried. The first three approaches, i.e. the linear combination of single sensor chatter indicators, the separate NN for multi-sensor classification approaches and the Sugeno fuzzy model (fuzzy model classification) showed a pretty high accuracy ranging between 95% and 96% but their accuracy for malfunctions ranges between 50 and 75%. Instead the last approach, i.e. the statistical inference classification based on conditional probability, showed a notable different behaviour. Its accuracy was slightly lower with a value of 94% but its insensitivity to malfunctions was high (90-92%). Therefore, the best performance are derived by this latter approach which allows to obtain both accuracy and robustness.

Kim & Ahn (2002) developed a decision making system in milling based on the spindle motor power monitoring and neural networks paradigm to evaluate the state of chip disposal. From the acquired data, selected features were extracted and combined into input vectors to be fed to a feed-forward back-propagation neural network system.

In traditional machining processes, operator is able to evaluate the process state and react adequately to any machine problem. Audible sound energy appears to be a good sensing technique that could adequately replace operator's experience based knowledge. Even if the audible sensing techniques have not been widely investigated in literature for the process condition monitoring of machining operations, one application in milling analysing the sound energy deriving from band sawing of Al alloy and C steel was developed with the aim to realize an automatic process monitoring system with cheap sensors (Rubio & Teti, 2009). A NN approach was then realized and applied; it showed successful results to monitor tool conditions.

2.4.2 Fuzzy logic

Nowadays, fuzzy logic (FL) is used in two different contexts. In the first context, it used as an extension of the many-valued logic (or multi-valued logic), i.e. the infinite-valued logic, but most widely it is associated with the fuzzy set theory (Klir & Folger, 1988). A fuzzy set is considered a set without clear boundary. They are an extension of the classical notion of set in which the membership of the elements in a set is assessed in binary terms (1 if the element belongs to the set, 0 otherwise). Instead, the fuzzy set theory introduces the concept of (membership function" as the gradual assessment of the membership of elements in a set. The shape of membership functions may be triangular or trapezoidal (the most common ones), rectangular, gaussian, sigmoidal, etc.

Figure 3 summarizes the main steps for the implementation of the most common fuzzy inference system.



Figure 3. Fuzzy inference system implementation steps (Teti, Jemielniak, & O'Donnell, 2010)

A decision support system based on fuzzy logic was designed to monitor the cutting force components during turning operations to estimate the tool wear (Balazinski & Jemielniak, 1998; Roy, 2015; Ren, Baron, Balazinski, Botez, & Bigras, 2015). The three components the FDSS are: a knowledge base consisting of if-then rules, an inference engine and a user interface. The system consist of the linguistic term set, fuzzy rules and inference engine, and user interface. The decision support system described above allows to accurately assess the tool wear monitoring.

Features extracted from acoustic emission signals and the consequent frequency analysis during the quasi orthogonal cutting of metal alloys have been used in a fuzzy logic system for tool wear and workpiece heat treatment monitoring (Teti, 1995; Teti & Manzoni, 1998). With a success rate higher than 75%, the system results adequate for monitoring scopes.

Achiche, Balazinski, Baron, & Jemielniak (2002) developed a fuzzy logic knowledge based system for tool wear monitoring using a genetic algorithm during. This system was compared to the classical tool wear estimation approaches (fuzzy logic and neural networks). However, the construction of a fuzzy logic knowledge base system requires appropriate skills and expertise. Therefore FL systems are rather difficult and complicated to implement manually. The fuzzy logic knowledge base system may be built using a genetic algorithm to overcome this problem. Furthermore, the system complexity can be set according to the accuracy to be achieved.

2.4.3 Genetic algorithms

There are several other methods for pattern recognition and decision making. One of them is genetic algorithms (GA), a search heuristic inspired by biological phenomena and particularly useful to solve complex problems. The first step is the development of the computer model able to represent the problem under investigation. The numerical representation of each element of the population is known as chromosome, generally a binary string. Then the population was ranked according to the fitness function. The strings that perform the best solutions are selected for the reproduction and the creation of the new population using genetic operators (e.g. crossover and mutation). Thus, the evolution of the population was performed according to both exploration, i.e. explore the workspace solution, and exploitation, i.e. search in the best solution area already identified . From a biology perspective, these algorithms are considered to be simple. However, these algorithms are considered sufficiently complex to catch the complexity of real world problems and provide good solutions.

2.5 Sensor fusion concept and paradigm

In machining operations, the use of signal features coming from a single sensor source may not be sufficient to detect the required process condition monitoring specifications. Therefore, the sensor fusion concept has been widely investigated in literature in order to combine signals coming from multiple different sensors and extract from them a sufficient number of SFs related to the tool and/or process conditions (Dimla Snr., 2000; Sick, 2002; Li, 2002; Segreto, Simeone, & Teti, 2014). The combined features allow to obtain more accurate, complete and robust information compared to that obtained using separate sources.

Reconfigurable monitoring system for sensor fusion research. The implementation of a multi-sensor fusion concept for process monitoring has been widely investigated not only in the literature but also in industrial projects (Teti, Segreto, Neugebauer, & Harzbecker, 2008; Teti, Segreto, & Harzbecker, 2008; Segreto & Teti, 2008). Sensors employed in these applications include acoustic emission, audible sound, cutting force, motor current, optical and vibration sensors for different machining processes, work materials and monitoring scopes. The monitored machining process are: broaching, drilling, orthogonal cutting, milling, and turning. The materials tested are: composite materials, Ni alloys, Ni–Ti alloys, steels, and Ti alloys. The monitoring scopes investigated are: chip form, machinability, tool wear, process and work material conditions.

Features extracted from both time and frequency domain are collected into feature vectors. The feature vectors represent the data input for pattern recognition paradigms (Duda & Hart, 1973). When the features belong to a single sensor, the feature vector corresponds to the input pattern vector, conversely if the significant signal features belong to different sensor sources, sensor fusion feature vectors are constructed so that the input pattern vector integrates all the features and the sensor fusion concept is realized.

In reconfigurable multi-sensor monitoring systems, pattern recognition and decision making are provided by the decision making support systems described in the previous paragraph.

Sensor fusion application to machining process monitoring. The neural network approach has been widely and successfully used for the multi-sensor process monitoring of machining operations, e.g. for the cutting of difficult-to-machine materials by monitoring both acceleration and cutting force signals (Nath, Rahman, & Andrew, 2007).

The neural network training was realized using three different configurations of signal feature vectors:

- single sensor (single cutting force or acceleration component)
- integration of the three cutting force components or three acceleration components:
- sensor fusion pattern vectors combining cutting force and acceleration feature vectors.
- The NN output was composed of coded values for process condition and machinability evaluation. The first configuration provided an accuracy range from 78% to 85%. Accuracy improved notably using the second configuration (92–97%). Finally the sensor fusion concept implementation allows to obtain the highest accuracy values (99–100%).
- The NN performance values described above have been achieved dealing with sensor fusion data instead of single sensor source. This highlights the neural network aptitude to manage the sensor fusion concept even based on incomplete or noisy dataset.

Wang, Hong, Wong, & Zhu (2007) combined force sensor and vision system for online monitoring and detection of tool breakage and tool wear during milling. During the machining operations, images of the tool flank have been captured for tool wear estimation. Two features are extracted in-process from the cutting force and appropriately pre-processed. These two features closely indicate flank wear. After each cutting pass, the features extracted from the force sensor signals and the measured flank wear values were fed to a self-organizing map network for the online prediction of the flank wear.

In addition tool breakage was detected using the force sensor features in the time domain. Their thresholds values are dynamically determined. Any in-process identified breakage is done through cutting force monitoring and then verified. The empirical findings highlight that this approach is adequate for tool condition monitoring in milling operations and regardless of cutting conditions.

3. Cognitive sensor monitoring of robot assisted polishing

Polishing is usually the last and critical stage of the manufacturing process of industrial tools and components. As several other machining operations have been carried out on the components to be polished, such components are characterized by a high added value when they are ready for polishing. Polishing is an abrasive machining process mainly used for finishing operations to achieve superior surface finish. Errors in the polishing steps, leading to unsatisfactory surface quality or compromised surface accuracy, which cannot be corrected, and generate therefore a high value loss. Nevertheless polishing is becoming more and more important and requested operation due to the increasing market qualitative demands.

Meanwhile polishing of flat surfaces is normally carried out using industrial machines and well documented and controllable processes, polishing of 3-dimensional components is still carried out by means of a series of manual operations performed by highly skilled and trained craftsmen using simple hand-held motorized tools (Weule, Timmermann, & Eversheim, 1990; Dambon, Demmer, & Peters, 2006). In addition, the choice of type and sequence of pads, pastes, as well as the polishing operations (e.g. motion, pressure) is left at the discretion of the individual craftsman, therefore the results may differ strongly. As a consequence, the result of the polishing process for a 3D part varies substantially depending on who carried out the operation. Also the evaluation of the polished surface is left to the subjective interpretation and judgment of the individual craftsman. Although surface roughness requirements are normally specified on the drawings, such specifications are not sufficient to describe the required characteristics of the surface. An excellent finish is expected at the end of the polishing process, i.e. roughness ranges equal to 0.1-0.5 μm (5-15 $\mu\text{-in}$).

During polishing, in order to remove scratches and burrs and to smooth rough surfaces, abrasive grains glued to the outside periphery of the rotating wheel are used. The wheels may be made of different materials, such as canvas, felt or leather. When the abrasive grains worn down, the wheel is replenished with new grains. The surface finishing depends on the grains size, for rough polishing grains size ranging from 20 to 80 mm in diameter are used, 90 to 120 mm for finish polishing and above 120 mm for fine finishing.

Meanwhile the majority of manufacturing processes has been successfully modelled, leading to reliable prediction of a number of dependent process parameters and process performance measures, reliable polishing models for automatic polishing (non-manual operations) are not existing and the limited attempts to date have been focused on flat surfaces. This is due to both the high complexity of the process kinematics, where the velocity vector of the single loose abrasive grains is undefined, and the high number of variables to be controlled (Tönshoff, Friemuth, & Becker, 2002). Recent studies highlighted the incredible performance obtained by the use of semi-automatic polishing machine in terms of time reduction and achieved quality requirements (Liao, Xi, & Liu, 2008; Eriksen, Arentoft, Grønbaek, & Bay, 2012).

Following the procedure for manual polishing is described, the same approach is used for automatic polishing, where the tool is held by a robot arm rather than an operator. Manual polishing is a highly repetitive process where the polisher performs a number of operations in an iterative way. Thus the operator performs several steps (Figure 4): realize the polishing (P),

evaluates the progress (E), determines the part as not completed (NC), broken (B), completed (C), or continues with the next (finer) level of polishing (F). Changing to a finer abrasive is a particularly critical step, since it involves cleaning of the part before starting to use a finer polishing abrasive material.

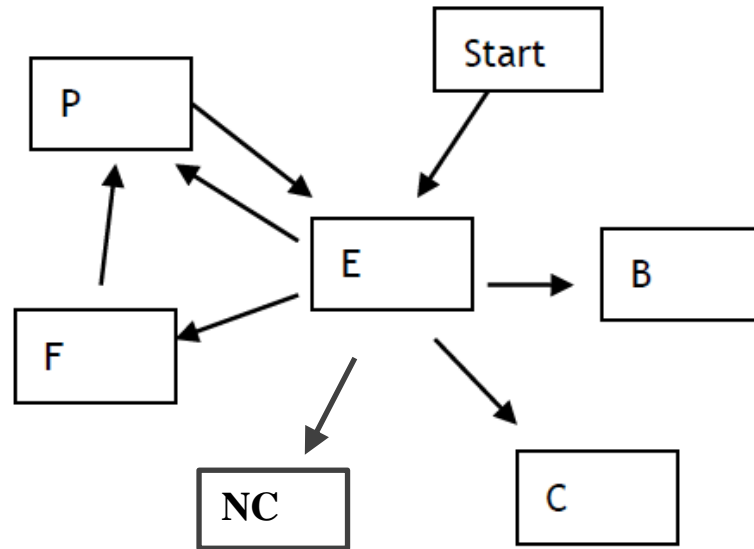


Figure 4. General steps of the polishing process (IFaCOM deliverable 4.1)

The F process is especially tricky since this involves cleaning of the part and a switch to a finer Inaccurate or insufficient cleaning or contamination might result in leftover large abrasives resulting in the failure of the polishing process about to start.

The time consumed by the polishing process ranges from a few minutes for small non-complex parts to several hours for hardened parts that require a high surface finish such as less than $Ra\ 0.01\mu\text{m}$. The hardness of the workpiece material has a strong effect on the material removal rate and therefore on the time needed to polish the surface

As shown in Figure 5, the time required by a polishing job is also largely dependent on the number of polishing stages required, increasing greatly when the part requires multiple steps, as each polishing step requires accurate cleaning of the part surface and tool change.

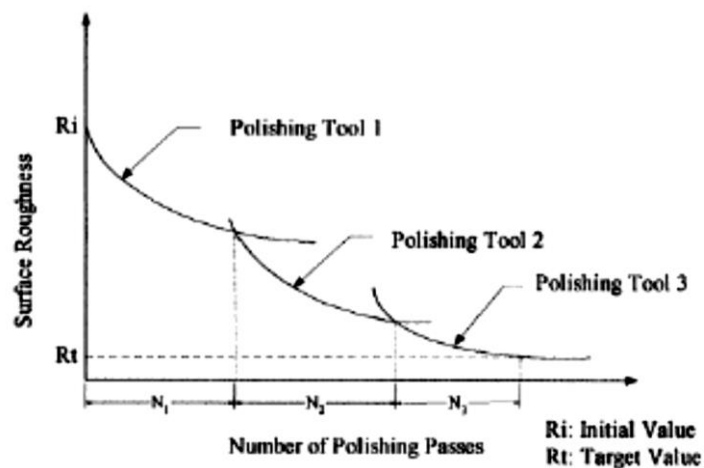


Figure 5. Evolution of surface roughness in polishing operation (IFaCOM deliverable 4.1)

Determination of the right moment of the tool change is critical and time consuming since requires proper cleaning for evaluation. If the tool is used for too short period, residual marks from the previous operation are not entirely removed and subsequent finer grains in the following polishing steps will not remove these marks. On the other hand, unnecessary long tool usage is no longer improving the surface roughness and moreover can lead to the deterioration of the surface.

On-line process control and monitoring approaches have been applied in order to the optimise the process safety and the products quality. Furthermore the on-line evaluation of surface roughness finishing using, for example, the scattered light sensors allows to reduce the time necessary for the operations carried out for the direct measurements of the finishing, i.e. stop the polishing process, remove the piece from the polishing machine, use the stylus profilometer. Kim, Ahn, & Lee (2009) and Oh & Lee (2011) developed a multi-sensor monitoring system including force and acoustic emission sensors in order to monitor the surface roughness of Stavax die steel workpieces (S136) during magnetic abrasive finishing operations. The signals have been fed to an artificial neural network (ANN). The results showed that the ANN successfully predict the surface roughness values.

3.1 Surface roughness

Sometimes the difference between rough and smooth surfaces can not be detected by touch and appearance. Therefore, especially in the field of engineering, the exact degree of roughness is of considerable importance, and it has a significant impact on the function of components and their cost. The dimension which we shall be dealing with are usually very small, i.e. microns (μm).

Changes in production processes parameters, such as feed rate and spindle speed, but also tool wear, can affect surface texture in different ways. therefore it is important analyse the surface texture and ideally the analysis should be provided over the total area. Furthermore the experience has shown that the a trace along a single track is usually adequate to obtain the required information. The first step in quantifying the texture of a surface is to obtain a digital representation of the surface under consideration.

Surfaces may be completely characterized by their roughness value, and roughness assessment must be converted into a qualitative and repeatable process. Unfortunately does not exist a single parameter able to catch the complexity of the surfaces. Therefore several profile parameters have been defined and they can be divided into three groups (Whitehouse, 2012):

- amplitude parameters: determined by peak or valley heights, or both, irrespective of horizontal spacing (e.g. Ra).
- spacing parameters: determined solely by the spacing of irregularities along the surface (e.g. Rq)
- hybrid parameters: determined by both amplitude and spacing (e.g. Rdq)

3.1.1 2 Profile roughness parameters

Following three main surface roughness parameters in bidimensional analysis have been reported.

Ra, (also known as Roughness Average) represents the arithmetic average of absolute values and it is expressed as:

$$R_a = \frac{1}{l} \int_0^l |f(x)| dx$$

This is one of the most commonly used parameters. Furthermore R_a (Figure 6) gives no information regarding the shape of the irregularities and makes no distinction between peaks and valleys (the area below the centre line is inverted and placed above the line).

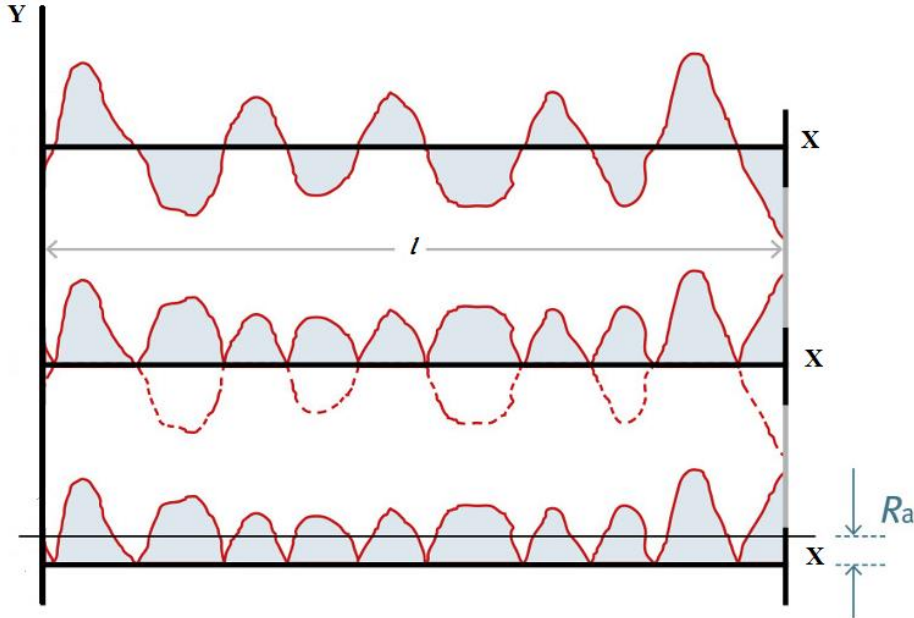


Figure 6. Roughness Average (R_a)

R_q (or R_{MS}) is another method of calculating an average roughness value. It represents the arithmetic average of absolute values and it is expressed as:

$$R_q = \sqrt{\frac{1}{l} \int_0^l y^2 dx}$$

R_{dq} is the Root Mean Square (RMS) slope of the profile within the sampling length (Figure 7) and it is calculated according to the following analytical formulation:

$$R_{dq} = \sqrt{\frac{1}{l} \int_0^l (\theta(x) - \bar{\theta})^2 dx}$$

Where θ is the slope of the profile at any given point and $\bar{\theta}$ is equal to $\frac{1}{l} \int_0^l \theta(x) dx$.

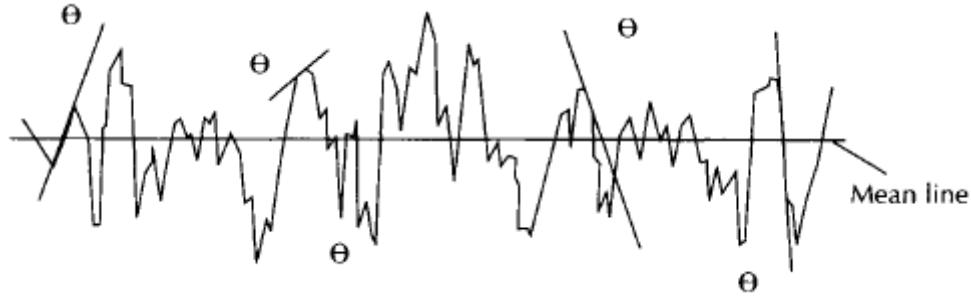


Figure 7. Standard deviation of surface slopes (Whitehouse, 2012)

3.1.2 3D Surface roughness parameters

Areal roughness parameters are defined in the ISO 25178 series. Nowadays many optical measurement instruments are able to measure the surface roughness over an area.

In a 3D profile image, S_a and S_q are respectively the Average Roughness and Root Mean Square Roughness evaluated over the complete 3D surface. Mathematically, S_a and S_q are evaluated as follows:

$$S_a = \iint_a |Z(x, y)| dx dy \quad S_q = \sqrt{\iint_a (Z(x, y,))^2 dx dy}$$

The S_a and S_q parameters represent an overall measure of the texture comprising the surface. S_q is typically used to specify optical surfaces and S_a is used for machined surfaces.

Three more parameters are considered: S_p (Max Peak Height), S_v (Max Valley Depth) and S_z (Max Height of Surface). These parameters are evaluated starting from the absolute highest and lowest points found on the surface. S_p is the height of the highest point, S_v , is the depth of the lowest point (expressed as a negative number) and S_z is the sum of the largest peak height value and largest pit or valley depth value within the sampling area. It is found from $S_z = S_p - S_v$.

3.2 Polishing of AISI 52100 steel

In the focus of the IFaCOM project, STRECON develops and offers special machinery solutions for the robot assisted polishing (RAP) of industrial tools and components among other needs developed for tool assembly and die adjustment in close proximity to the production line. STRECON is not having an active internal polishing production but developed a robot assisted polishing machine that can offer unique possibilities for automated, robust and repetitive generation of polished functional surfaces for various applications.

STRECON's focus within IFaCOM is in improving the measuring, repeatability and predictability characteristics of the polishing process by its product, the RAP-225 Robot Assisted Polishing (RAP) machine (Figure 8).

In order to establish a robust method for the detection of the polishing process end-point, i.e. determination of the right moment for tool and abrasive paste change, STRECON sensor system selection focuses on monitoring the progress of the surface quality during the polishing process by means of variation in VQCs (Vital Quality Characteristics), i.e. roughness and gloss of the polished surface.

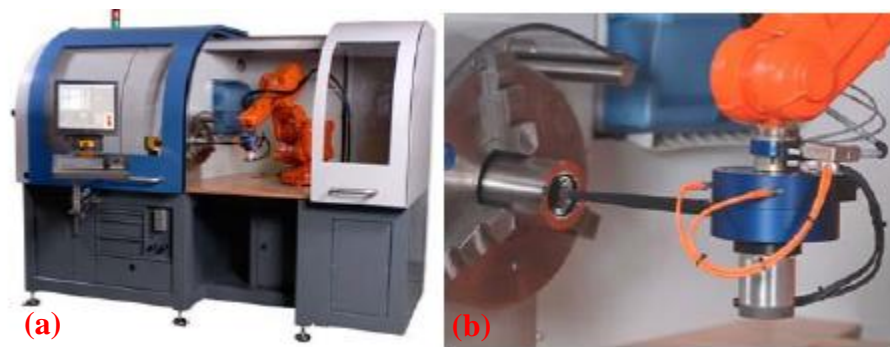


Figure 8. (a) STRECON® RAP-225 MACHINE for polishing tools, machine components and other similar applications with 2D rotation-symmetric geometry as well as simplified 3D geometries; (b) close-up of the vibration polishing module (right) (Pilný & Bissacco, 2015)

The RAP machine is used for performing automatic polishing operations of 3-dimensional components. The polishing tool, controlled by the robot arm, is normally moved in three different ways:

- High frequency reciprocating linear motion (where the tool “vibrates” on the surface).
- Continuous rotation, where a round spherical tool is rotating while in contact with the surface area to be polished (rotationally driven tool).
- Low frequency/low speed motion of the tool over the polished surface following a general tool path.

The workpiece motion, with defined peripheral speed, is present only in the case of rotational symmetric workpieces while the polishing tool is moved according to one of the ways described above. STRECON’s contribution consists of the following basic phases:

1. Execute polishing program
2. Visual assessment of the polishing operation by an expert and by using measurement equipment
3. Based upon the assessment either:
 - Continue with the current polishing step
 - Change to the next polishing step (finer abrasive)
 - Consider the part completed

Changing to a finer abrasive is a particularly critical step, since it involves cleaning of the part before starting to use a finer polishing abrasive material. Inaccurate or insufficient cleaning or contamination might result in leftover large abrasives resulting in the failure of the polishing process about to start.

Before the introduction of the RAP machine the polishing technology showed a very low level of automation. Due to the lack of feedback from sensors, the process requires multiple interactions of a skilled operator which evaluates the surface quality.

Determination of the right moment for tool change is an important step for obtaining the desired final result. The time consumed by a polishing job is largely dependent on the number of

polishing stages required, increasing greatly when the part requires multiple steps, as each polishing step requires accurate cleaning of the part surface and tool change. The process ranges from a few minutes for small non-complex parts to several hours for hardened parts that require a high surface finish such as less than Ra 0.01 μ m. Determination of the right moment of the tool change between is important and time consuming since requires proper cleaning for evaluation. If the tool is used for too short period, residual marks from the previous operation are not entirely removed and subsequent finer grains in the following polishing steps will not remove these marks. On the other hand, unnecessary long tool usage is no longer improving the surface roughness and moreover can lead to over polishing (deterioration) of the surface.

3.2.1 Experimental procedure and workpiece details

A robust method for the determination of the right moment for tool change has to be established by the process control. Recognition of the steady state in the polishing process when additional material removal would no longer improve the surface texture (roughness), resulting in an automatic process stop and/or change of tool to proceed to the next step of the polishing sequence would provide:

- Significant reduction in the cycle time of the polishing job
- Maintaining the specified geometrical tolerances (avoidance of an excessive material removal)

This will be based on monitoring of the progress in polishing process and critical process parameters, providing better repeatability, predictability and more consistent manufacturing with regards to form tolerance, surface roughness etc. It will also enable to cope with greater deviances of initial surface roughness resulting from preceding manufacturing operation in batches to be polished. As quite large deviations of identical parts in bathes has been experienced by STRECON (e.g. surface deterioration due to tool wear in turning).

Within IFaCOM, STRECON proposed to focus on the development of the RAP machine using the vibrating tool module (high frequency reciprocating linear motion of the polishing tool) when polishing rotationally symmetric parts. A simple turned cylindrical test piece of 40mm in diameter and 75 mm long split into 7 bands each of roughly 20 mm length has been used (Figure 9). The workpiece, called Unimax roll 1, is made of AISI 52100 alloy steel.



Figure 9. Initial test piece proposed by STRECON

3.3.2 Identification of possible vital parameters and sensor monitoring system implemented

In order to establish robust method for polishing process end-point detection (i.e. determination of the right moment for tool and abrasive paste change), STRECON's sensor system selection has focused on monitoring the progress in polishing process by means of variation in VQCs (roughness of the polished surface). The following parameters were identified as the "vital" parameters concerning the goal stated in the previous section:

- Surface roughness (its variation)
- Gloss of the surface

It is not necessary to precisely measure the polished surface roughness directly on the machine. Due to the precision required – Ra as low as 10 nm (normally between 40 and 10 nm) for plastic molds and coarse polishing environment (polishing paste, lubricant, loose particles from workpiece material and polishing tool), it would be expensive and impractical to implement sufficient measuring solution. Precise surface roughness measurement is preferable to perform outside of the RAP machine during the tool change, since the workpiece must be thoroughly cleaned before application of finer paste to proceed to subsequent polishing step. A cleaning process inside the RAP machine may be considered in order to save time of the process and reduce alignment problems when the workpiece is repositioned. The most effective and economic solution is to monitor the magnitude of variation in surface roughness over polishing time (number of polishing passes).

An optical instrument OS 500 from the company OptoSurf was used for on-line roughness and form measurement based on scattered light method. Light scattering is a surface measurement method for fast in line measurement of roughness, form and defects. The great advantage of the OS 500 is its insensitivity to vibration and water spray. Therefore the light scattering technique (Figure 10) is best suited to use in rough production environment where vibrations often cannot be avoided. Owing to the high data rates of 2000 data points/sec, a full 100% testing of components is possible.

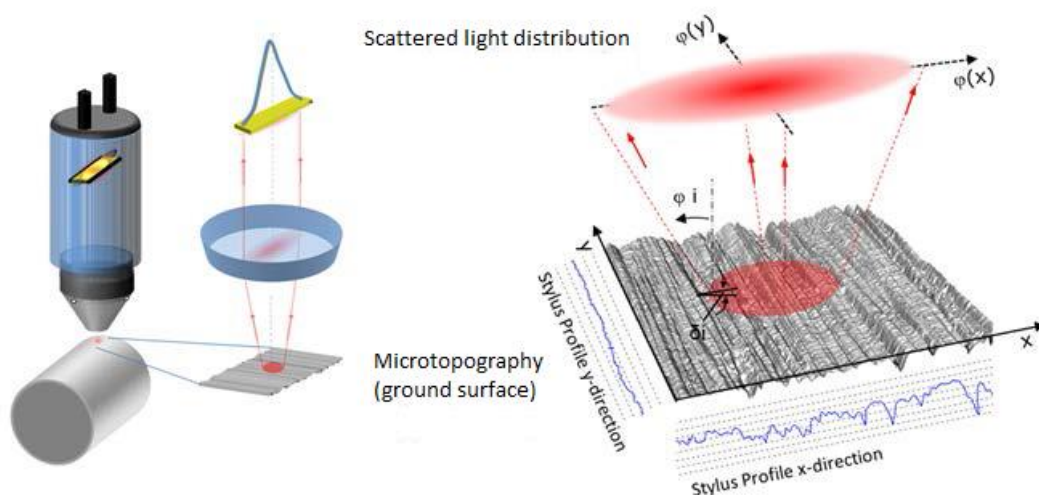


Figure 10. Measuring principle of Non-Contact Surface Metrology by means of Light Scattering

3.2.3 Sensor monitoring system

As regard the sensor monitoring system, a special sensorised arm for the RAP demonstrator including force, current and AE (acoustic emission) sensors has been developed.

The sensors are mounted on the machine as shown in Figure 11.

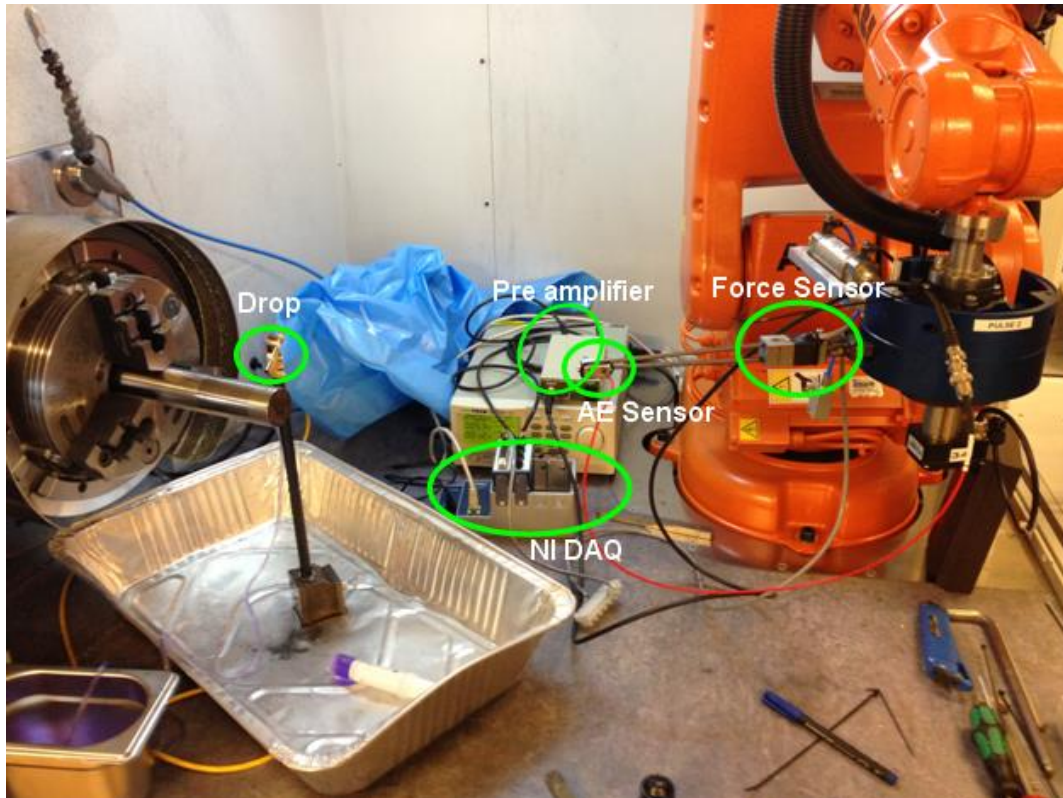




Figure 11. Sensors mounted on the RAP machine (IFaCOM deliverale 4.1)

The current sensor is in the electrical cabinet so it is not seen here. The drop system controls the amount of lubrication on the surface, and it is in turn controlled by the RAP software. The sensors are listed in the table below (Table 1).

Table 1. Sensors used in the monitoring of the process analysed

Sensor type	Sensor model	Picture
Acoustic Emission	Fuji Ceramics Corporation R-CAST M304A sensor + A1200 pre-amplifier	
Force sensor	Strain gauge sensor	
Voltage	Voltage sensor embedded in the electrical cabinet	N.A.

3.4 Experimental Test 1

During the Test1, 5 repetitions (5 workpiece, WP) of a stone polishing experiment with in-process monitoring has been carried out using the sensors described above which extract the following sensor signals: 3D forces (F_x – oscillation direction, F_y – tangential, F_z – Normal contact force), Acoustic Emission (AE) and Current.

Both in-line scattered light measurements of surface roughness (A_q) and reference areal topography measurements (S_a , S_z) have been collected.

The experiment presents one polishing step performed on fine turned surfaces, approx. $S_a = 0.3 \mu\text{m}$, $S_z = 2.5 \mu\text{m}$, using silicon carbide bonded abrasive of #800 grit size (412-1801). The process has been performed in 6 steps (on 6 bands or surfaces) with 5 repetitions, resulting in 5 workpieces polished. During the polishing of workpiece 4 (WP4) an error occurred in the detection and acquisition of the sensor signals, thus leading to the elimination of the polishing repetition of Test 1 carried out on WP4.

Process parameters used during the test are:

- Contact force: approx. 9 N;
- Oscillation: 1000 pulses/min;
- Stroke length: 1mm;
- Spindle speed: 200rpm;
- Feed rate: 1 mm/s;
- 1 pass = 17 mm;
- Sampling rate (for current and force sensor) = 2kHz;
- Sampling rate (for AE) = 1MHz.

Table 2 summarizes the number of passes for each band.

Table 2. Number of passes for each band

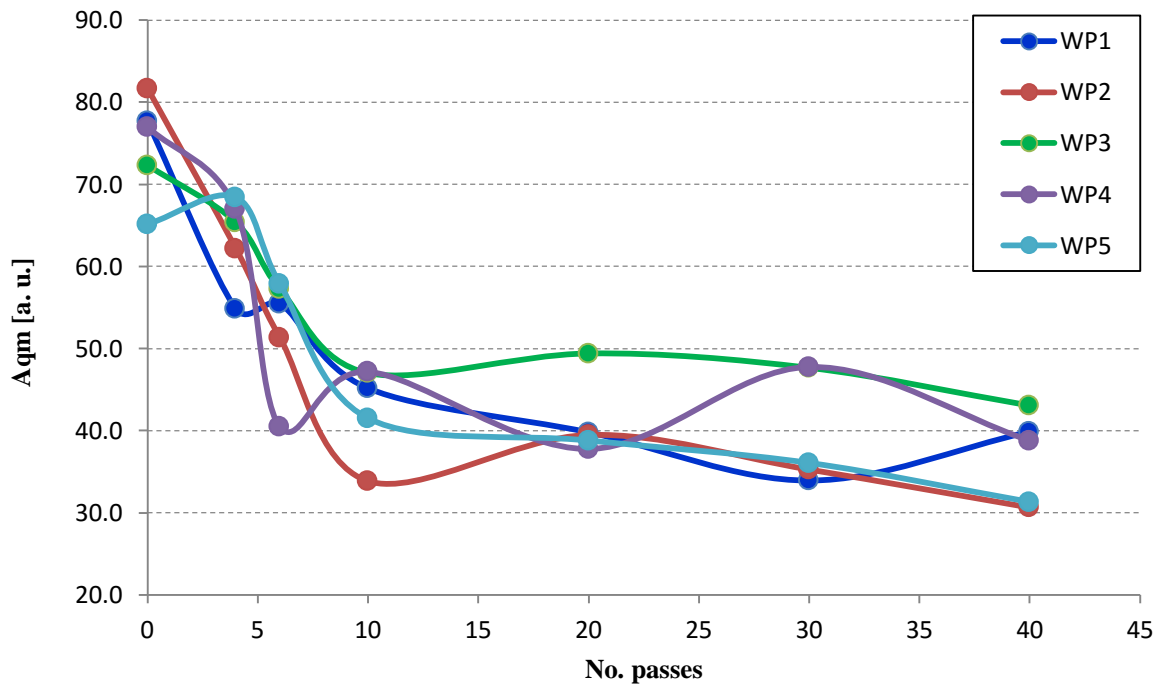
Band	initial (ini.)	1	2	3	4	5	6
No. passes	0	4	6	10	20	30	40

As regard measurements of surface roughness (A_q), scattered light measurements were performed with 50% overlapping in X and Y direction, covering 10 mm of the polished area in the centre of a polished band, discarding border areas and resulting in 6138 measurements per band (surface).

Table 3 reports the values in arbitrary unit of A_{qm} and A_{qs} measured for each workpiece in each band. Furthermore in Figure 12 the A_{qm} values are plotted versus pass number.

Table 3. Number of passes for each band and surface roughness values (Aqm and Aqs)_Test1

Band	No. passes	WP1		WP2		WP3		WP4		WP5	
		Aqm [A. u]	Aqs [A. u]	Aqm [A. u]	Aqs [A. u]	Aqm [A. u]	Aqs [A. u]	Aqm [A. u]	Aqs [A. u]	Aqm [A. u]	Aqs [A. u]
initial	0	77.6	7.6	81.7	6.1	72.3	6.1	77.0	1.5	65.1	6.8
B1	4	54.9	3.7	62.2	5.5	65.4	5.5	67.0	5.4	68.4	4.9
B2	6	55.5	4.1	51.3	4.6	57.3	4.6	40.5	2.6	57.9	4.5
B3	10	45.2	5.4	33.8	4.6	47.0	4.6	47.2	2.7	41.5	3.6
B4	20	39.8	4.4	39.5	6.6	49.4	6.6	37.8	4.6	38.8	5.3
B5	30	33.9	4.0	35.3	5.7	47.6	5.7	47.8	5.9	36.1	5.1
B6	40	39.9	5.5	30.6	6.6	43.1	6.6	38.8	6.4	31.3	5.0

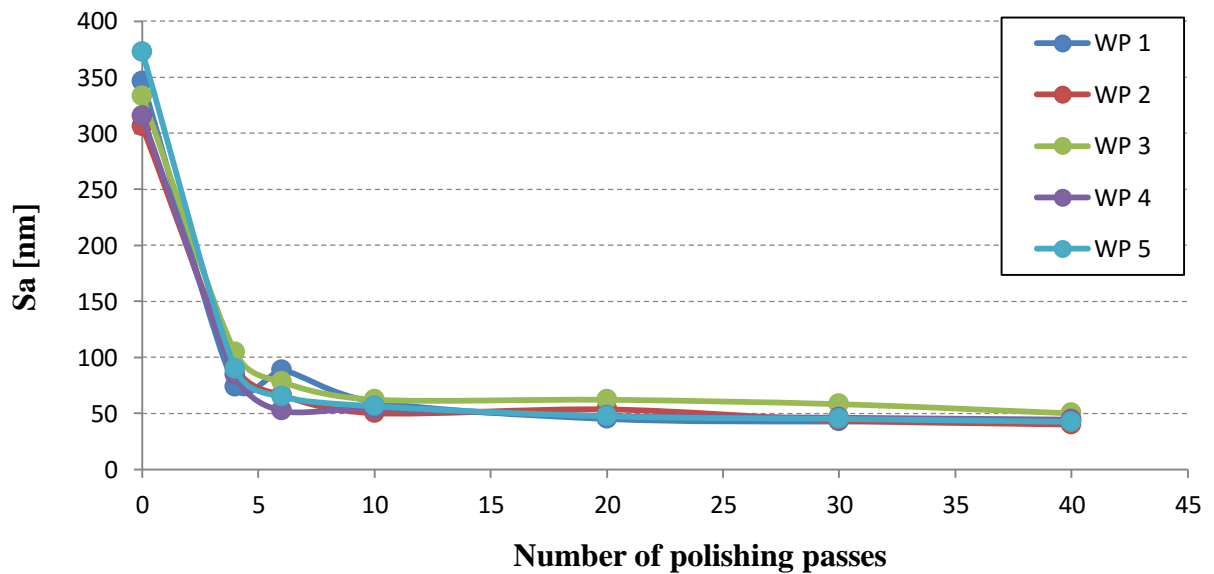
**Figure 12. Aqm roughness values versus number of passes_Test1**

Regarding the surface area measurements (Sa, Sz), they were performed using an optical confocal microscope. The data files were filtered using 2nd polynomial for removal of form (cylindrical WP). No additional filtering has been applied.

Table 4 reports the values in arbitrary unit of Sa and Sz measured for each workpiece in each band. Furthermore in Figure 13 the Sa and Sz values are plotted versus pass number.

Table 4. Number of passes for each band and surface roughness values (Sa and Sz)_Test1

	Meas. No.	Sa [nm]							Sz [nm]						
		ini.	B1	B2	B3	B4	B5	B6	ini.	B1	B2	B3	B4	B5	B6
WP 1	1	370	68	83	62	38	41	45	2931	1533	1312	3100	1812	1541	956
	2	345	64	67	62	44	45	42	2998	1400	1098	2174	443	712	512
	3	326	74	63	73	43	41	43	2677	1487	910	1514	794	451	1399
	4	379	86	121	46	51	40	41	2902	1441	1984	876	792	449	626
	5	312	77	109	58	51	47	48	2487	1874	1836	799	909	610	815
	AVG	346	74	88	60	45	43	44	2799	1547	1428	1692	950	753	862
s	29	9	26	10	6	3	3	212	189	465	963	513	455	346	
WP 2	1	374	129	57	51	48	47	42	2662	1974	938	759	920	863	558
	2	284	75	79	63	49	45	42	2510	1274	1270	1266	1201	469	489
	3	351	77	67	47	49	45	41	3554	1103	1211	835	691	607	473
	4	265	96	64	54	80	39	39	2370	1410	1142	815	1442	598	474
	5	257	85	65	36	42	43	35	2180	1438	1143	591	684	633	470
	AVG	306	92	66	50	54	44	40	2655	1440	1141	853	988	634	493
s	53	22	8	10	15	3	3	533	327	125	250	330	143	37	
WP 3	1	346	143	91	78	89	63	70	2142	1373	1212	1709	1217	922	1588
	2	396	68	105	67	55	59	56	2597	1349	2003	917	1707	934	2358
	3	348	80	75	59	65	73	44	2203	1217	1343	1091	1038	991	1105
	4	250	63	70	55	55	47	37	2325	1558	1592	1150	840	845	546
	5	326	168	50	52	48	49	44	1916	1636	1189	882	687	998	763
	AVG	333	104	78	62	62	58	50	2236	1427	1468	1150	1098	938	1272
s	53	48	21	10	16	11	13	250	169	339	332	395	62	723	
WP 5	1	365	108	61	55	50	39	44	2384	1890	940	1050	744	488	784
	2	414	89	70	52	51	45	32	2686	1124	1054	788	561	622	860
	3	312	96	66	61	61	58	66	2431	1391	1451	862	1530	989	797
	4	381	74	68	69	40	46	36	2309	1183	1273	955	720	655	654
	5	391	82	60	45	34	38	34	2724	1245	1256	663	483	1020	617
	AVG	373	90	65	56	47	45	43	2507	1367	1195	864	808	755	742
s	38	13	4	9	11	8	14	187	309	200	149	418	237	102	



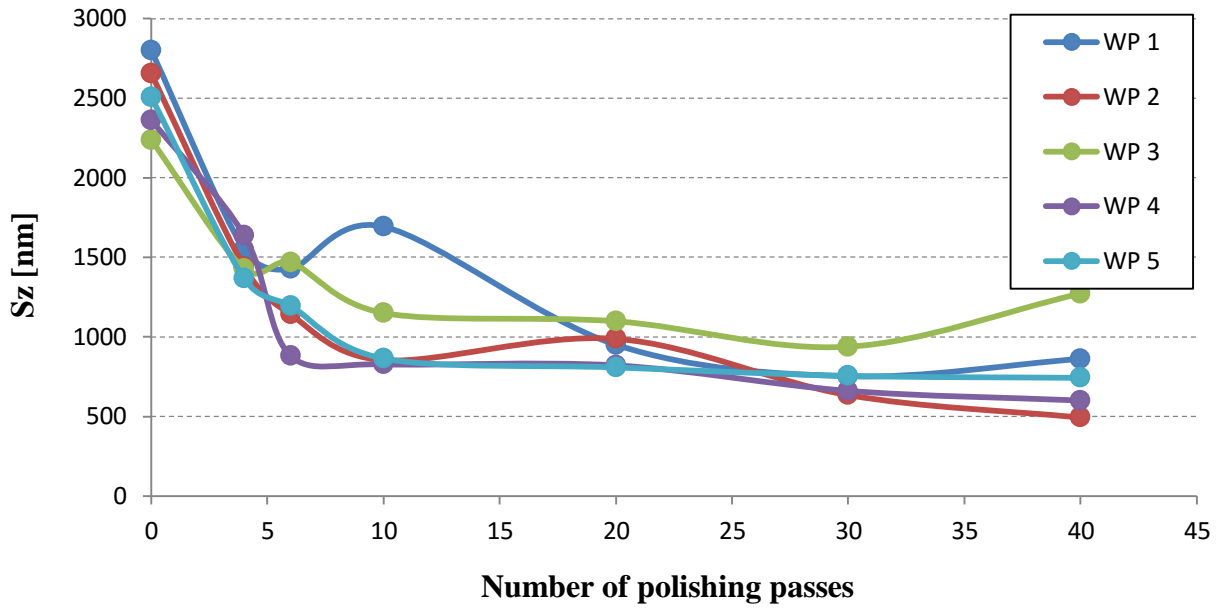


Figure 13. S_a and S_z roughness values versus number of passes_Test1

3.4.1 Features Extraction and selection for experimental Test1

To find correlations between sensorial data and surface roughness values, advanced signal processing, based on signal conditioning, feature extraction and data fusion, was applied to the multiple sensor signals acquired through the monitoring system.

Signal analysis in the time domain was performed to extract a number of conventional statistical features from each dataset. The following statistical features were extracted (Binsaeid, Asfour, Cho, & Onar, 2009; Teti, Jemielniak, & O'Donnell, 2010): mean average, variance, skewness, kurtosis and energy.

The results of the sensor signal conventional statistical feature extraction are reported for each of the workpieces that provided usable sensorial data: WP1, WP2, WP3, WP5. It is worth noting that during the polishing of WP4 an error occurred in the detection and acquisition of the sensor signals, thus leading to the elimination of the polishing repetition of Test 1 carried out on WP4.

The extracted sensor signal conventional statistical features are plotted versus pass number (or file number in the case of AE signals) for each valid workpiece together with the measured surface roughness S_a values. After the feature extraction phase, in order to perform the feature selection step, the plots of all the sensor signal conventional statistical features were examined in order to identify possible trends useful for correlation with the measured surface roughness.

The results of the trend classification are summarised in Table 5. As can be seen from the table, the following sensor signal conventional statistical features (with ** in Table 5) appear to display promising capabilities for the identification of correlations with surface roughness through the development of cognitive pattern recognition tools: $AE_{raw}Var$, $AE_{raw}Ene$, $AE_{RMS}Ave$, $AE_{RMS}Var$, $AE_{RMS}Ene$, $CurrentAve$, F_xVar , F_xEne , F_yAve , F_yVar , F_ySke , F_yKur , F_yEne , F_zVar , F_zEne .

Table 5. Visual checking of significant signals features_Test 1

		TEST1					LEGEND	
		WP1	WP2	WP3	WP4	WP5		
AE _{raw}	Variance	**	**	**		**	**	Acceptable trend
	Skewness	-	-	-		-	*	Uncertain trend
	Kurtosis	*	-	-		-	-	No trend
	Energy	**	**	**		**	-	Not usable signals
AE _{RMS}	Average	**	**	**		**		
	Variance	**	**	**		**		
	Skewness	-	-	-		-		
	Kurtosis	-	-	-		-		
	Energy	**	**	**		**		
Current	Average	**	**	*		*		
	Variance	*	-	-		*		
	Skewness	*	-	-		*		
	Kurtosis	*	-	-		*		
	Energy	-	-	*		*		
F _x	Average	-	-	-		-		
	Variance	**	**	**		**		
	Skewness	-	*	*		*		
	Kurtosis	*	*	*		*		
	Energy	**	**	**		**		
F _y	Average	**	**	**		**		
	Variance	*	**	**		**		
	Skewness	*	**	**		*		
	Kurtosis	*	**	**		*		
	Energy	-	**	**		**		
F _z	Average	-	-	*		**		
	Variance	**	**	**		*		
	Skewness	-	-	-		-		
	Kurtosis	*	*	*		**		
	Energy	*	**	**		**		

On the basis of the above selected features, two types of sensor fusion pattern vectors were constructed including the promising features from the different sensor signals but excluding the simultaneous presence of AE_{raw} and AE_{RMS} features to avoid redundancy.

The first sensor fusion pattern feature vector contains signal features of AE_{raw}, Current, F_x, F_y, F_z:

[AE_{raw}Var, AE_{raw}Ene, CurrentAve, F_xVar, F_xEne, F_yAve, F_yVar, F_ySke, F_yKur, F_yEne, F_zVar, F_zEne]

The second sensor fusion pattern feature vector contains the signal features of AE_{RMS}, Current, F_x, F_y, F_z:

[AE_{RMS}Ave, AE_{RMS}Var, AE_{RMS}Ene, CurrentAve, F_xVar, F_xEne, F_yAve, F_yVar, F_ySke, F_yKur, F_yEne, F_zVar, F_zEne]

The above sensor fusion pattern feature vectors can be alternatively utilized as input to neural network classification paradigms in order to obtain in output the acceptability assessment of the surface roughness of the polished part as described in the next paragraph.

3.4.2 Neural Network Pattern Recognition for Surface Roughness Identification

Based on the trend classification of the conventional statistical features extracted from the force, current and AE sensor signals triplet, a feature selection procedure was carried out in order to construct sensor fusion pattern feature vectors to be utilised as inputs to neural network (NN) based pattern recognition paradigms for the identification of surface roughness.

For each of the four polished workpieces (WP1, WP2, WP3, WP5) of the valid sensor monitoring signal detection of the Test 1 series, two NN training sets were built with input pattern feature vectors constructed by sensor data fusion of selected features from the sensor signals triplet: besides selected features from force and current signals, the input pattern feature vectors of NN training set 1 contain selected features from AE_{raw} signals, while the input pattern feature vectors of NN training set 2 comprise selected features from AERMS signals.

The input pattern feature vectors of NN training set 1 are as follows:

[$AE_{raw}Var$, $AE_{raw}Ene$, CurrentAve, F_xVar , F_xEne , F_yAve , F_yVar , F_ySke , F_yKur , F_yEne , F_zVar , F_zEne].

The input pattern feature vectors of NN training set 2 are as follows:

[$AE_{RMS}Ave$, $AE_{RMS}Var$, $AE_{RMS}Ene$, CurrentAve, F_xVar , F_xEne , F_yAve , F_yVar , F_ySke , F_yKur , F_yEne , F_zVar , F_zEne].

Each NN training set consists of 40 input pattern feature vectors, i.e. one input pattern feature vector per polishing pass, and each of these input pattern feature vectors is associated with the interpolated value of surface roughness for the corresponding polishing pass.

Reference areal topography measurements were performed using a confocal microscope. The data files were filtered using a 2nd polynomial to remove the cylindrical form of the WPs; no additional filtering was applied.

For each WP, 7 surface roughness average values, each based on five roughness measurements, were obtained with reference to the following 7 steps of the full polishing process: (1) before polishing; (2) after 4 polishing passes; (3) after 6 polishing passes; (4) after 10 polishing passes; (5) after 20 polishing passes; (6) after 30 polishing passes; (7) after completing the 40 polishing passes.

The surface roughness average measurement values were used to obtain, via power function fitting, surface roughness interpolation curves made of 40 data points associated to each of the 40 polishing passes (Figure 14).

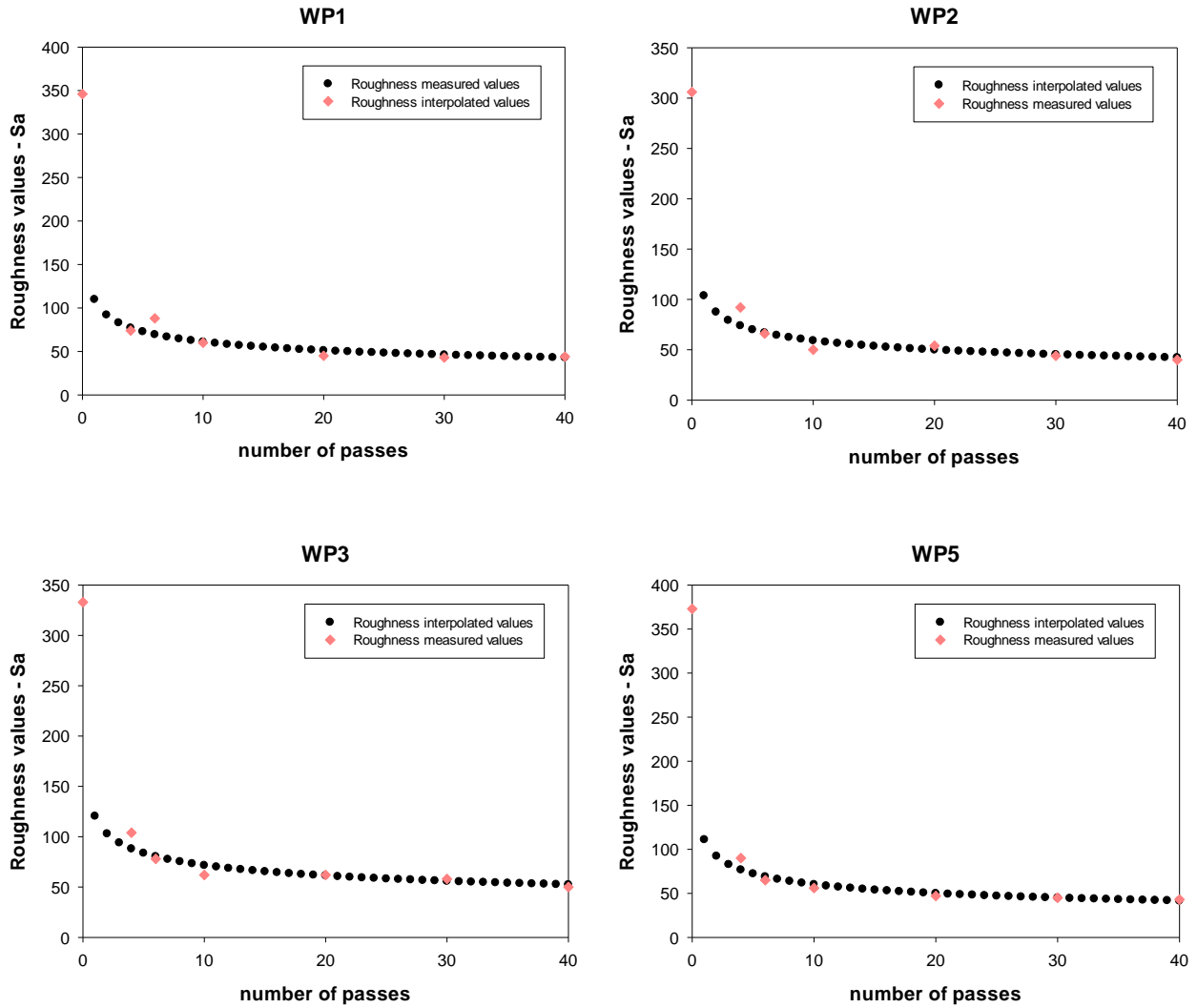


Figure 14. Surface roughness average measurement values and surface roughness interpolation curves for polished workpieces WP1, WP2, WP3, WP5

To perform NN learning, the input pattern feature vectors associated with the corresponding surface roughness interpolation values for each WP were fed to NN paradigms. For NN training set 1, containing input pattern vectors with AE_{raw} features, two NN configurations were used: 12-12-1 and 12-24-1, where 12 is the number of input nodes, equal to the number of features in the input pattern vector; 12 or 24 is the number hidden nodes, related to the number of input nodes; and 1 is the output node, yielding the NN predicted surface roughness value per polishing pass. For NN training set 2, comprising input pattern vectors with AE_{RMS} features, two NN configurations were used: 13-13-1 and 13-26-1, where 13 is the number of input nodes, equal to the number of features in the input pattern vector; 13 or 26 is the number hidden nodes, related to the number of input nodes; and 1 is the output node, yielding the NN predicted surface roughness value per polishing pass. The employed NN learning procedure was the leave-k-out method where k cases from the training set are put aside in turn, while the other cases are used for NN training. Once the NN training phase is completed, the k cases previously put aside are utilised as inputs to the trained NN for the testing phase. This NN learning procedure is particularly useful when the available training set is limited in size.

3.4.2.1 Discussion of results for NN training set 1

In the case of NN training set 1, for each WP and polishing pass the desired surface roughness interpolation value and the NN predicted surface roughness values obtained using the diverse NN configurations are summarised in Table 6. Figure 15 reports, for each WP, the plots of the 7 surface roughness average measurement values, the desired surface roughness interpolation values and the NN predicted surface roughness value obtained from the two NN configurations.

Table 6. NN training set 1: desired surface roughness interpolation values and NN predicted surface roughness values, obtained with the 12-12-1 and 12-24-1 NN configurations, for each WP and polishing pass

Pass #	WP1 surface roughness interpolation values	WP1 NN predicted surface roughness values		WP2 surface roughness interpolation values	WP2 NN predicted surface roughness values		WP3 surface roughness interpolation values	WP3 NN predicted surface roughness values		WP5 surface roughness interpolation values	WP5 NN predicted surface roughness values	
		12-12-1	12-24-1		12-12-1	12-24-1		12-12-1	12-24-1		12-12-1	12-24-1
1	109.78	102.85	201.24	103.53	139.38	12.20	120.35	168.71	528.69	110.91	95.46	131.41
2	91.93	92.43	83.75	87.42	80.86	81.51	102.90	86.77	78.60	92.17	92.45	95.01
3	82.87	85.37	93.71	79.19	73.54	86.50	93.89	95.25	301.08	82.71	82.24	81.57
4	76.98	74.63	61.21	73.82	81.37	78.53	87.98	85.08	85.92	76.60	82.70	79.09
5	72.71	71.47	73.87	69.91	68.96	67.25	83.65	84.19	82.72	72.17	65.98	67.60
6	69.39	69.07	69.38	66.86	65.09	63.79	80.28	79.90	80.12	68.74	63.54	60.23
7	66.71	61.88	68.03	64.40	65.13	62.55	77.53	72.29	75.37	65.97	70.82	70.46
8	64.47	64.57	63.61	62.33	66.09	65.27	75.22	79.34	79.79	63.66	65.84	65.60
9	62.55	61.09	61.12	60.57	60.57	59.88	73.25	72.35	73.78	61.69	62.51	62.97
10	60.89	62.23	62.44	59.03	58.25	60.00	71.52	67.24	71.39	59.98	58.35	58.23
11	59.42	59.89	61.89	57.67	59.19	58.12	70.00	69.31	68.01	58.47	59.53	57.10
12	58.11	56.70	55.12	56.46	57.16	56.46	68.64	69.58	67.86	57.13	57.54	58.70
13	56.93	56.00	54.85	55.37	53.42	53.15	67.41	64.46	63.56	55.92	52.85	52.19
14	55.86	58.09	56.38	54.38	52.58	52.29	66.29	68.56	66.55	54.82	55.95	56.83
15	54.88	57.87	54.36	53.47	53.00	52.96	65.26	69.52	69.17	53.82	56.32	52.55
16	53.98	59.43	59.93	52.63	52.47	54.38	64.32	66.60	68.29	52.90	54.75	53.61
17	53.15	52.66	53.45	51.86	52.79	55.49	63.44	64.79	63.93	52.05	51.77	52.95
18	52.38	47.09	49.32	51.14	51.46	52.06	62.63	61.98	63.11	51.26	53.98	53.60
19	51.66	50.93	49.53	50.47	50.04	50.74	61.87	61.91	59.83	50.53	51.35	52.00
20	50.99	52.23	52.43	49.84	49.70	49.71	61.15	61.54	61.72	49.84	47.56	50.48
21	50.35	50.81	50.07	49.25	49.87	49.92	60.48	57.27	55.61	49.20	45.53	42.63
22	49.76	51.14	49.68	48.70	48.74	49.48	59.85	56.87	58.10	48.59	52.54	51.13
23	49.19	48.95	48.30	48.17	48.37	48.44	59.25	56.60	56.82	48.02	51.53	50.51
24	48.66	46.75	48.96	47.68	46.68	45.20	58.68	58.08	57.20	47.47	47.15	47.22
25	48.16	47.50	46.60	47.20	48.70	48.86	58.14	59.14	58.29	46.96	44.95	43.89
26	47.67	49.24	48.19	46.75	44.92	46.98	57.63	60.91	60.32	46.47	44.03	-68.58
27	47.22	44.08	43.99	46.32	45.38	45.13	57.14	57.94	58.88	46.00	44.86	45.64
28	46.78	47.13	48.18	45.92	43.60	44.23	56.67	58.13	57.78	45.56	46.56	45.20
29	46.36	44.96	45.20	45.52	45.18	45.47	56.23	53.06	55.33	45.13	45.15	43.11
30	45.96	48.23	45.16	45.15	44.35	45.00	55.80	56.16	55.73	44.73	46.55	45.35
31	45.58	44.83	45.45	44.79	46.28	45.13	55.39	54.37	56.27	44.34	45.14	43.14
32	45.21	44.66	46.61	44.44	46.05	46.72	54.99	55.99	56.98	43.96	45.56	44.75
33	44.85	48.03	48.16	44.11	46.06	45.84	54.61	54.01	55.19	43.60	41.95	43.67
34	44.51	45.23	42.55	43.79	44.79	43.87	54.24	54.50	55.01	43.26	44.39	44.46
35	44.18	43.82	43.31	43.48	43.96	45.43	53.89	53.86	54.57	42.92	42.02	41.99
36	43.86	44.73	44.91	43.18	42.78	42.20	53.55	52.27	50.53	42.60	40.69	41.17
37	43.56	44.80	46.32	42.90	43.76	42.50	53.21	52.21	51.17	42.29	45.77	45.60
38	43.26	43.21	44.14	42.62	42.23	41.98	52.90	53.12	53.06	41.99	42.28	42.40
39	42.97	44.44	43.35	42.35	46.58	42.37	52.59	52.41	53.32	41.70	43.62	42.71
40	42.70	29.34	36.80	42.09	16.30	69.56	52.29	59.40	79.90	41.42	40.43	48.48

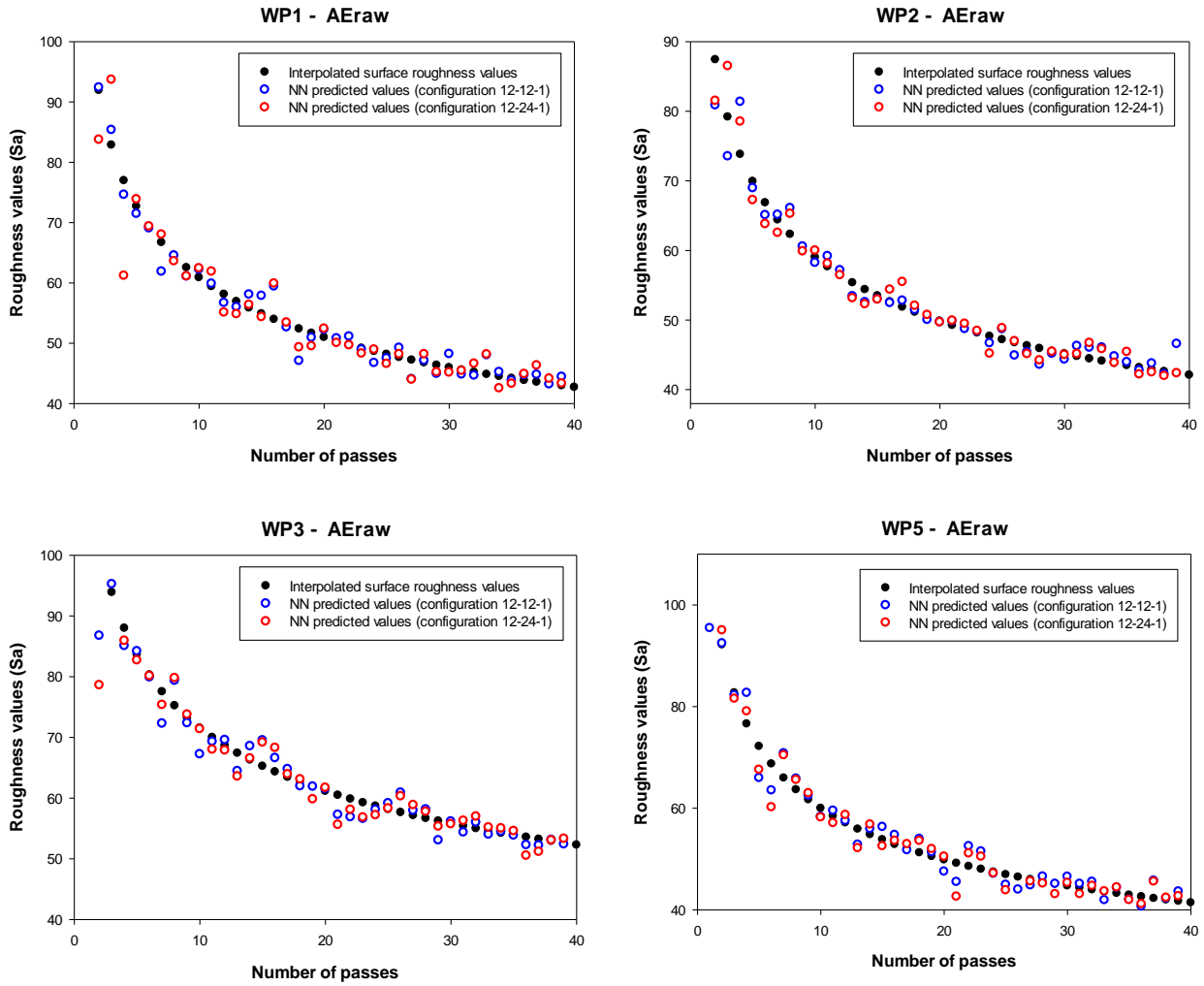


Figure 15. NN training set 1: WP1, WP2, WP3, WP5 plots of the 7 average surface roughness values, the desired surface roughness interpolation values and the NN predicted surface roughness values obtained using the 12-12-1 and 12-24-1 NN configurations

3.4.2.2 Discussion of results for NN training set 2

In the case of NN training set 2, for each WP and polishing pass the desired surface roughness interpolation value and the NN predicted surface roughness values obtained using the diverse NN configurations are summarised in Table 7. Figure 16 reports, for each WP, the plots of the 7 surface roughness average measurement values, the desired surface roughness interpolation values and the NN predicted surface roughness value obtained from the two NN configurations.

Table 7. NN training set 2: desired surface roughness interpolation values and NN predicted surface roughness values, obtained with the 13-13-1 and 13-26-1 NN configurations, for each WP and polishing pass

Pass #	WP1 surface roughness interpolation values	WP1 NN predicted surface roughness values		WP2 surface roughness interpolation values	WP2 NN predicted surface roughness values		WP3 surface roughness interpolation values	WP3 NN predicted surface roughness values		WP5 surface roughness interpolation values	WP5 NN predicted surface roughness values	
		13-13-1	13-26-1		13-13-1	13-26-1		13-13-1	13-26-1		13-13-1	13-26-1
1	109.78	70.63	22.58	103.53	432.12	337.37	120.35	254.80	405.00	110.91	186.20	114.34
2	91.93	92.22	83.31	87.42	93.82	94.16	102.90	90.42	86.08	92.17	127.10	84.32
3	82.87	92.42	90.30	79.19	74.90	73.46	93.89	101.63	105.06	82.71	87.36	87.14
4	76.98	75.08	72.67	73.82	79.58	79.06	87.98	85.61	87.40	76.60	70.99	76.39
5	72.71	71.79	71.19	69.91	70.00	67.71	83.65	82.76	83.73	72.17	66.16	67.43
6	69.39	70.10	65.80	66.86	65.99	66.56	80.28	80.17	81.77	68.74	61.45	20.57
7	66.71	65.37	65.85	64.40	63.65	64.17	77.53	74.27	74.66	65.97	67.72	69.37
8	64.47	65.63	64.00	62.33	65.09	66.86	75.22	80.30	80.48	63.66	67.06	69.33
9	62.55	63.13	60.71	60.57	56.38	57.86	73.25	75.63	74.74	61.69	63.96	63.36
10	60.89	62.46	63.16	59.03	59.32	59.00	71.52	68.60	70.59	59.98	62.32	61.39
11	59.42	58.16	61.14	57.67	60.60	59.38	70.00	67.88	67.93	58.47	55.14	55.28
12	58.11	57.58	56.65	56.46	55.57	58.01	68.64	67.14	66.53	57.13	55.93	58.43
13	56.93	54.15	57.56	55.37	51.56	52.14	67.41	64.22	64.43	55.92	53.04	51.28
14	55.86	57.53	58.68	54.38	53.62	54.04	66.29	66.38	67.27	54.82	53.80	53.72
15	54.88	58.51	57.64	53.47	54.46	52.60	65.26	66.14	66.45	53.82	87.99	54.66
16	53.98	57.94	56.46	52.63	53.74	54.32	64.32	65.42	66.12	52.90	56.77	55.12
17	53.15	51.90	53.11	51.86	51.85	51.84	63.44	64.58	61.70	52.05	51.54	51.44
18	52.38	49.83	49.74	51.14	51.96	52.02	62.63	65.26	64.08	51.26	52.23	51.94
19	51.66	52.32	50.72	50.47	50.42	49.74	61.87	60.67	59.87	50.53	50.88	49.98
20	50.99	52.08	52.54	49.84	49.44	49.58	61.15	63.20	61.89	49.84	49.70	49.69
21	50.35	50.31	50.51	49.25	49.25	49.67	60.48	55.34	56.12	49.20	46.80	44.26
22	49.76	49.92	49.10	48.70	47.97	48.16	59.85	57.64	58.36	48.59	51.38	53.03
23	49.19	49.90	-5.04	48.17	48.02	47.70	59.25	58.34	57.16	48.02	51.72	51.23
24	48.66	47.16	47.50	47.68	43.69	45.42	58.68	55.77	56.15	47.47	47.19	45.13
25	48.16	47.63	46.40	47.20	49.18	49.26	58.14	59.98	58.85	46.96	43.62	45.99
26	47.67	49.51	50.69	46.75	50.11	48.18	57.63	61.31	60.41	46.47	39.88	41.96
27	47.22	44.52	43.18	46.32	44.96	44.59	57.14	58.01	56.78	46.00	45.95	45.47
28	46.78	48.46	48.46	45.92	44.58	44.55	56.67	58.80	58.35	45.56	47.14	43.96
29	46.36	45.79	45.95	45.52	44.73	45.60	56.23	54.92	54.06	45.13	44.02	42.22
30	45.96	45.61	45.89	45.15	44.25	44.52	55.80	55.81	56.76	44.73	44.96	45.03
31	45.58	43.73	44.69	44.79	45.50	45.95	55.39	54.08	53.57	44.34	45.71	44.53
32	45.21	45.53	45.69	44.44	46.29	45.54	54.99	55.35	55.28	43.96	44.29	44.38
33	44.85	47.98	46.04	44.11	45.12	45.96	54.61	55.61	54.77	43.60	43.80	42.90
34	44.51	43.16	43.45	43.79	43.68	44.63	54.24	55.55	55.38	43.26	44.01	44.25
35	44.18	44.46	45.06	43.48	44.65	45.11	53.89	54.21	54.66	42.92	43.29	42.25
36	43.86	44.51	45.59	43.18	42.55	42.70	53.55	53.37	53.40	42.60	41.58	41.34
37	43.56	45.95	46.93	42.90	43.22	43.55	53.21	55.21	53.85	42.29	42.98	43.42
38	43.26	42.71	43.21	42.62	41.82	42.18	52.90	53.75	51.87	41.99	42.49	42.00
39	42.97	45.14	45.52	42.35	43.14	43.64	52.59	52.42	53.29	41.70	38.43	44.23
40	42.70	30.92	79.80	42.09	43.89	66.02	52.29	187.30	38.90	41.42	40.37	48.44

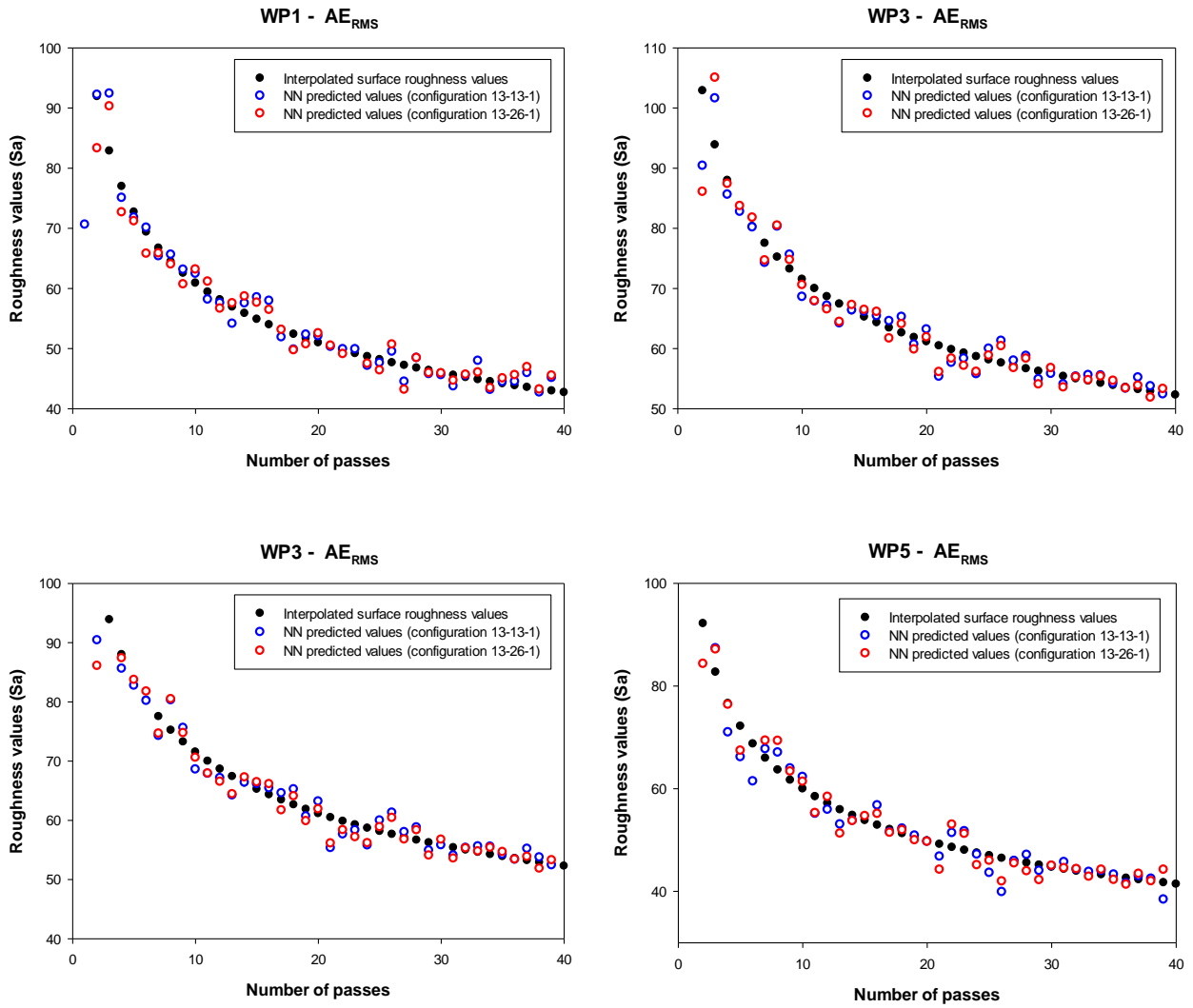


Figure 16. NN training set 2: WP1, WP2, WP3, WP5 plots of the 7 average surface roughness values, the desired surface roughness interpolation values and the NN predicted surface roughness values obtained using the 13-13-1 and 13-26-1 NN configurations

The overall performances of the NNs have been computed in terms of MAPE (Mean Absolute Percentage Error), i.e. the absolute differences between target values (y) and NN predicted values (\hat{y}_t) divided by the actual value:

$$MAPE = \frac{1}{n} \sum_{t=1}^n \left| \frac{y_t - \hat{y}_t}{y_t} \right|$$

The following table (Table 8) summarizes the NN results in terms of MAPE.

Table 8. NN results for training set 1 and training set 2 in terms of MAPE_Test1

	Training Set 1		Training Set 2	
	12-12-1	12-24-1	13-13-1	13-26-1
WP1	0.0366	0.0597	0.0431	0.1006
WP2	0.0495	0.0639	0.1065	0.0966
WP3	0.0407	0.1818	0.1217	0.0946
WP5	0.0401	0.1041	0.0780	0.0576

For all the workpiece polished, the overall NN best performances were obtained using the training set 1 with AE_{raw} signals. The training set 1 is composed by AE_{raw} signals, 12 input nodes, 12 hidden nodes and 1 output node.

The lowest MAPE value has been obtained for the WP1 (using the training set 1 and 12 hidden nodes) and it is equal to 0.0366, which means a prediction error of 3.66%. Instead, in the worst case scenario (WP3, using the training set 1 and 24 hidden node), the MAPE is equal to 0.1818 (prediction error of 18.18%).

3.5 Experimental Test 2

During the Test2, 5 repetitions of a (stone) polishing experiment with in-process monitoring has been carried out using the following sensors: 3D forces (F_x – oscillation direction, F_y – tangential, F_z – Normal contact force), Acoustic Emission (AE) and Current.

Both in-line scattered light measurements of surface roughness (A_q) and reference areal topography measurements (S_a , S_z) have been collected.

The experiment presents one polishing step using 9 μm diamond gel joke MAGIC and a plastic carrier made of PMMA. Initial surfaces were pre-polished to approx. $S_a = 0.1 \mu\text{m}$, $S_z = 1.1 \mu\text{m}$ using silicon carbide bonded abrasive of #400 grit size (412-1401). The process has been performed in 6 steps (on 6 bands or surfaces) with 5 repetitions, resulting in 5 workpieces polished. Process parameters used during the test are:

- Contact force: approx.. 5 N;
- Oscillation: 1000 pulses/min;
- stroke length: 1 mm;
- Spindle speed: 200 rpm;
- Feed rate: 1 mm/s;
- 1 pass = 15 mm;
- Sampling rate (for current and force sensor) = 2kHz;
- Sampling rate (for AE) = 1MHz.

Table 9 summarizes the number of passes for each band.

Table 9. Number of passes for each band

Band	initial (ini.)	1	2	3	4	5	6
No. passes	0	6	9	15	30	45	60

As regard measurements of surface roughness (Aq), scattered light measurements were performed with 50% overlapping in X and Y direction, covering 10 mm of the polished area in the centre of a polished band, discarding border areas and resulting in 6138 measurements per band (surface).

Table 10 reports the values in arbitrary unit of Aqm and Aqs measured for each workpiece in each band. Furthermore in Figure 17 the Aqm values are plotted versus pass number.

Table 10. Number of passes for each band and surface roughness values (Aqm and Aqs)_Test2

Band	No. passes	WP1		WP2		WP3		WP4		WP5	
		Aqm [A. u]	Aqs [A. u]	Aqm [A. u]	Aqs [A. u]	Aqm [A. u]	Aqs [A. u]	Aqm [A. u]	Aqs [A. u]	Aqm [A. u]	Aqs [A. u]
ini	0	46.5	1.5	44.7	1.5	50.4	2.4	53.0	2.0	50.9	2.2
B1	6	22.8	1.9	37.4	2.0	32.0	4.5	39.5	2.4	42.9	2.4
B2	9	22.0	1.5	29.0	2.4	38.6	2.3	31.9	2.2	39.5	2.5
B3	15	26.1	2.4	30.1	4.1	22.8	2.9	39.2	1.7	35.6	2.9
B4	30	20.3	2.4	18.3	3.1	23.6	4.1	27.1	1.8	27.9	2.5
B5	45	22.3	2.3	12.3	3.9	19.4	3.6	28.0	2.0	16.4	2.0
B6	60	19.0	1.8	22.3	6.5	19.4	2.5	29.5	2.4	19.2	1.8

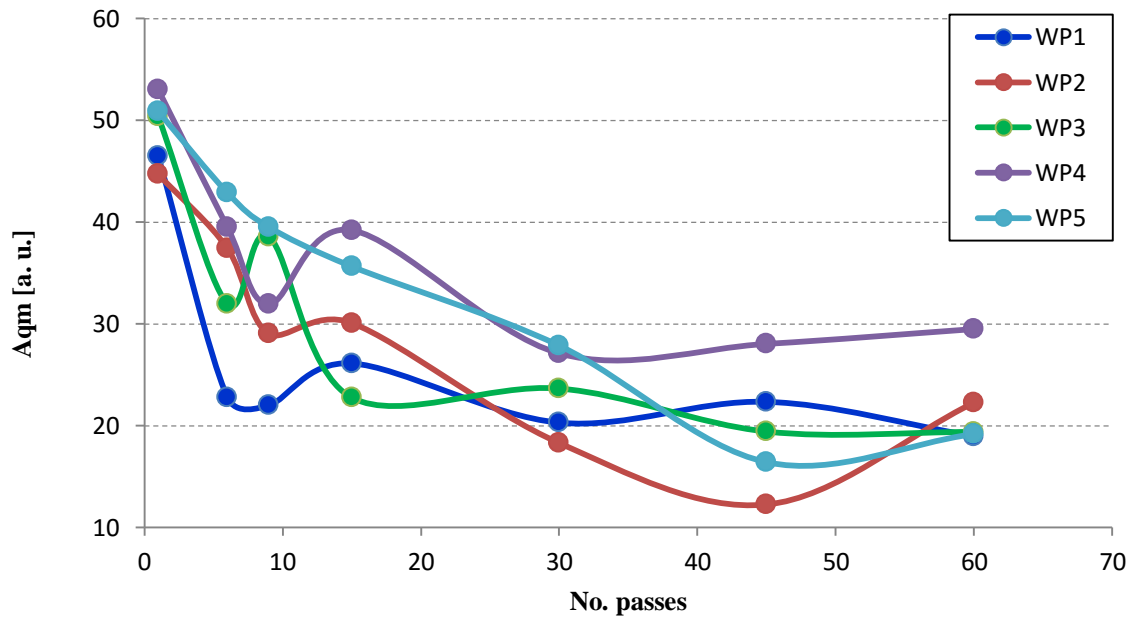


Figure 17. Aqm roughness values versus number of passes_Test2

In reference to areal topography measurements (Sa, Sz), Reference areal topography measurements were performed using an optical confocal microscope. The data files were filtered using 2nd polynomial for removal of form (cylindrical WP). No additional filtering has been applied.

Table 11 reports the values in arbitrary unit of Sa and Sz measured for each workpiece in each band. Furthermore in Figure 18 the Sa and Sz values are plotted versus pass number.

Table 11. Number of passes for each band and surface roughness values (Sa and Sz)_Test2

	Meas. No.	Sa [nm]							Sz [nm]						
		ini.	B1	B2	B3	B4	B5	B6	ini.	B1	B2	B3	B4	B5	B6
WP 1	1	87	62	60	79	63	58	77	1072	546	743	669	610	564	810
	2	95	61	61	66	55	64	76	1140	765	1380	656	664	662	935
	3	83	77	53	79	57	56	72	942	684	551	680	542	635	750
	4	98	41	49	67	60	58	66	1042	419	529	764	624	718	619
	5	101	83	64	82	61	57	70	1074	972	630	694	660	566	872
	AVG s	93 7.6	65 16.3	57 6.2	75 7.5	59 3.2	59 3.1	72 4.5	1054 72.1	677 211.3	767 353.0	693 42.3	620 49.3	629 65.7	797 121.2
WP 2	1	88	100	69	83	53	21	45	1078	792	599	999	596	344	543
	2	98	95	90	108	47	26	53	1111	877	776	1327	513	686	666
	3	99	96	62	85	50	29	54	1153	866	683	1052	538	394	594
	4	88	93	74	86	62	27	59	1121	883	684	892	585	306	644
	5	88	83	73	104	51	27	52	1001	749	773	1155	499	340	733
	AVG s	92 5.8	93 6.3	74 10.3	93 11.8	53 5.7	26 3.0	53 5.0	1093 57.9	833 59.7	703 73.8	1085 165.2	546 43.0	414 155.3	636 72.1
WP 3	1	106	84	93	70	65	38	60	1148	648	956	751	969	509	800
	2	107	69	95	66	73	42	66	1158	577	1066	737	797	665	653
	3	106	109	96	55	85	47	64	1115	1253	752	542	862	546	877
	4	96	95	106	69	82	50	53	1012	954	896	688	1176	554	647
	5	101	72	97	67	93	40	49	1217	847	837	666	962	539	495
	AVG s	103 4.7	86 16.6	97 5.0	65 6.0	80 10.9	43 5.0	58 7.2	1130 75.5	856 268.5	901 118.9	677 83.0	953 143.8	563 59.7	694 148.5
WP 4	1	113	85	105	98	62	65	77	1317	1082	1036	918	773	842	808
	2	110	102	71	96	73	70	82	1202	1015	738	996	1374	647	775
	3	116	97	102	102	70	80	71	1327	882	858	940	611	698	716
	4	112	82	102	118	66	78	73	1223	726	989	955	590	756	905
	5	103	86	116	104	60	75	69	1041	1031	984	888	548	786	703
	AVG s	111 4.9	90 8.6	99 16.8	104 8.6	66 5.4	74 6.1	74 5.2	1222 115.3	947 144.0	921 121.7	939 40.5	779 343.3	746 75.9	781 81.3
WP 5	1	101	133	124	98	103	58	48	1094	1312	1276	769	832	585	543
	2	116	87	119	97	85	43	55	1803	682	1125	763	1028	493	692
	3	105	116	116	99	75	43	45	1059	956	1010	733	902	527	491
	4	104	120	113	97	74	62	52	1095	943	1079	932	918	775	566
	5	102	120	114	96	79	60	48	1673	906	1063	849	797	733	601
	AVG s	106 6.0	115 17.0	117 4.4	97 1.1	83 11.9	53 9.4	50 3.9	1345 362.2	960 226.1	1111 101.2	809 81.0	895 89.2	623 125.3	579 74.9

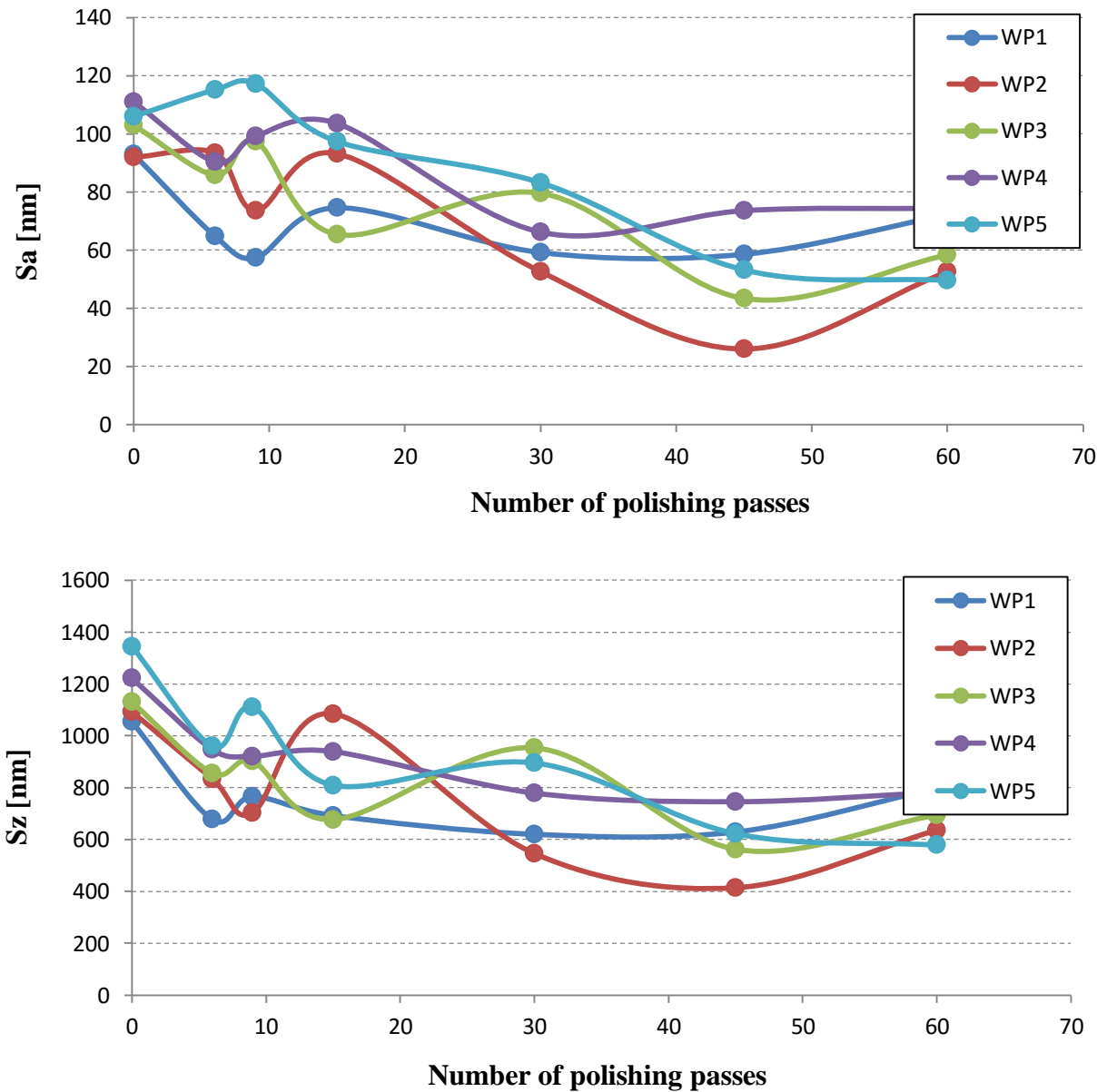


Figure 18. Sa and Sz roughness values versus number of passes_Test2

3.5.1 Features Extraction and selection for experimental Test2

To find correlations between sensorial data and surface roughness values, advanced signal processing, based on signal conditioning, feature extraction and data fusion, was applied to the multiple sensor signals acquired through the monitoring system.

Signal analysis in the time domain was performed to extract a number of conventional statistical features from each dataset. The following statistical features were extracted (Binsaeid, Asfour, Cho, & Onar, 2009; Teti, Jemielniak, & O'Donnell, 2010): mean average, variance, skewness, kurtosis and energy.

The results of the sensor signal conventional statistical feature extraction are reported for each of the workpieces: WP1, WP2, WP3, WP4, WP5.

The extracted sensor signal conventional statistical features are plotted versus pass number (or file number in the case of AE signals) for each valid workpiece together with the measured

surface roughness Sa values. After the feature extraction phase, in order to perform the feature selection step, the plots of all the sensor signal conventional statistical features were examined in order to identify possible trends useful for correlation with the measured surface roughness.

The results of the trend classification are summarised in Table 12. As can be seen from the table, the following sensor signal conventional statistical features (with ** in Table 12) appear to display promising capabilities for the identification of correlations with surface roughness through the development of cognitive pattern recognition tools: $AE_{raw}Var$, $AE_{raw}Ene$, $AE_{RMS}Ave$, $AE_{RMS}Var$, $AE_{RMS}Ene$, F_xAve , F_xVar , F_xSke , F_xEne , F_yAve , F_yEne , F_zAve , F_zEne .

Table 12. Visual checking of significant signals features_Test 2

		TEST2						
		WP1	WP2	WP3	WP4	WP5	LEGEND	
AE_{raw}	Variance	**	**	**	**	**	**	Acceptable trend
	Skewness	-	*	*	*	-	*	Uncertain trend
	Kurtosis	-	-	-	-	-	-	No trend
	Energy	**	**	**	**	**	-	No trend
AE_{RMS}	Average	**	**	**	**	**		
	Variance	**	**	**	**	*		
	Skewness	-	-	-	-	-		
	Kurtosis	-	-	-	-	-		
	Energy	**	**	**	**	**		
Current	Average	-	-	**	-	-		
	Variance	*	-	*	-	**		
	Skewness	-	-	-	-	-		
	Kurtosis	-	-	*	-	-		
	Energy	-	-	**	*	-		
F_x	Average	**	**	**	**	**		
	Variance	**	**	**	**	**		
	Skewness	-	**	**	**	**		
	Kurtosis	*	*	*	**	*		
	Energy	**	**	**	**	**		
F_y	Average	*	**	**	**	**		
	Variance	*	*	*	*	**		
	Skewness	-	-	-	-	**		
	Kurtosis	-	-	-	-	*		
	Energy	*	**	**	**	**		
F_z	Average	**	**	*	**	*		
	Variance	**	-	-	*	**		
	Skewness	-	-	-	*	-		
	Kurtosis	**	-	-	*	*		
	Energy	**	**	*	**	**		

On the basis of the above selected features, two types of sensor fusion pattern vectors can be constructed that include the promising features from the different sensor signals but exclude the simultaneous presence of AE_{raw} and AE_{RMS} features to avoid redundancy.

The first sensor fusion pattern feature vector will contain the signal features of AE_{raw} , Current, F_x , F_y , F_z :

$$[AE_{raw} Var, AE_{raw} Ene, F_x Ave, F_x Var, F_x Ske, F_x Ene, F_y Ave, F_y Ene, F_z Ave, F_z Ene]$$

The second sensor fusion pattern feature vector will contain the signal features of AE_{RMS} , Current, F_x , F_y , F_z :

$$[AE_{RMS}Ave, AE_{RMS}Var, AE_{RMS}Ene, F_xAve, F_xVar, F_xSke, F_xEne, F_yAve, F_yEne, F_zAve, F_zEne]$$

The above sensor fusion pattern feature vectors can be alternatively utilized as input to neural network classification paradigms in order to obtain in output the acceptability assessment of the surface roughness of the polished part as described in the next paragraph.

APPENDIX A reports, as an example, the selected features of the first pattern features vector for the WP1.

3.5.2 Neural Network Pattern Recognition for Surface Roughness Identification

Based on the trend classification of the conventional statistical features extracted from the force, current and AE sensor signals triplet, a feature selection procedure was carried out in order to construct sensor fusion pattern feature vectors to be utilised as inputs to neural network (NN) based pattern recognition paradigms for the identification of surface roughness.

For each of the five polished workpieces (WP1, WP2, WP3, WP4, WP5) of the valid sensor monitoring signal detection of the Test 1 series, two NN training sets were built with input pattern feature vectors constructed by sensor data fusion of selected features from the sensor signals triplet: besides selected features from force and current signals, the input pattern feature vectors of NN training set 1 contain selected features from AE_{raw} signals, while the input pattern feature vectors of NN training set 2 comprise selected features from AE_{RMS} signals.

The input pattern feature vectors of NN training set 1 are as follows: [$AE_{raw}Var$, $AE_{raw}Ene$, F_xAve , F_xVar , F_xSke , F_xEne , F_yAve , F_yEne , F_zAve , F_zEne].

The input pattern feature vectors of NN training set 2 are as follows: [$AE_{RMS}Ave$, $AE_{RMS}Var$, $AE_{RMS}Ene$, F_xAve , F_xVar , F_xSke , F_xEne , F_yAve , F_yEne , F_zAve , F_zEne].

Each NN training set consists of 60 input pattern feature vectors, i.e. one input pattern feature vector per polishing pass, and each of these input pattern feature vectors is associated with the interpolated value of surface roughness for the corresponding polishing pass.

Reference areal topography measurements were performed using a confocal microscope. The data files were filtered using a 2nd polynomial to remove the cylindrical form of the WPs; no additional filtering was applied.

For each WP, 7 surface roughness average values, each based on five roughness measurements, were obtained with reference to the following 7 steps of the full polishing process: (1) before polishing; (2) after 6 polishing passes; (3) after 9 polishing passes; (4) after 15 polishing passes; (5) after 30 polishing passes; (6) after 45 polishing passes; (7) after completing the 60 polishing passes.

The surface roughness average measurement values were used to obtain, via power function fitting, surface roughness interpolation curves made of 60 data points associated to each of the 60 polishing passes (Figure 19).

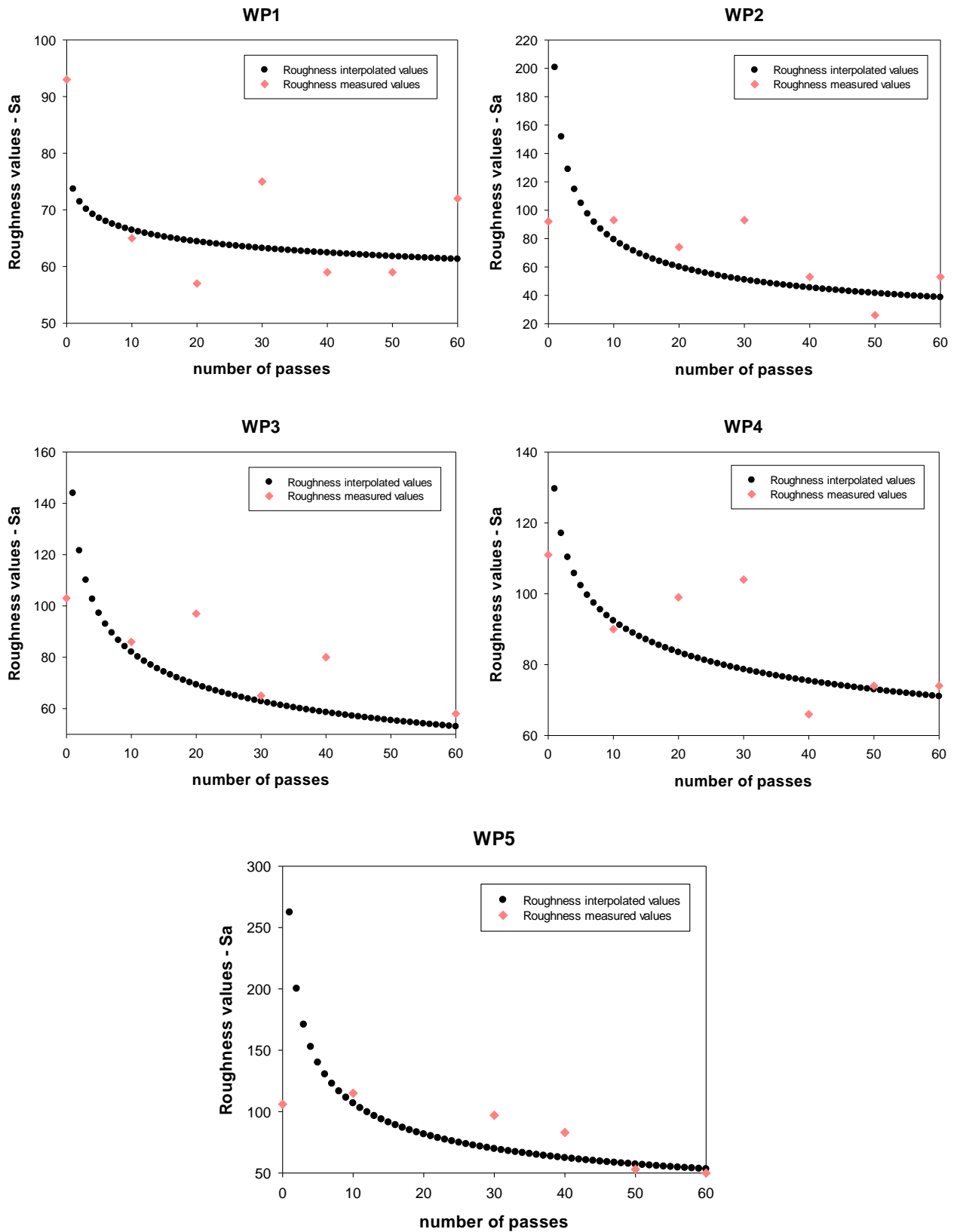


Figure 19. Surface roughness average measurement values and surface roughness interpolation curves for polished workpieces WP1, WP2, WP3, WP4, WP5

To perform NN learning, the input pattern feature vectors associated with the corresponding surface roughness interpolation values for each WP were fed to NN paradigms. For NN training set 1, containing input pattern vectors with AE_{raw} features, two NN configurations were used: 10-

10-1 and 10-20-1, where 10 is the number of input nodes, equal to the number of features in the input pattern vector; 10 or 20 is the number hidden nodes, related to the number of input nodes; and 1 is the output node, yielding the NN predicted surface roughness value per polishing pass. For NN training set 2, comprising input pattern vectors with AE_{RMS} features, two NN configurations were used: 11-11-1 and 11-22-1, where 11 is the number of input nodes, equal to the number of features in the input pattern vector; 11 or 22 is the number hidden nodes, related to the number of input nodes; and 1 is the output node, yielding the NN predicted surface roughness value per polishing pass. The employed NN learning procedure was the leave-k-out method where k cases from the training set are put aside in turn, while the other cases are used for NN training. Once the NN training phase is completed, the k cases previously put aside are utilised as inputs to the trained NN for the testing phase. This NN learning procedure is particularly useful when the available training set is limited in size.

3.5.2.1 Discussion of results for NN training set 2

In the case of NN training set 1, for each WP and polishing pass the desired surface roughness interpolation value and the NN predicted surface roughness values obtained using the diverse NN configurations are summarised in Table 13. Figure 20 reports, for each WP, the plots of the 7 surface roughness average measurement values, the desired surface roughness interpolation values and the NN predicted surface roughness value obtained from the two NN configurations.

Table 13. NN training set 1: desired surface roughness interpolation values and NN predicted surface roughness values, obtained with the 10-10-1 and 10-20-1 NN configurations, for each WP and polishing pass

Pass #	WP1 surface roughness interpolation values	WP1 NN predicted surface roughness values		WP2 surface roughness interpolation values	WP2 NN predicted surface roughness values		WP3 surface roughness interpolation values	WP3 NN predicted surface roughness values		WP4 surface roughness interpolation values	WP4 NN predicted surface roughness values		WP5 surface roughness interpolation values	WP5 NN predicted surface roughness values	
		10-10-1	10-20-1		10-10-1	10-20-1		10-10-1	10-20-1		10-10-1	10-20-1		10-10-1	10-20-1
1	73.6910	66.1577	71.4539	200.6600			143.9400			129.6500			262.3200		
2	71.4279	69.2002	67.3149	151.7559			121.5431			117.0904			200.1842		
3	70.1365	73.1620	108.6372	128.8786			110.0941			110.3153			170.9047		
4	69.2344	72.6606	62.5628	114.7706			102.6311			105.7474			152.7665		
5	68.5426	67.4602	68.1614	104.9001			97.1925			102.3349			140.0339		
6	67.9826	67.7204	67.4356	97.4689	63.6376	64.0282	92.9635	46.9966	116.9466	99.6287	102.3905	106.7907	130.4225	165.3628	157.9191
7	67.5126	67.5046	67.0340	91.5981	67.2205	64.9065	89.5319	77.0951	63.2254	97.3964	94.2689	95.7914	122.8127	187.9995	160.3316
8	67.1082	67.9738	67.0170	86.7992	62.4169	62.3112	86.6618	90.7644	86.5652	95.5033	96.5019	115.2635	116.5806	117.1270	91.1154
9	66.7534	66.6800	66.6691	82.7754	62.3782	62.4878	84.2066	81.4436	87.9268	93.8640	92.6777	93.5076	111.3466	110.9688	113.5175
10	66.4377	66.3122	65.9243	79.3343	61.6298	61.5703	82.0694	86.0132	86.8551	92.4214	93.6185	95.4240	106.8640	105.3964	97.5891
11	66.1533	66.5803	66.0311	76.3448	59.8173	60.9053	80.1829	75.2265	79.1331	91.1355	89.7610	92.5960	102.9647	99.4234	99.3618
12	65.8948	65.8096	65.8521	73.7141	61.0440	60.4251	78.4985	80.3008	81.0627	89.9773	91.0599	91.4523	99.5292	104.5671	103.8854
13	65.6579	65.7604	65.1114	71.3743	59.5197	59.7698	76.9803	75.3876	76.1522	88.9248	88.2021	89.0379	96.4703	94.4496	95.1624
14	65.4393	65.6417	65.2764	69.2742	60.6471	60.7599	75.6008	75.7439	73.9150	87.9613	85.5122	86.0441	93.7220	89.4443	90.1979
15	65.2365	64.9644	64.9388	67.3746	59.5873	60.0352	74.3387	73.2080	65.7176	87.0737	85.8145	85.4714	91.2338	84.2610	83.7631
16	65.0473	65.3328	65.3869	65.6448	60.1971	59.5416	73.1773	76.2280	77.7332	86.2515	85.3373	86.5010	88.9661	90.5879	92.4922
17	64.8701	65.4072	64.8202	64.0604	58.8143	58.5554	72.1028	69.8418	70.2483	85.4863	85.4527	84.5858	86.8873	90.2495	91.4844
18	64.7034	64.4137	64.5389	62.6017	59.3939	59.8297	71.1042	69.9678	71.4000	84.7710	83.1468	87.3619	84.9719	86.3477	82.6546
19	64.5462	65.3173	64.5952	61.2524	58.1945	58.4733	70.1723	73.3384	68.6736	84.1000	84.1338	85.1568	83.1989	79.0504	81.9463
20	64.3974	64.1429	64.2724	59.9992	58.0554	58.5130	69.2995	68.2052	71.2668	83.4682	84.1840	82.3963	81.5511	81.7567	78.8186
21	64.2561	64.4315	64.4394	58.8310	57.6261	57.7767	68.4794	67.9315	68.6271	82.8717	82.3505	82.6300	80.0140	88.4941	83.1903
22	64.1218	64.3501	64.8786	57.7384	57.3683	57.3234	67.7065	67.1298	67.4673	82.3069	82.8088	81.3474	78.5754	82.8850	79.4974
23	63.9936	63.8910	64.1094	56.7132	57.5971	57.4987	66.9761	66.3787	65.1973	81.7709	82.1332	81.6696	77.2249	84.0703	80.6231
24	63.8712	63.8019	64.0646	55.7488	56.6720	57.2437	66.2842	67.8154	67.0830	81.2609	79.8700	80.0896	75.9537	74.3766	70.1187
25	63.7540	63.3595	64.1069	54.8392	57.7737	57.5956	65.6272	61.7083	63.2006	80.7747	81.7680	81.2781	74.7541	74.0393	73.1908
26	63.6415	63.9182	63.9255	53.9792	56.7830	57.4592	65.0022	64.6868	62.4772	80.3103	79.0848	79.2347	73.6193	66.6435	71.6144
27	63.5335	63.2513	51.6693	53.1644	57.3702	57.1974	64.4064	62.7513	64.7241	79.8660	79.3819	80.3653	72.5437	74.0514	71.2789
28	63.4297	63.9666	63.4202	52.3909	56.2966	56.2694	63.8374	63.0624	62.1642	79.4402	78.7124	77.4673	71.5220	75.4985	71.8527
29	63.3296	63.3317	63.7760	51.6552	56.5358	56.4778	63.2931	63.0522	61.5241	79.0315	77.6572	76.1663	70.5499	71.6776	69.4322
30	63.2330	63.3415	63.3703	50.9543	55.9614	55.9176	62.7717	62.4602	62.0916	78.6386	77.6155	77.3013	69.6232	70.5072	68.8183
31	63.1398	62.8360	62.8298	50.2854	56.7865	56.6261	62.2715	62.1308	60.4562	78.2605	76.6435	77.7601	68.7385	73.8180	70.1196
32	63.0497	62.4789	62.5834	49.6461	55.6993	55.8611	61.7910	61.9657	61.8660	77.8961	77.7833	78.4642	67.8927	74.5229	68.2858
33	62.9624	63.3210	63.3116	49.0343	56.2971	56.2974	61.3287	62.2116	60.3311	77.5445	76.6529	76.6912	67.0828	65.0373	66.9283
34	62.8779	62.6627	62.6583	48.4479	55.5815	55.5173	60.8836	59.5355	59.5484	77.2049	78.7462	77.8309	66.3063	68.6959	67.8463
35	62.7959	61.9361	62.6335	47.8852	55.4572	55.7036	60.4545	58.9005	58.5498	76.8767	75.7213	76.9573	65.5609	67.0018	64.4076
36	62.7164	62.4147	62.5652	47.3446	54.5802	54.6312	60.0404	57.2377	60.4084	76.5590	79.3327	76.7124	64.8445	58.3860	59.3699
37	62.6391	62.1206	62.2866	46.8248	53.9469	53.9854	59.6404	58.6119	59.2785	76.2512	74.1277	72.9824	64.1553	62.4707	60.7785
38	62.5640	63.0189	64.0140	46.3242	54.9000	54.7815	59.2535	60.7553	58.5536	75.9529	76.1601	77.5035	63.4915	62.8428	63.4776
39	62.4909	62.0755	61.8896	45.8418	54.7618	55.0364	58.8792	61.0891	58.9600	75.6634	77.2184	75.2050	62.8516	58.6466	60.7307

40	62.4197	61.7769	61.9882	45.3765	54.8328	54.8281	58.5166	57.7216	57.2624	75.3824	76.2052	76.1244	62.2340	60.8239	66.4238
41	62.3504	62.4415	62.4516	44.9272	54.5362	54.0005	58.1651	56.3399	57.8382	75.1092	75.0791	75.3447	61.6376	63.5093	63.8527
42	62.2828	61.6997	62.2574	44.4930	54.9555	54.4722	57.8241	55.1310	55.9681	74.8436	76.4340	75.5609	61.0610	62.8655	62.5724
43	62.2169	62.5516	62.6237	44.0730	53.5101	53.5012	57.4930	57.6896	57.9685	74.5852	76.2094	75.3484	60.5033	62.9341	59.9404
44	62.1526	61.8162	61.7119	43.6666	54.5909	54.3287	57.1714	55.3541	56.0249	74.3336	74.6138	74.5094	59.9632	55.7353	57.4948
45	62.0897	62.1345	62.2231	43.2729	53.7876	53.4648	56.8588	54.6826	55.1769	74.0884	74.8511	73.1944	59.4400	63.2691	60.9946
46	62.0284	62.0849	62.4251	42.8913	53.3581	53.3801	56.5547	54.6878	54.7387	73.8494	72.6843	73.9699	58.9326	59.7820	58.9234
47	61.9684	62.1392	62.4515	42.5212	54.4048	54.3167	56.2587	56.3915	55.6899	73.6163	73.2323	72.6522	58.4404	61.4057	58.8402
48	61.9097	62.5230	63.0653	42.1619	54.0811	54.1754	55.9704	56.4518	57.7316	73.3888	72.4527	72.5856	57.9625	60.1395	58.5854
49	61.8523	61.5347	62.1356	41.8130	54.8585	54.4842	55.6895	58.5663	58.1864	73.1667	73.2349	73.7120	57.4983	60.1807	55.3668
50	61.7961	61.9416	62.0402	41.4740	55.0688	55.0734	55.4157	55.3363	56.8384	72.9498	74.8204	74.1357	57.0470	53.7231	58.4891
51	61.7410	62.4512	62.5643	41.1443	54.5464	54.8883	55.1486	56.0712	57.6386	72.7377	73.1150	71.1774	56.6082	58.9943	58.2145
52	61.6871	62.0350	62.1244	40.8236	53.8004	54.6436	54.8879	53.3378	55.1707	72.5304	74.5239	73.5747	56.1811	60.7772	60.2584
53	61.6342	61.9508	62.3460	40.5114	54.2999	54.3138	54.6334	57.0980	56.1204	72.3276	74.2040	75.6378	55.7653	58.2088	55.2554
54	61.5824	61.8273	62.1983	40.2074	54.1901	54.3278	54.3848	56.4750	56.6227	72.1291	76.7274	73.1429	55.3602	56.0805	54.7980
55	61.5316	62.7030	62.1474	39.9112	54.3629	54.4147	54.1418	56.3580	56.3067	71.9348	73.1004	72.6403	54.9655	51.3285	53.4903
56	61.4817	0.0819	25.7939	39.6224	53.4511	53.5962	53.9043	55.4168	55.5432	71.7445	74.6742	71.7707	54.5806	54.0987	54.5081
57	61.4328	40.9926	48.1926	39.3408	53.2883	53.2715	53.6720	55.3912	55.6003	71.5581	73.1020	75.0209	54.2051	51.4655	52.4875
58	61.3847	62.9836	63.0155	39.0660	29.0953	36.0204	53.4448	57.5151	56.6160	71.3754	57.0530	42.7711	53.8387	56.3142	56.5352
59	61.3375	64.3334	60.3505	38.7978	267.7936	132.0055	53.2223	40.8218	3.7570	71.1963	-8.7569	8.2492	53.4810	41.5986	55.4233
60	61.2911	68.4443	68.9582	38.5359	36.4585	34.3487	53.0045	97.3991	237.4063	71.0206	156.9046	180.4063	53.1315	46.0853	111.70

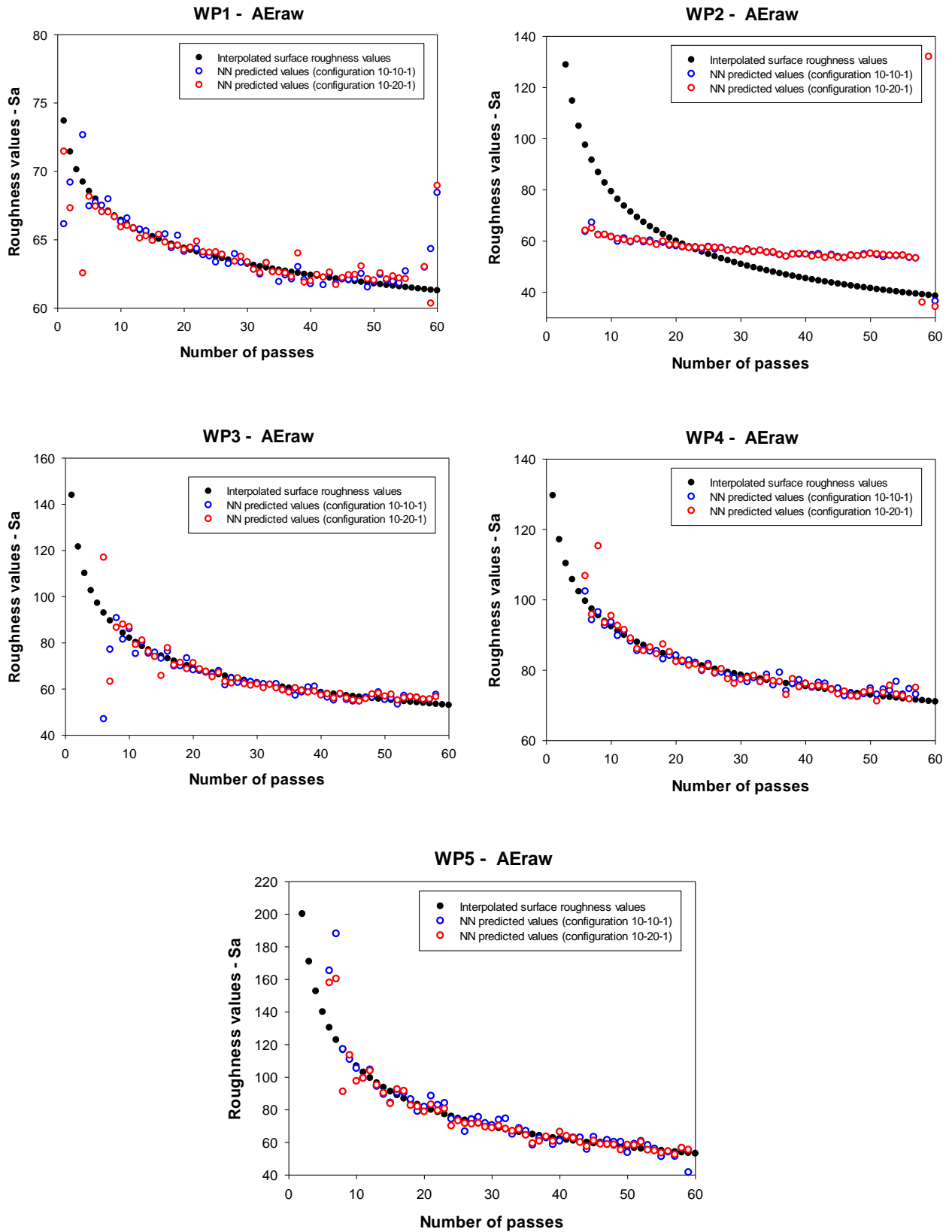


Figure 20. NN training set 1: WP1, WP2, WP3, WP4, WP5 plots of the desired surface roughness interpolation values and the NN predicted surface roughness values obtained

3.5.2.2 Discussion of results for NN training set 2

In the case of NN training set 2, for each WP and polishing pass the desired surface roughness interpolation values and the NN predicted surface roughness values obtained using the two NN configurations are summarised in Table 14. As can be noticed from the table, the initial 5 polishing passes were not considered for NN training and testing as they precede the first surface roughness measurements on each polished WP that were performed after 6 polishing passes. Figure 21 reports, for each WP, the plots of surface roughness average measurement values, desired surface roughness interpolation values and NN predicted surface roughness value obtained using the two NN configurations.

40	62.4197	61.8401	61.9481	45.3765	44.66417	45.45334	58.5166	57.3663	64.5069	75.3824	75.80721	76.1414	62.2340	64.2654	63.6223
41	62.3504	62.4821	62.7517	44.9272	28.35848	42.65319	58.1651	58.3607	64.6500	75.1092	74.53106	74.4506	61.6376	63.6325	62.0331
42	62.2828	61.7649	61.7798	44.4930	43.53790	43.52159	57.8241	56.0623	64.3467	74.8436	75.80992	76.3658	61.0610	63.3525	63.0822
43	62.2169	62.3787	62.5811	44.0730	42.70401	41.29146	57.4930	58.6675	65.3317	74.5852	75.12776	74.7708	60.5033	60.9057	62.0175
44	62.1526	62.0327	61.9340	43.6666	43.50244	42.50039	57.1714	55.3309	64.1370	74.3336	73.69640	74.4156	59.9632	56.8048	56.2740
45	62.0897	62.7395	62.1275	43.2729	41.22353	41.23141	56.8588	54.5833	64.2107	74.0884	73.71872	73.3512	59.4400	63.1856	62.6220
46	62.0284	62.2474	62.0943	42.8913	41.36918	40.77108	56.5547	55.8493	64.1563	73.8494	71.90728	73.4699	58.9326	60.8006	60.6601
47	61.9684	62.4316	62.0933	42.5212	42.64372	41.73190	56.2587	56.2107	64.5632	73.6163	73.03865	74.3772	58.4404	59.5318	58.0466
48	61.9097	62.4865	62.6603	42.1619	43.60847	43.42529	55.9704	58.7104	65.1704	73.3888	72.80769	72.3143	57.9625	60.4301	58.3976
49	61.8523	61.9954	61.9446	41.8130	43.30162	42.97072	55.6895	58.6849	65.0894	73.1667	72.99185	74.9392	57.4983	59.4244	58.6342
50	61.7961	62.0474	61.5671	41.4740	46.89216	46.38957	55.4157	54.9234	64.4725	72.9498	74.35489	74.7930	57.0470	56.4724	56.1700
51	61.7410	62.7562	62.4168	41.1443	43.60823	43.65486	55.1486	57.2642	64.6197	72.7377	71.96960	72.1891	56.6082	56.8466	57.2135
52	61.6871	61.9326	61.7346	40.8236	43.03515	43.10767	54.8879	54.9767	64.0986	72.5304	71.99384	73.0091	56.1811	58.4900	58.6529
53	61.6342	62.2522	61.6931	40.5114	42.42447	42.06324	54.6334	57.1453	64.7729	72.3276	71.99262	72.6788	55.7653	58.3903	59.1033
54	61.5824	62.0628	62.1500	40.2074	43.12738	42.85550	54.3848	56.3588	64.3475	72.1291	71.31455	71.3876	55.3602	55.0300	55.6031
55	61.5316	62.3906	62.4327	39.9112	42.20431	42.24894	54.1418	55.5223	64.5284	71.9348	73.28075	72.9532	54.9655	55.0078	55.7022
56	61.4817	135.052	47.5367	39.6224	39.56671	40.54712	53.9043	55.0493	64.0815	71.7445	71.47693	71.3559	54.5806	52.3211	49.9007
57	61.4328	51.2654	30.8384	39.3408	38.24240	39.37584	53.6720	55.6634	64.4502	71.5581	72.83909	72.8905	54.2051	50.7471	52.8339
58	61.3847	63.0106	62.4861	39.0660	39.22278	58.15832	53.4448	57.8049	64.6001	71.3754	28.72913	32.6488	53.8387	55.8343	57.5431
59	61.3375	62.9039	63.4727	38.7978	33.29983	21.61634	53.2223	168.6976	47.4353	71.1963	49.45456	45.6368	53.4810	74.3317	26.4545
60	61.2911	59.7257	70.7436	38.5359	78.584	35.788	53.0045	264.6645	163.0339	71.0206	71.60638	25.5462	53.1315	91.7703	4.8810

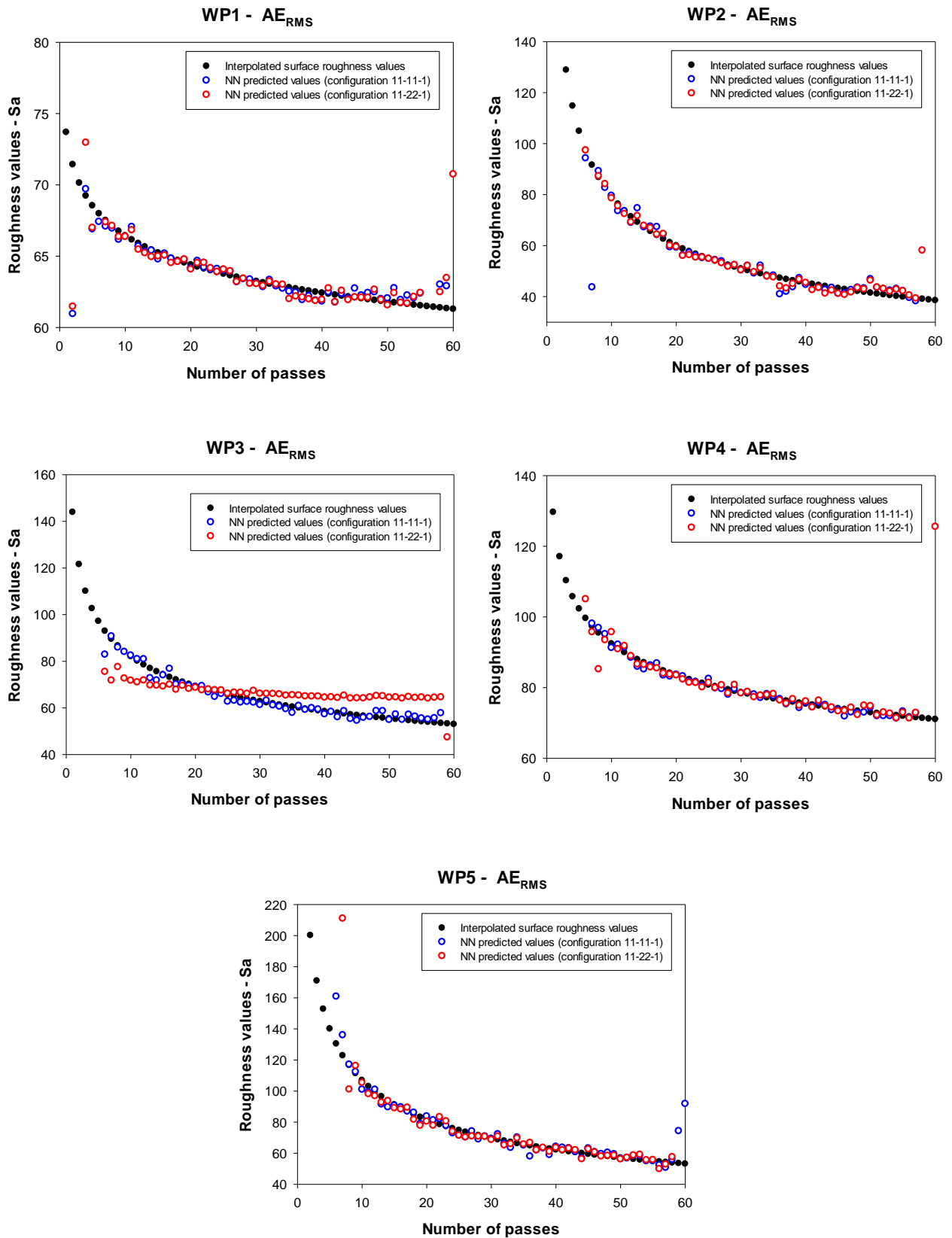


Figure 21. NN training set 2: WP1, WP2, WP3, WP4, WP5 plots of the desired surface roughness interpolation values and the NN predicted surface roughness values obtained

The overall performances of the NNs have been computed in terms of MAPE (Mean Absolute Percentage Error), i.e. the absolute differences between target values (y) and NN predicted values (\hat{y}_t) divided by the actual value:

$$MAPE = \frac{1}{n} \sum_{t=1}^n \left| \frac{y_t - \hat{y}_t}{y_t} \right|$$

The following table (Table 15) summarizes the NN results in terms of MAPE.

Table 15. NN results for training set 1 and training set 2 in terms of MAPE_Test2

	<i>Training Set 1</i>		<i>Training Set 2</i>	
	<i>10-10-1</i>	<i>10-20-1</i>	<i>11-11-1</i>	<i>11-22-1</i>
WP1	0.0339	0.0361	0.0995	0.0783
WP2	0.2629	0.2028	0.0618	0.0549
WP3	0.0504	0.1044	0.1245	0.1256
WP4	0.0515	0.0632	0.0383	0.0366
WP5	0.0548	0.0564	0.0508	0.0704

In the test 2 it is not possible to define the best NN overall configuration.

The lowest MAPE value has been obtained for the WP1 (using the training set 1, 10 input nodes, 10 hidden nodes and 1 output node), and it is equal to 0.0339, which means a prediction error of 3.39%. Instead, in the worst case scenario (WP3, using the training set 2 and 22 hidden node), the MAPE is equal to 0.1256 (prediction error of 12.56%).

4. Cognitive sensor monitoring of drilling of composite materials

4.1 Characteristics of composite materials

Nowadays, composite materials with a worldwide increase in technologies are more and more replacing traditional materials due to their excellent properties. It is possible to observe a dynamic growth of applications of composite materials in automotive and aerospace industries due to their lightness and stiffness to improve products quality and efficiency.

Composite materials can be defined as a mixture of two or more materials which are not homogenous and chemically different one from each other, combined in order to obtain a product that has specific chemical and physical properties, different from the original elements. The two major elements are reinforcement and matrix. The first one is in the form of strong *fibres*, which play the role of “reinforcement”. The fibrous reinforcement represents the discontinuous phase used to enhance the strength, the toughness and the rigidity of the matrix, with which it must constitute a good chemical-physical bond. The reinforcement is used to absorb the load; it is possible to study the best fibres orientation (Figure 22) in relation to external loads in order to obtain maximum resistance of the material with less material and, therefore, with the maximum saving in weight. In fact, the reinforcement, and the resulting strength of the final product, reach the maximum value in the longitudinal direction to the fibres, and the minimum in the transverse direction, along which fracture may occur even for relatively low loads. Fibres are distributed in a weaker base called *matrix* which serves to distribute them and to transmit the load to the fibres. Materials of different physical and chemical properties, when properly combined, produce a material with different characteristics from its constituent components. The main beneficial characteristics of composite materials includes high strength, stiffness and corrosion resistance (Campbell, 2010).

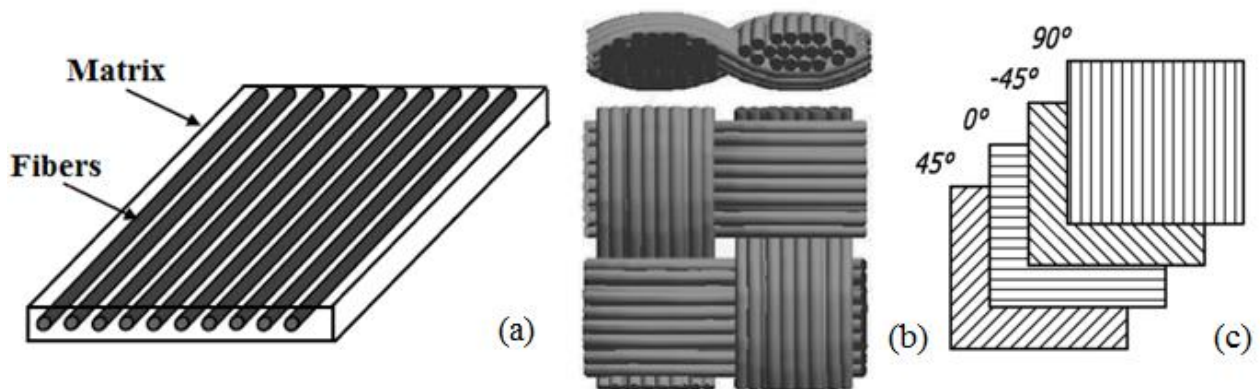


Figure 22. (a) Unidirectional fibres orientation; (b) Bidirectional fibre orientations; (c) Laying-up sequence of unidirectional-ply

4.2 Classification of composite laminates

The classification of the composite materials can be made on the basis of multiple criteria. One of the most common classification is according to the type of components used in the realization

of the composite material, with particular reference to the type of matrix and the reinforcing fibre type. Since the field of possible applications is mostly influenced by the type of material used for the matrix is commonly used to classify the composite materials according to its characteristics. Therefore the composite materials can be distinguished into: *metal matrix composites (MMC)*, *ceramic matrix composites (CMC)* and *polymer matrix composites (FRP)*.

The mechanical properties of *metal matrix composites* make them particularly interesting as an alternative to conventional alloys used in the aerospace industry and in all applications where a resistance at medium-high temperatures ($> 250\text{ }^{\circ}\text{C}$) is required.

The metal matrix composites are realized by incorporating, in a metal or a metal alloy (for example, aluminium, magnesium, titanium, zinc), specific materials, commonly referred to as reinforcements, consisting of: continuous or discontinuous fibres of boron, graphite, silicon carbide, tungsten or molybdenum; ceramic particles of silicon carbide, alumina or boron carbide. The *ceramic matrix composites* are constituted by refractory materials (e.g. oxides, carbides, nitrides) so they can be used with high temperatures, up to $1500\text{ }^{\circ}\text{C}$. They consist of particular fibres, such as those of carbon I and Silicon carbide (SiC), able to retain their mechanical properties at high temperatures (Balasubramanian, 2016).

These materials are characterized by lightness, rigidity, high breaking strength and fragility. This latter limits their use in most applications.

Due to the excellent physical properties of the final product, the *polymer matrix composites*, also known as FRP (Fibre Reinforced Plastic), have been widely used in different sectors including aerospace, automotive and civil engineering.

Composite materials can be also distinguished according to the type of reinforcement used. The fibres may be of carbon, glass, steel or aluminium and differ from each other for their mechanical properties (e.g. elastic modulus, breaking strength, specific weight) as well as chemical and electrical properties. It is important to highlight that, with constant Young's modulus, the carbon fibres have a lower density and a resistance six times higher than steel or aluminium¹.

The most commonly used reinforcing fibres are substantially three: Glass fibres (Fiberglass), Carbon fibres (Carbon fibre) and Aramid fibres (Kevlar).

The Carbon Fibre Reinforced Plastic (CFRP) materials are the widely used composite in aerospace sector mainly for their lightness and resistance (Wilhelm, 2001). The advantages of carbon fibres are: high elastic modulus, light weight, high resistance to fatigue and compression, low thermal expansion coefficient, good electrical conductivity, a good resistance to high temperatures (2000°C) in non-oxidizing atmosphere and a good resistance to medium temperatures (400°C) in oxidizing atmosphere.

Therefore, the composite materials made up of resin and carbon reinforcements have an excellent combination of low weight, high mechanical strength and high rigidity.

In the last decades there was an increasing percentage of composite materials employed in airplane realization². In general the application of CFRP reduces the overall weight of the airplane, and increases its efficiency and safety, also reducing fuel consumption.

¹ <http://classroom.materials.ac.uk/caseRoto.php>

² Hexcel Corporation, Aerostrategy

4.3 Drilling operations

Drilling is a cutting process which allows to obtain, through material removal, holes that normally act as housing for bolted or riveted junctions.

Drilling processing of composite materials is a challenge for manufacturing engineers (Zitoune, Vijayan, & Collombet, 2010) due to material fragmentation and delamination that occurs during the drilling operation which affect aesthetics and processed surface quality (Jain & Yang, 1994).

Drilling tools can be divided into different types depending on the processes for which they are designed but the most widely used are the twist-drill bits (Figure 23).

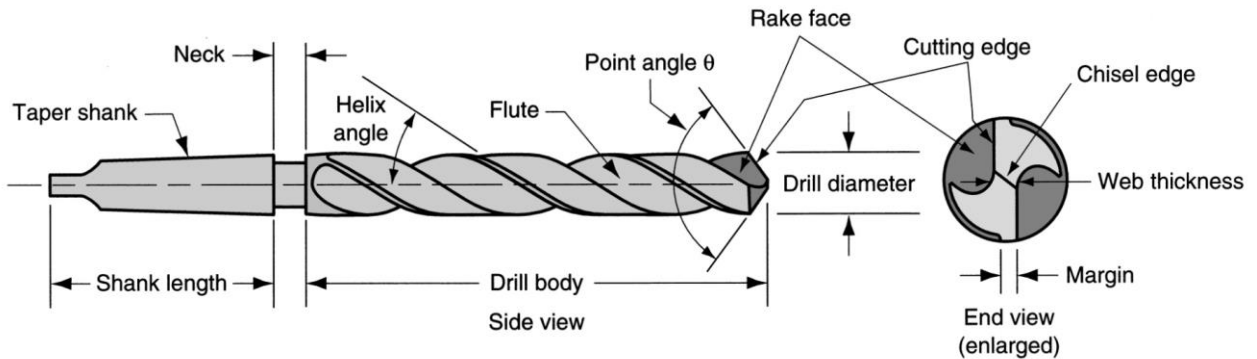


Figure 23. Standard geometry of a twist drill (Groover, 2010)

The standard twist drill has two opposite helicoidal grooves. The angle between the spiral *flutes* and the tool axis is called *helix angle*, which usually varies between 30° and 35° degrees. The flutes are necessary for the extraction of chips from the hole. Although it is desirable for the flute openings to be large to provide maximum clearance for the chips, the body of the drill must be supported over its length. This support is provided by the *web*, which is the thickness of the drill between the flutes.

The last part of the body of the twist drill has a conical shape. A typical value for the *point angle* is 118°. Finally there is the *chisel edge*. Connected to the chisel edge are two *cutting edges* (sometimes called *lips*). The portion of each flute adjacent to the cutting edge acts as the *rake face* of the tool.

The bit is also equipped with *margins*, which drive the tools into the hole and realizes the finishing of the cylindrical wall. The bit ends, on the other side, with a cylindrical or conical *shank*, which serves to fix it to the drill spindle.

A typical automated drilling operation is performed by a drill press in which all drilling parameters (e.g. feed rate and spindle speed) are set and controlled.

The drilling process involves two basic motions (El-Hofy, 2013) (Figure 24):

- The primary (or cutting) motion represents the rotation around the tool axis. The cutting speed is measurable by the following relation:

$$V_t = \frac{\pi * n * D}{1000}$$

where:

D is the bit diameter;

n is the spindle rotation speed.

- The second motion is called the feed motion (V_a). It is obtained from the motion of the tool perpendicular to the work-piece. The feed of the main spindle is calculated as follows:

$$V_a = f_r * n$$

where:

f_r is the feed per revolution.

The feed rate (f) or forward ratio is the ratio between forward speed F_s and spindle rotation speed:

$$f = \frac{V_a}{n}$$

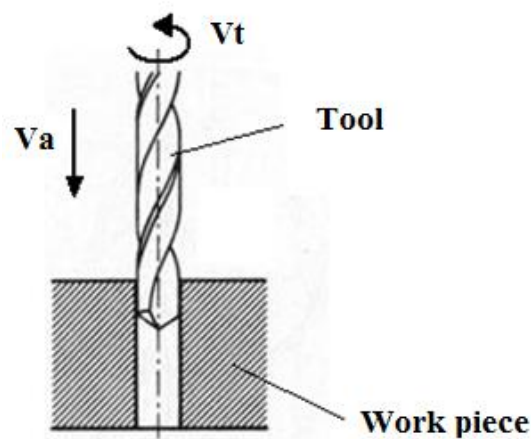


Figure 24. Drilling basic motions

Frequently composite laminates are produced through overlapping of multiple layers, in order to form a multi-layered material, in which each layer has a different orientation of fibres. For this reason, the composite laminate acquires anisotropy and inhomogeneity properties, which make it, light and strong, but also hard to be machined (Sheikh-Ahmad & Davim, 2012). Drilling is a particularly hostile operation for composite laminates, because high concentrated efforts and vibrations generated during such processing may cause widespread damages. Such damages cause problems from an aesthetical point of view but it can also compromise finished part mechanical properties.

Although several application of non-traditional machining operations to hole-making of composite laminates, such as laser machining (Herzog, Jaeschke, Meier, & Haferkamp, 2008) and water-jet machining (Azmir & Ahsan, 2009), have been developed, mechanical drilling operations using conventional or special drill bits are primary applications for composite laminates.

Among various drilling operations for composite laminates, conventional drilling with twist drill bits and various special drill bits is the first operation attracting extensive attention and to be studied systematically. According to the main purpose of the scientific papers reported in literature dealing with the conventional drilling of composites materials, they can be divided into four groups (Liu, Tang, & Cong, 2012):

- Papers investigating the correlation between input (e.g. feed rate, drill bit geometry, spindle speed) and output variables (e.g. delamination and holes quality) (Davim, Reis, & António, 2004; Arul, Vijayaraghavan, Malhotra, & Krishnamurthy, 2006; Davim, Rubio, & Abrao, 2007; Shyha, Soo, Aspinwall, & Bradley, 2010);
- Papers analysing the effects of the drill bit geometry on thrust force and quality of drilled holes (Tsao & Hocheng, 2005; Hocheng & Tsao, 2006; Shyha, Aspinwall, Soo, & Bradley, 2009; Durão, et al., 2010);
- Papers investigating the effects of the tool wear on thrust force and quality of drilled holes (Iliescu, Gehin, Gutierrez, & Giro, 2010; Isbilir & Ghassemieh, 2012; Isbilir & Ghassemieh, 2013; Raj & Karunamoorthy, 2016);
- Papers focusing on the minimization of delamination (Stone & Krishnamurthy, 1996; Capello, 2004; Tsao, 2006)

4.4 Tool wear analysis

The use of a specific cutting tool influences both the quality and the cost of the machined parts. The tool must guarantee the following two properties:

- The tool must remove material;
- The tool must allow to achieve an adequate surface finishing

One of the main limits during drilling of polymer matrix composites with conventional twist drills such as high speed steel, is the excessive tool wear which are subjected to such tools.

In fact, while a tip of high speed steel can be used for drilling hundreds of holes in carbon steel before completely wear out, the same tool, drilling composite materials is able to drill less than ten holes.

The tool wear, i.e. the progressive removal of material from the tools surface, is linked to the combined effect of high temperature, chemical characteristics of the material and high stresses to which the tool and workpiece are subjected during machining.

Further causes may be the following:

- Wear by abrasion: produced by the sliding of a hard and rough surface on a softer one;
- Wear for bond: originated by the high contact pressures between chip and tool which causes welds between the surfaces in contact;
- Wear by diffusion: produced by the migration of atoms through the tool-chip interface.

The combined effect of mechanical and thermal stresses can cause both chipping, i.e. removal of metal particles near the cutting edge due to impacts or excessive pressures, and plastic deformation due to high temperatures in the cutting zone.

The mechanisms of tool wear can occur on both tool flank (flank wear) and tool crater (crater wear), the two most widely parameters used for tool wear measurement (Figure 25). However

flank wear is most commonly used for wear monitoring due to their trend during machining (Sheikh-Ahmad & Davim, 2012).

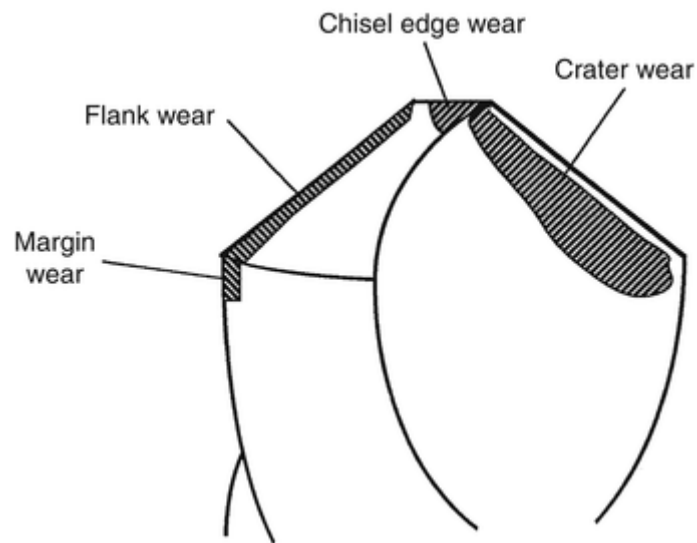


Figure 25. Schematic representation of twist drill (Stephenson & Agapiou, 2006)

The first one is the result of a friction between the machined surface of the workpiece and the tool flank. Flank wear appears in the form of so-called wear land and is measured by the width of this wear land, VB . Cutting forces increase significantly with flank wear. The second one is the result of the action of the chip sliding on the tool surface. In Figure 26 the tool wear as a function of cutting time is reported (wear curve). Crater wear follows almost the same growth curve.

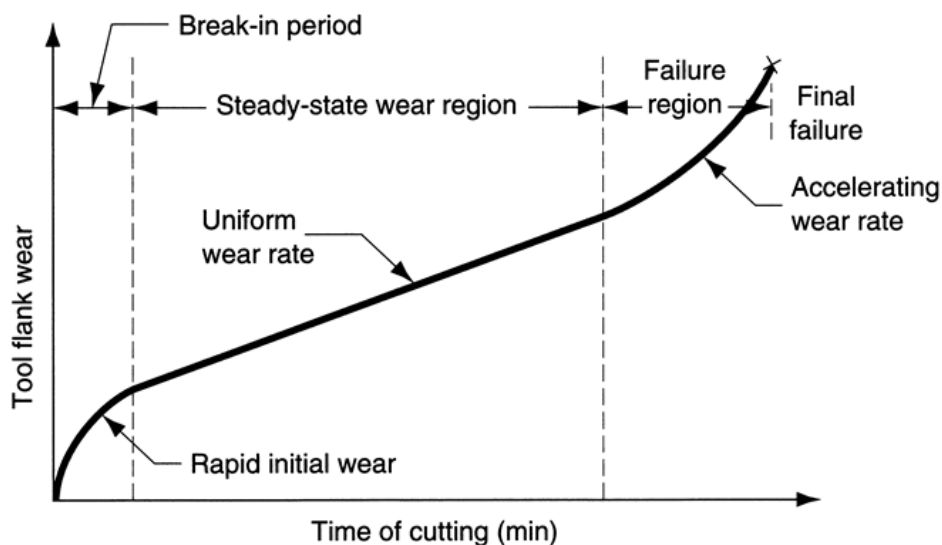


Figure 26. Tool wear as a function of cutting time (Marinov, 2004)

As cutting proceeds, the amount of tool wear increases gradually. The tool wear must be lower than a certain limit in order to avoid tool failure, this value is known as tool life (generally in the steady state wear region) and it depends on the operating conditions. The duration of the life of the tool T is defined generally by imposing a limit to the value VB . When this limit is exceeded, the tool must be changed.

Parameters, which affect the rate of tool wear are: cutting conditions (cutting speed V , feed f , depth of cut d), cutting tool geometry (tool orthogonal rake angle), properties of work material. From these parameters, cutting speed is the most important one. As cutting speed is increased, wear rate increases, so the same wear criterion is reached in less time, i.e. tool life decreases with cutting speed.

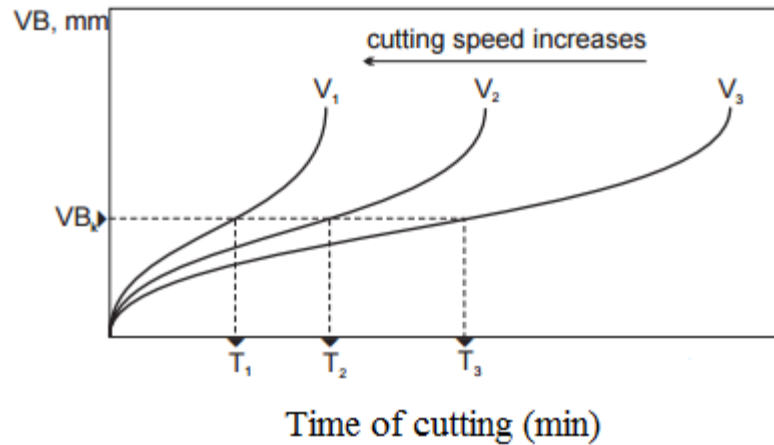


Figure 27. Effect of cutting speed on tool wear and tool life for three cutting speeds

In general, the tool life can be expressed as:

- a function of the dimensional tolerances permitted on the workpiece;
- as a function of the tolerances of surface roughness of the workpiece;
- as a function of a given parameter for the quality of the holes;
- as a function of the limit fixed for the tool wear.

4.5 Hole quality evaluation for drilling of composite laminates

Drilling of composite materials is a widespread machining process in aerospace industry. Frequently the parts realized in composite materials should be assembled to other parts using mechanical joints due to the difficulties to realize welding operations or adhesive joints.

The drilled holes reduce the laminate's resistance to stress so they are subjected to strict quality requirements. As far as geometric requirements, the holes must be in the right position, have the set diameter and the right shape. Other quality parameters are, e.g., surface roughness at drilled hole wall, delamination, fuzzing, spalling.

In the drilled area the mechanical properties of the material are lower compared to others areas. This phenomenon depends mainly on the effects of thrust force and torque that occurs during drilling. During drilling operations, both the resistance to cutting and the friction between the drill bit and the workpiece prevent the tool penetration into the workpiece and cause growing thrust forces and torques. Hence these signals are the most widely monitored in literature dealing with drilling operations.

Usually the thrust force and torque are considered the sum of two effects: the indentation of the chisel edge and the cut of the main edges (López De Lacalle, Rivero, & Lamikiz, 2009).

A recent study conducted in 2014 using the Taguchi method analyses the influence of process parameters on thrust force and torque. The analysis reveals that the feed rate is the most

significant factor affecting the thrust force, while the cutting speed contributes the most to the torque (Neseli, 2004).

It has been found in literature that the thrust force produced during drilling operations directly affect the quality of drilled holes (Ho-Cheng & Dharan, 1990; Chen W.-C. , 1997; Khashaba, Seif, & Elhamid, 2007).

4.5.1 Delamination

The drilling process impact the workpiece surface quality that has different acceptance levels depending on the company. Nevertheless, workpiece quality can be affected by different non-compliance. However delamination is one of the most common parameters used for the evaluation of hole quality (Zhang , Wang, & Liu, 2001; Won & Dharan, 2002; Davim & Reis, 2003; Bhatnagar, Singh, & Nayak, 2004; Babu & Pradhan, 2007; Romoli & Dini, 2008). Achieving a lower thrust force is the first priority during drilling process since thrust force is highly related to delamination. The primary mode of failure is delamination, which happens in drilling of laminate material, when thrust force exceeds a certain value, it would cause layers of multilayer material such as CFRP to become separated. This failure would cause the material a significant loss of mechanical toughness, and would extremely diminish interlaminar strength. Avoiding delamination becomes the main objective of drilling CFRP material since the CFRP material continues to grow in the aerospace and automobile industries (Lenin, Ramkumar, & Senthilkumar, 2015).

The delamination can be defined as an inter-laminar failure occurring at both the top and the bottom of the stack surface around the drilled hole.

The exit delamination (or push-down delamination at hole exit) is generally more severe than the entry delamination (or peel-up delamination) (Dharan & Won, 2000). This two types of damage mechanisms have different causes and effects. Peel-up delamination is caused by the cutting force pushing the abraded and cut materials to the flute surface. At the beginning of the contact, the cutting edge of the drill will abrade the laminate. As the drill moves forward it tends to pull the abraded material along the flute and the material spirals up before being effectively cut. Normally, a reduction in the feed rate adopted can reduce this effect. On the other hand, push-out delamination is a damage that occurs in interlaminar regions, so it on both fibre nature and resin type and respective properties. This damage is a consequence of the thrust force applied by the drill bit on the uncut laminate plies of the workpiece. At a certain point, the loading exceeds the interlaminar bond strength and delamination occurs, before the laminate is totally penetrated by the drill (Durão, et al., 2010). This damage can be reduced using by proper optimization of process variables (cutting speed, feed rate and drill point geometry) (Singh & Bajpai, 2013).

In the following figure (Figure 28) the phenomenon has been schematized:

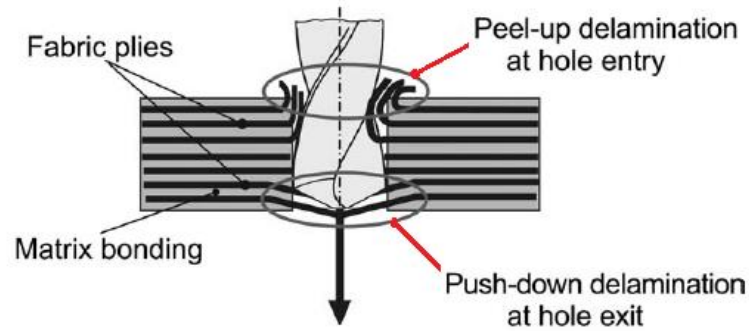


Figure 28. Entry and exit delamination representation (Faraz, Biermann, & Weinert, 2009)

The delamination damage (entry and exit) was estimated in terms of delamination factor, F_d (Figure 29), according to the following relationship proposed by (Chen W.-C. , 1997):

$$F_d = \frac{D_{max}}{D_a}$$

where:

D_{max} is the diameter of the circumference including the damaged area

D_a is the actual measured hole diameter (Rawat & Attia, 2009)

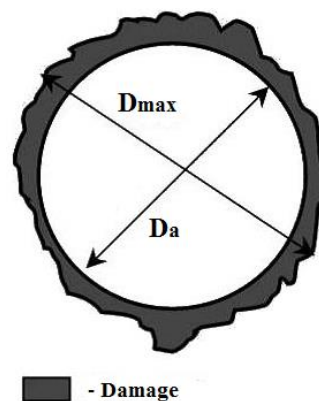


Figure 29. Delamination factor

As some of these defects are not visible in a visual inspection, it is needed to establish non-destructive testing (NDT) in order to be able to determine the existence of internal damages, like delamination, between the laminate plies. Carbon/epoxy laminates are opaque, so radiography is needed for plate damage evaluation after drilling (Marques, Durão, Magalhães, & Tavar, 2007). Another measure of delamination is the delamination area. The amount of delamination at the hole exit was characterized by the delaminated area around the hole A_d and not just by the maximum damaged diameter D_{max} . The damaged area A_d is more difficult to assess with respect to the D_{max} and delamination factor F_d (Davim, Rubio, & Abrao, 2007). Figure 30 shows two holes with the same delamination factor F_d . It is possible to notice that the magnitudes of the damaged area is completely different. This example shows that the delamination factor F_d alone is insufficient when the material generates irregular damages, especially in CFRP material.

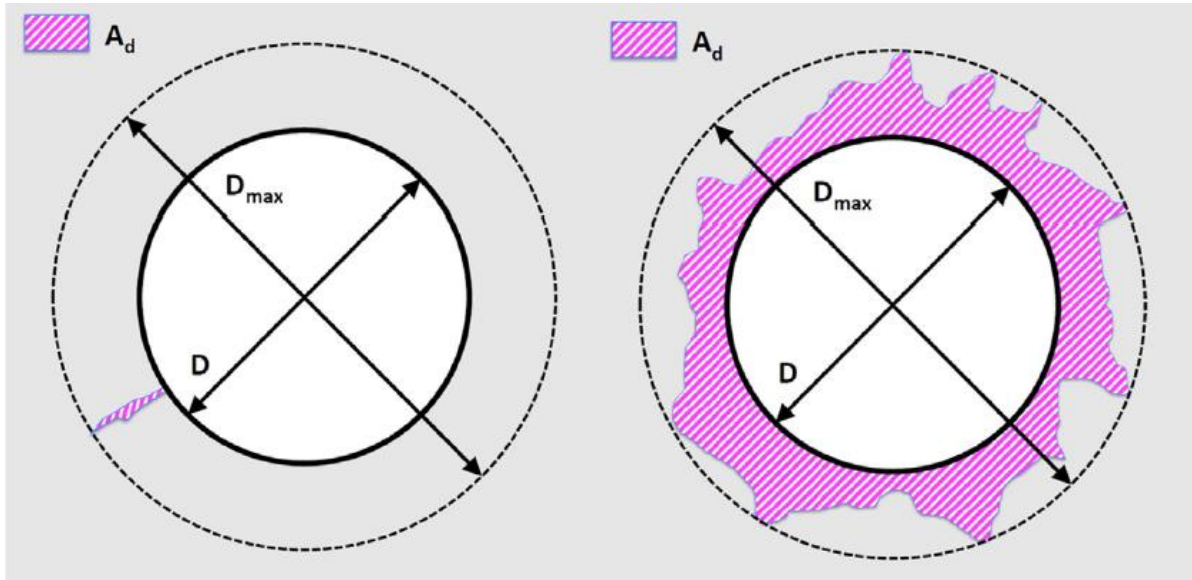


Figure 30. Representation of holes delamination factor and delaminated area (Voß, Henerichs, Rupp, Kuster, & Wegener, 2016)

Based on the delamination factor F_d formula and the damaged area around the bore (A_d), (Davim, Rubio, & Abrao, 2007) developed an adjusted delamination factor measure in order to measure the percentage of the damaged area in the circular ring:

$$F_{da} = F_d + \frac{A_d}{(A_{max} - A_0)} (F_d^2 - F_d), \quad F_d \in [1; \infty]$$

where

A_{max} is the circular area of diameter D_{max}

A_0 is the area belonging to the bore diameter D

4.5.2 Spalling and fuzzing

Due to their anisotropy, and non-homogeneity, CFRP materials cause also two of the most common defects in drilling, i.e. fuzzing (uncut fibres) and spalling (shingling) (Arul, Vijayaraghavan, Malhotra, & Krishnamurthya, 2006).

Spalling is a type of defect caused by the actions of both chisel edge and cutting edges. Some studies reveal that the spalling damages increase with the feed rate but decreases with the spindle speed. Nevertheless, the effect of the feed rate is often greater than that of the spindle speed one (Zhang L. , 2013) it develops in two stages. The first begins when the thrust force, produced by the chisel edge, reaches a critical value and ends at the time when the chisel edge penetrates through the last layer. A valid action of the chisel against the spalling can appreciate it through a photographic examination of the surface leaving the drilled material.

In the proximity of the drilling axis a small clique emerges and it grows according to the fibres direction, along the exit surface (Figure 31). Therefore there will be a rapid development of spalling, also as a result of the actions of thrust and rotation of the cutting edges, as can be seen in Figure 31 (b) and (c). The region in which there is the maximum extension of this fault is the main one, while during the cutting phase it generates a secondary region.

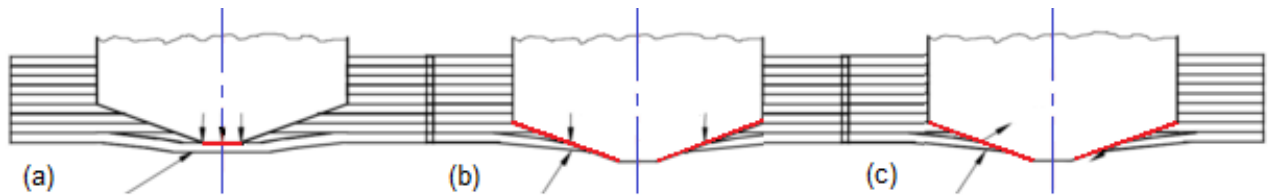


Figure 31. Formation process of the spalling defect: (a) Thrust action of the chisel edge; (b) Thrust action of the cutting edges; (c) Twist action of the cutting edges.

The following formula was used to assess the magnitude of the spalling. In the following formula, l represents the average of the spalling lengths at the two sides of the exit holes:

$$l = \frac{l_1 + l_2}{2}$$

l_1 and l_2 are shown in Figure 32.

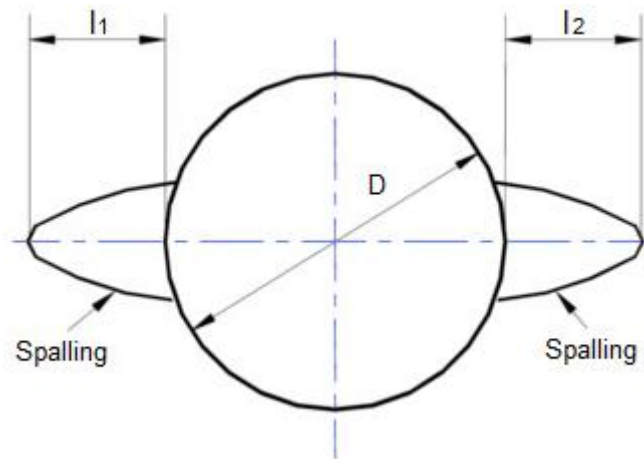


Figure 32. Spalling defect (Zhang L. , 2013)

There often exist small amount of uncut fibres nearly the edge of the hole in spalling areas. This defect is also known as fuzzing (Figure 33).

According to (Feito, Díaz-Álvarez, Díaz-Álvarez, Cantero, & Miguélez, 2014) fuzzing increased with point angle and feed.

Some of the causes are the following:

- The fibres, within the zone in which the angle between the cutting speed and the direction of the fibres is acute, are difficult to cut;
- The last surface layer at the hole exit is a free surface so that the fibres are not subjected to shear deformation.

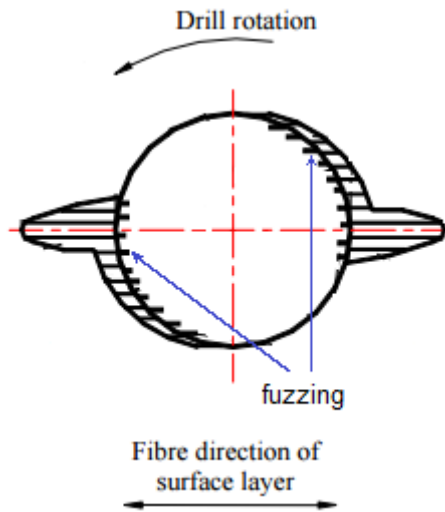


Figure 33. Uncut fibres – fuzzing (Zhang, Chen, Chen, & Zhang, 2001)

Voß, Henerichs, Rupp, Kuster, & Wegener (2016) define three parameters to measure and describe the extent of uncut fibres when drilling CFRP.

The first measure represent the relative circumferential length at 95% of D (Figure 34):

$$F_{L,95\%} = \frac{L_{95\%} - L_{f,95\%}}{L_{95\%}} \quad [0; 1]$$

where

$L_{95\%}$ is the complete circumferential length at 95% of D

$L_{f,95\%}$ represent the uncovered circumferential length at 95% of D due to the presence of uncut fibres (in red in Figure 34)

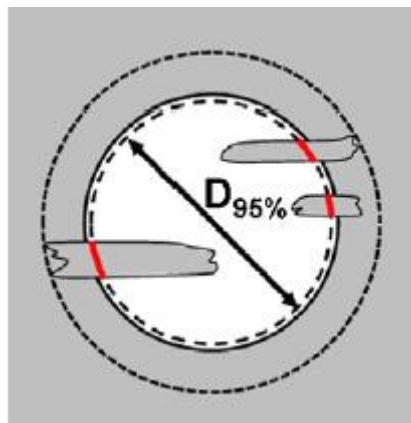


Figure 34. Covered relative circumference (Voß, Henerichs, Rupp, Kuster, & Wegener, 2016)

Another parameter, F_n , describes the number of uncut fibres.

The last parameter, $F_{A,cov}$, represents the covered relative bore area by uncut fibres (Figure 35) and it is calculated as follows:

$$F_{A_{cov}} = \frac{A_0 - A_{free}}{A_0} = \frac{A_{cov}}{A_0} \quad [0; 1]$$

where

A_0 is the circular bore area

A_{free} is the uncovered bore area

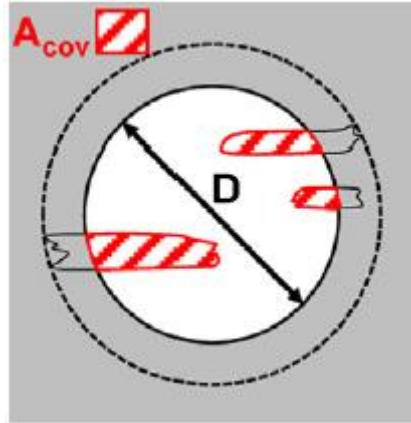


Figure 35. Covered relative bore area (Voß, Henerichs, Rupp, Kuster, & Wegener, 2016)

The delamination factor represents a good approach to easily and quickly assess the extent of delamination (Davim & Reis, 2003a; Davim & Reis, 2003b). However, as discussed in Section 4.5.1, the delamination factor is not sufficient to accurately define and measure hole quality assessment. Therefore a formula which take into account different parameters should be useful.

4.5.3 Diameter error and circularity

The dimensional accuracy of the holes was measured in terms of hole diameter error, given by the difference between actual (D_a) and nominal hole diameter (D_n) divided by nominal hole diameter (Sadek, Meshreki, & Attia, 2012):

$$D_{error} = \frac{D_a - D_n}{D_n} * 100$$

A negative error indicates an undersized hole with respect to the nominal size.

There must be paid attention also to the circularity of holes after machining. The anisotropic properties of composite materials make them difficult to machine and they are the main cause the roundness error (Piquet, Ferret, Lachaud, & Swider, 2000).

For each position of the drill's cutting edges in relation to fibre orientation, there exists a different relative reinforcement direction. Therefore such behaviour is present in each single ply of the laminate.

This defect can be carefully observed in Figure 36 where D is the diameter in practica; D_a is the actual diameter, and D_n is the nominal diameter.

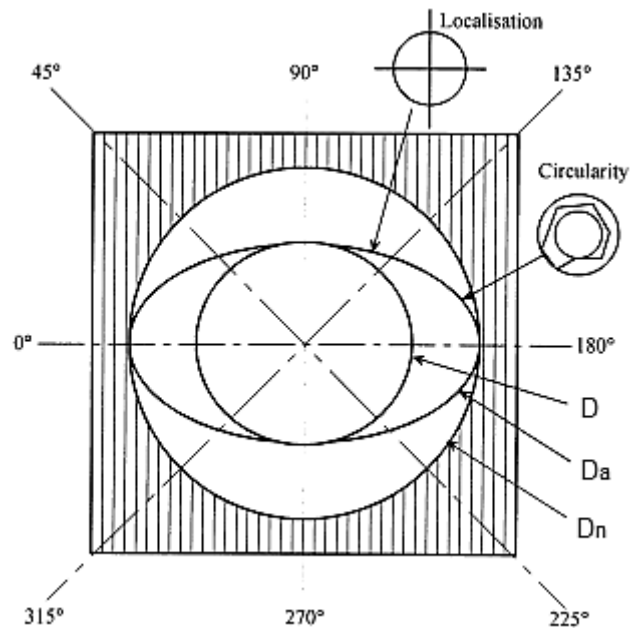


Figure 36. Hole defects observed in a unidirectional plate

4.5.4 Roughness

Drilled holes surface roughness is one another significant parameters to assess the quality of a hole.

A study conducted in 2009 (Rahman, Mamat, & Wagiman, 2009) proves that the surface roughness is mostly influenced by spindle speed and feed rate while tool diameter gives less influence on the value of surface roughness. Hence as the spindle and feed rate increases, the surface roughness will decrease.

In composite materials an excessive value of this parameter is a symptom of an incorrect execution of the hole, that is to say that the fibres are not cut in an appropriate manner. A high level of roughness of the hole compromises the mechanical properties of the laminate favouring the propagation of cracks and making the composite less inert to atmospheric agents.

In 1997 the roughness value of the inner wall of the holes was investigated using the SEM by (Ogawa, et al., 1997). It was found that the major cutting edge of the drill is more influent in the quality of the drilled hole wall than the chisel edge in small diameter drilling.

4.6 Drilling of CFRP/CFRP stacks

The aerospace industry is particularly interested in employing lightweight materials in order to reach the target in lowering costs by enhancing efficiency and reducing emissions in order to improve, i.e. decrease, global environmental impact. Notable materials that attract the aerospace industry due to the fact that they satisfy the emerging requirements of the sector are composite materials. Composite materials are notable for their high specific strength, high specific stiffness, excellent corrosion resistance and good fatigue resistance. Therefore, the employment of composite materials, especially carbon fibre reinforced plastics, in the manufacturing of new generation aircrafts has highly increased. In some cases, the percentage of carbon fibre reinforced plastics has reached up to over 50% of the whole vehicle weight. However, these carbon fibre reinforced plastics are considered to have several problems concerning low

machinability due to their physical proprieties. These plastics are anisotropic, nonhomogeneous and reinforced by abrasive fibres. These properties lead to machining issues such as rapid tool wear and can determine severe damage generation in the workpiece. The most common machining process of composite materials employed in the aerospace sector is drilling for hole-making required for riveting and fastening of aircraft assemblies. Carbon fibre reinforced plastics, better known as CFRP, are one of the most widely employed composite materials in the aerospace industry. Drilling of CFRP laminates may produce several defects such as entry/exit delamination, geometric/dimensional errors, interlaminar delamination, fibre pull-out, thermal damage. These defects can be critical to the geometrical and dimensional tolerances and surface integrity due to the tight requirements concerning those criteria in the aerospace industry. These defects may result in out-of-tolerance assembly and long-term structural properties decline. Usually, the CFRP laminates are manually drilled. The cutting tools are usually replaced well ahead with respect to the set tool wear thresholds in order to avoid damages and defects produced from tool wear and catastrophic tool failure. A way for improving the productivity and control in the aerospace manufacturing industry is automation of the drilling processes. Quality control of the machined workpiece should be carried out by adequate monitoring and control of the drilling process parameters.. An on-line real time multiple sensor monitoring of the drilling process variables is highly useful in the control and automation of the drilling processes. In this work, an intelligent sensor monitoring system is implemented with reference to the drilling process of CFRP/CFRP stack laminates for the aeronautical industry. In the following paragraphs, the experimental setup in terms of workpiece material, machine tool, drill bits as well as the plan of the experimental testing campaign are illustrated.

4.6.1 Workpiece details

The workpiece to be employed for the experimental drilling tests is represented by CFRP/CFRP stacks, with the aim to reproduce the real aeronautical industry operating conditions, in which the CFRP laminates are superimposed and then drilled together to allow for subsequent riveting. the CFRP/CFRP stacks under study are composed by two overlaid symmetrical and balanced laminates. Each laminate has a thickness of 5 mm and is made up of 26 prepreg unidirectional plies stacked according to the following sequence $[\pm 45^\circ/0^\circ/\pm 45/90^\circ/\pm 45^\circ/0^\circ/-45^\circ/90^\circ/45^\circ/90^\circ]_s$. A very thin fiberglass/epoxy ply, reinforced with $0^\circ/90^\circ$ fabric (areal weight 80 g/m²) is laid on the top and bottom of each laminate. The prepreg plies are made of Toray T300 carbon fibres and CYCOM 977-2 epoxy matrix. Laminates were fabricated by hand layup, vacuum bag moulding (Figure 37a) and autoclave curing (180 min at 180 °C and 6 bar) (Figure 37b).

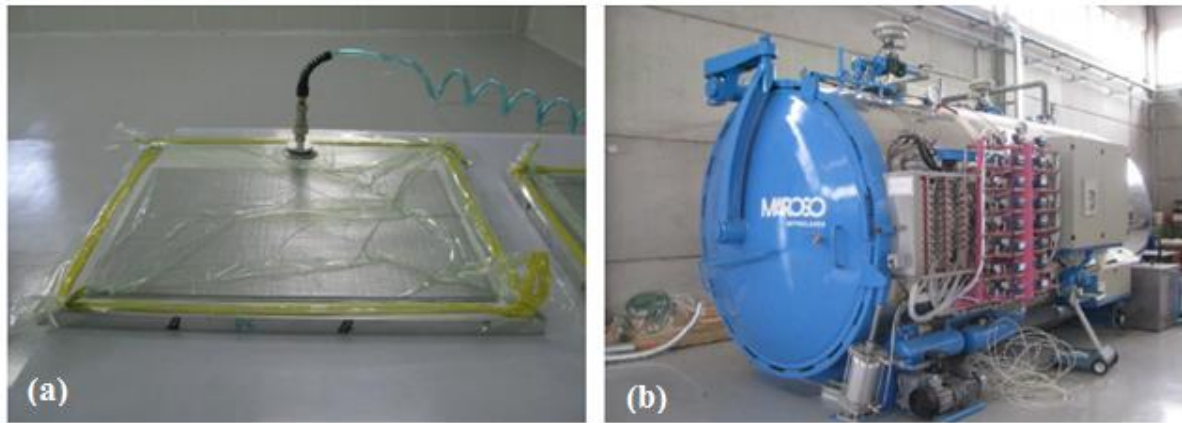


Figure 37. (a) Vacuum bag moulding; (b) Autoclave

The surface texture of the laminates on the bag side is very irregular compared to the mould side. Therefore, the two CFRP laminates of each stack were placed with the bag side in contact in order to realize the drilling process in the severest possible conditions. Figure 38 shows the surface texture on the bag side and the mould side as well as the stratification of the laminates.

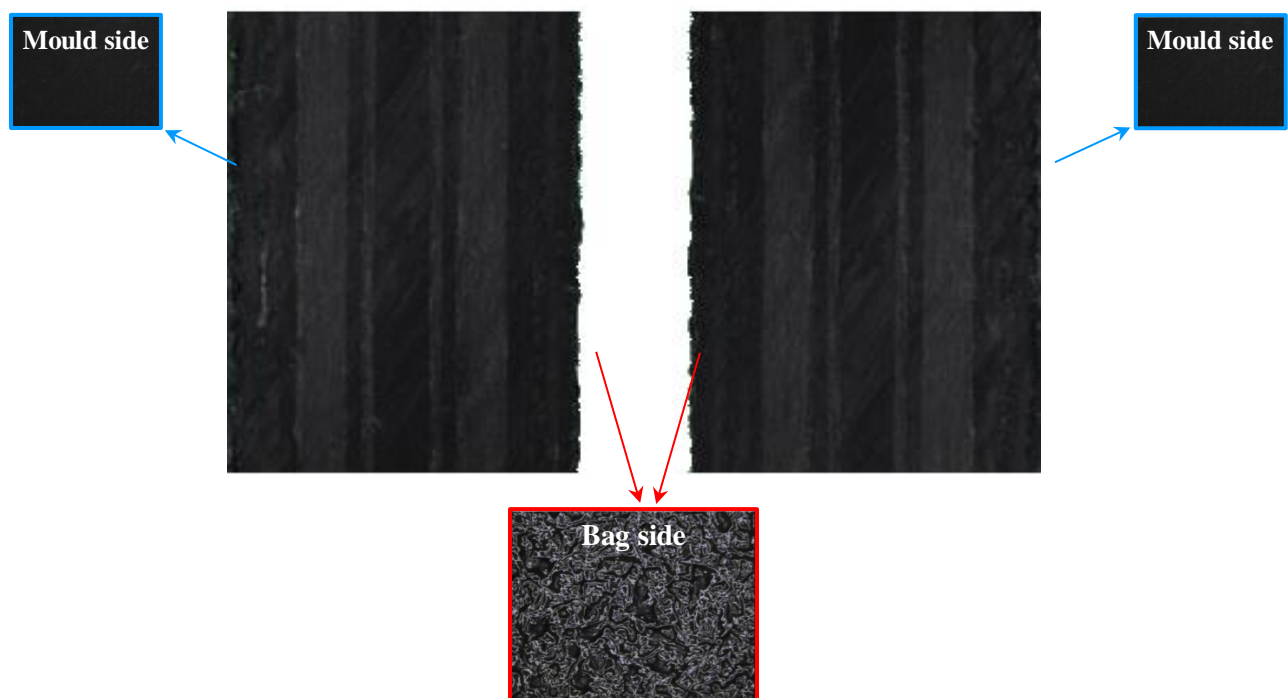


Figure 38. Laminates profiles and their surface textures

4.6.2 Experimental procedure

In order to identify the influence of the cutting parameters on the machinability of the composite material under study in terms of tool wear and quality of the holes, different cutting conditions were adopted for the experimental drilling tests: three feed values (0.11 mm/rev, 0.15 mm/rev and 0.20 mm/rev) and three different spindle speeds (2700 rpm, 6000 rpm and 9000 rpm) were employed, as shown in Table 16. For each experimental condition, 60 consecutive holes were realized with the same drill bit.

Table 16. Experimental testing conditions

		Spindle Speed (rpm)		
		2700	6000	9000
Feed (mm/rev)	0.11	-	x	-
	0.15	x	x	x
	0.20	-	x	-

A 2-flute 6.35 mm diameter with 125° point angle twist drill made of tungsten carbide (WC) was used in the experimental campaign. Figure 39 reports a microscopic view of the tool before drilling. The CNC drilling centre and the sensors used for the monitoring of CFRP/CFRP stacks drilling have been reported in Figure 40.

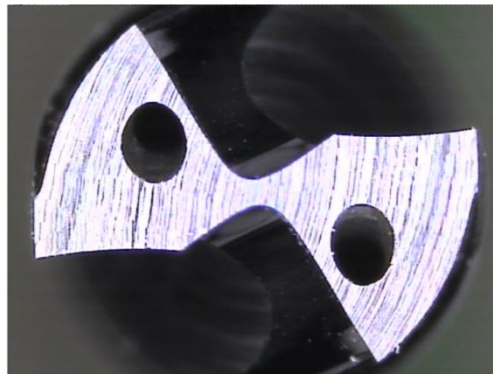


Figure 39. Drill bit geometry

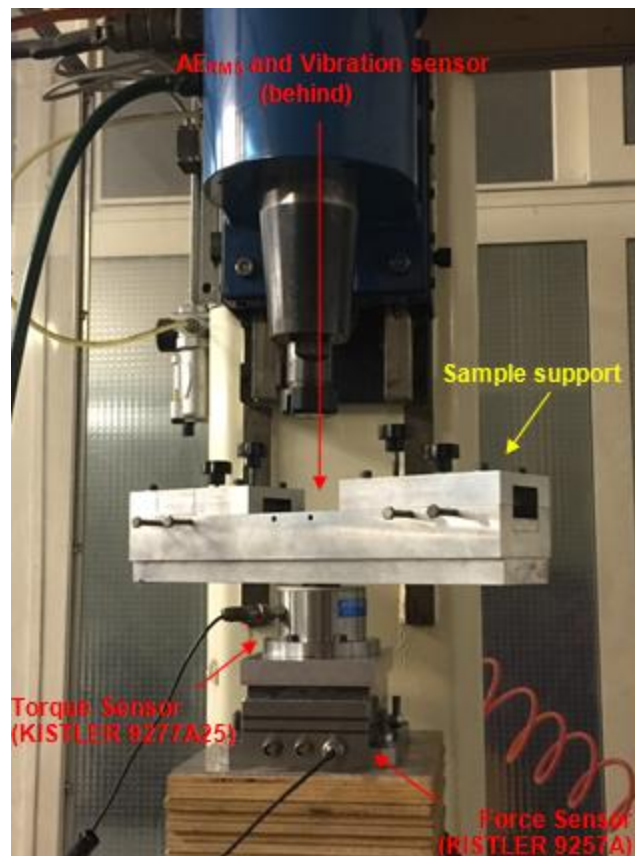


Figure 40. Drilling centre used for the experimental campaign

The thrust force and cutting torque were measured using two Kistler piezoelectric dynamometers, respectively the model 9257A and the model 9277A25. The Acoustic Emission (AE) RMS and acceleration of vibrations have been acquired by the Montronix® BV100-AX sensor.

4.7 Multiple sensor monitoring system

The multiple sensor monitoring system employed during the experimental drilling tests comprised the following sensors:

- Force sensor;
- Torque sensor;
- Acoustic Emission (AE) sensor;
- Vibration Acceleration sensor.

Force and Torque sensor

A Kistler-9257A piezoelectric dynamometer was employed to acquire the thrust force along the z-direction, F_z (Figure 41a). The cutting torque about the z axis, M_z , was acquired using a Kistler-9277A25 piezoelectric dynamometer (Figure 41b).

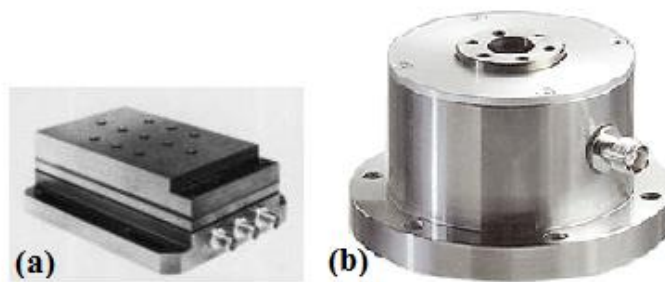


Figure 41. (a) Kistler-9257A piezoelectric dynamometer; (b) Kistler-9277A25 piezoelectric dynamometer

Two Kistler 5007 amplifiers (Figure 42) were employed for the force and torque signals. The time constant setup was set to “long”. The selected scale in mechanical unit (M.U.) / V was 100. Calibration was necessary for both force and torque after each single drilling test. The transducer sensitivity values to be set are suggested by the technical data sheets of the two piezoelectric dynamometers. As regards force, the values are equal to $-7.5 \text{ pC} / \text{N}$ for the force components along the x and y axes, F_x and F_y , and $-3.5 \text{ pC} / \text{N}$ for the force component along the z axis, F_z , which represents the thrust force of the drilling process. Conversely, the value to be set for the torque component about the z axis, M_z , is $-2.5 \text{ pC} / \text{Ncm}$.



Figure 42. Kistler 5007 amplifiers

Acoustic Emission and Vibration acceleration sensor

The acoustic emission and vibration acceleration signals were acquired using the Montronix BV100™ broadband vibration sensor, provided with two channels to measure both the vibrations and the high frequency acoustic emission (AE) signals. (Figure 43a). The analogue acoustic emission and vibration acceleration sensor signals were then amplified by a Montronix TSVA4G amplifier (Figure 43b). The AE amplifier specifications are reported in the following Table 17.

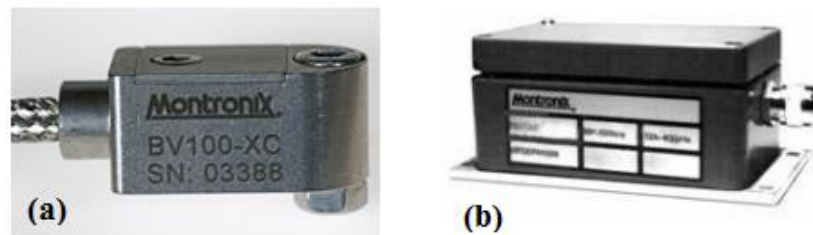


Figure 43. (a) Vibration and high frequency Acoustic Emission sensor - Montronix BV100™; (b) Montronix TSVA4G amplifier

Table 17. AE Amplifier Specifications

Gain Settings:	1, 2, 5, 10, 20, 40, 80, 200, 400, 800
Gain Error	±2%
Output Voltage	0 to 10 V
Power provided to Sensor	+ 15 VDC @ 4mA constant current
Amplifier Power Requirements	+15 VDC @ 80mA -15 VDC @ -60 mA
Temperature Range	0° to 60° C
Connectors	PG9 threaded fittings, sensor-specific
Weight	680 g

The amplifier was configured with the settings reported in Figure 44.

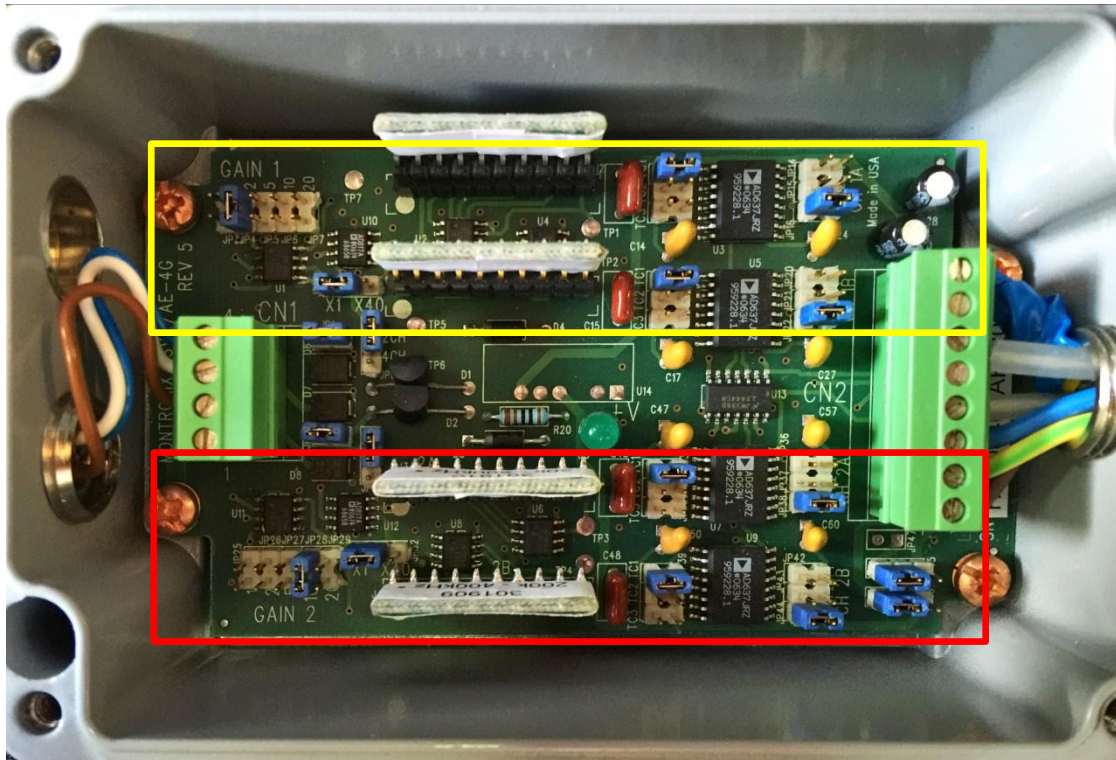


Figure 44. Acoustic Emission and Vibration Acceleration amplifier settings

The amplifier has two channels:

- the yellow on the top (channel 1) is dedicated to the Acceleration signals amplification
- the red on the bottom (channel 2) is dedicated to the AE signals amplification

The gain set for Acceleration signals is equal to 2 while the gain set for the AE_{RMS} signals is equal to 10 in order to properly visualize the signals without exceeding the maximum threshold of 10 V imposed by the data acquisition (DAQ) board.

Both the AE and Acceleration signals have been acquired as Root Mean Square (RMS) signals. RMS is a technique used to rectify a RAW signal and convert it to an amplitude envelope, which is easier to view. The rectification process converts all the numbers into positive values rather than positive and negative.

During the experimental tests the RMS conversion time constant was set to $TC1 = \text{short}$, corresponding to a time constant of 0.12 ms.

The output low-pass filter cut-off frequency was set to $F3 = \text{high}$ for both channels.

Signal Acquisition

The analogue signal from the Thrust Force, cutting Torque, Vibration Acceleration and AE_{RMS} sensors were digitalized by the National Instruments DAQ device NI USB-6361 (Figure 45). The specifications of the device are reported in Table 18.



Figure 45. Data acquisition device - NI USB-6361

Table 18. Data acquisition device NI USB-6361

Analog Inputs (AI)	16
Max AI Sampling Rate (1-Channel)	2MS/s
Max Total AI Throughput	2MS/s
Analog Outputs (AO)	2
Max AO Update Rate	2.86 MS/s
Digital I/O Lines	24
Max Digital I/O Rate	10 MHz
Triggering	Analog, Digital

According to the Nyquist-Shannon sampling theorem, the sampling rate was set equal to 10kHz. The sampling theorem provides a prescription for the nominal sampling interval required to avoid aliasing, i.e. the effect that causes different signals to become indistinguishable when sampled. The theorem states that *the sampling frequency should be at least twice the highest frequency contained in the signal*:

$$f_s \geq 2 * f_c$$

where:

f_s is the signal sampling frequency and f_c is the highest frequency observed in the signal.

The data acquisition software used is the NI SignalExpress 2014. The software allows to quickly acquire, analyse and visualize data using the software interface shown in Figure 46.

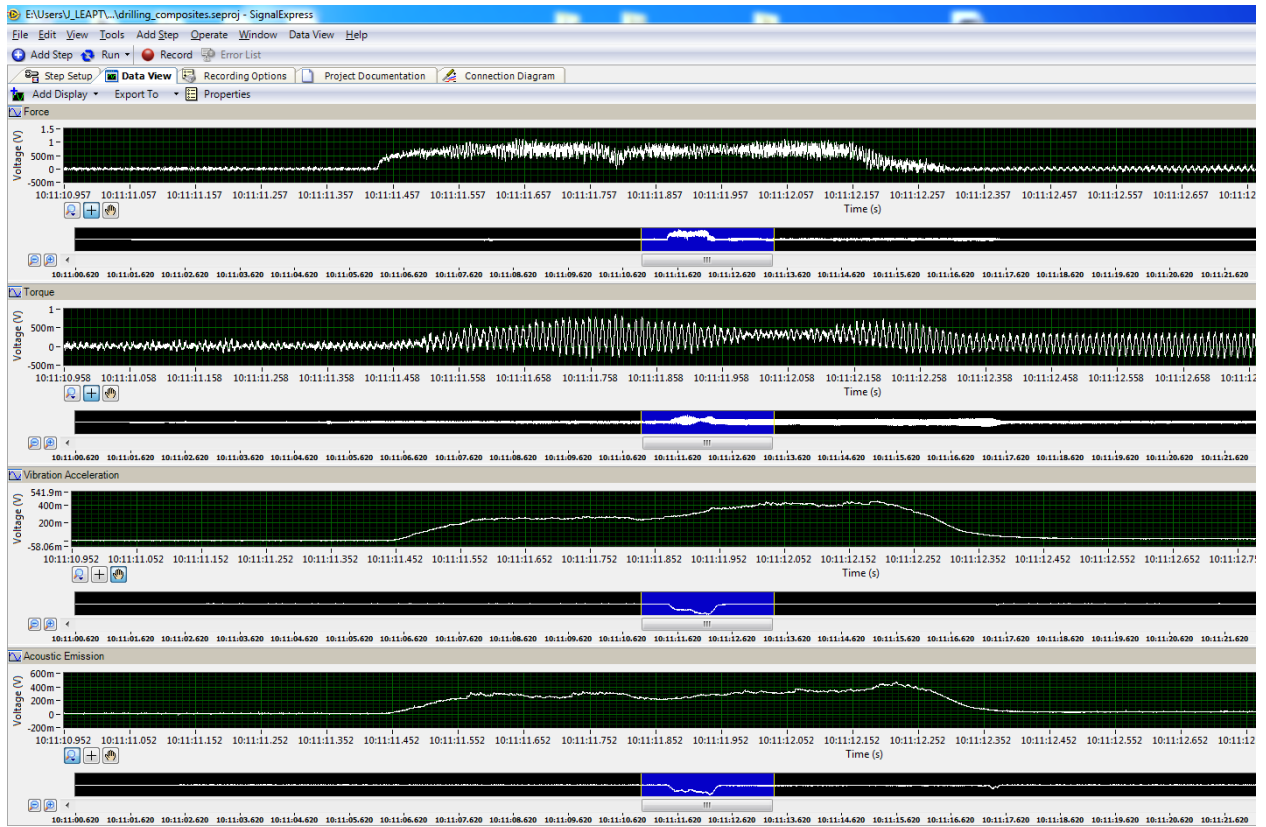


Figure 46. NI SignalExpress software interface

4.8 Advanced signal processing

The file format of the data acquired using NI SignalExpress is *tdms*. In order to process the signals in MATLAB it was necessary convert them into *mat* files.

Each mat file contains 5 columns: *Sample Time*, *Thrust Force Values*, *Torque Values*, *Acoustic Emission RMS values* and *Vibration Acceleration values*.

The raw sensor signals acquired during the drilling tests included portions corresponding to the time instants before and after the actual machining process. With the aim to extract information only when the tool is actually removing material, signal conditioning was carried out in the following way (Teti, Jemielniak, & O'Donnell, 2010) : examination of the raw signal to identify the actual machining portions; removal of the initial and final signal portions, and final verification and acceptance of the conditioned signal (Figure 47). The identification of the start and end of the actual machining portion was carried out on the basis of thresholds fixed on the moving average of the thrust force signals. The torque, the AE_{RMS} and the vibrations acceleration signals were segmented at the same start and end points of the thrust force signal, completing the full set of conditioned signals from a given drilling test with equal duration and number of samplings.

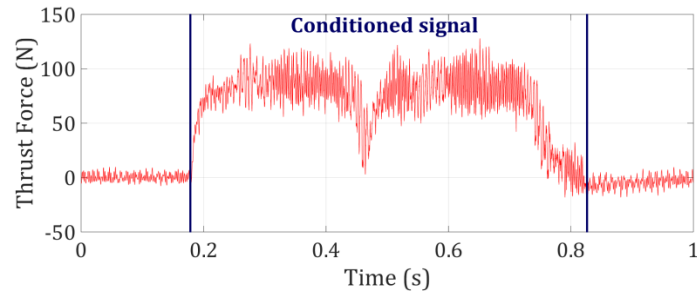
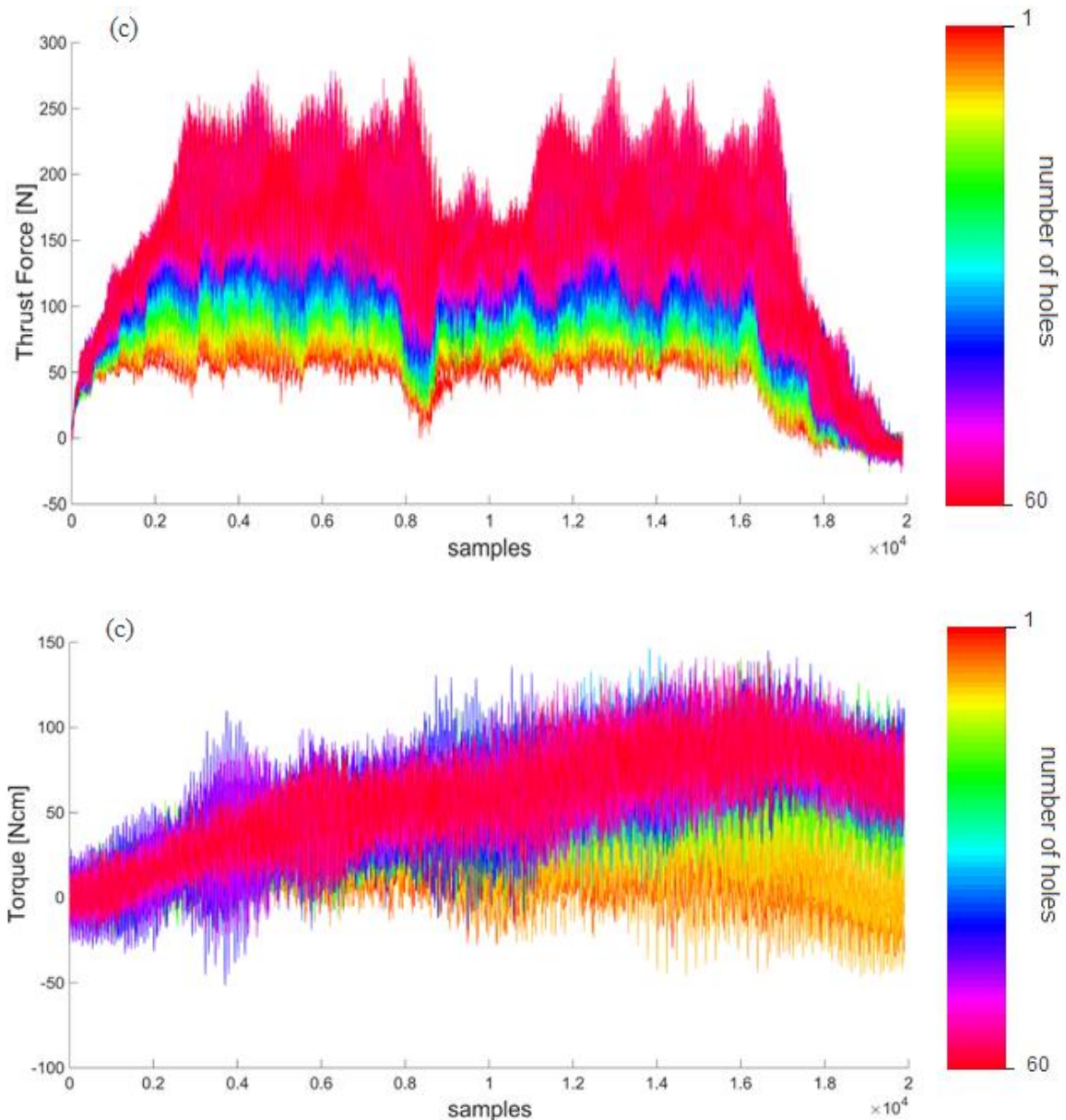


Figure 47. Thrust force raw signal and its corresponding conditioned signal for hole n. 6 (6000 rpm, 0.20 mm/rev).

Figure 48 a,b,c,d shows the plots of the thrust force, torque, acoustic emission and vibration acceleration signals as a function of the number of holes for the operating conditions 6000 rpm – 0.15 mm/rev. The plots relative to the other operating conditions listed in Table 16 are reported in APPENDIX B.



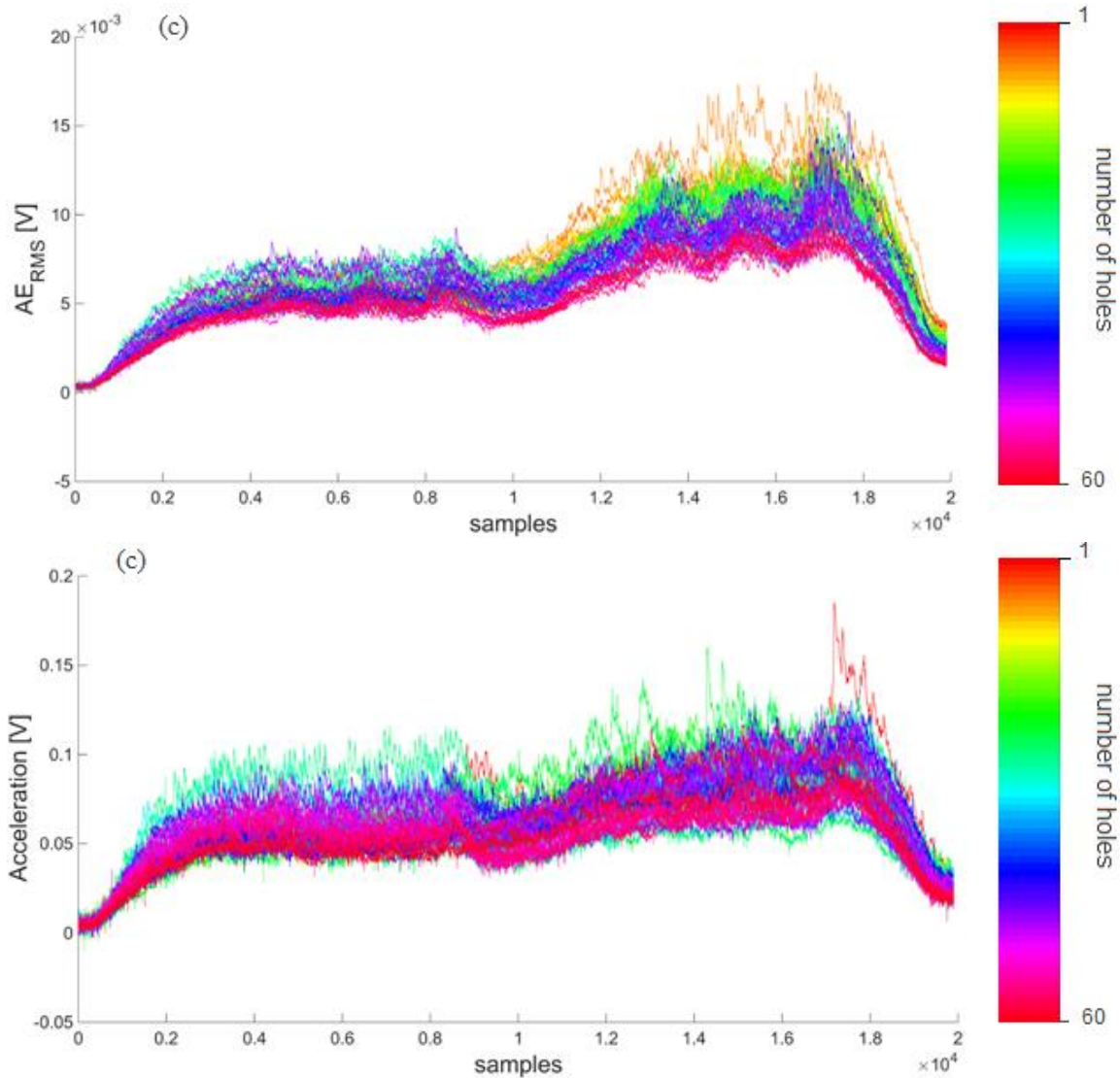


Figure 48. (a) thrust force; (b) torque; (c) acoustic emission; (d) vibration acceleration - operating conditions 6000 rpm – 0.15 mm/rev

4.9 Features extraction

To find correlations between sensorial data, tool state and hole quality assessment, advanced signal processing, based on signal conditioning, feature extraction and data fusion, was applied to the multiple sensor signals acquired through the monitoring system.

4.9.1 Time domain features

Signal analysis in the time domain was performed to extract a number of conventional statistical features from each dataset. The following statistical features were extracted (Binsaeid, Asfour, Cho, & Onar, 2009; Teti, Jemielniak, & O'Donnell, 2010):

- Arithmetic Mean: The mean of amplitude values of raw data signal. It represents the central value of a discrete set of numbers;
- Variance: The variance of amplitude values. It measures how far a set of numbers is spread out;
- Kurtosis: Fourth central moment. It is a measure of the “peakedness” of the probability

distribution of the signal raw data;

- Skewness: The 3rd central moment. It is a measure of the asymmetry of the probability distribution of the signal raw data;
- Signal Power: it is defined as the measured area under the rectified signal envelope. This is another measurement of the signal amplitude; however, it is sensitive to amplitude as well as duration, and it is less dependent on operating frequency.

The above described features have been plotted for each operating condition and for all the 60 drilled holes. The following figures report, as an example, the values of the statistical features related to the thrust force as a function of the number of drilled holes (Figure 49). From a simple visual examination, the values of some of the statistical features seem to increase with increasing number of holes.

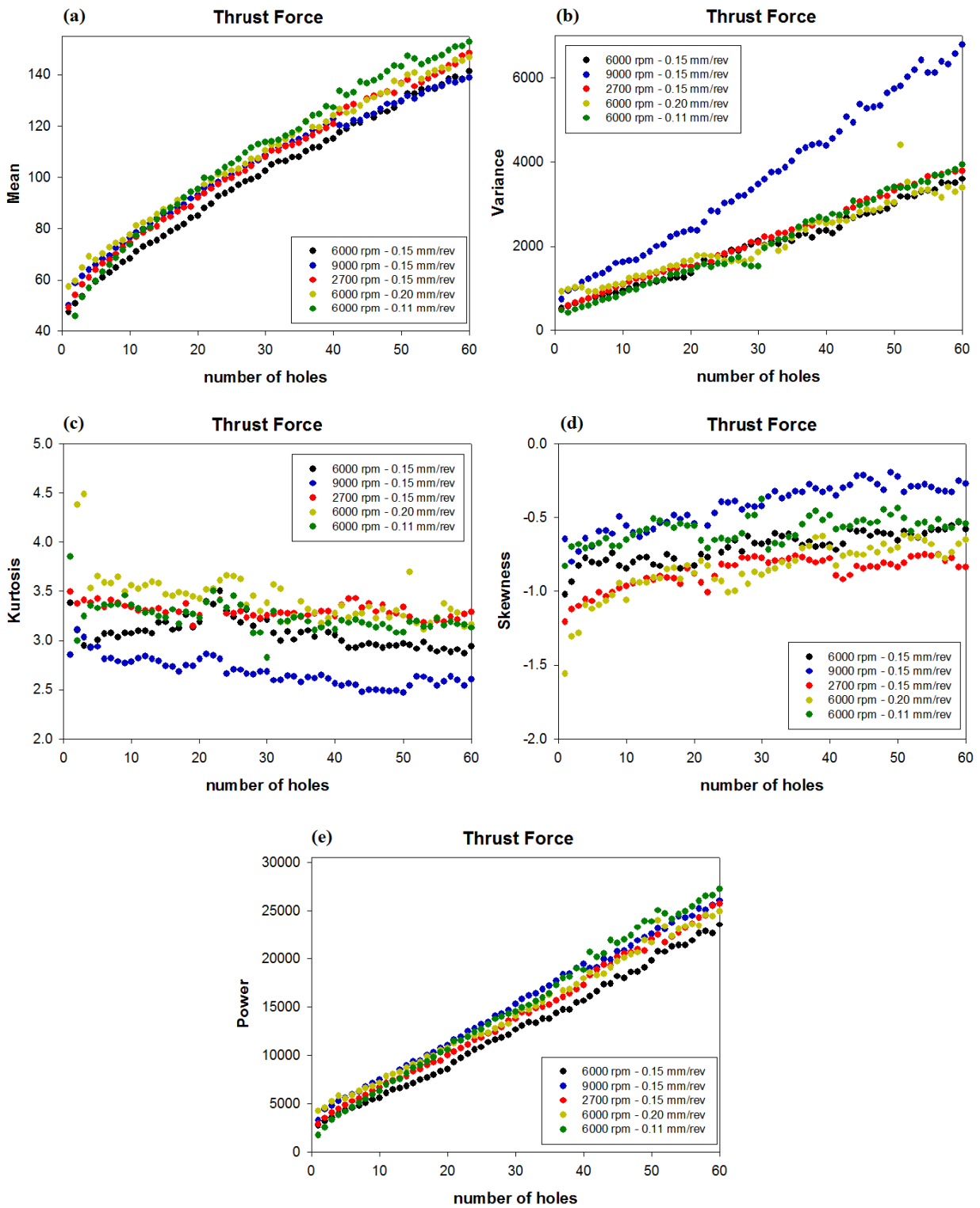


Figure 49. Thrust force statistical features plots for all operating conditions: (a) Arithmetic Mean; (b) Variance; (c) Kurtosis; (d) Skewness; (e) Power

4.9.2 Frequency domain features

In order to complete the signals analysis, a number of frequency domain features were calculated using the fast Fourier Transform (FFT). More specifically there is a relationship between the peaks obtained in the fft and the influence of fibre cutting angle during the drilling process. Using the MATLAB function *fft*, the discrete Fourier Transform was calculated for each signal

type: Force (Figure 50), Torque, AE_{RMS} and Acceleration. The *fft* function was used to convert the signal to the frequency domain, so the new input length, that is the next power of 2 from the original signal length (*nextpow2*), was identified. This will pad the signal X with trailing zeros in order to improve the performance of *fft*.

The following parameters were used:

```

Fs = 10000;           % Sampling frequency
T = 1/Fs;             % Sampling period
L = length(Curr_Force) % Length of signal (depends on the operating
                      % conditions)

```

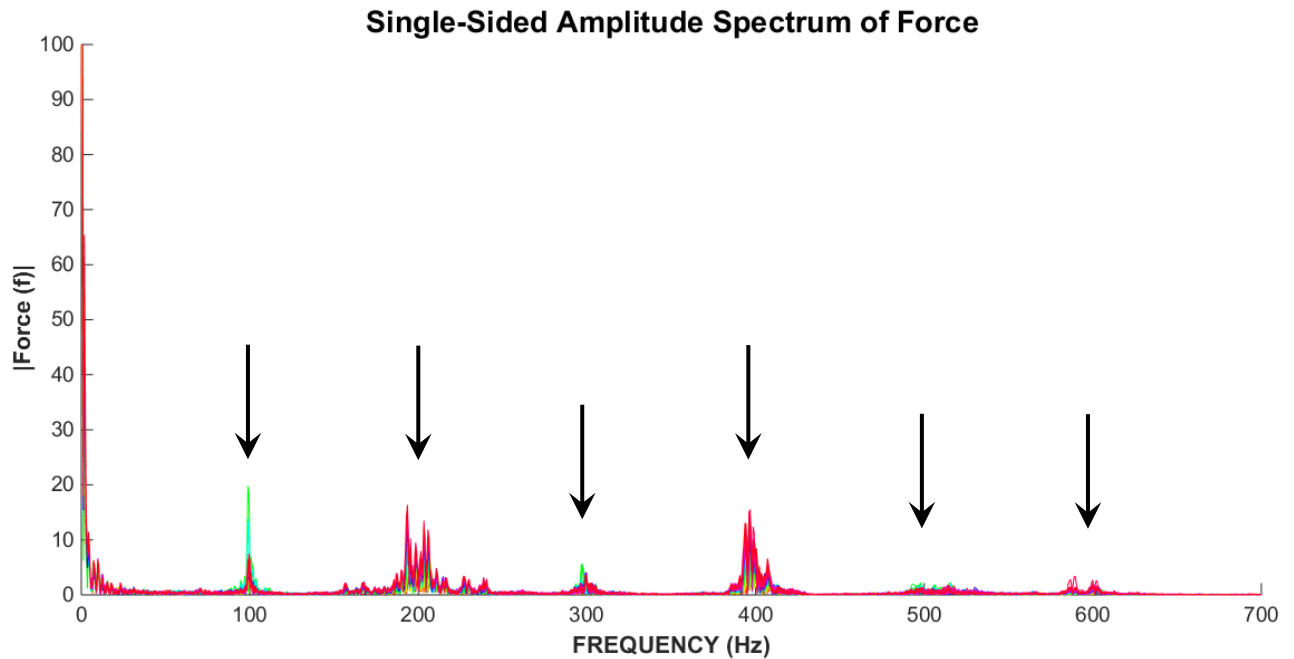


Figure 50. Single-Sided Amplitude Spectrum of Force (6000 rpm – 0.15 mm/rev)

As reported in Figure 50, the Single-Sided Amplitude Spectrum of Force highlights the presence of some peaks corresponding to different frequency values. Therefore, the peak analysis was conducted to investigate the evolution of the peaks with increasing number of holes. In particular, the frequency peaks corresponding to 1, 2, 3, 4, 5, 6 times the revolution frequency of the drill bit proved to be relevant for the sensor signals.

Figure 51 shows the values of the peaks at 100, 200, 300, 400, 500 and 600 Hz as a function of the number of holes for the experimental test performed at 6000 rpm and 0.15 mm/rev (the revolution frequency in this case is equal to $6000 \text{ rpm} / 60 = 100 \text{ Hz}$). From a simple visual examination of Fig. 50, the amplitude of some of the peaks seem to increase with increasing number of holes. The statistical based procedure implemented for the selection of the most relevant features among those extracted in the time domain as well as in the frequency domain is illustrated in paragraph 4.12 of this chapter.

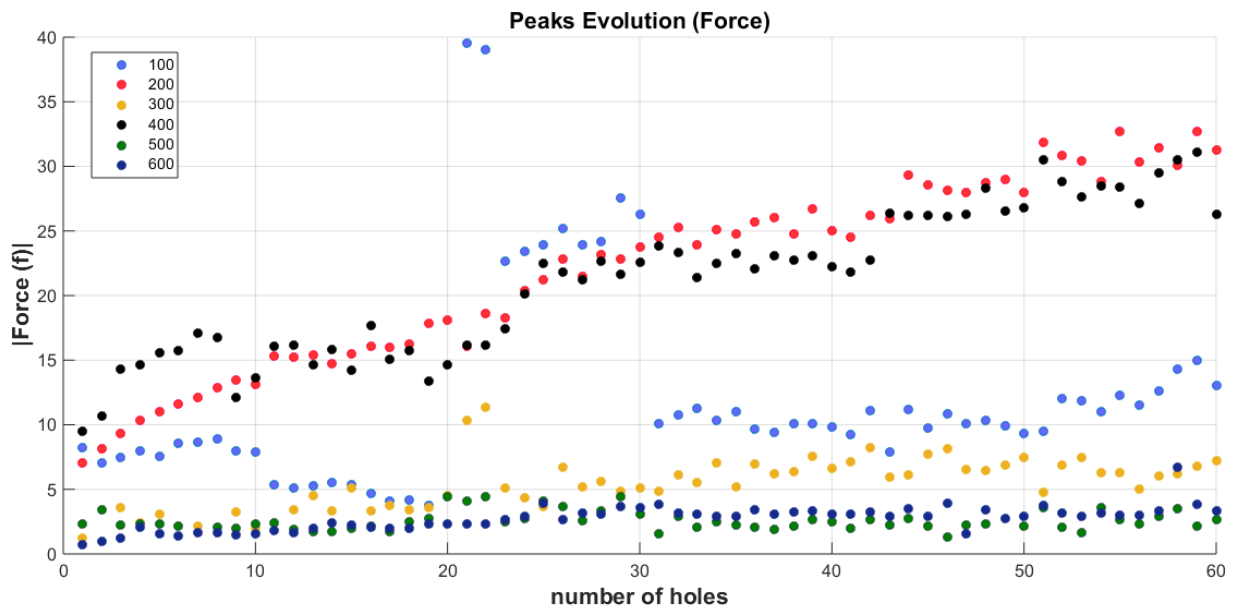


Figure 51. Evolution of peaks detected in frequency domain using discrete Fourier Transform (6000 rpm – 0.15 mm/rev)

4.10 Tool wear

According to the literature, the most widely used parameter for the monitoring of the tool wear during drilling operations is the flank wear (Park, Beal, Kim, Kwon, & Lantrip, 2013; Zitoune, El Mansori, & Krishnaraj, 2013; Sousa, Sousa, Jackson, & Machado, 2014), in terms of VB and VB_{max} values in mm.

To measure flank wear of the drill bits during the experimental drilling tests, a Tesa Visio V-200 optical measuring machine (Figure 52a) was employed. Tools have been settled on a support (Figure 52b) to make the measuring process repeatable and the drills have been notched to identify the left and right side.

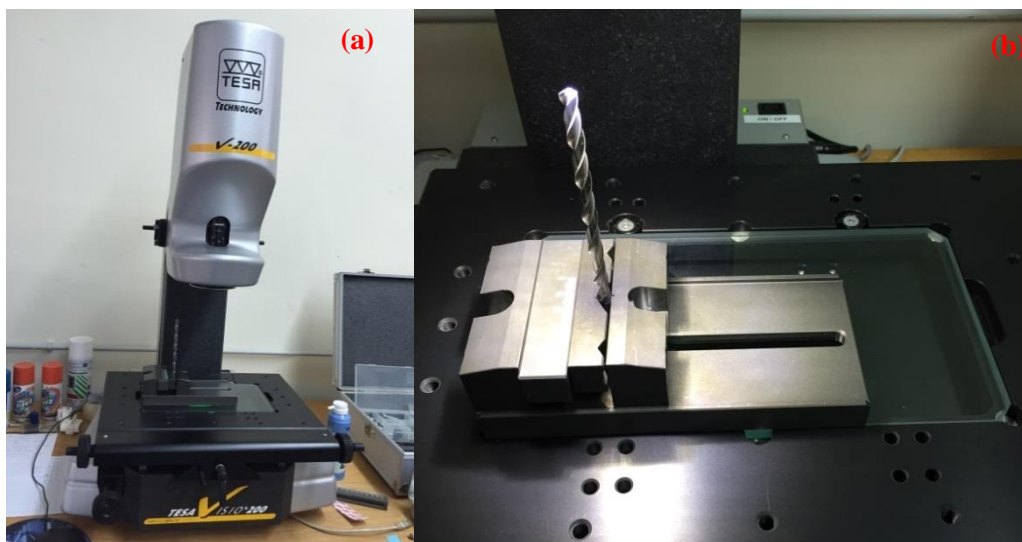


Figure 52. (a) drill secured in the vine; (b) optical measuring machine Tesa Visio V-200

In order to evaluate the tool wear, after every 10 consecutive drilled holes the flank wear (VB and VB_{max}) was measured. The VB (mm) and VB_{max} (mm) were evaluated according to the reference proposed by Dolinšek & Kopač (1999) and Dolinšek, Šuštaršič, & Kopač (2001) and calculated for both left and right cutting edges as in Figure 53.

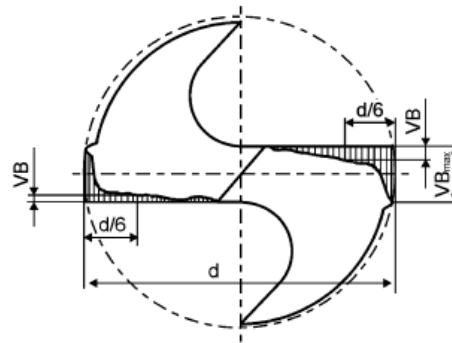


Figure 53. Tool wears types for the determination of tool-life during drilling (Dolinšek, Šuštaršič, & Kopač, 2001)

For each drilling condition, 6 VB and 6 VB_{max} values were obtained to describe the tool wear development. The values have been plotted with 5 different colours corresponding to each experimental testing condition in Figure 54.

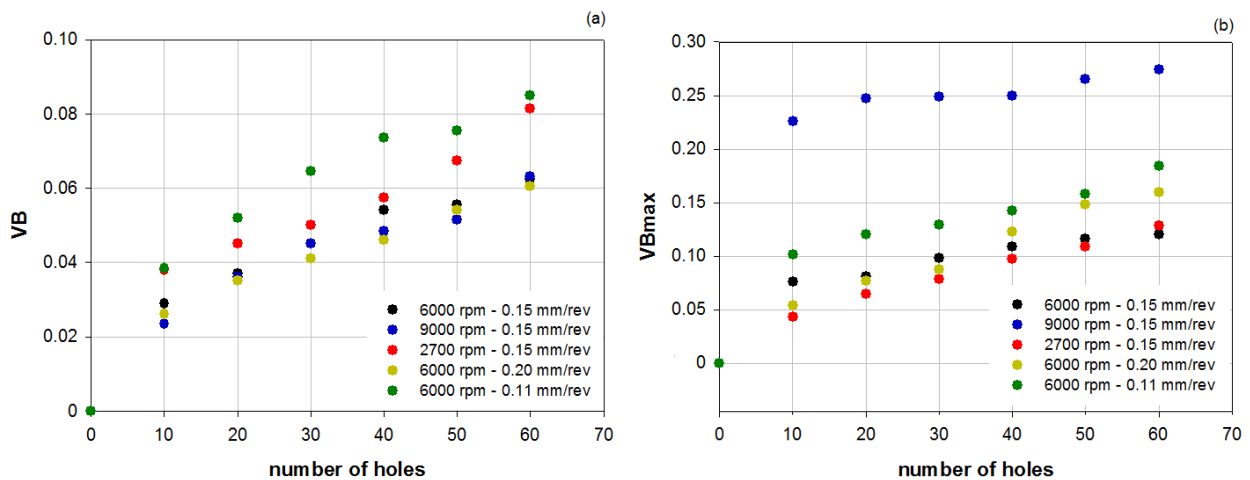


Figure 54. Measured flank wear values: (a) VB and (b) VB_{max}

It is possible to notice that there is a rising trend in the evolution of tool wear in each operating conditions. A 3rd order polynomial interpolation of the VB values was applied to construct the tool wear curves (Figure 55) and to correlate the sensor signals and the tool wear.

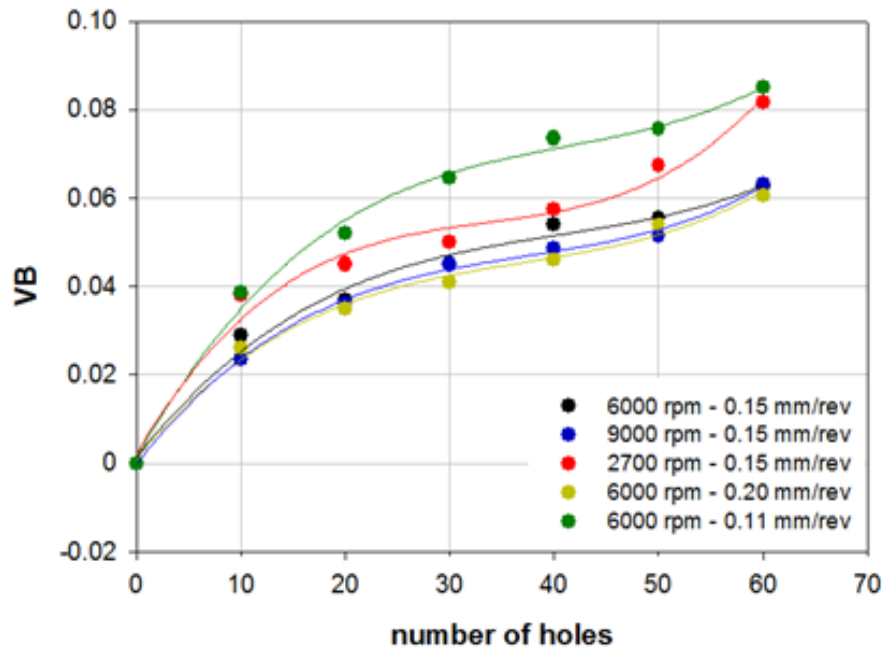


Figure 55. Measured flank wear values and interpolated tool wear curves

4.11 Hole quality assessment

For each drilling condition both entry and exit delamination were estimated. The delamination damage (entry and exit) was estimated in terms of delamination factor, F_d , according to the following relationship proposed by Chen (1997):

$$F_d = \frac{D_{max}}{D_a}$$

The holes delamination measures were evaluated using the Tesa Visio V-200 optical measuring machine. Figure 56 reports the images of the 1st, 30th and 60th hole at the top of the stacks. Figure 57 reports the images of the 1st, 30th and 60th hole at the bottom of the stacks.

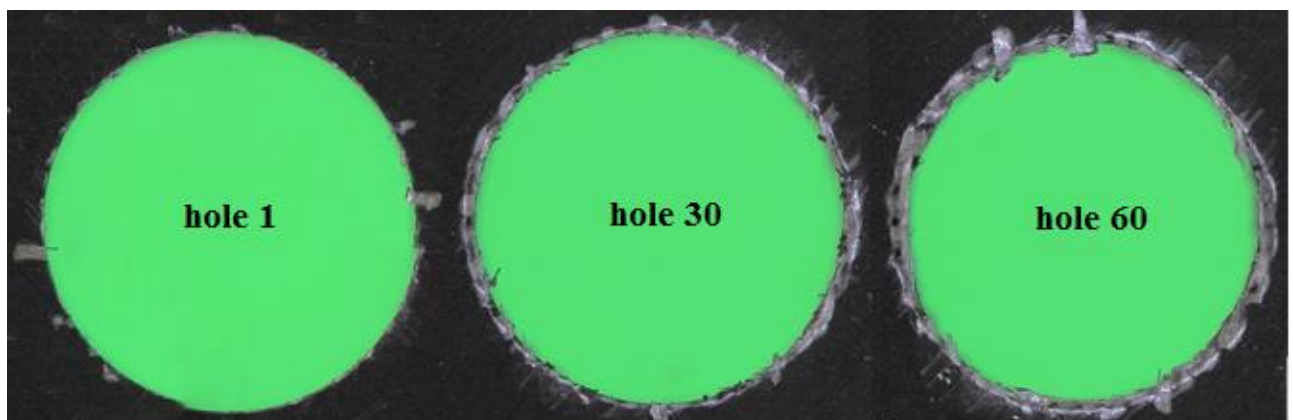


Figure 56. Entry delamination (6000 rpm - 0.20 mm/rev) for holes 1,30 and 60

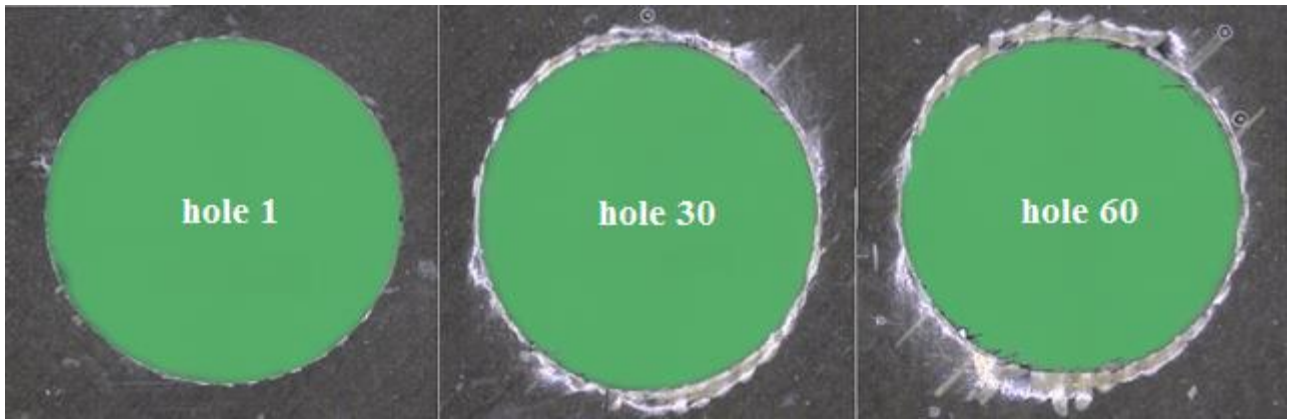


Figure 57. Exit delamination (6000 rpm - 0.20 mm/rev) for holes 1,30 and 60

It can be noticed that for each drilling condition, the entry delamination remained approximately constant or shows no significant trend with increasing number of holes (Figure 58a), whereas the exit delamination showed a significant growth with the number of holes (Figure 58b).

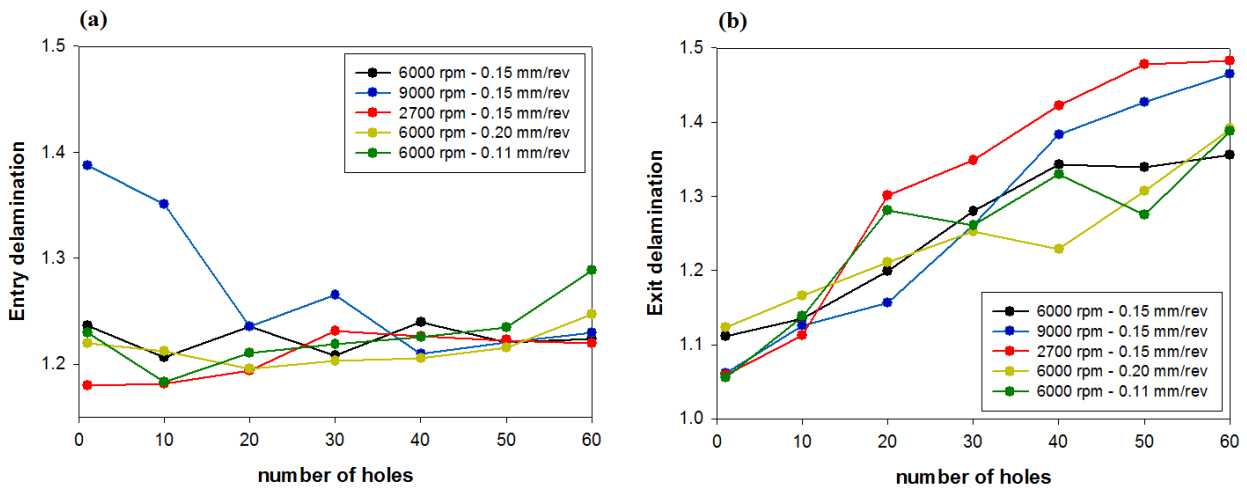


Figure 58. (a) Measured entry delamination; (b) Measured exit delamination

The delaminated area assessment, expressed in mm^2 , was also calculated for each exit hole (Figure 59) and plotted versus the number of holes Figure 60.

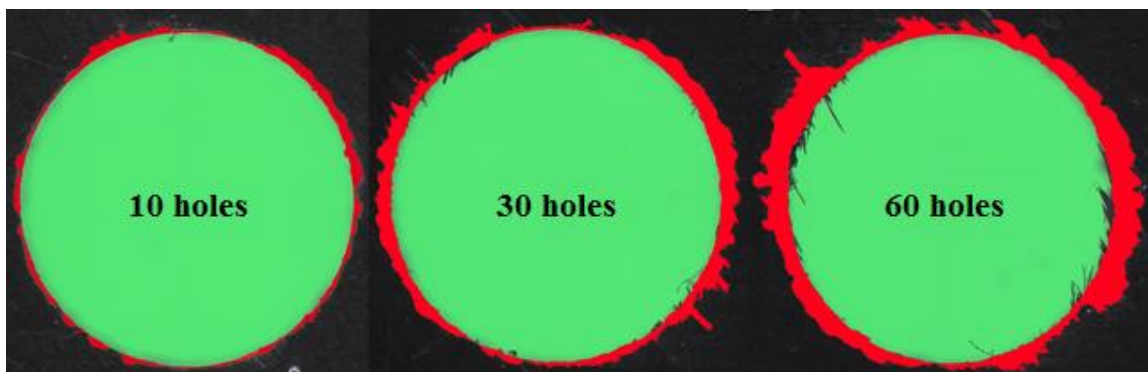


Figure 59. Delaminated area (6000 rpm - 0.20 mm/rev) for holes 1,30 and 60

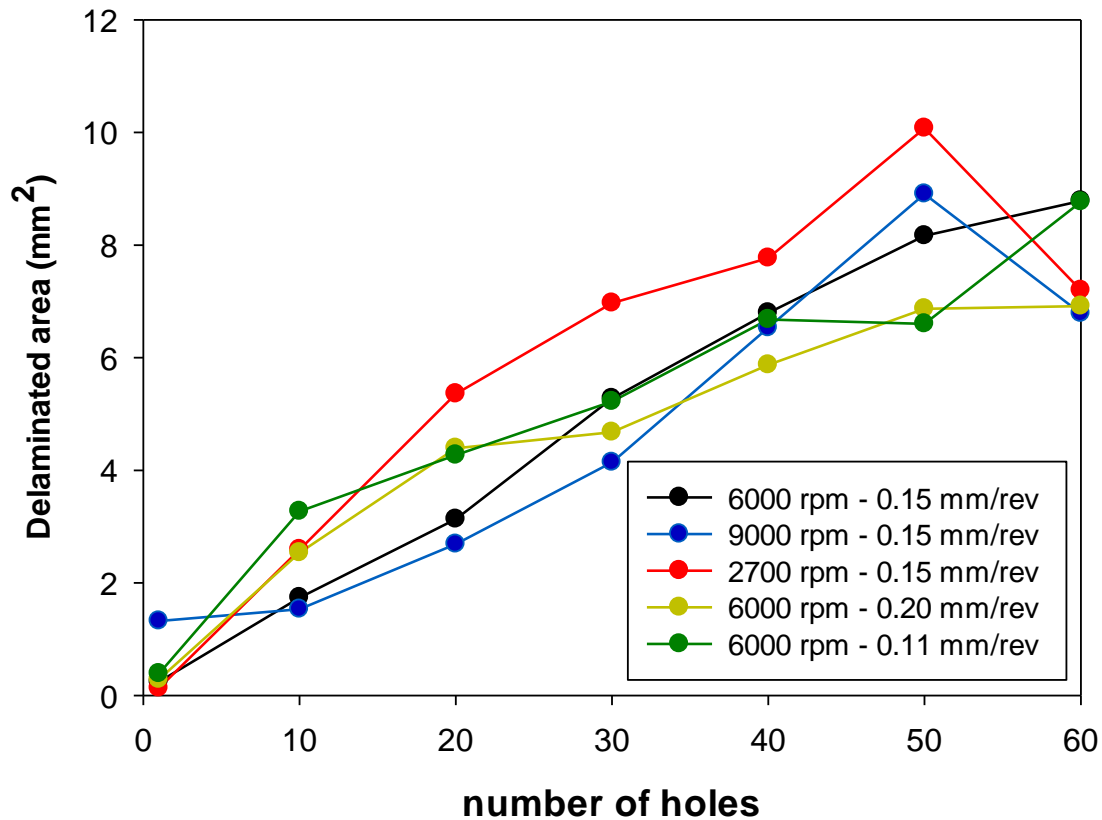


Figure 60. Measured delaminated area

4.12 Features selection

With the aim to find correlations between the features extracted from the acquired sensor signals and the process conditions, an advanced sensor monitoring procedure based on sensor fusion approach is implemented in this work. Sensor fusion is realized by combining features from sensor signals of different nature to construct Feature Pattern Vectors (FPVs) that can be fed to cognitive paradigms for pattern recognition and decision making. The number of features of a FPV is a key factor that determines the size of the hypothesis space containing all hypotheses that can be learned from data (Hastie, Tibshirani, & Friedman, 2001). The more the features, the larger the hypothesis space, e.g. the linear increase of the number of features leads to the exponential increase of the hypothesis space.

Moreover, not all the extracted features may be relevant to the pattern recognition output, and they may even include undesired noise.

Therefore, feature selection is necessary to choose the most relevant features with reference to the output of interest. In this work, a statistical feature selection procedure based on the calculation of the statistical correlation between the extracted features and output parameters has been investigated.

The statistical procedure highlights significant positive correlations between both the time and frequency domain features described in the previous sections and tool state and quality assessment (see APPENDIX C for a detailed analysis of correlations).

To investigate whether the correlation coefficient between the two measures is statistically significant, t-test has been applied. Specifically, to test the null hypothesis (H_0) that the couples of the measures are not correlated, the test statistic is calculated using Student's t-distribution with $\nu = n - 2$ degrees of freedom. More specifically, the correlation coefficient, r , was calculated in terms of the Pearson correlation coefficient as follows:

$$r = \frac{\sum(x_i - \bar{x}) - (y_i - \bar{y})}{[\sum(x_i - \bar{x})^2 \sum(y_i - \bar{y})^2]^{1/2}}$$

The t value was calculated according to the following formula:

$$t = \frac{r}{\sqrt{1 - r^2}} * \sqrt{n - 2}$$

The critical value depends on the number of samples, n , and the desired confidence interval $1-\alpha$. For the case under study, in which $n=60$ and $1-\alpha=0.99$, the critical value $t_{60;0.99}$ is equal to 2.39. Therefore the acceptance region is $-t < 2.39 < t$.

The selection of features has been achieved in two ways: at first, all the features meeting the t-test correlation criterion were selected, secondly a minimum subset of features without learning performance deterioration was selected in order to avoid the noise caused by irrelevant and redundant features which don't affect learning performances.

Therefore the first features considered relevant for the monitoring scope are the ones having a strong correlation with the considered outputs for at least three different experimental cutting conditions (see APPENDIX B for further details):

- Conventional Statistical Features: F_{mean} , F_{variance} , F_{skewness} , F_{power} , T_{mean} and $AER_{\text{msvariance}}$
- Frequency domain features: $F_{\text{peak}_{2x}}$, $F_{\text{peak}_{4x}}$, $F_{\text{peak}_{6x}}$, $T_{\text{peak}_{2x}}$, and $T_{\text{peak}_{4x}}$

In order to avoid redundant and irrelevant features, they have been further reduced to the following:

- Conventional Statistical Features: F_{mean} , F_{variance} , F_{skewness} , F_{power} , and T_{mean}
- Frequency domain features: $F_{\text{peak}_{2x}}$, $F_{\text{peak}_{4x}}$, and $F_{\text{peak}_{6x}}$

Both configurations of features have been tested to predict tool wear and hole quality parameters as discussed in the next section.

4.13 Neural network paradigm for decision making

To find correlations between sensor signal features and tool condition (VB) and hole quality (Exit delamination factor and Delaminated Area), a neural network (NN) based cognitive paradigm was developed to recognise feature patterns by correlating input FPVs to their corresponding outputs (Teti, Jemielniak, & O'Donnell, 2010).

Different FPVs with diverse combinations of selected features were fed to the NN based cognitive paradigms for pattern recognition on tool state and hole quality. The first FPV was made up of the selected time domain features. The second FPV was composed by the selected frequency domain features. Finally, a FPV with selected time and frequency domain features

was fed to the neural network. The optimal feature combination for pattern vector construction was identified by evaluating the pattern recognition performance of each FPV type.

Each sensor fusion FPV was associated to its matching flank wear value (VB), exit delamination factor (F_d) and delaminated area to create input-output vectors for NN learning. For each drilling condition, 60 input-output vectors (i.e. one for each drilled hole) were built to form the related NN learning set.

Three-layer cascade-forward backpropagation NNs were setup, one for each drilling condition, and an algorithm to train and test different numbers of hidden layer nodes was implemented using the corresponding NN learning sets. The training and testing procedure required to partition the initial 60 input-output vectors into training, validation and test subsets according to the following percentages: training subset = 70%; validation subset = 15%; testing subset = 15% (Moller, 1993).

The performance of the trained NN is evaluated solely on the basis of the test subset results. However, the NN pattern recognition performance may be significantly affected by the specific partitioning into training, validation and testing subsets. To overcome this issue, a bootstrap resampling technique was applied to randomly generate the subsets several times in order to better estimate the pattern recognition performance of the NN.

According to the bootstrap procedure, from the original 60 input-output vectors, the training ($l=42$ samples), validation ($m=9$ samples) and testing ($n=9$ samples) subsets were resampled $K=60$ times with replacement. Thus, the overall pattern recognition performance was estimated by combining the recognition rates obtained from all the $K=60$ resamplings.

The NN performances were evaluated in terms of both *root mean square error* (RMSE), i.e. the standard deviation of the differences between NN predicted values (\hat{y}_t) and target values (y), and *mean absolute percentage error* (MAPE), i.e. the absolute differences between target values (y) and NN predicted values (\hat{y}_t) divided by the actual value. Their analytical expressions are:

$$RMSE = \sqrt{\frac{\sum_{t=1}^n (\hat{y}_t - y)^2}{n}} \quad MAPE = \frac{1}{n} \sum_{t=1}^n \left| \frac{y_t - \hat{y}_t}{y_t} \right|$$

Even if the MAPE is one of the most common performance measures adopted in literature (Jahan Hossain & Ahmad, 2014; Ghorbani & Moetakef-Imani, 2015; Varol, Canakci, & Ozsahin, 2015; Huang, Chang, Kuo, Li, & You, 2015) it has the drawbacks that it can't be used if there are zero target values, there is no upper limit to the percentage error (Tofallis, 2015). Therefore it was used in combination with the RMSE to evaluate the NNs performance.

Initially, NNs were trained and tested using sensor fusion FPVs containing the six selected time domain features, F_{mean} , F_{variance} , F_{skewness} , F_{power} , T_{mean} and $AERms_{\text{variance}}$, and the five selected frequency domain features, $F_{\text{peak}_{2x}}$, $F_{\text{peak}_{4x}}$, $F_{\text{peak}_{6x}}$, $T_{\text{peak}_{2x}}$, and $T_{\text{peak}_{4x}}$, separately. Subsequently, these time and frequency domain features have been used together to train the NNs. Table 19 and Figure 61 report the results of the analysis and the overall performances of the NNs.

Table 19. NN performances in terms of RMSE and MAPE

NO FULL CORRELATION- Experimental condition	Selected time domain features (6)				Selected frequency domain features (5)				Selected time-frequency domain features (11)			
	RMSE	Hidden nodes	MAPE	Hidden nodes	RMSE	Hidden nodes	MAPE	Hidden nodes	RMSE	Hidden nodes	MAPE	Hidden nodes
TOOL WEAR (VB)												
6000 rpm - 0.15 mm/rev	0.003082	16	0.04297	16	0.006588	5	0.08352	13	0.006037	15	0.07211	15
9000 rpm - 0.15 mm/rev	0.001238	7	0.04823	7	0.003323	5	0.07443	5	0.0023	12	0.07585	11
2700 rpm - 0.15 mm/rev	0.001478	7	0.02888	13	0.008079	10	0.1456	10	0.003223	12	0.0678	15
6000 rpm - 0.20 mm/rev	0.002222	10	0.06113	10	0.003757	8	0.08928	6	0.002858	12	0.07	14
6000 rpm - 0.11 mm/rev	0.00145	10	0.02913	16	0.006115	5	0.1151	5	0.002472	11	0.04723	11
EXIT DELAMINATION FACTOR (F_d)												
6000 rpm - 0.15 mm/rev	0.006462	6	0.003617	6	0.01797	5	0.01071	6	0.01249	16	0.007133	11
9000 rpm - 0.15 mm/rev	0.008541	6	0.004781	6	0.03204	5	0.01783	5	0.01972	12	0.01058	11
2700 rpm - 0.15 mm/rev	0.01062	7	0.005716	7	0.06641	6	0.03851	6	0.02295	11	0.01299	11
6000 rpm - 0.20 mm/rev	0.002543	7	0.071	7	0.003896	7	0.08995	6	0.003085	15	0.07511	14
6000 rpm - 0.11 mm/rev	0.0186	6	0.01084	6	0.03454	5	0.02136	9	0.02547	12	0.01505	12
DELAMINATED AREA												
6000 rpm - 0.15 mm/rev	1.107	6	0.2465	10	1.253	5	0.3258	5	1.75	19	0.3921	25
9000 rpm - 0.15 mm/rev	1	7	0.2505	6	1.205	6	0.2614	5	1.427	12	0.3136	12
2700 rpm - 0.15 mm/rev	1.05	8	0.2519	7	1.729	5	0.6175	10	1.41	16	0.3843	22
6000 rpm - 0.20 mm/rev	1.14	11	0.2619	8	0.9827	6	0.2298	6	1.194	12	0.3163	18
6000 rpm - 0.11 mm/rev	0.9402	10	0.175	10	1.065	5	0.1943	7	1.014	11	0.1979	14

FULL CORRELATION- Experimental condition	Selected time domain features (5)				Selected frequency domain features (3)				Selected time-frequency domain features (8)			
	RMSE	Hidden nodes	MAPE	Hidden nodes	RMSE	Hidden nodes	MAPE	Hidden nodes	RMSE	Hidden nodes	MAPE	Hidden nodes
TOOL WEAR (VB)												
6000 rpm - 0.15 mm/rev	0.003047	7	0.05324	7	0.006142	7	0.08372	5	0.00424	11	0.07013	7
9000 rpm - 0.15 mm/rev	0.001139	10	0.06353	10	0.002979	3	0.09747	8	0.001376	8	0.05519	8
2700 rpm - 0.15 mm/rev	0.001074	12	0.02379	12	0.007412	7	0.1813	7	0.001725	8	0.04121	9
6000 rpm - 0.20 mm/rev	0.002204	6	0.05638	7	0.003879	3	0.1026	3	0.002219	16	0.05285	16
6000 rpm - 0.11 mm/rev	0.001376	11	0.04389	13	0.007998	3	0.1612	3	0.00143	8	0.04126	10
EXIT DELAMINATION FACTOR (F_d)												
6000 rpm - 0.15 mm/rev	0.005076	7	0.002879	7	0.01912	4	0.0105	6	0.007223	8	0.004196	8
9000 rpm - 0.15 mm/rev	0.0076	7	0.004336	7	0.02814	3	0.01504	3	0.01061	8	0.006098	8
2700 rpm - 0.15 mm/rev	0.008547	10	0.004598	10	0.06126	8	0.03531	10	0.01535	10	0.008561	10
6000 rpm - 0.20 mm/rev	0.002017	5	0.06203	10	0.004112	9	0.1054	4	0.002004	11	0.05346	8
6000 rpm - 0.11 mm/rev	0.01614	9	0.008775	14	0.0326	4	0.02003	4	0.02125	11	0.0137	9
DELAMINATED AREA												
6000 rpm - 0.15 mm/rev	0.9706	8	0.1894	5	1.152	9	0.2269	8	1.155	8	0.2786	8
9000 rpm - 0.15 mm/rev	0.08835	8	0.1967	5	0.1073	8	0.2097	4	0.1031	9	0.2262	9
2700 rpm - 0.15 mm/rev	0.8475	7	0.2751	8	1.495	3	0.8237	3	1.193	9	0.4721	9
6000 rpm - 0.20 mm/rev	0.9667	8	0.2804	8	0.8517	4	0.2141	5	0.9537	9	0.273	9
6000 rpm - 0.11 mm/rev	0.8556	5	0.2765	5	1.054	3	0.2022	3	0.9805	11	0.2323	11

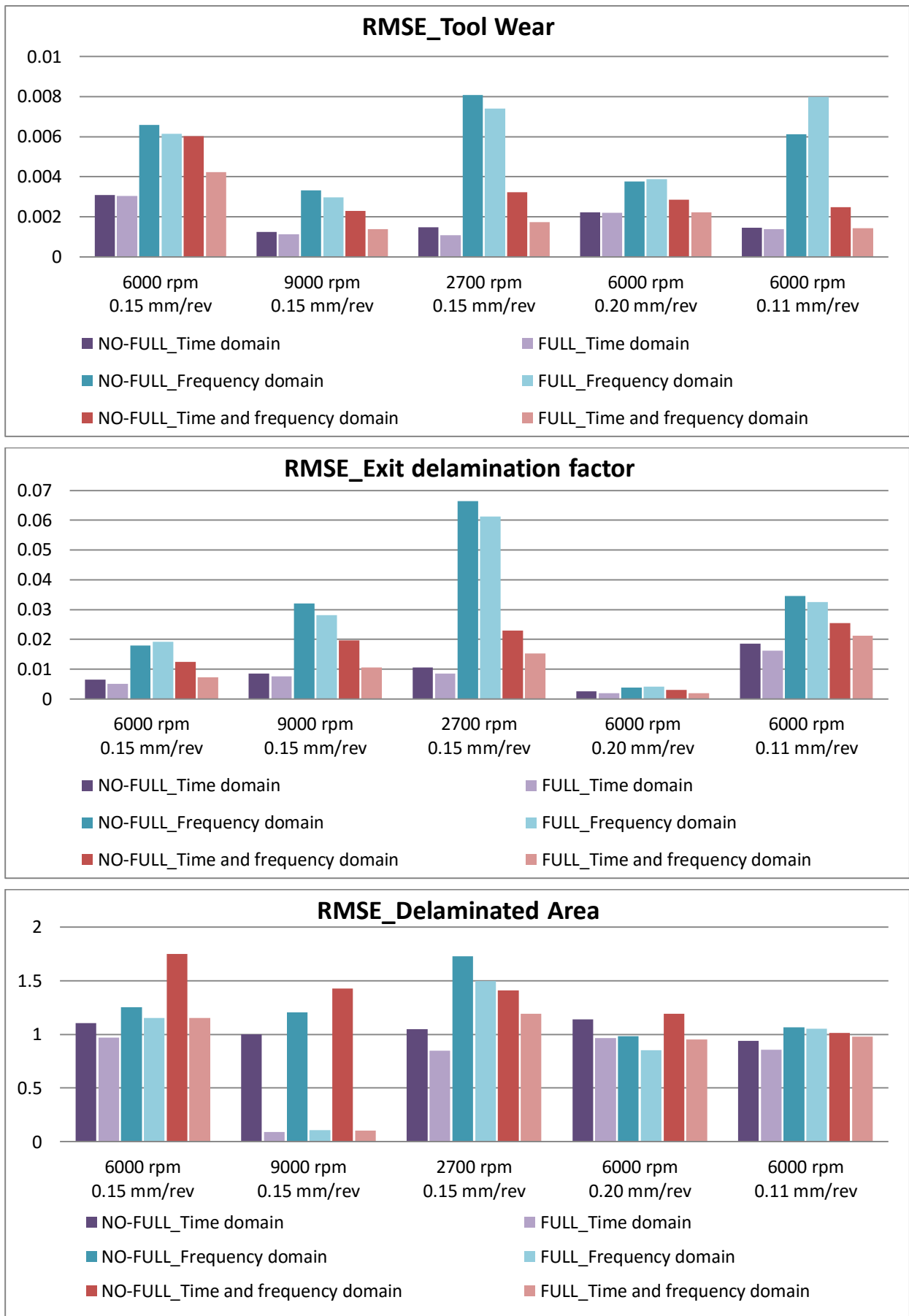


Figure 61. Results comparison

4.14 Discussion of results

The analysis of results shows that for each operating condition and considering both RMSE and MAPE performance indicators, the selected time domain features were the best to predict the output parameters. The frequency domain features did not improve the prediction even if they get good performances.

As far as tool wear, the overall best performance was obtained for drilling condition 9000 rpm and 0.15 mm/rev using a NN with 7 hidden nodes. Regarding the exit delamination factor the overall best performance was obtained for drilling condition 6000 rpm and 0.20 mm/rev using a NN with 7 hidden nodes. Finally, concerning the delaminated area the overall best performance was obtained for drilling condition 6000 rpm and 0.11 mm/rev using a NN with 10 hidden nodes. The NN performance values related to the delaminated area prediction are not very satisfactory compared to the other prediction performance values. The lowest MAPE value is 0.175, which means a prediction error of 17.50%, and 0.2619 (prediction error of 26.19%) in the worst scenario.

The second configuration of selected features was tested. Once again, the analysis of results shows that for each operating condition and considering both RMSE and MAPE, the selected time domain features were the best to predict the output parameters. The frequency domain features didn't improve the prediction even if they get good performances. Furthermore, the RMSE and MAPE values are considerably better than the previous case. More specifically as far as tool wear, the overall best performance was obtained for drilling condition 2700 rpm and 0.15 mm/rev using a NN with 12 hidden nodes. Regarding the exit delamination factor prediction, the overall best performance was obtained for drilling condition 6000 rpm and 0.20 mm/rev using a NN with 5 hidden nodes. Finally, concerning the delaminated area prediction, the overall best performance was obtained for drilling condition 2700 rpm and 0.15 mm/rev using a NN with 7 hidden nodes. The NN performance values, although better than for the previous case, are not very satisfactory here too. The lowest MAPE value is 0.1894, which means a prediction error of 18.94%, and the highest value is equal to 0.2804 (prediction error of 28.04%) in the worst case scenario.

Figures reported in APPENDIX D show, for each drilling condition, the full results of the optimal NN configurations obtained by varying the number of hidden nodes.

The results show that, in both scenarios, the time domain features perform better in predicting the output variables and that the second features selection displayed the highest pattern recognition performance as reported in Table 20.

Table 20. Overall results

Experimental condition	Selected time domain features (6)		Selected time domain features (5)	
	RMSE	MAPE	RMSE	MAPE
TOOL WEAR (VB)				
6000 rpm - 0.15 mm/rev	0.003082	0.04297	0.003047	0.05324
9000 rpm - 0.15 mm/rev	0.001238	0.04823	0.001139	0.06353
2700 rpm - 0.15 mm/rev	0.001478	0.02888	0.001074	0.02379
6000 rpm - 0.20 mm/rev	0.002222	0.06113	0.002204	0.05638
6000 rpm - 0.11 mm/rev	0.00145	0.02913	0.001376	0.04389
EXIT DELAMINATION FACTOR (F_d)				
6000 rpm - 0.15 mm/rev	0.006462	0.003617	0.005076	0.002879
9000 rpm - 0.15 mm/rev	0.008541	0.004781	0.0076	0.004336
2700 rpm - 0.15 mm/rev	0.01062	0.005716	0.008547	0.004598
6000 rpm - 0.20 mm/rev	0.002543	0.071	0.002017	0.06203
6000 rpm - 0.11 mm/rev	0.0186	0.01084	0.01614	0.008775
DELAMINATED AREA				
6000 rpm - 0.15 mm/rev	1.107	0.2465	0.9706	0.1894
9000 rpm - 0.15 mm/rev	1.000	0.2505	0.08835	0.1967
2700 rpm - 0.15 mm/rev	1.050	0.2519	0.8475	0.2751
6000 rpm - 0.20 mm/rev	1.140	0.2619	0.9667	0.2804
6000 rpm - 0.11 mm/rev	0.940	0.1750	0.8556	0.2765

The drilled hole quality evaluations were utilized to set up a criterion for tool change execution, required when the tool wear is responsible for a drilled hole quality which is no more acceptable. As the lower limit of the tolerance range corresponds to the nominal diameter, any negative hole diameter error is unacceptable. For each drilling condition, the occurrence of negative hole diameter errors was detected and associated to the flank wear value and the exit delamination factor.

Figure 62 shows that, under all drilling conditions, the hole diameter error becomes negative when the flank wear, VB, reaches the typical value of 0.04 mm, which can be used as a threshold to determine the need for tool change due to undersized hole diameter.

The figure also shows that, for all drilling conditions, the exit delamination factor grows with the number of holes and reaches approximately 1.2 when the flank wear attains 0.04 mm. Also the delaminated area shows a growing trend according to the number of holes drilled, and its value is about 3.7-4 mm² when the tool wear is almost equal to 0.04 mm. This suggests that the flank wear threshold could also be associated to the second hole quality parameter represented by the exit delamination factor (Rawat & Attia, 2009) and delaminated area.

Accordingly, if the NN paradigm allows for reliable predictions of tool wear development, it is also capable to effectively support on-line decision making on drill bit change execution.

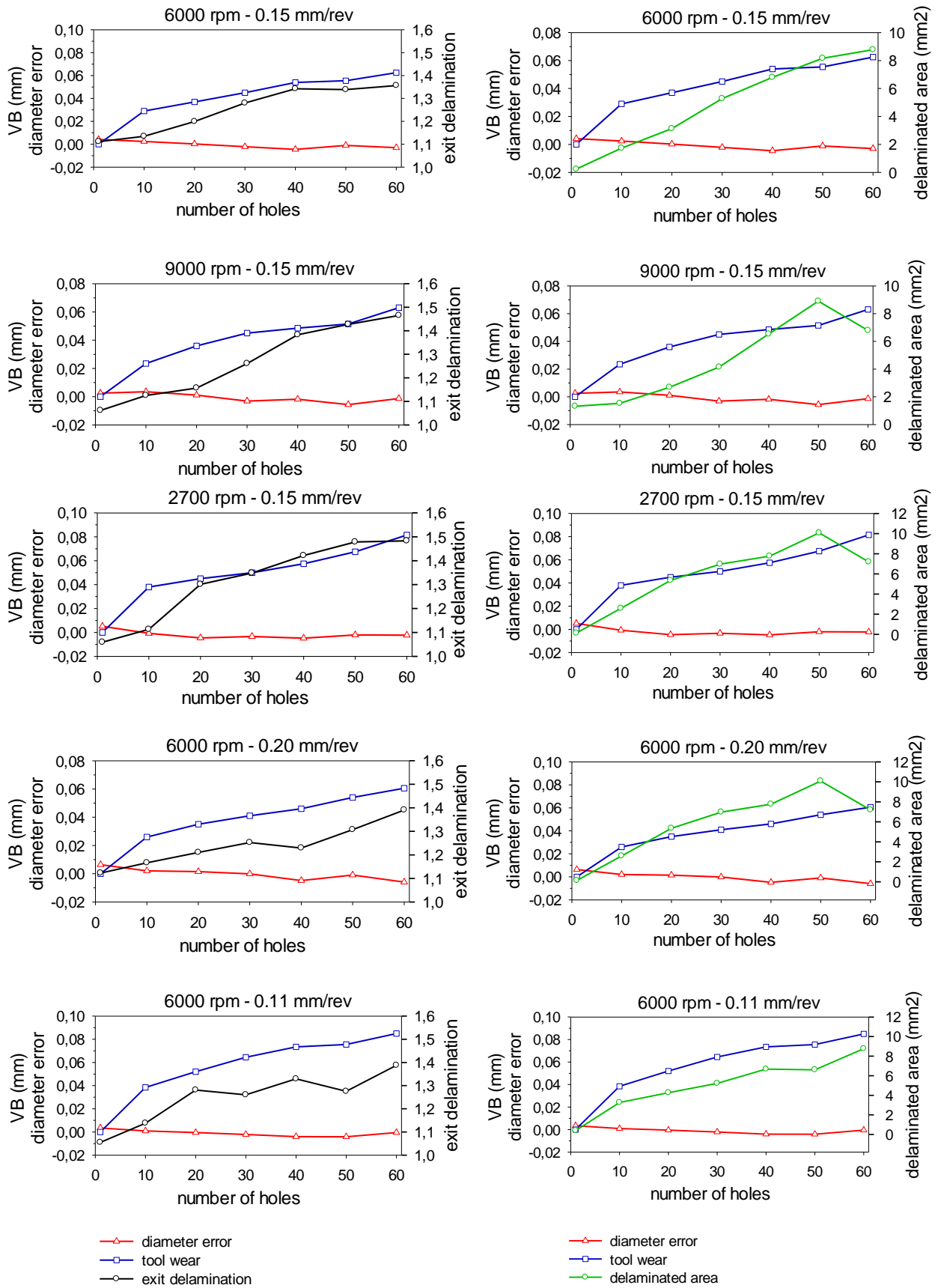


Figure 62. Exit diameter error, tool flank wear, exit delamination and delaminated area measures for all drilling conditions

5. Conclusions and future developments

The research activities developed in this thesis, focused on cognitive sensor monitoring of machining processes for zero defect manufacturing, were carried out within the framework of the international research project EC FP7 CP-IP “IFaCOM – Intelligent Fault Correction and self Optimizing Manufacturing systems” (2011-2015; FoF NMP – 285489) and the national MIUR PON Project on “Development of eco-compatible materials and technologies for robotised drilling and assembly processes – STEP FAR” (2014-2016).

The results obtained within the IFaCOM project, related to cognitive sensor monitoring of robot assisted polishing were presented through the implementation of an industrial demonstrator at STRECON A/S, Denmark, of the sensor monitoring system, integrating the corresponding decision making paradigm. The demonstrator was presented and fully functioning at the final project meeting which took place in Norway during the first half of 2015.

The surface roughness measurements and the extracted features resulted to be correlated and the developed cognitive paradigm was able to predict when the required surface roughness has been reached. However neural network parameters may be optimized, i.e. number of hidden nodes, transfer function, and different neural network configurations may be trained and tested.

Regarding the STEP FAR project, multiple sensor process monitoring was implemented in the drilling of CFRP/CFRP stacks for assembly of aircraft fuselage panels, with the aim to support on-line decision making on tool change execution through cognitive tool wear prediction and hole quality assessment. Thrust force, torque, acoustic emission RMS and vibration acceleration signals were acquired during experimental drilling tests under different rotational speed and feed conditions. Advanced sensor signal processing techniques, comprising signal conditioning, statistical feature extraction and data fusion, were implemented to construct sensor fusion pattern vectors with the aim to find correlations with tool state via neural network based pattern recognition paradigms.

The NN performance results indicated that, for all drilling conditions, the extracted statistical features and used as input sensor fusion pattern vector allow to obtain very accurate results in terms of tool wear and exit delamination factor prediction. The NN prediction of tool wear was highly accurate, with the minimum and maximum RMSE values respectively equal to $1.074e-3$ and $3.047e-3$. Also the exit delamination factor prediction showed good results with MAPE values equal to $2.017e-3$ and $1.614e-2$ as the minimum and maximum values respectively. Therefore, these outcomes highlight the strong correlations existing between signal features, tool wear level and exit delamination factor.

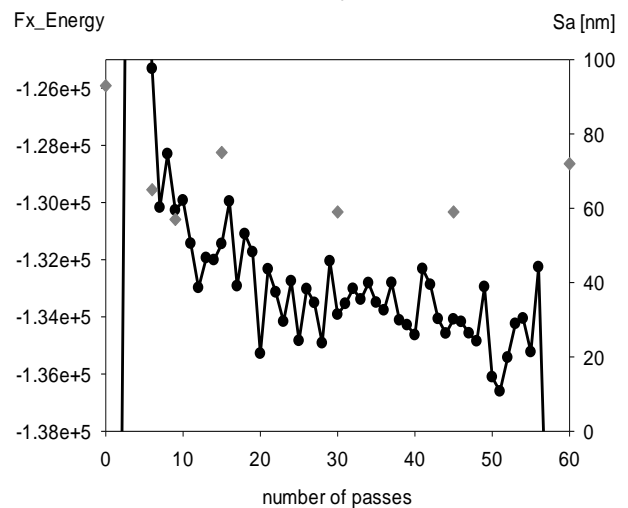
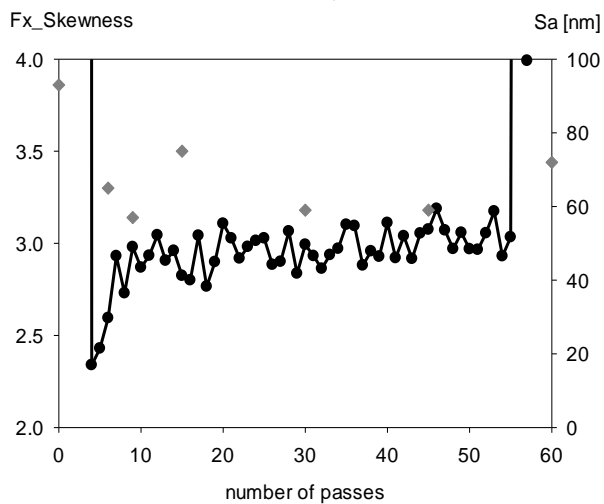
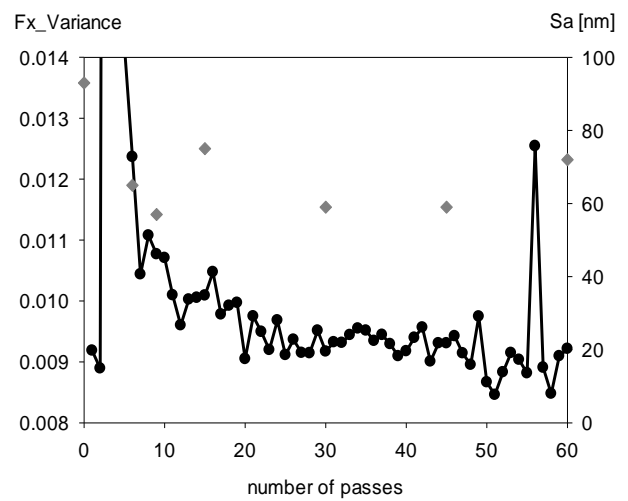
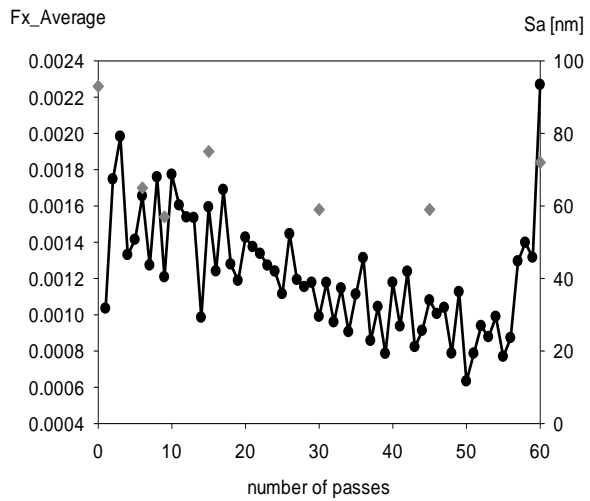
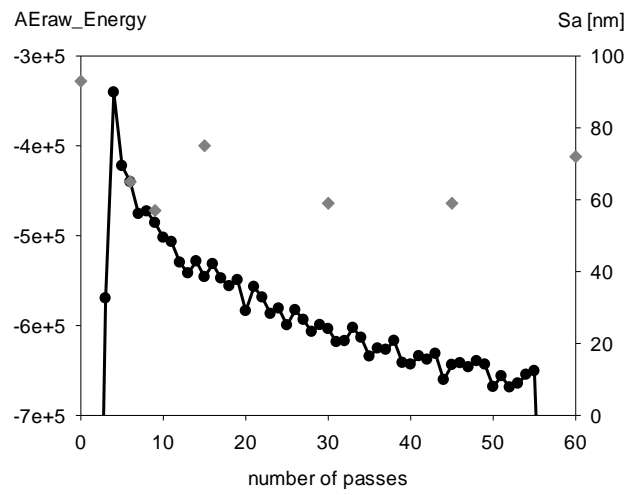
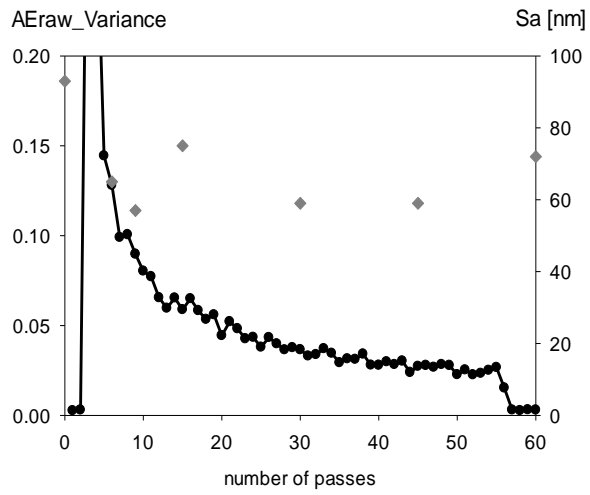
Although the delaminated area was not accurately predicted by the developed NN paradigm, it shows significant correlation with the extracted signal features and the other considered outputs. Indeed, the prediction of tool wear can be used to forecast the quality of the drilled holes. A significant correspondence between hole diameter error, delaminated area and exit delamination factor with tool wear level was observed: in particular, a tool wear threshold, $VB = 0.04$, was identified, in proximity of which unacceptable hole quality is generated, i.e. negative diameter error values.

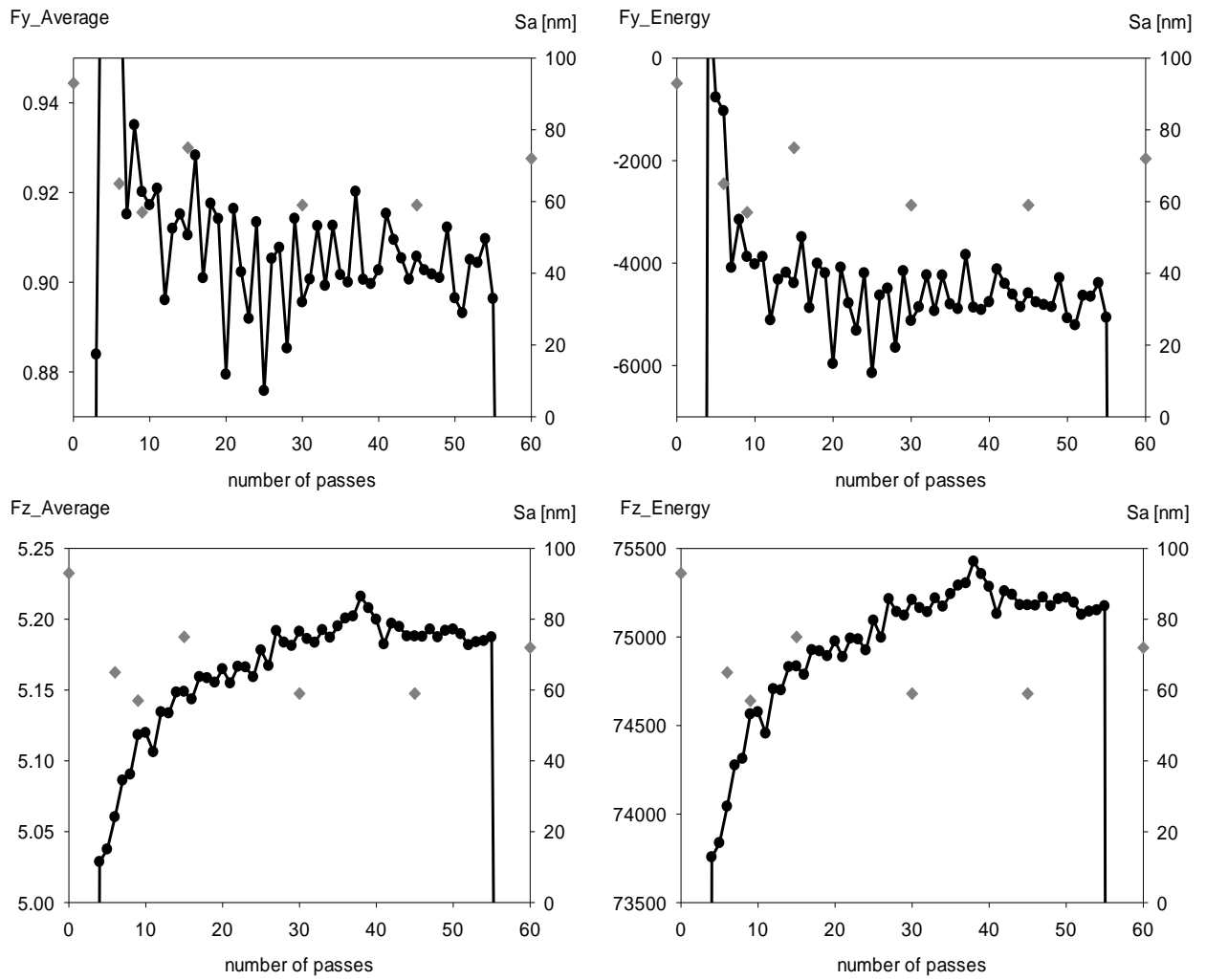
As a result, via on-line prediction of tool wear during drilling, taking into account the identified flank wear threshold, the cognitive sensor monitoring paradigm can provide diagnosis and prognosis services to support decision making on tool change execution, which is highly functional for drilling automation.

These results pave the way for the definition of future developments of this application that can be identified in the following research directions:

- The delaminated area measure should be further improved on the basis of recent approaches reported in literature (Voß, Henerichs, Rupp, Kuster, & Wegener, 2016);
- An automatic software tool based on digital image analysis may be developed in order to detect and measure the hole quality parameters;
- A comprehensive measure of drilled holes quality should be formulated taking into account different parameters;
- Even if the frequency signal features do not improve the NN performances, they result statistically correlated to the process output and, therefore, relevant to monitor the drilling process. Furthermore, the peaks position are useful in order to observe the influence of the fibre cutting angle during the drilling process. The connection between the tool cutting edges, the direction of the fibre in the composite laminate and the coefficient of the mathematical model representing the drilling operation may be investigated.

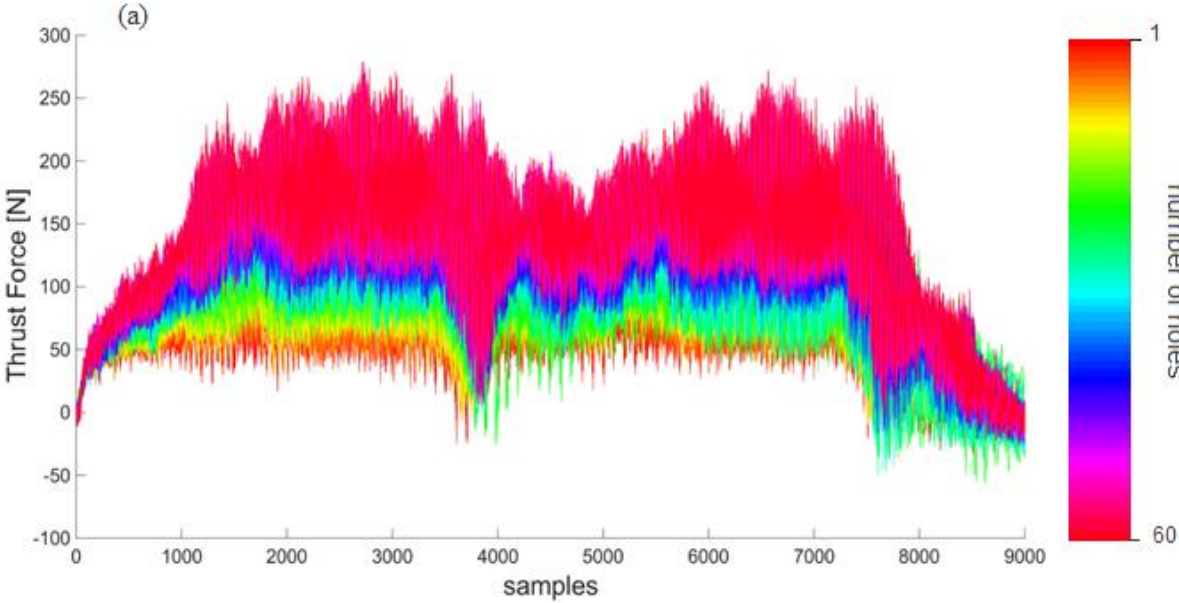
APPENDIX A

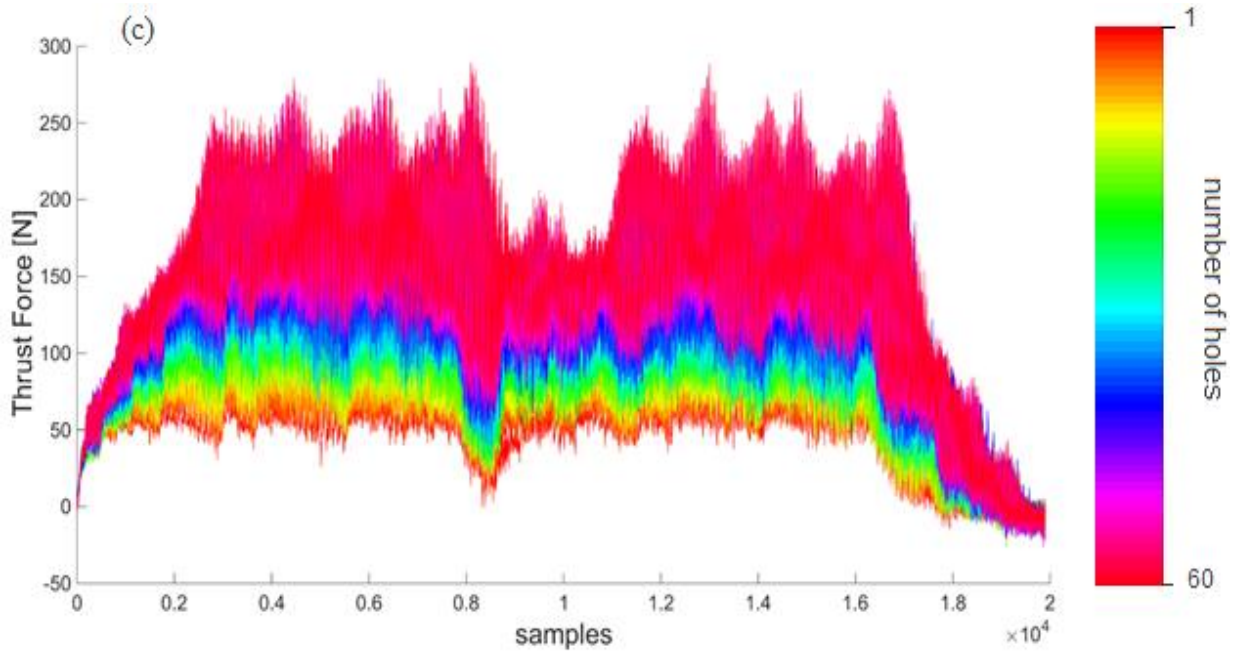
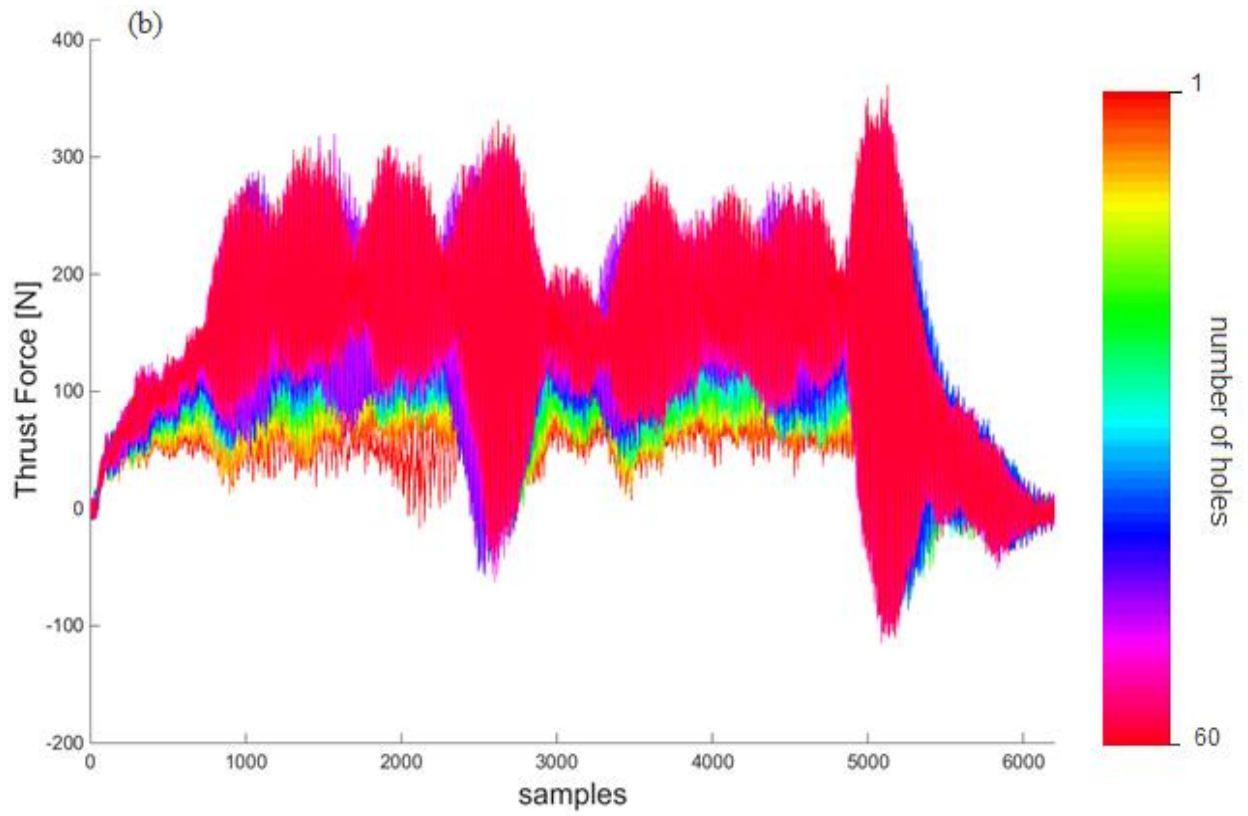


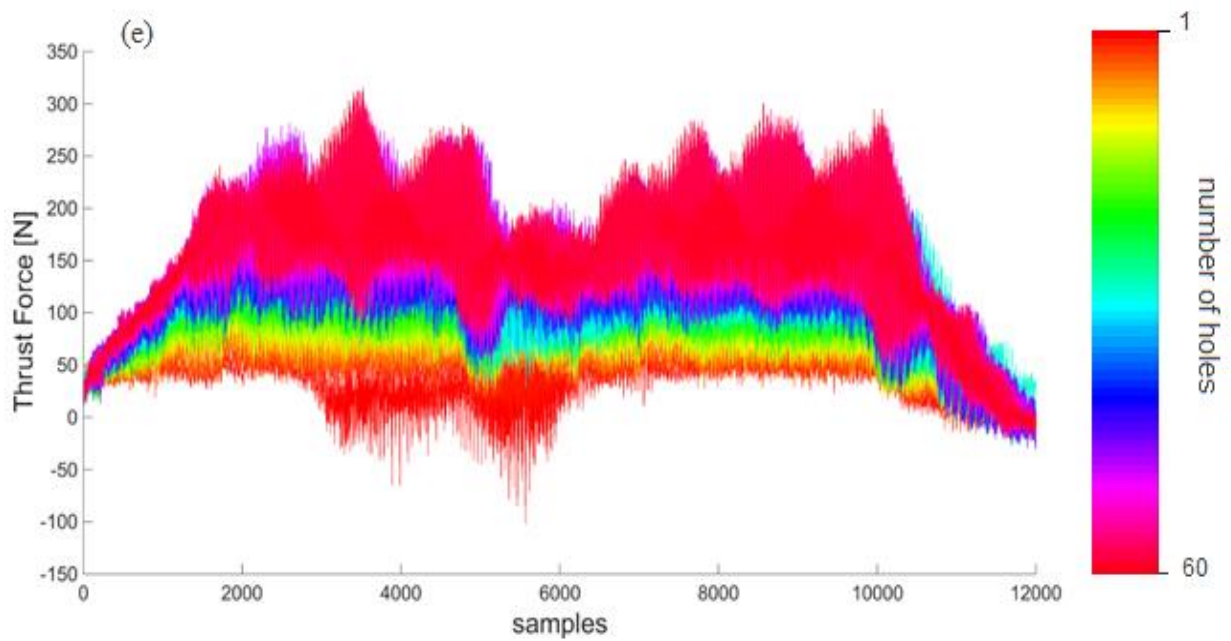
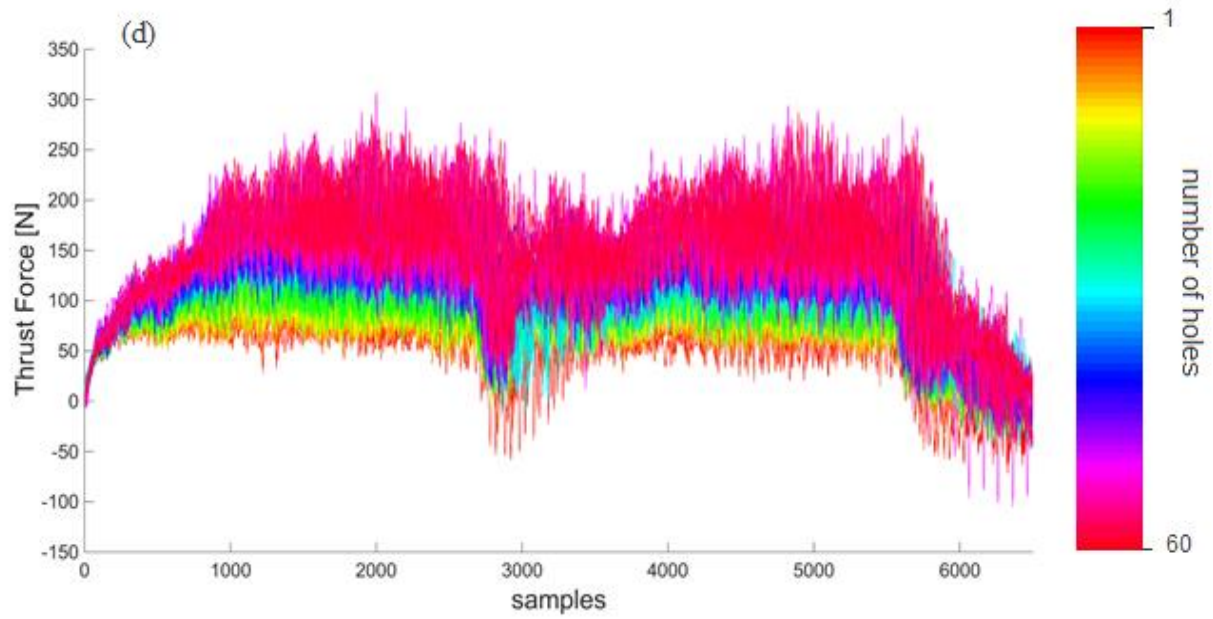


APPENDIX B

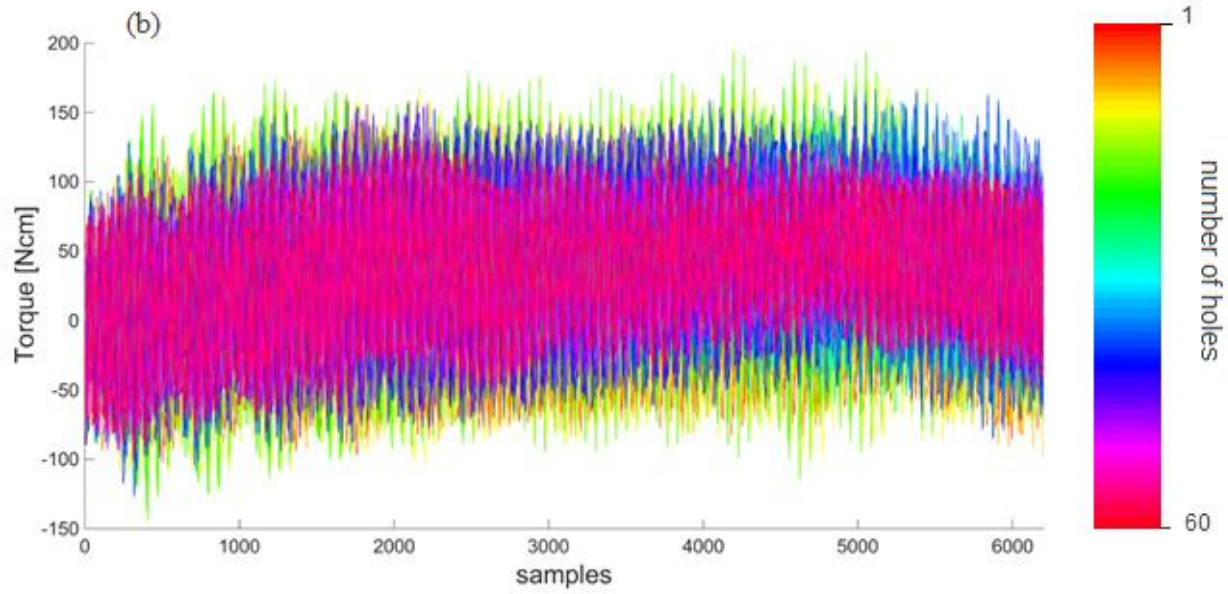
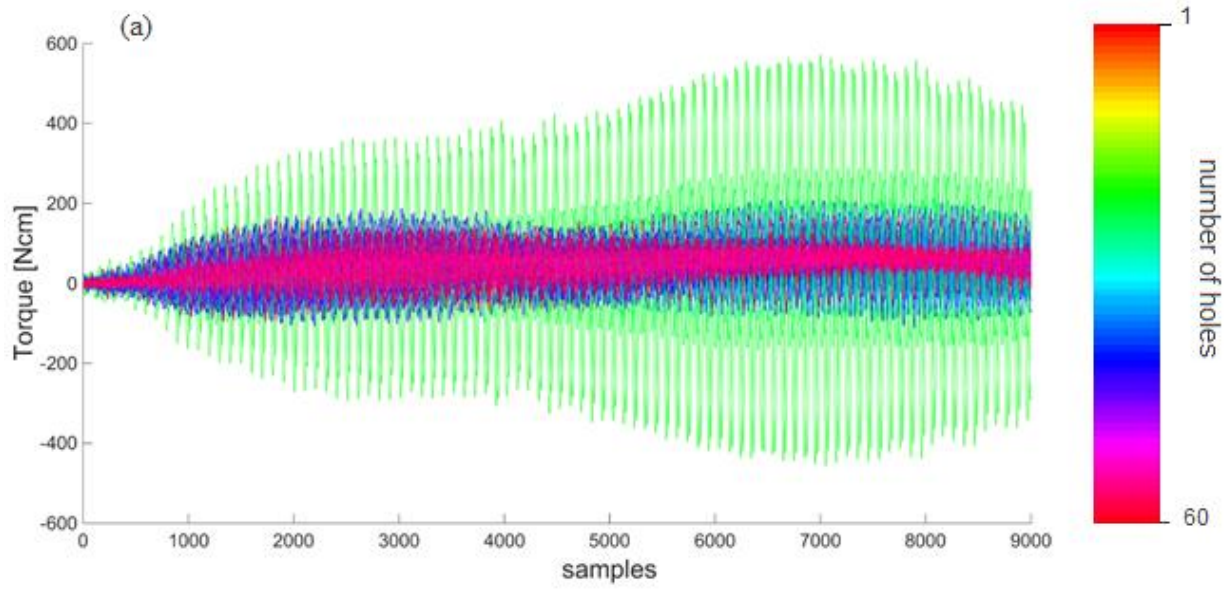
The following figures show the plots of the thrust force signals [N] as a function of the number of holes for all the operating conditions reported in Table 16 where (a) 6000 rpm – 0.15 mm/rev; (b) 9000 rpm – 0.15 mm/rev; (c) 2700 rpm – 0.15 mm/rev; (d) 6000 rpm – 0.20 mm/rev; (e) 6000 rpm- 0.11 mm/rev.

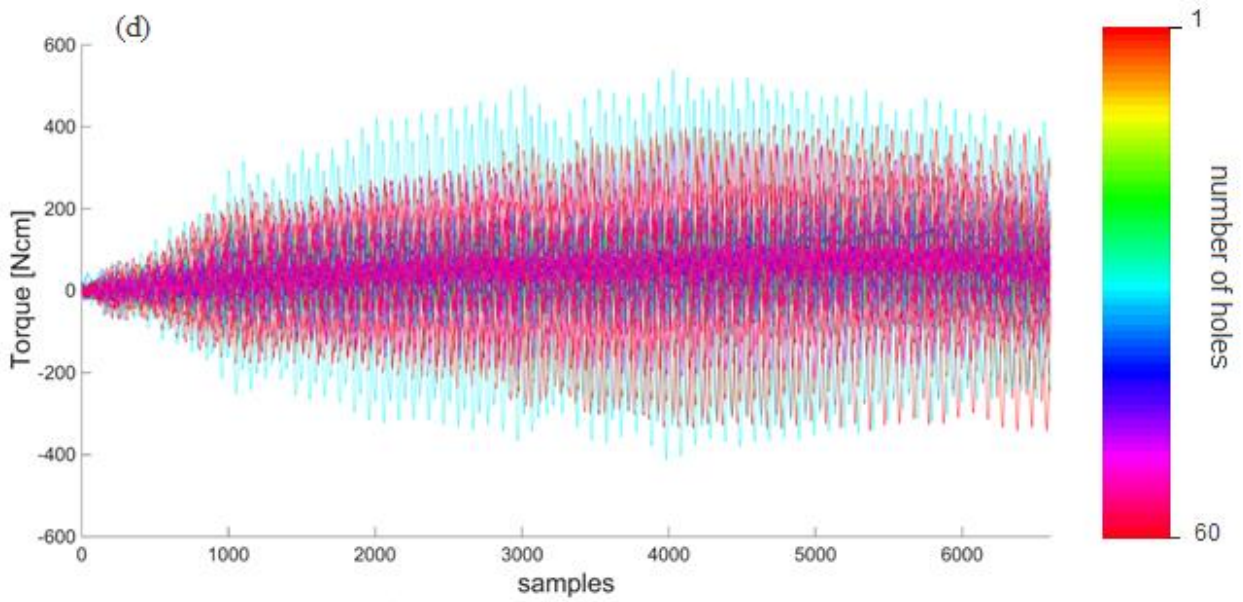
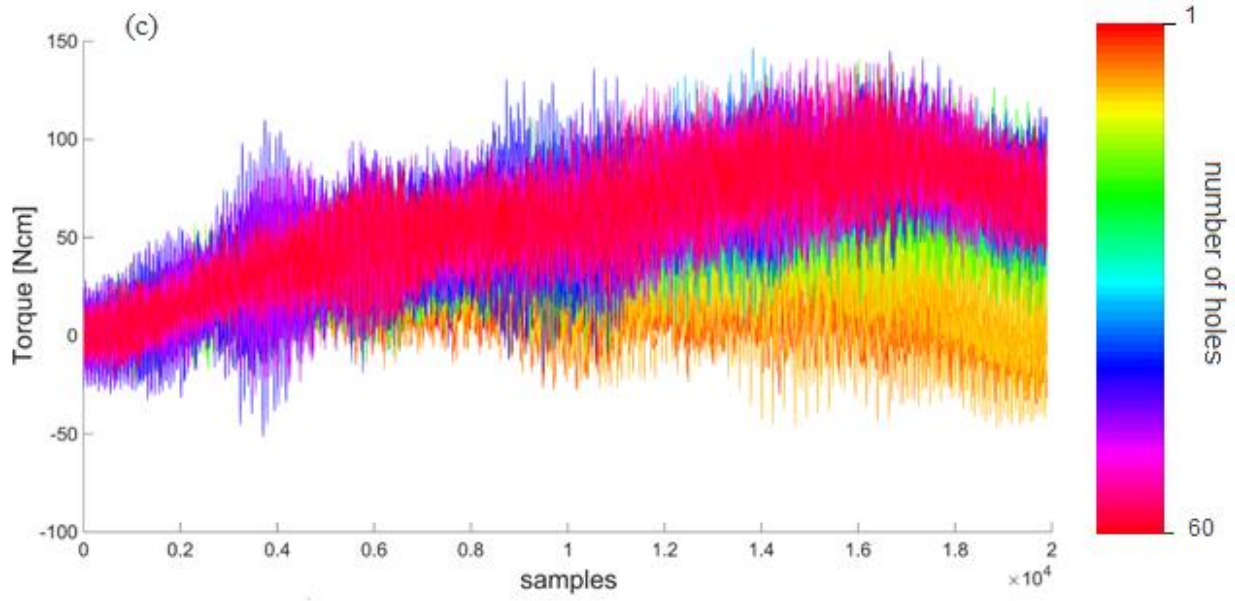


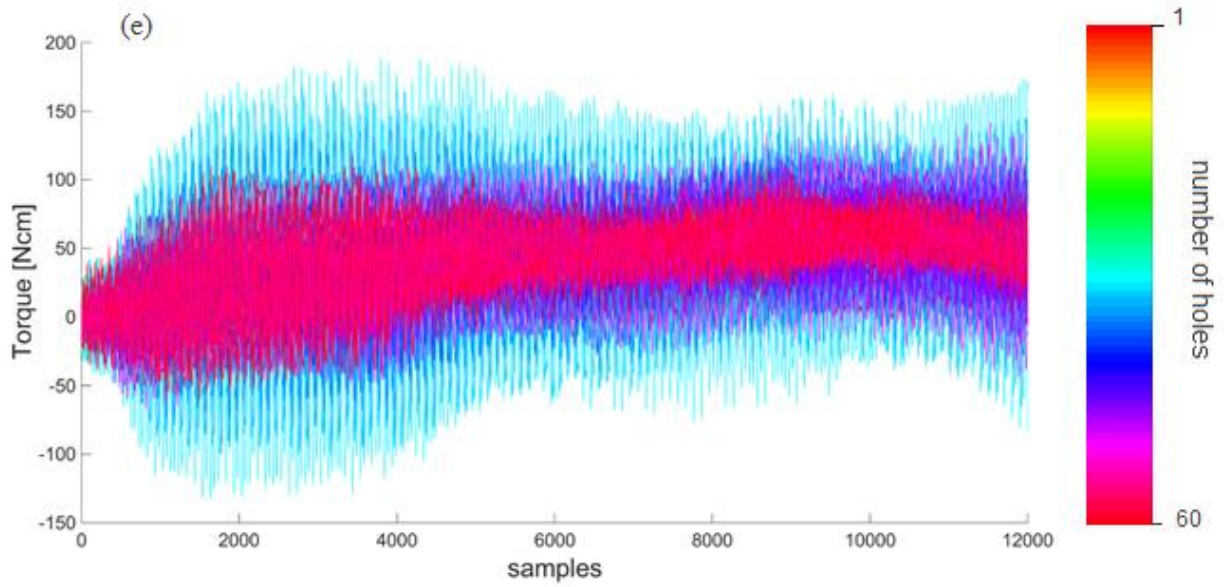




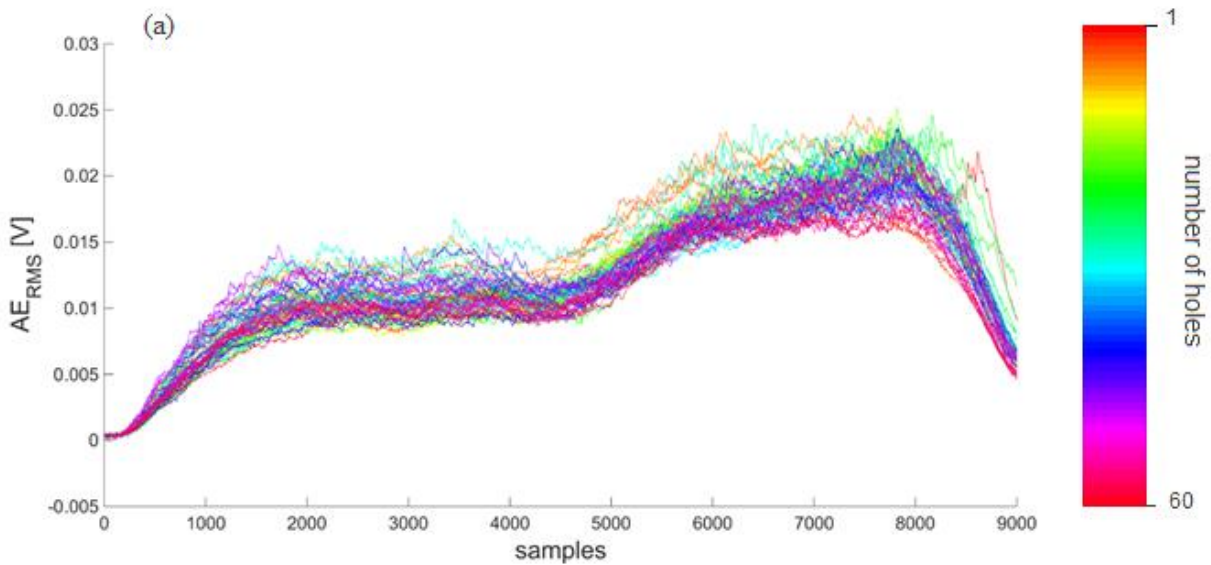
The following figures show the plots of the torque signals [N] as a function of the number of holes for all the operating conditions reported in Table 16 where (a) 6000 rpm – 0.15 mm/rev; (b) 9000 rpm – 0.15 mm/rev; (c) 2700 rpm – 0.15 mm/rev; (d) 6000 rpm – 0.20 mm/rev; (e) 6000 rpm- 0.11 mm/rev.

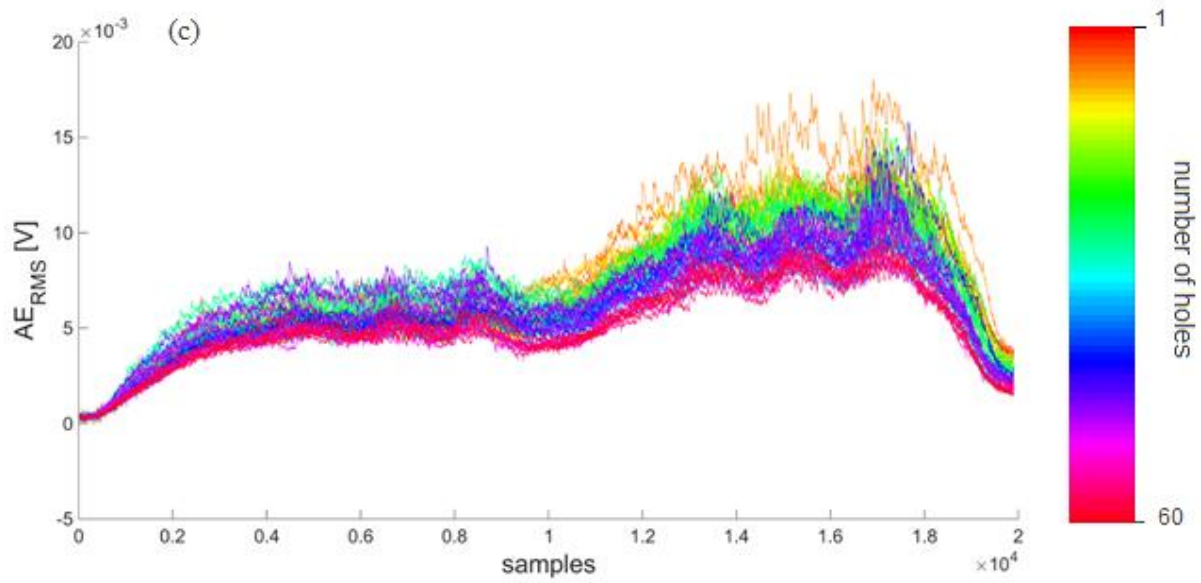
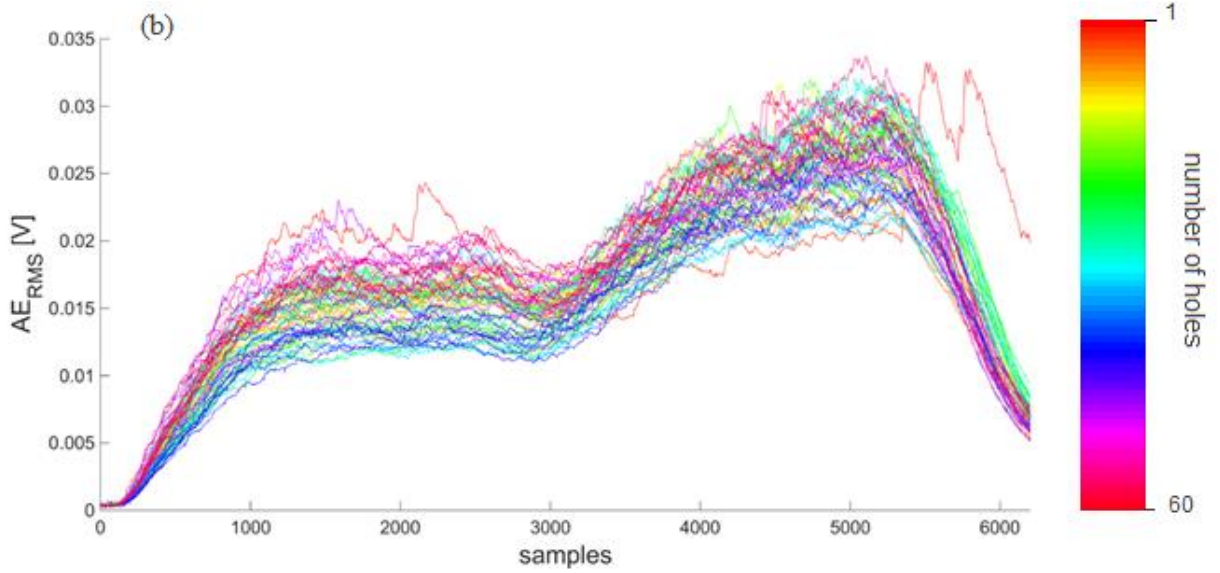


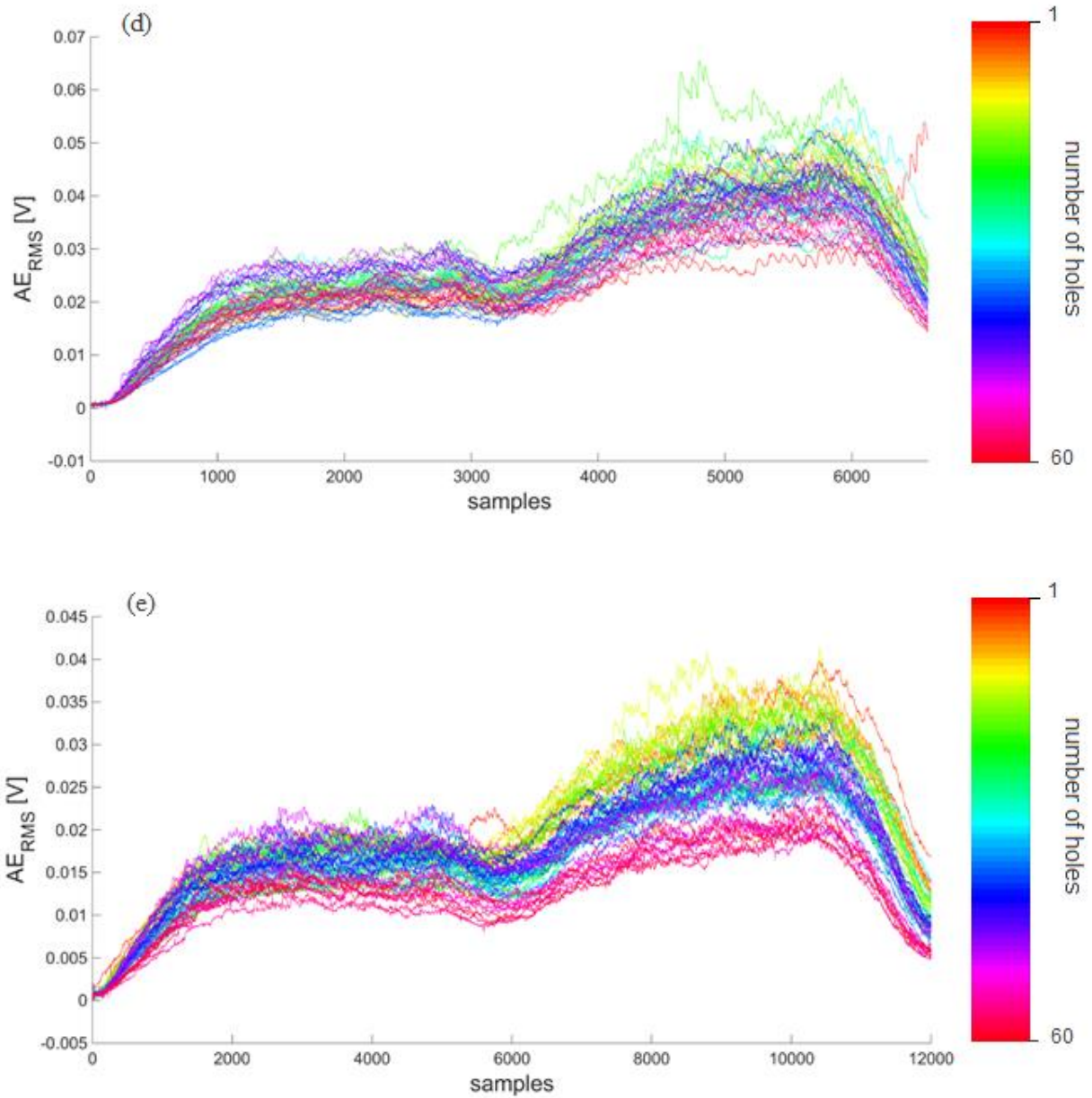




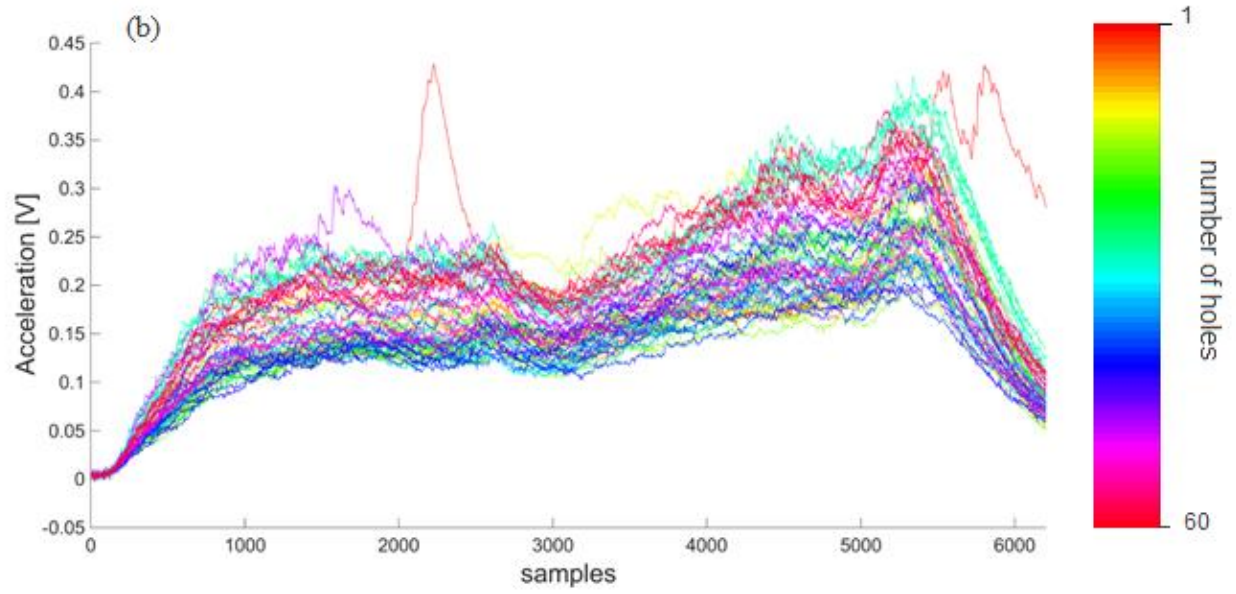
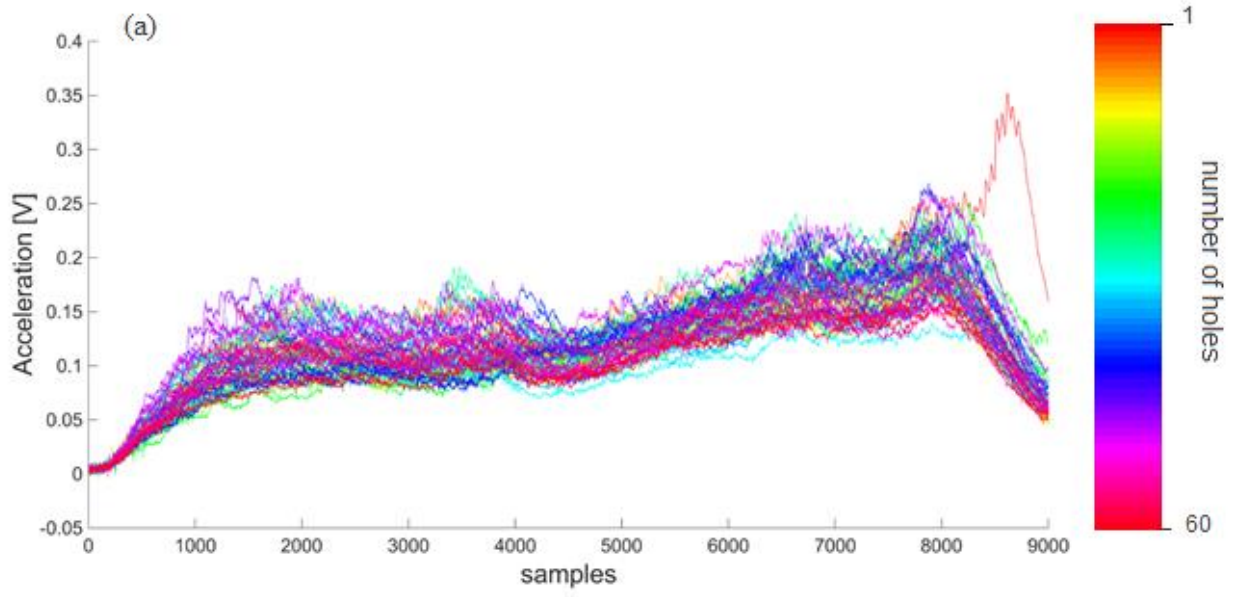
The following figures show the plots of the AE_{RMS} signals [N] as a function of the number of holes for all the operating conditions reported in Table 16 where (a) 6000 rpm – 0.15 mm/rev; (b) 9000 rpm – 0.15 mm/rev; (c) 2700 rpm – 0.15 mm/rev; (d) 6000 rpm – 0.20 mm/rev; (e) 6000 rpm- 0.11 mm/rev.

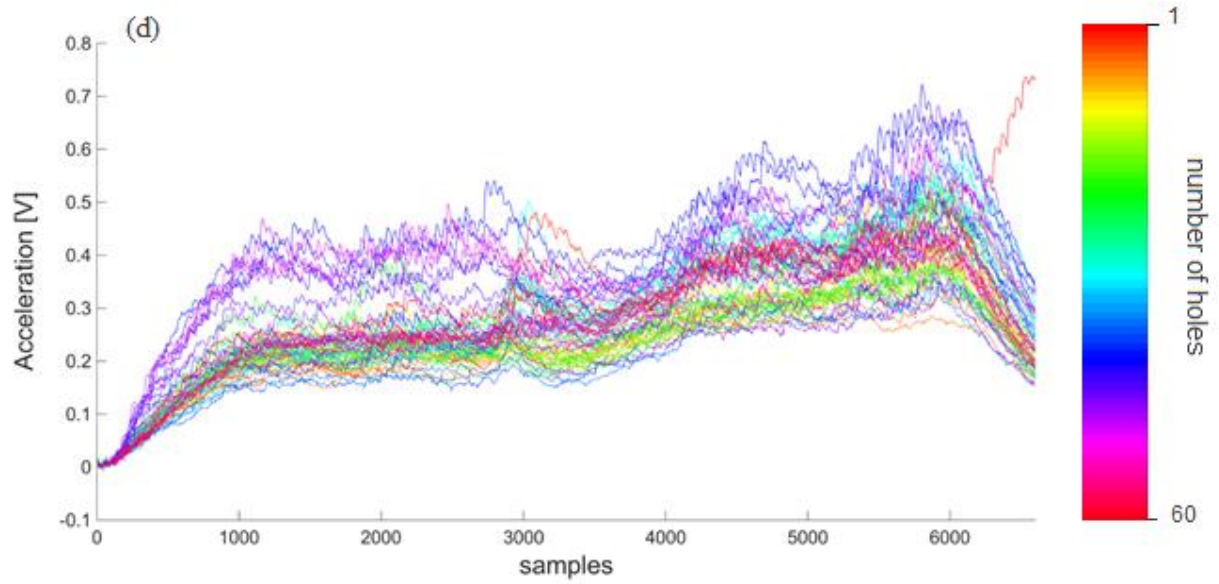
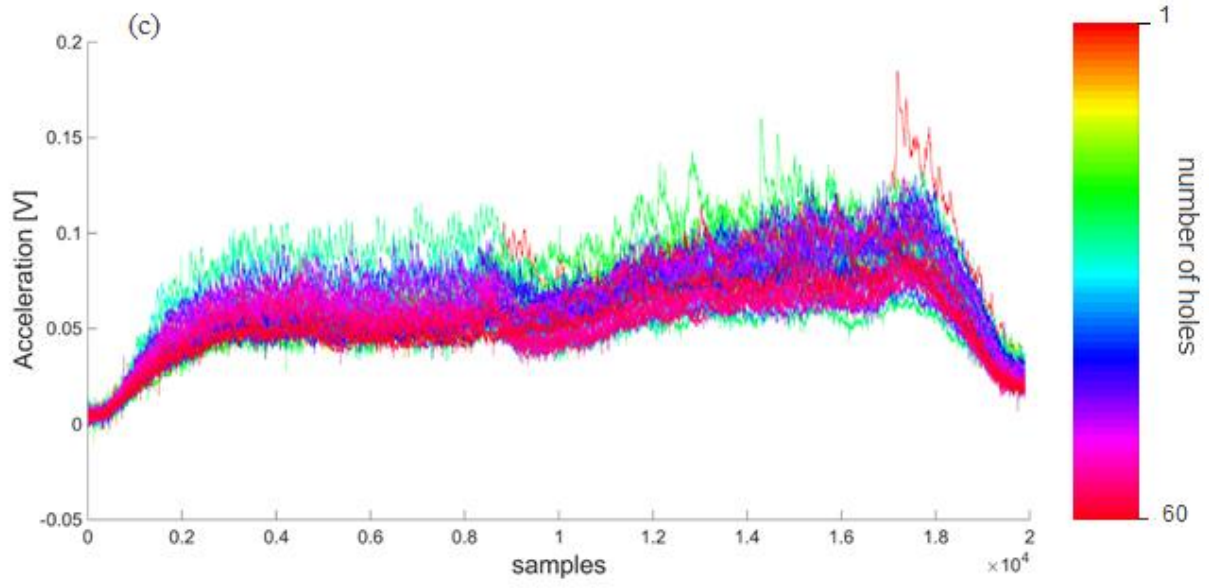


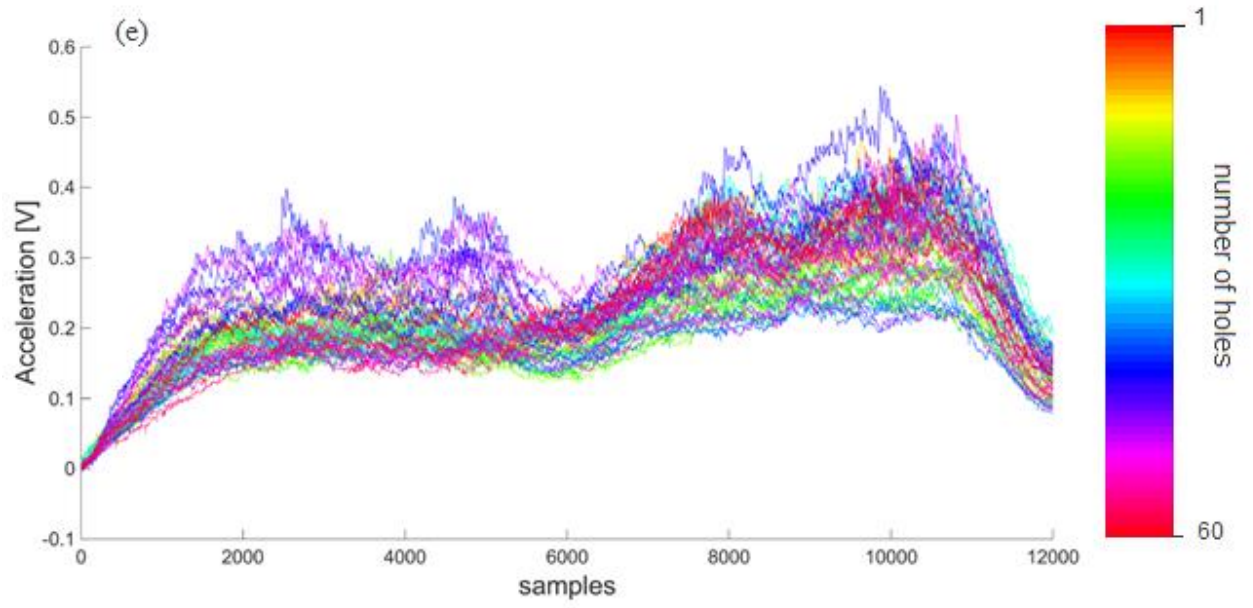




The following figures show the plots of the vibrations acceleration signals [N] as a function of the number for holes of all the operating conditions reported in Table 16 where (a) 6000 rpm – 0.15 mm/rev; (b) 9000 rpm – 0.15 mm/rev; (c) 2700 rpm – 0.15 mm/rev; (d) 6000 rpm – 0.20 mm/rev; (e) 6000 rpm- 0.11 mm/rev.







APPENDIX C

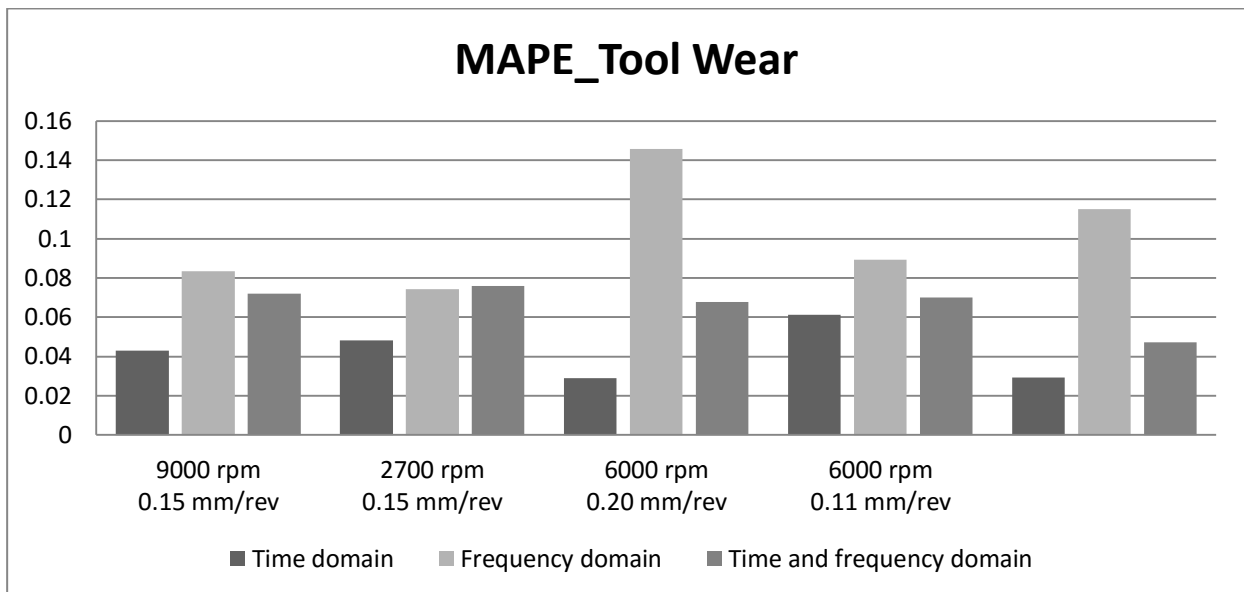
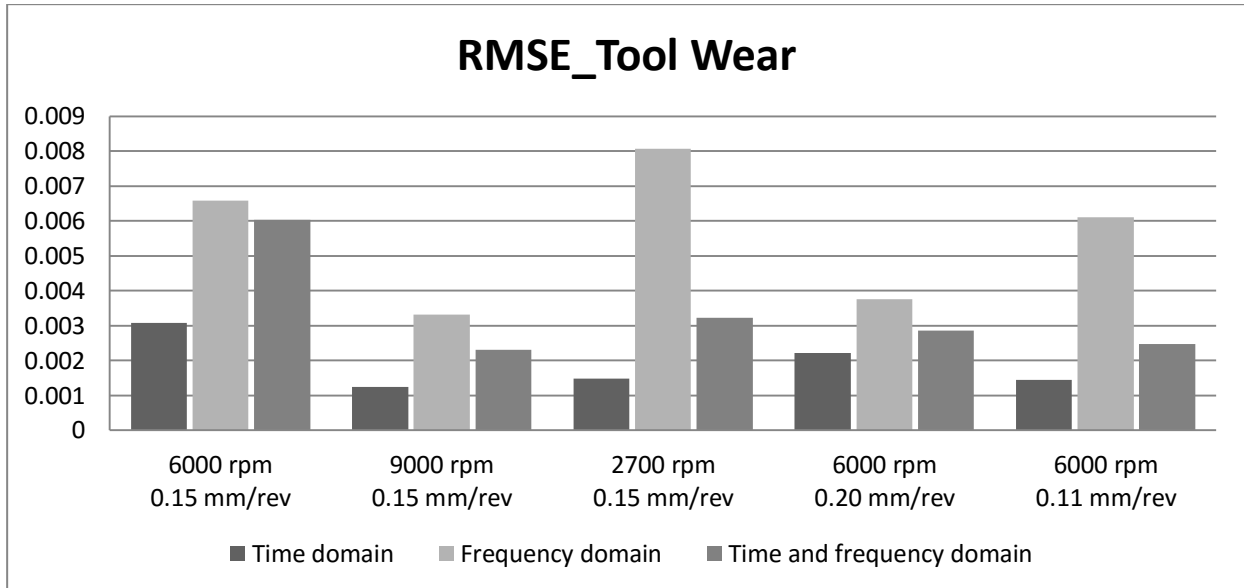
The following tables report the synthesis of the correlation analysis described in section 4.12. The value “1” means that there is correlation between the two variables, instead “0” means that there is no correlation between the variables.

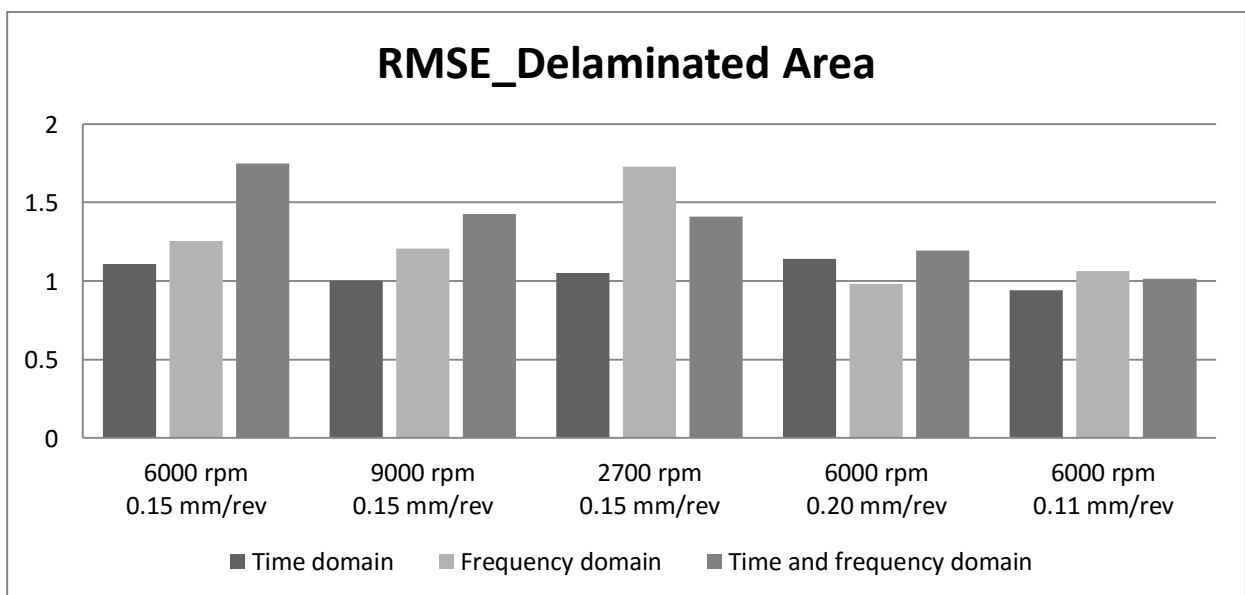
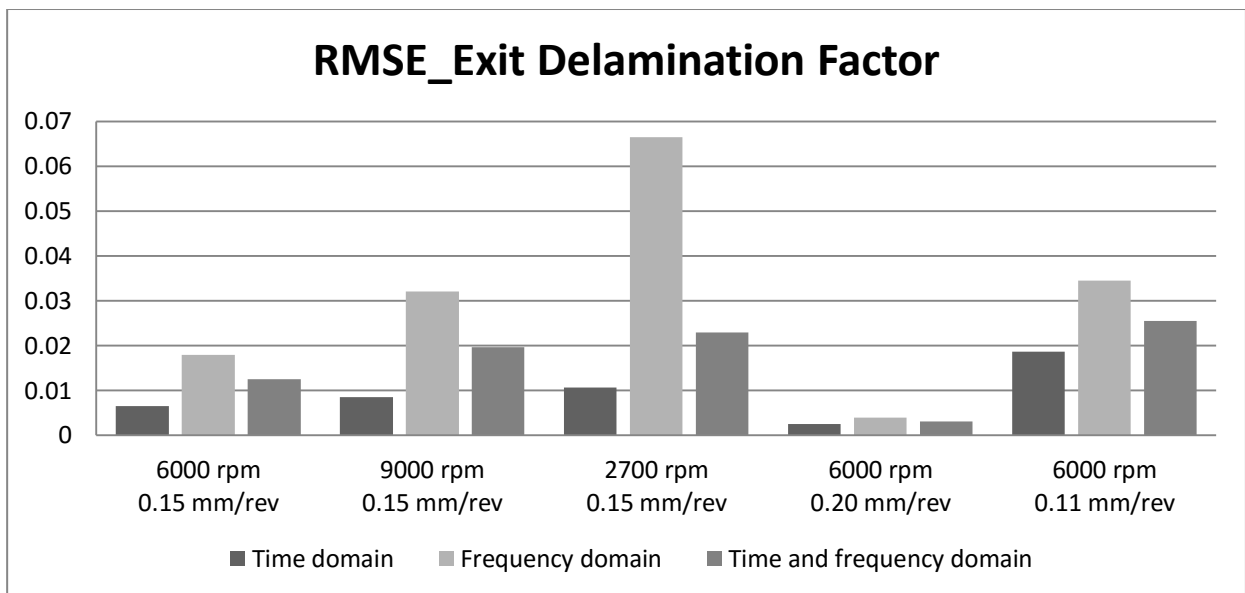
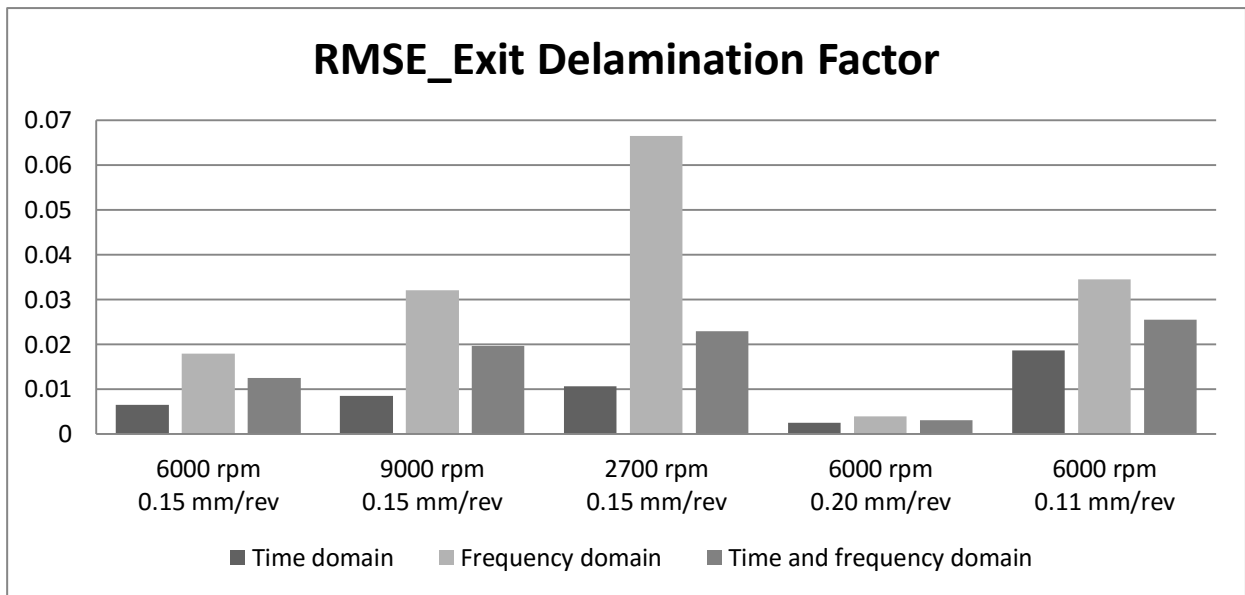
	TIME DOMAIN FEATURES																			
	Force					Torque					Vibration Acceleration					AErms				
	M.	V.	K.	S.	P.	M.	V.	K.	S.	P.	M.	V.	K.	S.	P.	M.	V.	K.	S.	P.
	TOOL WEAR - VB																			
6000 rpm 0.15 mm/rev	1	1	0	1	1	1	0	0	0	0	0	0	0	0	0	0	0	0	0	0
9000 rpm 0.15 mm/rev	1	1	0	1	1	1	0	1	0	0	1	1	0	0	1	0	1	0	1	1
2700 rpm 0.15 mm/rev	1	1	0	1	1	1	1	0	0	1	0	0	0	0	0	0	0	1	0	0
6000 rpm 0.20 mm/rev	1	1	0	1	1	1	0	0	0	0	1	1	0	0	1	0	0	1	0	0
6000 rpm 0.11 mm/rev	1	1	0	1	1	1	1	0	0	1	0	0	0	0	0	0	0	1	0	0
NO-FULL	X	X	-	X	X	X	-	-	-	-	-	-	-	-	-	-	-	X	-	-
FULL	X	X	-	X	X	X	-	-	-	-	-	-	-	-	-	-	-	-	-	-
	EXIT DELAMINATION FACTOR																			
6000 rpm 0.15 mm/rev	1	1	0	1	1	1	0	0	0	0	0	0	0	0	0	0	0	1	0	0
9000 rpm 0.15 mm/rev	1	1	0	1	1	1	0	1	0	0	1	0	0	0	1	0	1	0	1	0
2700 rpm 0.15 mm/rev	1	1	0	1	1	1	1	0	0	1	0	0	0	0	0	0	0	1	0	0
6000 rpm 0.20 mm/rev	1	1	0	1	1	1	0	0	0	0	1	1	0	0	1	0	0	1	0	0
6000 rpm 0.11 mm/rev	1	1	0	1	1	1	1	0	0	1	0	0	0	0	0	0	0	1	0	0
NO-FULL	X	X	-	X	X	X	-	-	-	-	-	-	-	-	-	-	-	X	-	-
FULL	X	X	-	X	X	X	-	-	-	-	-	-	-	-	-	-	-	-	-	-
	DELAMINATED AREA																			
6000 rpm 0.15 mm/rev	1	1	0	1	1	1	0	0	0	0	0	0	0	0	0	0	0	1	0	0
9000 rpm 0.15 mm/rev	1	1	0	1	1	1	0	1	0	0	1	1	0	0	1	1	1	0	1	1
2700 rpm 0.15 mm/rev	1	1	0	1	1	1	1	0	0	1	0	0	0	0	0	0	0	1	0	0
6000 rpm 0.20 mm/rev	1	1	0	1	1	1	0	0	0	0	1	1	1	0	1	0	0	1	0	0
6000 rpm 0.11 mm/rev	1	1	0	1	1	1	1	0	0	1	0	0	0	0	0	0	0	1	0	0
NO-FULL	X	X	-	X	X	X	-	-	-	-	-	-	-	-	-	-	-	X	-	-
FULL	X	X	-	X	X	X	-	-	-	-	-	-	-	-	-	-	-	-	-	-

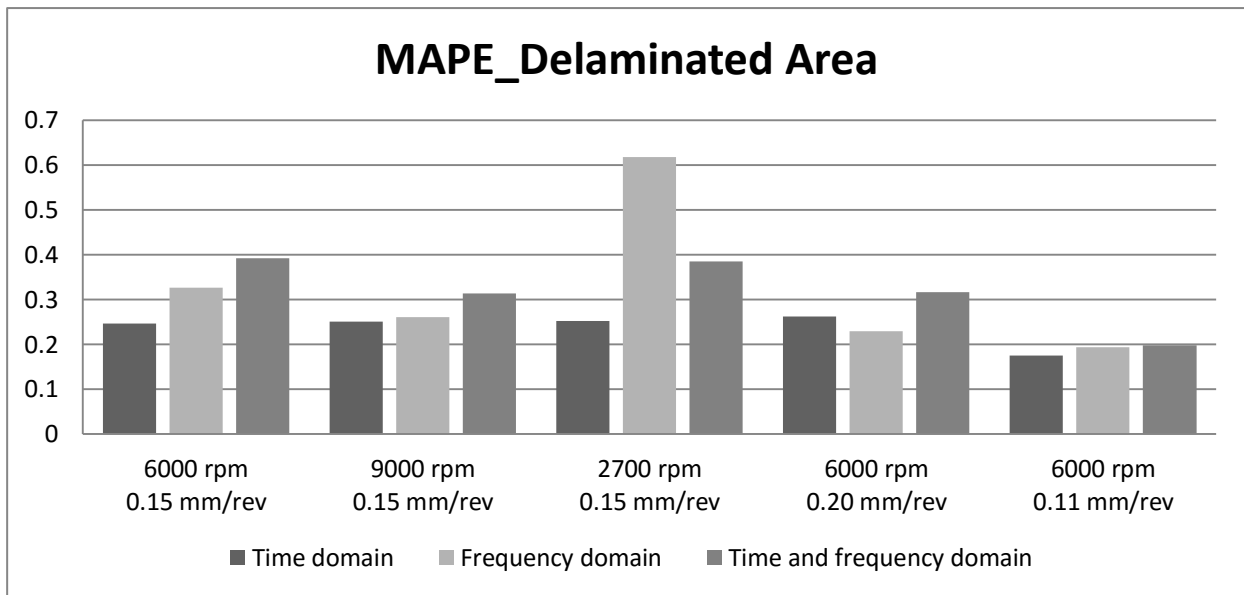
Force												Vibration Acceleration			AErms		
1xFreq.	2xFreq	3xFreq	4xFreq	5xFreq	6xFreq	8xFreq	1xFreq.	2xFreq	3xFreq.	4xFreq	5xFreq.	1xFreq	2xFreq	4xFreq	1xFreq.	2xFreq	4xFreq
TOOL WEAR - VB																	
1	1	1	1	0	1	0	0	1	0	1	0	0	0	-	0	0	-
0	1	-	1	-	1	-	0	1	-	1	-	-	0	-	-	0	-
-	1	-	1	-	1	1	-	0	0	0	-	-	0	0	-	0	0
1	1	1	1	1	1	1	0	0	1	1	0	1	1	-	0	0	-
1	1	1	1	1	1	1	1	1	1	1	0	0	0	0	0	0	0
-	X	-	X	-	X	-	-	X	-	X	-	-	-	-	-	-	-
-	X	-	X	-	X	-	-	-	-	-	-	-	-	-	-	-	-
EXIT DELAMINATION FACTOR																	
1	1	1	1	0	1	0	0	1	0	1	0	0	0	-	0	0	-
0	1	-	1	-	1	-	0	1	-	1	-	-	0	-	-	0	-
-	1	-	1	-	1	1	-	0	0	0	-	-	0	0	-	0	0
1	1	1	1	1	1	1	1	0	1	1	0	1	0	-	0	0	-
1	1	1	1	1	1	1	1	1	1	1	0	0	0	0	0	0	0
-	X	-	X	-	X	-	-	X	-	X	-	-	-	-	-	-	-
-	X	-	X	-	X	-	-	-	-	-	-	-	-	-	-	-	-
DELAMINATED AREA																	
1	1	1	1	0	1	0	1	1	0	1	0	0	0	-	0	0	-
0	1	-	1	-	1	-	0	1	-	1	-	-	0	-	-	0	-
-	1	-	1	-	1	1	-	0	0	0	-	-	0	0	-	0	0
1	1	1	1	1	1	1	1	1	0		-	1	1	0	0	1	0
1	1	0	1	1	1	1	1	1	1	1	0	0	0	0	0	0	0
-	X	-	X	-	X	-	-	X	-	X	-	-	-	-	-	-	-
-	X	-	X	-	X	-	-	-	-	-	-	-	-	-	-	-	-

APPENDIX D

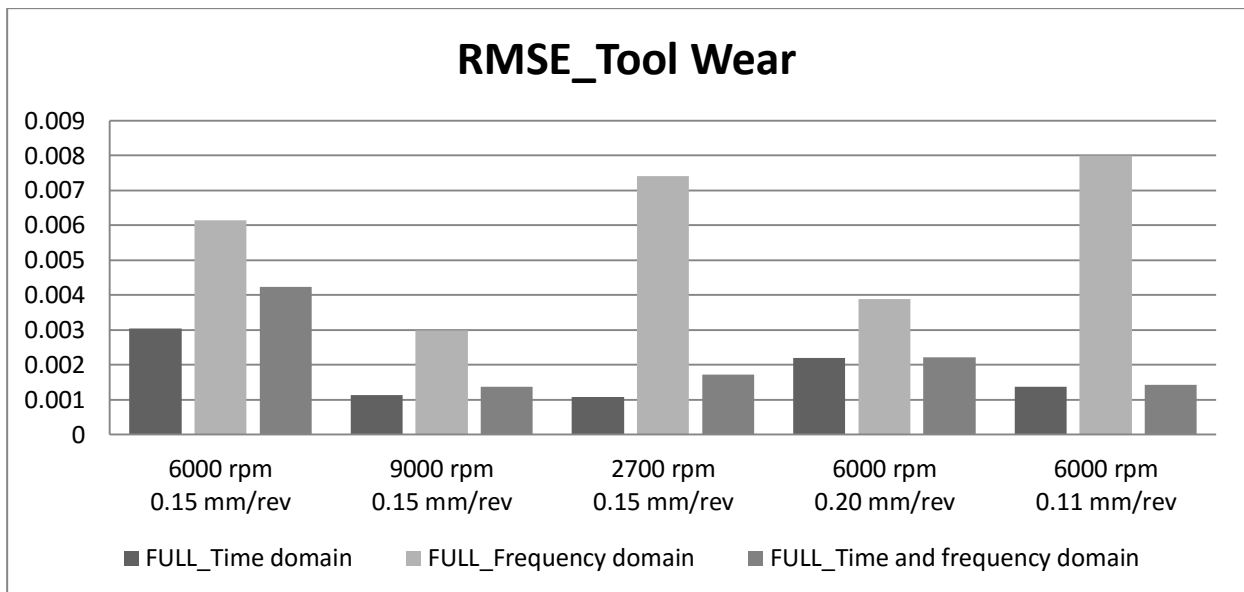
- Time domain features: F_{mean} , F_{variance} , F_{skewness} , F_{power} , T_{mean} and $A\text{Erms}_{\text{variance}}$
- Frequency domain features: $F_{\text{peak}_{2x}}$, $F_{\text{peak}_{4x}}$, $F_{\text{peak}_{6x}}$, $T_{\text{peak}_{2x}}$, and $T_{\text{peak}_{4x}}$
- Time and frequency domain features: F_{mean} , F_{variance} , F_{skewness} , F_{power} , T_{mean} , $A\text{Erms}_{\text{variance}}$, $F_{\text{peak}_{2x}}$, $F_{\text{peak}_{4x}}$, $F_{\text{peak}_{6x}}$, $T_{\text{peak}_{2x}}$, and $T_{\text{peak}_{4x}}$

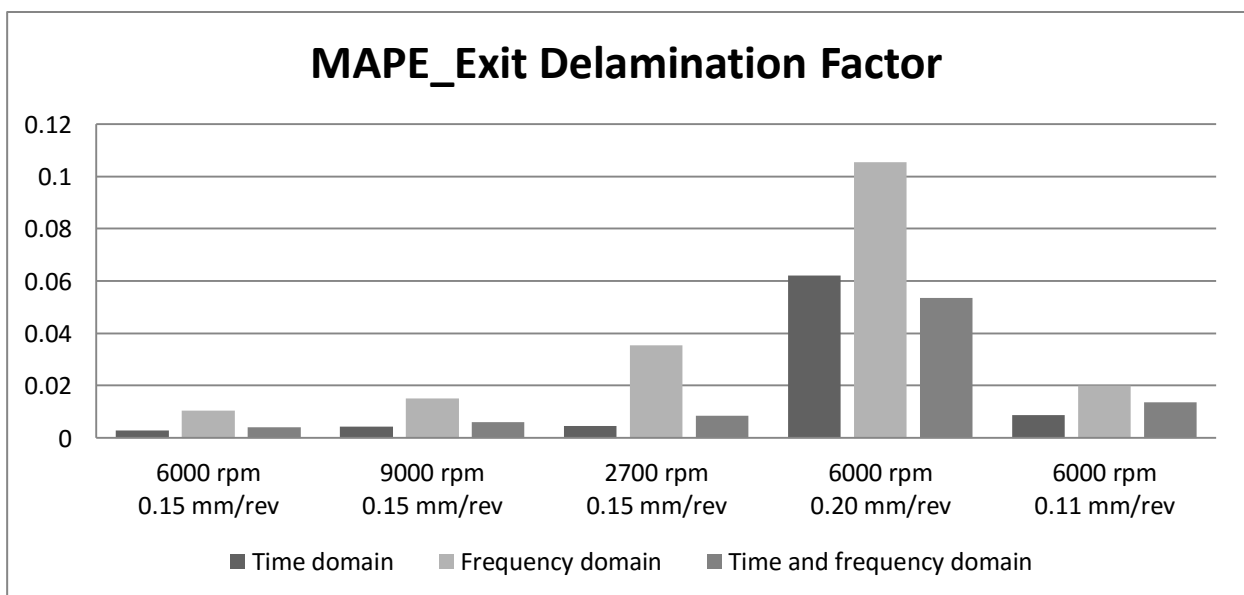
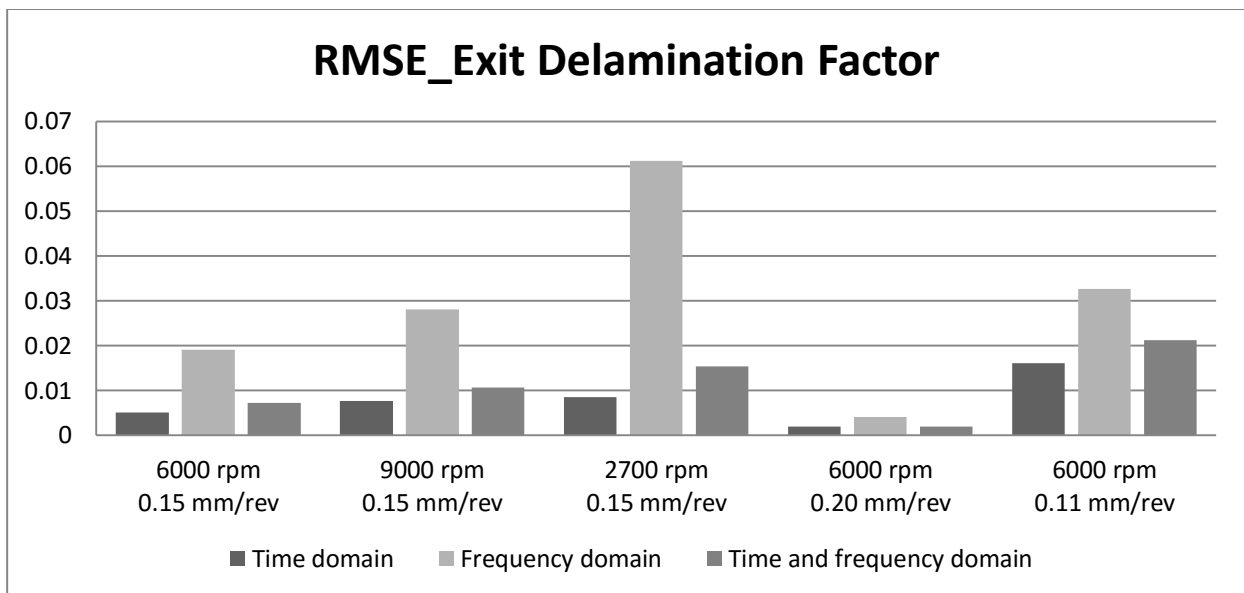
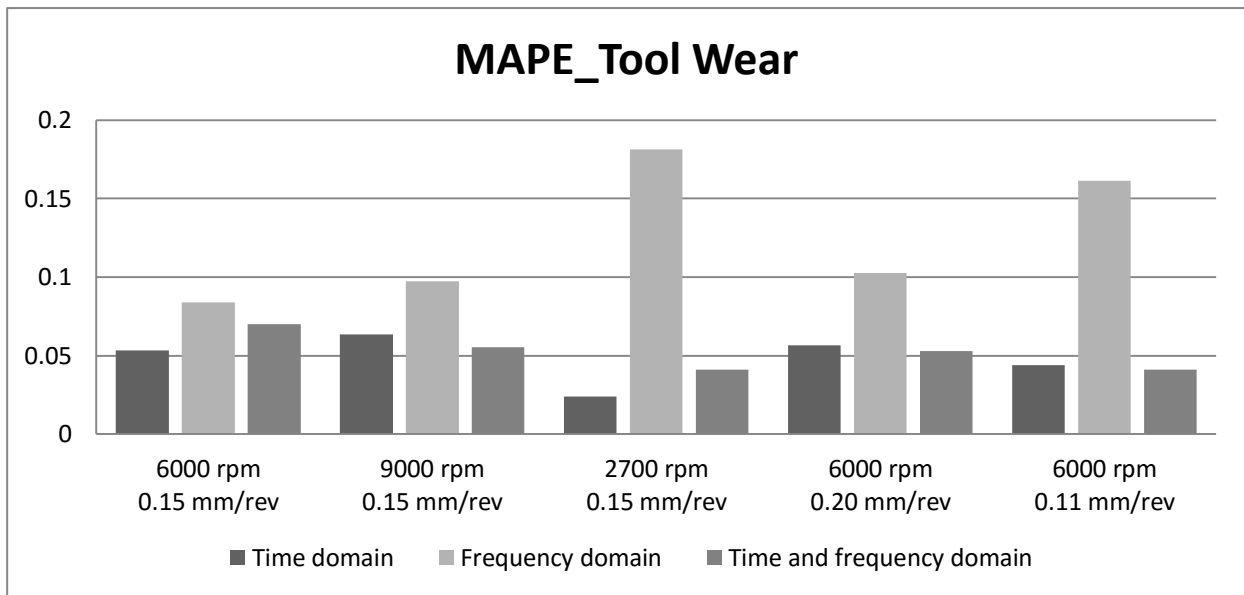


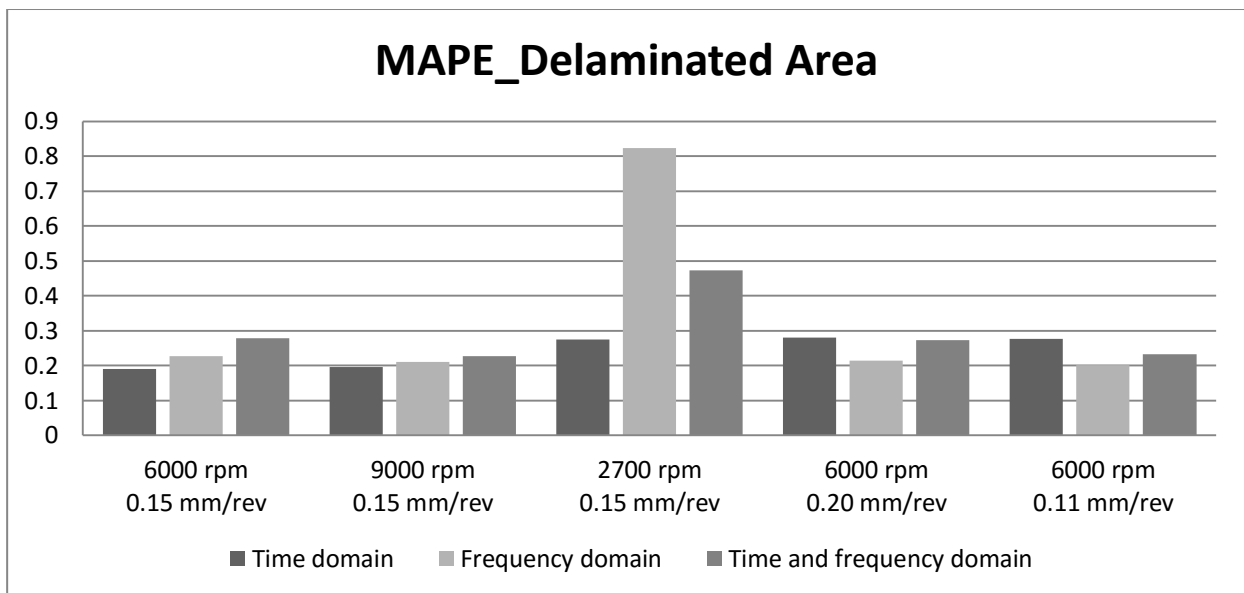
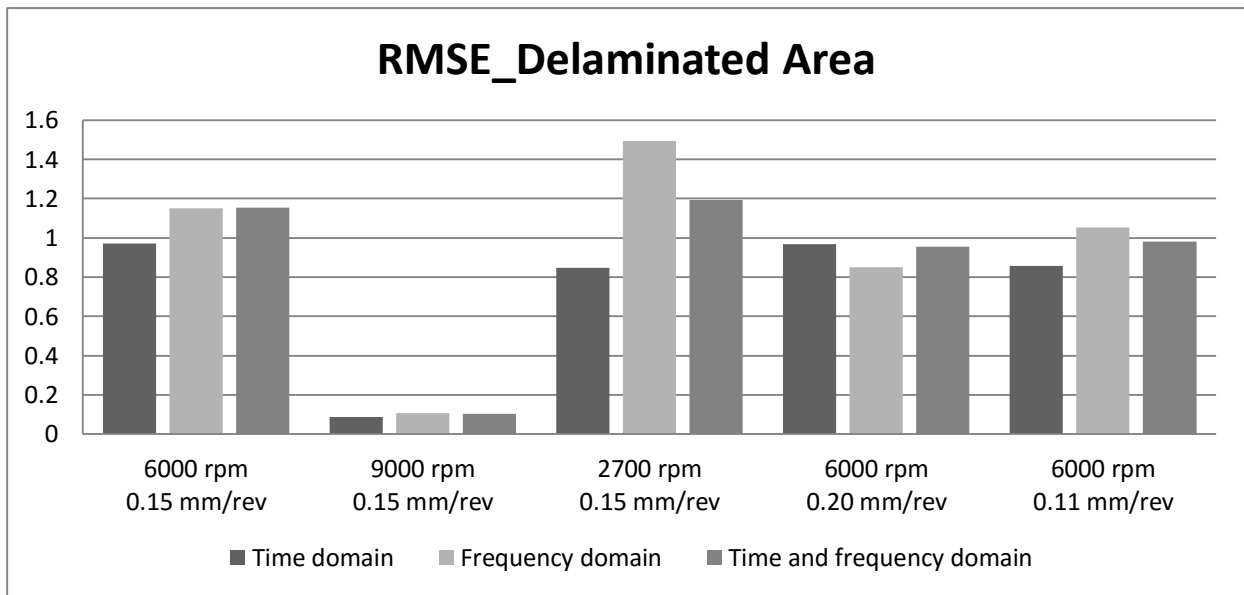




- Time domain features: F_{mean} , F_{variance} , F_{skewness} , F_{power} , and T_{mean}
- Frequency domain features: $F_{\text{peak}_{2x}}$, $F_{\text{peak}_{4x}}$, and $F_{\text{peak}_{6x}}$
- Time and frequency domain features: F_{mean} , F_{variance} , F_{skewness} , F_{power} , T_{mean} , $F_{\text{peak}_{2x}}$, and $F_{\text{peak}_{4x}}$, $F_{\text{peak}_{6x}}$







References

- Abouelatta, O., & Mádl, J. (2001). Surface roughness prediction based on cutting parameters and tool vibrations in turning operations. *Journal of Materials Processing Technology*, 118(1-3), 269-277.
- Abu-Zahra, N., & Yu, G. (2000). Analytical model for tool wear monitoring in turning operations using ultrasound waves. *International Journal of Machine Tools and Manufacture*, 40(11), 1619-1635.
- Achiche, S., Balazinski, M., Baron, L., & Jemielniak, K. (2002). Tool wear monitoring using genetically-generated fuzzy knowledge bases. *Engineering Applications of Artificial Intelligence*, 15(3-4), 303-314.
- Ahn, J., Shen, Y., Kim, H., Jeong, H., & Cho, K. (2001). Development of a sensor information integrated expert system for optimizing die polishing. *Robotics and Computer-Integrated Manufacturing*, 17(4), 269-276.
- Al-Habaibeh, A., & Gindy, N. (2000). New approach for systematic design of condition monitoring systems for milling processes. *Journal of Materials Processing Technology*, 107(1-3), 243-251.
- Altintas, Y., & Park, S. (2004). Dynamic compensation of spindle-integrated force sensors. *CIRP Annals - Manufacturing Technology*, 53(1), 305-308.
- Andreasen, J., & De Chiffre, L. (1998). An Automatic System for Elaboration of Chip Breaking Diagrams. *CIRP Annals*, 47(1), 35-40.
- Arrazola, P., Arriola, I., Davies, M., Cooke, A., & Dutterer, B. (2008). The Effect of Machinability on Thermal Fields in Orthogonal Cutting of AISI 4140 Steel. *CIRP Annals*, 57(1), 65-68.
- Arul, S., Vijayaraghavan, L., Malhotra, S., & Krishnamurthy, R. (2006). Influence of tool material on dynamics of drilling of GFRP composites. *International Journal of Advanced Manufacturing Technology*, 29((7-8)), 655-662.
- Arul, S., Vijayaraghavan, L., Malhotra, S., & Krishnamurthy, R. (2006). The effect of vibratory drilling on hole quality in polymeric composites. *International Journal of Machine Tools and Manufacture*, 46((3-4)), 252-259.
- Axinte, D. (2006). Approach into the use of probabilistic neural networks for automated classification of tool malfunctions in broaching. *International Journal of Machine Tools and Manufacture*, 46(12-13), 1445-1448.
- Axinte, D. (2007). An experimental analysis of damped coupled vibrations in broaching. *International Journal of Machine Tools and Manufacture*, 47(14), 2182-2188.
- Axinte, D., & Gindy, N. (2003). Tool Condition Monitoring in Broaching. *Wear*, 254(3-4), 370-382.
- Axinte, D., Boud, F., Penny, J., Gindy, N., & Williams, D. (2005). Broaching of Ti-6-4 - Detection of workpiece surface anomalies on dovetail slots through process monitoring. *CIRP Annals - Manufacturing Technology*, 54(1), 87-90.
- Axinte, D., Gindy, N., Fox, K., & Unanue, I. (2004). Process monitoring to assist the workpiece surface quality in machining. *International Journal of Machine Tools and Manufacture*, 44(10), 1091-1108.

- Axinte, D., Natarajan, D., & Gindy, N. (2005). An approach to use an array of three acoustic emission sensors to locate uneven events in machining - Part 1: Method and validation. *International Journal of Machine Tools and Manufacture*, 45(14), 1605-1613.
- Azmir, M. A., & Ahsan, A. K. (2009). A study of abrasive water jet machining process on glass/epoxy composite laminate. *Journal of Materials Processing Technology*, 209(20), 6168-6173.
- Azouzi, R., & Guillot, M. (1997). On-line prediction of surface finish and dimensional deviation in turning using neural network based sensor fusion. *International Journal of Machine Tools and Manufacture*, 37(9), 1201-1217.
- Babu, P., & Pradhan, B. (2007). Effect of damage levels and curing stresses on delamination growth behavior emanating from circular holes in laminated FRP composite. *Composites (Part A: Applied Science and Manufacturing)*, 38, 2412–2421.
- Balasubramanian, M. (2016). Introduction to Composite Materials. In *Fibrous and Textile Materials for Composite Applications* (p. 1-38). Rana, Sohail, Figueiro, Raul.
- Balazinski, M., & Jemielniak, K. (1998). Tool Conditions Monitoring Using Fuzzy Decision Support System. *CIRP International Conference on Automatic Supervision, Monitoring and Adaptive Control in Manufacturing*, (p. 115-122). Miedzeszyn.
- Bhatnagar, N., Singh, I., & Nayak, D. (2004). Damage investigations in drilling of glass fiber reinforced plastic composite laminates. *Materials and Manufacturing Processes*, 19(6), 995–1007.
- Bhattacharyya, P., Sengupta, D., & Mukhopadhyay, S. (2007). Cutting force-based real-time estimation of tool wear in face milling using a combination of signal processing techniques. *Mechanical Systems and Signal Processing*, 21(6), 2665-2683.
- Biermann, D., Kirschner, M., Pantke, K., Tillmann, W., & Herper, J. (2013). New coating systems for temperature monitoring in turning processes. *Surface and Coatings Technology*, 215, 376-380.
- Binsaeid, S., Asfour, S., Cho, S., & Onar, A. (2009). Machine ensemble approach for simultaneous detection of transient and gradual abnormalities in end milling using multisensor fusion. *Journal of Materials Processing Technology*, 209, 4728–4738.
- Brophy, B., Kelly, K., & Byrne, G. (2002). AI-based condition monitoring of the drilling process. *Journal of Materials Processing Technology*, 124(3), 305-310.
- Bukkapatnam, S., Kumara, S., & Lakhtakia, A. (2000). Fractal estimation of flank wear in turning. *Journal of Dynamic Systems, Measurement and Control, Transactions of the ASME*, 122(1), 89-94.
- Bukkapatnam, S., Kumara, S., Lakhtakia, A., & Srinivasan, P. (2002). The neighborhood method and its coupling with the wavelet method for signal separation of chaotic signals. *Signal Processing*, 82(10), 1351-1374.
- Byrne, G., & O'Donnell, G. (2007). An integrated force sensor solution for process monitoring of drilling operations. *CIRP Annals - Manufacturing Technology*, 56(1), 88-92.
- Byrne, G., Dornfeld, D., & Denkena, B. (2003). Advancing cutting technology. *CIRP Annals - Manufacturing Technology*, 52(2), 483-507.

- Byrne, G., Dornfeld, D., Inasaki, I., Ketteler, G., König, W., & Teti, R. (1995). Tool Condition Monitoring (TCM) - The Status of Research and Industrial Application. *CIRP Annals - Manufacturing Technology*, 44(2), 541-567.
- Byrne, G., Dornfeld, D., Inasaki, I., Ketteler, G., König, W., & Teti, R. (1995). Tool Condition Monitoring (TCM) - The Status of Research and Industrial Application. *CIRP Annals - Manufacturing Technology*, 44(2), 541-567.
- Campbell, F. (2010). Introduction to Composite Materials. In *Structural Composite Materials*. Materials Park, Ohio: ASM International.
- Capello, E. (2004). Workpiece damping and its effect on delamination damage in drilling thin composite laminates. *Journal of Materials Processing Technology*, 148(2), 186-195.
- Carolan, T., Kidd, S., Hand, D., Wilcox, S., Wilkinson, P., Barton, J., . . . Reuben, R. (1997). Acoustic emission monitoring of tool wear during the face milling of steels and aluminium alloys using a fibre optic sensor. Part 1: Energy analysis. *roceedings of the Institution of Mechanical Engineers, Part B: Journal of Engineering Manufacture*, 211(4), p. 299-309.
- Carolan, T., Kidd, S., Hand, D., Wilcox, S., Wilkinson, P., Barton, J., . . . Reuben, R. (1997). Acoustic emission monitoring of tool wear during the face milling of steels and aluminium alloys using a fibre optic sensor. Part 2: Frequency analysis. *Proceedings of the Institution of Mechanical Engineers, Part B: Journal of Engineering Manufacture*, 211(4), p. 311-319.
- Chang, H.-K., Kim, J.-H., Kim, I., Jang, D., & Han, D. (2007). In-process surface roughness prediction using displacement signals from spindle motion. *International Journal of Machine Tools and Manufacture*, 47(6), 1021-1026.
- Chen, L., Bender, P., Renton, P., & El-Wardany, T. (2002). Integrated Virtual Manufacturing Systems for Process Optimisation and Monitoring. *CIRP Annals*, 51(1), 409-412.
- Chen, W.-C. (1997). Some Experimental Investigations in the Drilling of Carbon Fiber-Reinforced Plastic (CFRP) Composite Laminates. *International Journal of Machine Tools and Manufacture*, 37(8), 1097-1108.
- Choudhury, S., Jain, V., & Rama Rao, C. (1999). On-line monitoring of tool wear in turning using a neural network. *International Journal of Machine Tools and Manufacture*, 39(3), 489-504.
- Daisuke, H., & Tomoharu, N. (2001). 2-D Artificial Cellular Neural Network and its application to chase game. *IEEJ Transactions on Electronics, Information and Systems*, 6, 1071-1079.
- Dambon, O., Demmer, A., & Peters, J. (2006). Surface Interactions in Steel Polishing for the Precision Tool Making. *CIRP Annals - Manufacturing Technology*, 55(1), 609-612.
- Daubechies, I. (1990). The Wavelet Transform, Time-Frequency Localization and Signal Analysis. *IEEE Transactions on Information Theory*, 36(5), 961-1005.
- Davies, M., Ueda, T., M'Saoubi, R., Mullany, B., & Cooke, A. (2007). On The Measurement of Temperature in Material Removal Processes. *CIRP Annals - Manufacturing Technology*, 56(2), 581-604.
- Davim, J., & Reis, P. (2003). Drilling carbon fiber reinforced plastics manufactured by autoclave—experimental and statistical study. *Materials & Design*, 24(5), 315-324.

- Davim, J., & Reis, P. (2003). Study of Delamination in Drilling Carbon Fiber Reinforced Plastics (CFRP) Using Design Experiments. *Composite Structures*, 59, 481-487.
- Davim, J., Reis, P., & António, C. (2004). Drilling fiber reinforced plastics (FRPs) manufactured by hand lay-up: Influence of matrix (Viapal VHP 9731 and ATLAC 382-05). *Journal of Materials Processing Technology*, 155-156((1-3)), 1828-1833.
- Davim, J., Rubio, J., & Abrao, A. (2007). A novel approach based on digital image analysis to evaluate the delamination factor after drilling composite laminates. *Composites Science and Technology*, 67(9), 1939–1945.
- Davim, J., Rubio, J., & Abrao, A. (2007). A novel approach based on digital image analysis to evaluate the delamination factor after drilling composite laminates. *Composites Science and Technology*, 67(9), 1939-1945.
- Dharan, C., & Won, M. (2000). Machining parameters for an intelligent machining system for composite laminates. *International Journal of Machine Tools and Manufacture*, 40, 415–426.
- Dimla Snr., D. (2000). Sensor signals for tool-wear monitoring in metal cutting operations - a review of methods. *International Journal of Machine Tools and Manufacture*, 40(8), 1073-1098.
- Dimla, S. D., & Lister, P. (2000). On-line metal cutting tool condition monitoring. I: force and vibration analyses. *International Journal of Machine Tools and Manufacture*, 40(5), 739-768.
- Dolinšek, S., & Kopač, J. (1999). Acoustic emission signals for tool wear identification. *Wear*, 225-229, 295–303.
- Dolinšek, S., Šuštaršič, B., & Kopač, J. (2001). Wear mechanisms of cutting tools in high-speed cutting processes. *Wear*, 250(1-12), 349-356.
- Dong, J., Subrahmanyam, K., Wong, Y., Hong, G., & Mohanty, A. (2006). Bayesian-inference-based neural networks for tool wear estimation. *International Journal of Advanced Manufacturing Technology*, 30(9-10), 797-807.
- Duda, R., & Hart, P. (1973). *Pattern Classification and Scene Analysis*. New York: John Wiley and Sons.
- Durão, L., Gonçalves, D., Tavares, J., de Albuquerque, V., Aguiar Vieira, A., & Torres Marques, A. (2010). Drilling tool geometry evaluation for reinforced composite laminates. *Composite Structures*, 92(7), 1545-1550.
- E. Brinksmeier, R. J. (s.d.). *Drilling of Multi-Layer Composite Materials consisting of Carbon Fiber Reinforced Plastics (CFRP)*. University of Bremen Faculty of Production Technology, Division of Manufacturing Processes.
- El-Hofy, H. A.-G. (2013). *Fundamentals of Machining Processes: Conventional and Nonconventional Processes*. CRC Press.
- Eriksen, R., Arentoft, M., Grønbaek, J., & Bay, N. (2012). Manufacture of functional surfaces through combined application of tool manufacturing processes and Robot Assisted Polishing. *CIRP Annals - Manufacturing Technology*, 61(1), 563-566.
- Faraz, A., Biermann, D., & Weinert, K. (2009). Cutting edge rounding: An innovative tool wear criterion in drilling CFRP composite laminates. *International Journal of Machine Tools & Manufacture*, 49, 1185-1196.

- Feito, N., Díaz-Álvarez, J., Díaz-Álvarez, A., Cantero, J., & Miguélez, M. (2014). Experimental Analysis of the Influence of Drill Point Angle and Wear on the Drilling of Woven CFRPs. *Materials*, 7(6), 4258-4271.
- Gandarias, E., Dimov, S., Pham, D., Ivanov, A., Popov, K., Lizarralde, R., & Arrazola, P. (2006). New Methods for Tool Failure Detection in Micromilling. *Proceedings of IMechE*, 220(2), p. 137-144.
- Ghorbani, H., & Moetakef-Imani, B. (2015). Specific cutting force and cutting condition interaction modeling for round insert face milling operation. *International Journal of Advanced Manufacturing Technology*, 11, in press.
- Ghosh, N., Ravi, Y., Patra, A., Mukhopadhyay, S., Paul, S., Mohanty, A., & Chattopadhyay, A. (2007). Estimation of tool wear during CNC milling using neural network-based sensor fusion. *Mechanical Systems and Signal Processing*, 21(1), 466-479.
- Govekar, E., Gradisek, J., & Grabec, I. (2000). Analysis of AE Signals and Monitoring of Machining Processes. *Ultrasonics*, 38, 598-603.
- Groover, M. P. (2010). *Fundamentals of Modern Manufacturing: Materials, Processes, and Systems* (4th ed.). John Wiley & Sons, Inc.
- Grzesik, W., & Bernat, P. (1998). An investigation of the cutting process for chip breaking monitoring in turning of steels. *Journal of Manufacturing Science and Engineering, Transactions of the ASME*, 120(3), 555-562.
- Gu, S., Ni, J., & Yuan, J. (2002). Non-stationary signal analysis and transient machining process condition monitoring. *International Journal of Machine Tools and Manufacture*, 42(1), 41-51.
- Guo, Y., & Ammala, S. (2005). Real-time acoustic emission monitoring for surface damage in hard machining. *International Journal of Machine Tools and Manufacture*, 45(14), 1622-1627.
- Guo, Y., & Ammala, S. (2005). Real-time acoustic emission monitoring for surface damage in hard machining. *International Journal of Machine Tools and Manufacture*, 45(14), 1622-1627.
- Halgamuge, S., & Glesner, M. (1994). Neural networks in designing fuzzy systems for real world applications. *Fuzzy Sets and Systems*, 65(1), 1-12.
- Hastie, T., Tibshirani, R., & Friedman, J. (2001). *The Elements of Statistical Learning; Data mining, Inference and Prediction*. New York: Springer-Verlag.
- Herzog, D., Jaeschke, P., Meier, O., & Haferkamp, H. (2008). Investigations on the thermal effect caused by laser cutting with respect to static strength of CFRP. *International Journal of Machine Tools and Manufacture*, 48(12-13), 1464-1473.
- Ho-Cheng, H., & Dharan, C. (1990). Delamination during drilling in composite laminates. *Journal of engineering for industry*, 112(3), 236-239.
- Hocheng, H., & Tsao, C. (2006). Effects of special drill bits on drilling-induced delamination of composite materials. *International Journal of Machine Tools and Manufacture*, 46((12-13)), 1403-1416.
- Hong, G., Rahman, M., & Zhou, Q. (1996). Using neural network for tool condition monitoring based on wavelet decomposition. *International Journal of Machine Tools and Manufacture*, 36(5), 551-566.

- Huang, B., & Chen, J. (2003). An in-process neural network-based surface roughness prediction (INN-SRP) system using a dynamometer in end milling operations. *International Journal of Advanced Manufacturing Technology*, 21(5), 339-347.
- Huang, J.-C., Chang, H., Kuo, C.-G., Li, J.-F., & You, Y.-C. (2015). Prediction surface morphology of nanostructure fabricated by nano-oxidation technology. *Materials*, 8(12), 8437-8451.
- Hundt, W., Leuenberger, D., Rehsteiner, F., & Gygax, P. (1994). An Approach to Monitoring of the Grinding Process Using Acoustic Emission (AE) Technique. *CIRP Annals - Manufacturing Technology*, 43(1), 295-298.
- Hutton, D., & Hu, F. (1999). Acoustic emission monitoring of tool wear in end-milling using time-domain averaging. *Journal of Manufacturing Science and Engineering, Transactions of the ASME*, 121(1), 8-12.
- Iliescu, D., Gehin, D., Gutierrez, M., & Girod, F. (2010). Modeling and tool wear in drilling of CFRP. *International Journal of Machine Tools and Manufacture*, 50(2), 204-213.
- Inasaki, I. (1998). Application of acoustic emission sensor for monitoring machining processes. *Ultrasonics*, 36(1-5), 273-281.
- Isbilir, O., & Ghassemieh, E. (2012). Delamination and wear in drilling of carbon-fiber reinforced plastic composites using multilayer TiAlN/TiN PVD-coated tungsten carbide tools. *Journal of Reinforced Plastics and Composites*, 31(10), 717-727.
- Isbilir, O., & Ghassemieh, E. (2013). Comparative study of tool life and hole quality in drilling of CFRP/titanium stack using coated carbide drill. *Machining Science and Technology*, 17(3), 380-409.
- J.R. Ferreira, N. C. (s.d.). *Machining optimization in carbon fibre reinforced composite materials*. UNICAMP-Universida de Estadual de Campinas, Departamento de Enga. de Fabricacao, Campinas-SP, Brazil.
- Jahan Hossain, M., & Ahmad, N. (2014). A neuro-fuzzy approach to select cutting parameters for commercial die manufacturing. *Procedia Engineering*, 90, 753-759.
- Jain, S., & Yang, D. (1994). Delamination-Free Drilling of Composite Laminates. *Journal of engineering for industry*, 116(4), 475-481.
- Jemielniak, K. (2000). Some aspects of AE application in tool condition monitoring. *Ultrasonics*, 38(1), 604-608.
- Jemielniak, K. (2001). Some aspects of acoustic emission signal pre-processing. *Journal of Materials Processing Technology*, 109(3), 242-247.
- Jemielniak, K. O. (1998). Catastrophic tool failure detection based on acoustic emission signal analysis. *CIRP Annals - Manufacturing Technology*, 47(1), 31-34.
- Jemielniak, K., & Arrazola, P. (2008). Application of AE and cutting force signals in tool condition monitoring in micro-milling. *CIRP Journal of Manufacturing Science and Technology*, 1(2), 97-102.

- Jemielniak, K., & Bombiński, S. (2006). Hierarchical strategies in tool wear monitoring. *Proceedings of the Institution of Mechanical Engineers, Part B: Journal of Engineering Manufacture*, 220(3), 375-381.
- Jemielniak, K., & Szafarczyk, M. (1992). Detection of Cutting Edge Breakage in Turning. *CIRP Annals - Manufacturing Technology*, 41(1), 97-100.
- Jemielniak, K., Bombiński, S., & Aristimuno, P. (2008). Tool condition monitoring in micromilling based on hierarchical integration of signal measures. *CIRP Annals - Manufacturing Technology*, 57(1), 121-124.
- Jemielniak, K., Kwiatkowski, L., & Wrzosek, P. (1998). Diagnosis of tool wear based on cutting forces and acoustic emission measures as inputs to a neural network. *Journal of Intelligent Manufacturing*, 9(5), 447-455.
- Jemielniak, K., Kwiatkowski, L., & Wrzosek, P. (1998). Diagnosis of tool wear based on cutting forces and acoustic emission measures as inputs to a neural network. *Journal of Intelligent Manufacturing*, 9(5), 447-455.
- Jun, M., Burak Ozdoganlar, O., DeVor, R., Kapoor, S., Kirchheim, A., & Schaffner, G. (2002). Evaluation of a spindle-based force sensor for monitoring and fault diagnosis of machining operations. *International Journal of Machine Tools and Manufacture*, 42(6), 741-751.
- Kamarthi, S., & Pittner, S. (1997). Fourier and wavelet transform for flank wear estimation - A comparison. *Mechanical Systems and Signal Processing*, 11(6), 791-809.
- Kamarthi, S., Kumara, S., & Cohen, P. (2000). Flank wear estimation in turning through wavelet representation of acoustic emission signals. *Journal of Manufacturing Science and Engineering, Transactions of the ASME*, 122 (1), pp., 122(1), 12-19.
- Kannatey-Asibu Jr., E., & Dornfeld, D. (1982). A study of tool wear using statistical analysis of metal-cutting acoustic emission. *Wear.*, 76(2), 247-261.
- Karpuschewski, B., Wehmeier, M., & Inasaki, I. (2000). Grinding monitoring system based on power and acoustic emission sensors. *CIRP Annals - Manufacturing Technology*, 49(1), 235-240.
- Khashaba, U., Seif, M., & Elhamid, M. (2007). Drilling analysis of chopped composites. *Composites: Part A*, 38, 61-70.
- Kim, H., Ahn, J., Kim, S., & Takata, S. (2002). Real Time Drill Wear Estimation Based on Spindle Motor Power. *Journal of Materials Processing Technology*, 124(3), 267-273.
- Kim, H.-Y., & Ahn, J.-H. (2002). Chip disposal state monitoring in drilling using neural network based spindle motor power sensing. *International Journal of Machine Tools and Manufacture*, 42(10), 1113-1119.
- Kim, J.-D., & Kim, D.-S. (1997). Development of a combined-type tool dynamometer with a piezo-film accelerometer for an ultra-precision lathe. *Journal of Materials Processing Technology*, 71(3), 360-366.
- Kim, S., Ahn, B., & Lee, S. (2009). Characterization of Magnetic Abrasive Finishing Using Sensor Fusion. *Transactions of the Korean Society of Mechanical Engineers*, 33(5), 514-520.
- Klir, G., & Folger, T. (1988). *Fuzzy Sets, Uncertainty and Information*. Engelwood-Cliffs: Prentice-Hall.

- Klocke, F., Wirtz, G., & Veselovac, D. (2009). Design approach for adaptive axial force control in gun drilling. *ASME International Mechanical Engineering Congress and Exposition, 11*, p. 583-588.
- Kohonen, T. (1989). *Self-Organization and Associative Memory* (Vol. 8). Berlin: Springer-Verlag Berlin Heidelberg.
- Korkut, I. (2003). A dynamometer design and its construction for milling operation. *Materials and Design, 24*(8), 631-637.
- Kuljanic, E., Totis, G., & Sortino, M. (2009). Development of an intelligent multisensor chatter detection system in milling. *Mechanical Systems and Signal Processing, 23*(5), 1704-1718.
- Kunpeng, Z., San, W., & Soon, H. (2012). Signal processing for tool condition monitoring: From wavelet analysis to sparse decomposition. *Mechatronics and Manufacturing Engineering: Research and Development, 115-157*.
- Kurada, S., & Bradley, C. (1997). A review of machine vision sensors for tool condition monitoring. *Computers in Industry, 34*(1), 55-72.
- Kwak, J.-S. (2006). Application of wavelet transform technique to detect tool failure in turning operations. *International Journal of Advanced Manufacturing Technology, 28*(11-12), 1078-1083.
- Kwak, J.-S., & Song, J.-B. (2001). Trouble diagnosis of the grinding process by using acoustic emission signals. *International Journal of Machine Tools and Manufacture, 41*(6), 899-913.
- Lee, J., Choi, D., Kim, J., & Chu, C. (1995). Real-time Tool Breakage Detection for NC Milling Process. *CIRP Annals, 44*(1), 59-62.
- Lenin, V., Ramkumar, R., & Senthilkumar, M. (2015). Experimental Investigation of Thrust Force in Drilling of Glass Fiber Reinforced Plastic (GFRP) Composite Laminates. *International Journal of Engineering Research & Technology (IJERT), 4*(2), 633-637.
- Li, X. (2002). A brief review: Acoustic emission method for tool wear monitoring during turning. *International Journal of Machine Tools and Manufacture, 42*(2), 157-165.
- Li, X., Dong, S., & Yuan, Z. (1999). Discrete wavelet transform for tool breakage monitoring. *International Journal of Machine Tools and Manufacture, 39*(12), 1935-1944.
- Li, X., Ouyang, G., & Liang, Z. (2008). Complexity measure of motor current signals for tool flute breakage detection in end milling. *International Journal of Machine Tools and Manufacture, 48*(3-4), 371-379.
- Liao, L., Xi, F., & Liu, K. (2008). Modeling and control of automated polishing/ deburring process using a dual-purpose compliant toolhead. *International Journal of Machine Tools & Manufacture, 48*(12-13), 1454-1463.
- Liu, C., Li, Y., & Shen, W. (2014). A wavelet-based characteristic vector construction method for machining condition monitoring. *IEEE International Conference on Automation Science and Engineering*, (p. 304-308).
- Liu, D., Tang, Y., & Cong, W. (2012). A review of mechanical drilling for composite laminates. *Composite Structures, 94*(4), 1265-1279.

- López De Lacalle, L., Rivero, A., & Lamikiz, A. (2009). Mechanistic model for drills with double point-angle edges. *International Journal of Advanced Manufacturing Technology*, 40((5-6)), 447-457.
- Mallat, S. (1989). A theory for multiresolution signal decomposition: the wavelet representation. *IEEE Transactions on Pattern Analysis and Machine Intelligence*, 11(7), 674 - 693.
- Mannan, M., Kassim, A., & Jing, M. (2000). Application of image and sound analysis techniques to monitor the condition of cutting tools. *Pattern Recognition Letters*, 21(11), 969-979.
- Marinescu, I., & Axinte, D. (2008). A critical analysis of effectiveness of acoustic emission signals to detect tool and workpiece malfunctions in milling operations. *International Journal of Machine Tools and Manufacture*, 48(10), 1148-1160.
- Marinescu, I., & Axinte, D. (2009). A time-frequency acoustic emission-based monitoring technique to identify workpiece surface malfunctions in milling with multiple teeth cutting simultaneously. *International Journal of Machine Tools and Manufacture*, 49(1), 53-65.
- Marinov, V. (2004). Tool Wear and Tool Life . In *Manufacturing Technology* (p. 77-80).
- Marques, A., Durão, L., Magalhães, A., & Tavar, J. (2007). Delamination analysis of carbon fibre reinforced laminates. *ICCM International Conferences on Composite Materials*.
- Mezentsev, O., Zhu, R., DeVor, R., Kapoor, S., & Kline, W. (2002). Use of radial forces for fault detection in tapping. *International Journal of Machine Tools and Manufacture*, 42(4), 479-488.
- Moller, M. (1993). Neural Networks. 6, 525-533.
- Nath, C., Rahman, M., & Andrew, S. (2007). A study on ultrasonic vibration cutting of low alloy steel. *Journal of Materials Processing Technology*, 192-193, 159-165.
- Neseli, S. (2004). Optimization of process parameters with minimum thrust force and torque in drilling operation using taguchi method. *Advances in Mechanical Engineering*, art. no. 925382.
- Ogawa, K., Aoyama, E., Inoue, H., Hirogaki, T., Nobe, H., Kitahara, Y., . . . Gunjima, M. (1997). Investigation on cutting mechanism in small diameter drilling for GFRP (thrust force and surface roughness at drilled hole wall). *Composite Structures*, 38((1-4)), 343-350.
- Oh, J., & Lee, S. (2011). Prediction of surface roughness in magnetic abrasive finishing using acoustic emission and force sensor data fusion. *Proceedings of the Institution of Mechanical Engineers, Part B: Journal of Engineering Manufacture*, 225(6), 853-856.
- Oliveira, J., Ferraz Jr., F., Coelho, R., & Silva, E. (2008). Architecture for machining process and production monitoring based in open computer numerical control. *Journal of Engineering Manufacture*, 222(12), 1605-1612.
- Park, K.-H., Beal, A., Kim, D., Kwon, P., & Lantrip, J. (2013). A Comparative Study of Carbide Tools in Drilling of CFRP and CFRP-Ti Stacks. *Journal of Manufacturing Science and Engineering*, 136(1).
- Pilný, L., & Bissacco, G. (2015). Development of on the machine process monitoring and control strategy in Robot Assisted Polishing. *CIRP Annals - Manufacturing Technology*, 64, 313-316.

- Piquet, R., Ferret, B., Lachaud, F., & Swider, P. (2000). Experimental analysis of drilling damage in thin carbon/epoxy plate using special drills. *Composites Part A: Applied Science and Manufacturing*, 31(10), 1107-1115.
- Prakash, M., Kanthababu, M., & Rajurkar, K. (2015). Investigations on the effects of tool wear on chip formation mechanism and chip morphology using acoustic emission signal in the microendmilling of aluminum alloy. *International Journal of Advanced Manufacturing Technology*, 77(5-8), 1499-1511.
- Pritschow, G., & Kramer, C. (2005). Open system architecture for drives. *CIRP Annals - Manufacturing Technology*, 54(1), 375-378.
- Pujana, J., Arrazola, P., & Villar, J. (2008). In-process high-speed photography applied to orthogonal turning. *Journal of Materials Processing Technology*, 202((1-3)), 475-485.
- Qiao, X., & Zhu, C. (2012). Active control of milling chatter based on the built-in force actuator. *Journal of Mechanical Engineering*, 48(1), 185-192.
- Quan, Y., Zhou, M., & Luo, Z. (1998). On-line robust identification of tool-wear via multi-sensor neural-network fusion. *Engineering Applications of Artificial Intelligence*, 11(6), 717-722.
- Rahman, A., Mamat, A., & Wagiman, A. (2009). Effect of Machining Parameters on Hole Quality of Micro Drilling for Brass. *Modern Applied Science*, 3(5), 221-230.
- Raj, D., & Karunamoorthy, L. (2016). Study of the Effect of Tool Wear on Hole Quality in Drilling CFRP to Select a Suitable Drill for Multi-Criteria Hole Quality. *Materials and Manufacturing Processes*, 31(5), 587-592.
- Rawat, S., & Attia, H. (2009). Characterization of the dry high speed drilling process of woven composites using Machinability Maps approach. *CIRP Annals*, 58(1), 105-108.
- Rawat, S., & Attia, H. (2009). Characterization of the dry high speed drilling process of woven composites using Machinability Maps approach. *CIRP Annals - Manufacturing Technology*, 58(1), 105-108.
- Ren, Q., Baron, L., Balazinski, M., Botez, R., & Bigras, P. (2015). Tool wear assessment based on type-2 fuzzy uncertainty estimation on acoustic emission. *Applied Soft Computing Journal*, 31, 14-24.
- René de Jesús, R.-T., Gilberto, H.-R., Iván, T.-V., & Carlos, J.-C. (2004). FPGA based on-line tool breakage detection system for CNC milling machines. *Mechatronics*, 14(4), 439-454.
- Rogers, L. (1979). The application of vibration signature analysis and acoustic emission source location to on-line condition monitoring of anti-friction bearings. *Tribology International*, 12(2), 51-58.
- Romoli, L., & Dini, G. (2008). Experimental study on the influence of drill wear in CFRP drilling process. *Proceedings of the Sixth CIRP International Conference on Intelligent Computation in Manufacturing Engineering*. Naples.
- Roy, S. (2015). An application of ANFIS-based intelligence technique for predicting tool wear in milling. *Advances in Intelligent Systems and Computing*, 343, 299-306.
- Rubio, E., & Teti, R. (2009). Cutting parameters analysis for the development of a milling process monitoring system based on audible energy sound. *Journal of Intelligent Manufacturing*, 20(1), 43-54.

- Ryabov, O., Mori, K., & Kasashima, N. (1996). An in-process direct monitoring method for milling tool failures using a laser sensor. *CIRP Annals - Manufacturing Technology*, 45(1), 97-100.
- Ryabov, O., Mori, K., & Kasashima, N. (1996). An In-process Direct Monitoring Method for Milling Tool Failures Using a Laser Sensor. *CIRP Annals*, 45(1), 97-100.
- Sadek, A., Meshreki, M., & Attia, M. (2012). Characterization and optimization of orbital drilling of woven carbon fiber reinforced epoxy laminates. *CIRP Annals*, 61(1), 123-126.
- Salgado, D., & Alonso, F. (2006). Tool wear detection in turning operations using singular spectrum analysis. *Journal of Materials Processing Technology*, 171(3), 451-458.
- Salgado, D., Alonso, F., Cambero, I., & Marcelo, A. (2009). In-process surface roughness prediction system using cutting vibrations in turning. *International Journal of Advanced Manufacturing Technology*, 43(1-2), 40-51.
- Saravanan, S., Yadava, G., & Rao, P. (2006). Condition monitoring studies on spindle bearing of a lathe. *International Journal of Advanced Manufacturing Technology*, 28(9), 993-1005.
- Scheffer, C., & Heyns, P. (2001). Wear monitoring in turning operations using vibration and strain measurements. *Mechanical Systems and Signal Processing*, 15(6), 1185-1202.
- Scheffer, C., & Heyns, P. (2004). An industrial tool wear monitoring system for interrupted turning. *Mechanical Systems and Signal Processing*, 18(5), 1219-1242.
- Schmidhuber, J., Wierstra, D., Gagliolo, M., & Gomez, F. (2007). Training recurrent networks by evoluno. *Neural Computation*, 19(3), 757-779.
- Segreto, T., & Teti, R. (2008). Sensor Fusion of Acoustic Emission and Cutting Force for Tool Wear Monitoring during Composite Materials Machining. *6th CIRP International Conference on ICME*, (p. 221-226). Naples.
- Segreto, T., Simeone, A., & Teti, R. (2014). Principal component analysis for feature extraction and NN pattern recognition in sensor monitoring of chip form during turning. *CIRP Journal of Manufacturing Science and Technology*, 7(3), 202-209.
- Sheikh-Ahmad, J., & Davim, J. P. (2012). Tool wear in machining processes for composites. In H. Hocheng (A cura di), *Machining Technology for Composite Materials: Principles and Practice* (p. 116-150). Philadelphia (USA): Woodhead Publishing.
- Shi, D., Axinte, D., & Gindy, N. (2007). Development of an online machining process monitoring system: A case study of the broaching process. *International Journal of Advanced Manufacturing Technology*, 34((1-2)), 34-46.
- Shinno, H., & Hashizume, H. (1997). In-process monitoring method for machining environment based on simultaneous multiphenomena sensing. *CIRP Annals - Manufacturing Technology*, 46(1), 53-X11.
- Shyha, I., Aspinwall, D., Soo, S., & Bradley, S. (2009). Drill geometry and operating effects when cutting small diameter holes in CFRP. *International Journal of Machine Tools and Manufacture*, 49((12-13)), 1008-1014.

- Shyha, I., Soo, S., Aspinwall, D., & Bradley, S. (2010). Effect of laminate configuration and feed rate on cutting performance when drilling holes in carbon fibre reinforced plastic composites. *Journal of Materials Processing Technology*, 210(8), 1023-1034.
- Sick, B. (2002). On-line and indirect tool wear monitoring in turning with artificial neural networks: A review of more than a decade of research. *Mechanical Systems and Signal Processing*, 16(4), 487-546.
- Singh, I., & Bajpai, P. (2013). Machining Behavior of Green Composites. A Comparison with Conventional Composites. In V. Thakur, *Green Composites from Natural Resources* (p. 267-280). CRC Press.
- Smith, D., Smith, S., & Tlustý, J. (1998). High performance milling torque sensor. *Journal of Manufacturing Science and Engineering, Transactions of the ASME*, 120(3), 504-514.
- Song, D.-Y., Otani, N., Aoki, T., Kamakoshi, Y., Ohara, Y., & Tamaki, H. (2005). A new approach to cutting state monitoring in end-mill machining. *International Journal of Machine Tools and Manufacture*, 45((7-8)), 909-921.
- Sousa, J., Sousa, M., Jackson, M., & Machado, A. (2014). Comparison of the steel machining performance of new and reground cemented carbide drills. *Journal of Engineering Manufacture*, 228(3), 376–387.
- Specht, D. (1990). Probabilistic neural networks. *Neural Networks*, 3(1), 109-118.
- Stephenson, D. A., & Agapiou, J. S. (2006). *Metal Cutting Theory and Practice*. CRC Press - Taylor & Francis Group.
- Stone, R., & Krishnamurthy, K. (1996). A neural network thrust force controller to minimize delamination during drilling of graphite-epoxy laminates. *International Journal of Machine Tools and Manufacture*, 36(9), 985-1003.
- Sun, J., Hong, G., Rahman, M., & Wong, Y. (2004). Identification of feature set for effective tool condition monitoring by acoustic emission sensing. *International Journal of Production Research*, 42(5), 901-918.
- Tansel, I., Mekdeci, C., & McLaughlin, C. (1995). Detection of tool failure in end milling with wavelet transformations and neural networks (WT-NN). *International Journal of Machine Tools and Manufacture*, 35(8), 1137-1147.
- Tarnag, Y., & Lee, B. (1999). Amplitude demodulation of the induction motor current for the tool breakage detection in drilling operations. *Robotics and Computer-Integrated Manufacturing*, 15(4), 313-318.
- Teti, R. (1995). Fuzzy Logic Approach to Sensor Monitoring during Machining. *WILF 95*, (p. 189-199). Naples.
- Teti, R., & Kumara, S. (1997). Intelligent computing methods for manufacturing systems. *CIRP Annals - Manufacturing Technology*, 46(2), 629-652.
- Teti, R., & Manzoni, A. (1998). Tool Wear State Identification by Fuzzy Logic Processing of Fused Sensor Data. *1st CIRP International Seminar on ICME*, (p. 687-691). Capri.

- Teti, R., Jawahir, I., Jemielniak, K., Segreto, T., Chen, S., & Kossakowska, J. (2006). Chip Form Monitoring through Advanced Processing of Cutting Force Sensor Signals. *CIRP Annals*, 55(1), 75-80.
- Teti, R., Jemielniak, K., & O'Donnell, G. (2010). Advanced monitoring of machining operations. *CIRP Annals - Manufacturing Technology*, 59(2), 717-739.
- Teti, R., Segreto, T., & Harzbecker, C. (2008). Sensor monitoring based optimisation during turning of titanium alloys. *4th I*PROMS, Virtual International Conference on Innovative Production Machines and Systems*, (p. 547-554). Berlin.
- Teti, R., Segreto, T., Neugebauer, R., & Harzbecker, C. (2008). Process Acceptability in Turning of Ti alloys Based on Cutting Force Sensor Monitoring. *3rd International Conference on High Performance Cutting*, (p. 241-250). Dublin.
- Tofallis, C. (2015). A Better Measure of Relative Prediction Accuracy for Model Selection and Model Estimation. *Journal of the Operational Research Society*, 66, 1352-1362.
- Tönshoff, H., Friemuth, T., & Becker, J. (2002). Process Monitoring in Grinding. *CIRP Annals - Manufacturing Technology*, 51(2), 551-557.
- Tsao, C. (2006). The effect of pilot hole on delamination when core drill drilling composite materials. *International Journal of Machine Tools and Manufacture*, 46((12-13)), 1653-1661.
- Tsao, C., & Hocheng, H. (2005). Computerized tomography and C-Scan for measuring delamination in the drilling of composite materials using various drills. *International Journal of Machine Tools and Manufacture*, 45(11), 1282-1287.
- Varol, T., Canakci, A., & Ozsahin, S. (2015). Modeling of the prediction of densification behavior of powder metallurgy Al-Cu-Mg/B4C composites using artificial neural networks. *Acta Metallurgica Sinica (English Letters)*, 28(2), 182-195.
- Venuvinod, P., & Djordjevich, A. (1996). Towards Active Chip Control. *CIRP Annals*, 45(1), 83-86.
- Verl, A., Heisel, U., Walther, M., & Maier, D. (2009). Sensorless automated condition monitoring for the control of the predictive maintenance of machine tools. *CIRP Annals - Manufacturing Technology*, 58(1), 375-378.
- Voß, R., Henerichs, M., Rupp, S., Kuster, F., & Wegener, K. (2016). Evaluation of bore exit quality for fibre reinforced plastics including delamination and uncut fibres. *CIRP Journal of Manufacturing Science and Technology*, 12, 56-66.
- Wang, W., Hong, G., Wong, Y., & Zhu, K. (2007). Sensor fusion for online tool condition monitoring in milling. *International Journal of Production Research*, 45(21), 5095-5116.
- Weule, H., Timmermann, S., & Eversheim, W. (1990). Automation of the Surface Finishing in the Manufacturing of Dies and Molds. *CIRP Annals - Manufacturing Technology*, 39(1), 299-303.
- Whitehouse, D. (2012). *Surfaces and their Measurement*. Boston: Butterworth-Heinemann.
- Wilhelm, M. (2001). Aircraft Applications. In *ASM Handbook: Composite* (Vol. 21). D.B. Miracle and S.L. Donaldson.

- Won , M., & Dharan, C. (2002). Drilling of aramid and carbon fiber polymer composites. *Journal of Manufacturing Science and Engineering (Transactions of the ASME)*, 128, 778-783.
- Wong, Y., Nee, A., Li, X., & Reisdorf, C. (1997). Tool condition monitoring using laser scatter pattern. *Journal of Materials Processing Technology*, 63(1-3), 205-210.
- Wu, S., Li, P., Yan, Z., Zhang, L., Qiu, X., & Yang, J. (2014). Wavelet packet analyses of acoustic emission signal for tool wear in high speed milling. *Key Engineering Materials*, 589-590, 600-605.
- Wu, Y., & Du, R. (1996). Feature extraction and assessment using wavelet packets for monitoring of machining processes. *Mechanical Systems and Signal Processing*, 10(1), 29-53.
- Yang, G., Hou, J., Zhou, W., Zhu, L., & Duan, H. (2014). Non-contact temperature measurement by infrared pyrometer in high speed milling. *Applied Mechanics and Materials*, 668-669, 969-972.
- Zhang , L., Wang, L., & Liu, X. (2001). A mechanical model for predicting critical thrust forces in drilling composite laminates. *Proceedings of the Institution of Mechanical Engineers (Part B: Journal of Engineering Manufacture)*, 215, p. 135-146.
- Zhang, H., Chen, W., Chen, D., & Zhang, L. (2001). Assessment of the Exit Defects in Carbon Fibre-Reinforced Plastic Plates Caused by Drilling. *Key Engineering Materials*, 196, 43-52.
- Zhang, L. (2013). Mechanics and Modeling of Machining Polymer Matrix Composites Reinforced by Long Fibers. In J. Davim, *Machining Composites Materials* (p. 1-38). Wiley-ISTE.
- Zhou, Z., Chen, Y., Fuh, J., & Nee, A. (2000). Integrated condition monitoring and fault diagnosis for modern manufacturing systems. *CIRP Annals - Manufacturing Technology*, 49(1), 387-390.
- Zhu, K., Wong, Y., & Hong, G. (2009). Multi-category micro-milling tool wear monitoring with continuous hidden Markov models. *Mechanical Systems and Signal Processing*, 23(2), 547-560.
- Zitoune, R., El Mansori, M., & Krishnaraj, V. (2013). Tribo-functional design of double cone drill implications in tool wear during drilling of copper mesh/CFRP/wovenply. *Wear*, 302, 1560–1567.
- Zitoune, R., Vijayan, K., & Collombet, F. (2010). Study of drilling of composite material and aluminium stack. *Composite Structures*, 92(5), 1246–1255.